

University of Kentucky

UKnowledge

Theses and Dissertations--Toxicology and
Cancer Biology

Toxicology and Cancer Biology

2012

RELATIONSHIPS BETWEEN TELOMERIC SEQUENCES AND STRUCTURES, DNA REPLICATION, AND THE FUNCTION OF THE WERNER SYNDROME PROTEIN

Deanna Edwards

University of Kentucky, run_fast_pre@yahoo.com

[Right click to open a feedback form in a new tab to let us know how this document benefits you.](#)

Recommended Citation

Edwards, Deanna, "RELATIONSHIPS BETWEEN TELOMERIC SEQUENCES AND STRUCTURES, DNA REPLICATION, AND THE FUNCTION OF THE WERNER SYNDROME PROTEIN" (2012). *Theses and Dissertations--Toxicology and Cancer Biology*. 3.
https://uknowledge.uky.edu/toxicology_etds/3

This Doctoral Dissertation is brought to you for free and open access by the Toxicology and Cancer Biology at UKnowledge. It has been accepted for inclusion in Theses and Dissertations--Toxicology and Cancer Biology by an authorized administrator of UKnowledge. For more information, please contact UKnowledge@lsv.uky.edu.

STUDENT AGREEMENT:

I represent that my thesis or dissertation and abstract are my original work. Proper attribution has been given to all outside sources. I understand that I am solely responsible for obtaining any needed copyright permissions. I have obtained and attached hereto needed written permission statements(s) from the owner(s) of each third-party copyrighted matter to be included in my work, allowing electronic distribution (if such use is not permitted by the fair use doctrine).

I hereby grant to The University of Kentucky and its agents the non-exclusive license to archive and make accessible my work in whole or in part in all forms of media, now or hereafter known. I agree that the document mentioned above may be made available immediately for worldwide access unless a preapproved embargo applies.

I retain all other ownership rights to the copyright of my work. I also retain the right to use in future works (such as articles or books) all or part of my work. I understand that I am free to register the copyright to my work.

REVIEW, APPROVAL AND ACCEPTANCE

The document mentioned above has been reviewed and accepted by the student's advisor, on behalf of the advisory committee, and by the Director of Graduate Studies (DGS), on behalf of the program; we verify that this is the final, approved version of the student's dissertation including all changes required by the advisory committee. The undersigned agree to abide by the statements above.

Deanna Edwards, Student

Dr. David Orren, Major Professor

Dr. Liya Gu, Director of Graduate Studies

RELATIONSHIPS BETWEEN TELOMERIC SEQUENCES AND STRUCTURES,
DNA REPLICATION, AND THE FUNCTION OF THE WERNER SYNDROME
PROTEIN

DISSERTATION

A dissertation submitted in partial fulfillment of the requirements for the degree
of Doctor of Philosophy in the College of Medicine at the University of Kentucky

By

Deanna Nicole Edwards

Lexington, Kentucky

Director: Dr. David Orren, Professor of Toxicology

Lexington, Kentucky

2012

Copyright © Deanna Nicole Edwards 2012

ABSTRACT OF DISSERTATION

RELATIONSHIPS BETWEEN TELOMERIC SEQUENCES AND STRUCTURES, DNA REPLICATION, AND THE FUNCTION OF THE WERNER SYNDROME PROTEIN

All human chromosomes end with protective structures called telomeres, which consist of thousands of double-stranded TTAGGG repeats and end in a 3' guanine-rich overhang. These structures shorten normally during each round of replication, and extremely short telomeres along with telomere dysfunction are thought to contribute to the development of aging and cancer. Although many proteins have roles in telomere maintenance, WRN, which is a 3' to 5' helicase that is deficient in the premature aging disorder Werner's syndrome, has been proposed to play multiple roles at telomeres. In this study, I focus on the effect of telomeric sequences and/or structures formed during DNA replication or recombination and how WRN functions at these sites. This study suggests that WRN may promote proper replication of telomeres by accurately aligning telomeric sequences during replication fork regression, potentially the first step in responding to a blockage, such as DNA damage. However, even in the presence of WRN, replication of telomeric sequences is difficult, possibly due to the ability of G-rich sequences to form secondary structures such as G-quadruplexes. I demonstrate that the translesion polymerase pol η , as well as a variety of other polymerases, is unable to synthesize past an intramolecular G-quadruplex formed from telomeric sequence on the template strand. Furthermore, in physiological salt concentrations, WRN favors binding and unwinding a structure that mimics a strand invasion intermediate over other similar structures especially when it possesses G-telomeric sequence. In addition, WRN promotes unwinding of these structures in a direction that would promote additional annealing and strand invasion, supporting a role for WRN in promoting telomeric recombination and formation of a T-loop, a proposed protective structure specific to telomeres. Overall, the data suggest that telomeres may pose problems in replication due to the G-rich, repeating nature of the structures, while WRN may aid in promoting proper replication at these and other replication blocks. Furthermore, WRN may play a role in promoting additional formation of T-loops and other telomeric recombination, thus supporting the relationship of WRN, telomere maintenance, and potentially development of certain aging characteristics.

KEYWORDS: Werner Protein, Telomeres, Replication, Homologous Recombination, T-loops

Deanna Nicole Edwards

Student's Signature

08/29/2012

Date

RELATIONSHIPS BETWEEN TELOMERIC SEQUENCES AND STRUCTURES,
DNA REPLICATION, AND THE FUNCTION OF THE WERNER SYNDROME
PROTEIN

By

Deanna Nicole Edwards

David K. Orren, Ph.D.

Director of Dissertation

Liya Gu, Ph.D.

Director of Graduate Studies

08/29/2012

Date

...to my family.

ACKNOWLEDGEMENTS

Initially, I would like to express many thanks to my Dissertation Director, Dr. David Orren, for his direction and assistance during my research as well as the construction of this dissertation, as he has played a vital role to my scientific development throughout this entire process. Additionally, I would like to thank my entire Dissertation Committee, Dr. John D'Orazio, Dr. Isabel Mellon, Dr. Peter Mirabito, and Dr. Robert Dickson, each of whom provided critical insight that was essential to my training and education.

I extend my gratitude to all my current and former laboratory colleagues, but thanks are especially due to Dr. Amrita Machwe and Dr. Enerlyn Lozada for their encouragement, technical support, and critical thought. I would also like to thank Rajashree Karale, a rotating student in the lab, for her assistance with the polymerase studies.

I owe my thanks to the Graduate Center for Toxicology Chair, Dr. Mary Vore for her extensive work for the departmental National Institute of Environmental Health Sciences (NIEHS) training grant from which I was fortunate to receive funding.

Finally, I would like to thank numerous family and friends for their tireless support throughout this entire process. My parents, David and Debra Edwards, taught me from an early age that hard work and perseverance were a

requirement for every undertaking I pursue in life. They, along with my sister Danielle, have been tremendously supportive throughout this process. Thanks are also due to my grandparents, Bill Irvan, Charlotte Irvan, and Hazel Edwards, as well as numerous extended family members for their inspiration and support.

Finally, I would like to recognize the organizations that provided funding for my studies and laboratory work including the University of Kentucky Graduate School, the National Institute of Environmental Health Sciences, and the National Institutes of Health.

TABLE OF CONTENTS

Acknowledgements.....	iii
List of Tables	vii
List of Figures	viii
Chapter 1: Introduction	
Werner syndrome.....	1
WRN functions in genome and telomere maintenance	2
Telomere structure and function.....	3
Telomere length and protection determines cell fate	6
The Werner syndrome protein, WRN	10
Research objectives	13
Chapter 2: The effect of G-quadruplexes on DNA polymerase progression	
Introduction.....	18
Methods.....	21
Results	26
Discussion	51
Chapter 3: Fidelity of WRN-mediated regression of model replication forks with repeating sequences	
Introduction.....	59
Methods.....	61
Results	68
Discussion	90
Chapter 4: Recombination-related structural preference of WRN at physiological salt concentrations	
Introduction.....	96
Methods.....	99
Results	103

Discussion	123
Chapter 5: Telomere sequence specificity of recombination intermediates of WRN at physiological salt concentrations	
Introduction.....	130
Methods.....	132
Results	138
Discussion	168
Chapter 6: Conclusions and future directions.....	175
Replication of G-quadruplex forming sequences	177
Roles for WRN during telomeric replication and recombination.....	180
Relevance of results in context of Werner Syndrome	186
Relevance of results in context of normal aging phenotypes (including cancer) and implications for delaying age-related health problems and for cancer therapy.....	189
Appendix.....	192
List of Abbreviations	192
References	195
Vita.....	218

LIST OF TABLES

Table 2.1	Oligonucleotides used to construct primer/template substrates....	23
Table 2.2	Description of polymerases used	38
Table 3.1	Oligonucleotides used to construct model replication forks and daughter duplexes.....	62
Table 3.2	Restriction enzymes used to test repeat alignment	67
Table 4.1	Oligonucleotides used to construct HR-related substrates	100
Table 5.1	Oligonucleotides used to construct model strand invasion intermediates.....	133

LIST OF FIGURES

Figure 1.1	Protective telomere-specific proteins and structures	5
Figure 1.2	Telomere length hypothesis and aging/cancer	7
Figure 1.3	RecQ helicase family of proteins	11
Figure 2.1	G-quadruplex structure	19
Figure 2.2	Primer/template substrates	24
Figure 2.3	Template sequence of 4xGGG/*P31 forms an intramolecular G-quadruplex	27
Figure 2.4	Effect of temperature and KCl concentration on G-quadruplex stability	35
Figure 2.5	Replicative and translesion polymerases are blocked by an intramolecular G-quadruplex	40
Figure 2.6	Human pol η is capable of misincorporation upon encountering an intramolecular G-quadruplex	44
Figure 2.7	Human pol η extends from a misincorporated nucleotide	49
Figure 3.1	Model replication fork and partial duplex substrates	64
Figure 3.2	Protocol for WRN-mediated fork regression repeat alignment analysis	69
Figure 3.3	Analysis of experimental approach on dinucleotide repeat substrates	71
Figure 3.4	Regression of model replication fork with (TTAGGG) _{3.5}	74
Figure 3.5	Alignment analysis of (TTAGGG) _{3.5} repeats	77
Figure 3.6	Regression of model replication fork with (AC) _{10.5}	81
Figure 3.7	Alignment analysis of (AC) _{10.5} repeats	84

Figure 3.8	Alignment analysis of (TTAGGG) _{3.5} repeats following RecG-mediated fork regression	88
Figure 4.1	HR-related substrates	101
Figure 4.2	WRN preferentially unwinds model strand invasion intermediates	106
Figure 4.3	WRN more stably binds model strand invasion intermediates near the single-stranded/double-stranded junction	108
Figure 4.4	WRN unwinds the non-invading strand of a model strand invasion intermediate	112
Figure 4.5	Invading strand complementarity enhances WRN-mediated unwinding	117
Figure 4.6	BLM directionality and structural preferences are similar to WRN	120
Figure 4.7	Structural preferences of UvrD differ from WRN	124
Figure 5.1	Model strand invasion intermediate substrates	135
Figure 5.2	Telomeric sequence on 3' flap does not affect WRN-mediated unwinding	140
Figure 5.3	WRN preferentially unwinds model strand invasion intermediates with G-telomeric sequence on the 5' flap	142
Figure 5.4	WRN preferentially binds G-telomeric sequence	145
Figure 5.5	At least three G-telomeric repeats are required for efficient WRN-mediated unwinding	147
Figure 5.6	Enhanced unwinding of G-telomeric sequence not due to G-quadruplex secondary structure	149
Figure 5.7	A sequence with three G-telomeric repeats does not form a G-quadruplex	152
Figure 5.8	Location of G-telomeric repeats does not affect unwinding	155

Figure 5.9	More efficient unwinding with presence of longer G-runs	157
Figure 5.10	WRN-mediated unwinding is altered at lower temperatures	159
Figure 5.11	WRN-mediated unwinding reduced by Watson-Crick hairpin of 5' flap	162
Figure 5.12	G-telomeric mobile junctions are more effectively unwound	165
Figure 5.13	BLM preferentially unwinds model strand invasion intermediates with G-telomeric sequence	167
Figure 6.1	Graphic demonstrating downstream consequences of nonfunctional WRN	188

CHAPTER 1

INTRODUCTION

WERNER SYNDROME

Otto Werner first described the rare premature aging disease, Werner Syndrome (WS), in 1904 [Werner 1904], and since its discovery, only 1100 affected individuals have been discovered worldwide [Goto, Miller et al. 1996], with most of the cases occurring in the Japanese population [Goto 1997]. WS is an autosomal recessive disorder due to defects in a single gene product, WRN [Yu, Oshima et al. 1996; Matsumoto, Shimamoto et al. 1997]. WS patients prematurely develop several characteristics of normal human aging, including graying hair and baldness, cataracts, atherosclerosis, diabetes, and osteoporosis [Epstein, Martin et al. 1966; Goto, Miller et al. 1996; Goto 1997]. As compared to cancers that arise during normal aging, WS is more closely associated with mesenchymal-derived malignancies [Goto, Miller et al. 1996; Goto 1997]. As opposed to other progerias, individuals with WS develop normally during childhood but begin exhibiting these characteristics in early adulthood, typically perishing by their late forties [Epstein, Martin et al. 1966; Goto 1997]. Since the external phenotype is developed after normal growth as a result of a single defective protein, WS is often used as a simplified model of human aging.

WRN FUNCTIONS IN GENOME AND TELOMERE MAINTENANCE

In addition to the dramatic external phenotype, WRN deficiency leads to several genomic anomalies that suggest the WRN protein functions in DNA metabolism. Most notably, WS cells are characterized by genomic instability [Salk, Au et al. 1981; Goto, Miller et al. 1996], suggesting WRN normally suppresses illegitimate recombination. Further examination of WRN-deficient cells revealed they are particularly sensitive to nucleotide depletion by hydroxyurea and DNA damaging agents that block replication, including interstrand crosslinkers and topoisomerase inhibitors [Lebel and Leder 1998; Pichierri, Franchitto et al. 2001; Poot, Yom et al. 2001]. Even in the absence of exogenous agents, WS cells undergo an extended S-phase [Fujiwara, Higashikawa et al. 1977; Takeuchi, Hanaoka et al. 1982; Poot, Hoehn et al. 1992; Goto, Miller et al. 1996], indicative of difficult replication in the absence of WRN.

Although WRN may function in genome-wide maintenance, WRN localizes to telomeres during S phase [Crabbe, Verdun et al. 2004; Opresko, Otterlei et al. 2004], suggesting WRN plays a specific role at telomeres. WS cells, which possess a reduced replicative lifespan compared to controls, are able to continue dividing with expression of telomerase, an RNA-based reverse transcriptase that adds additional telomeric repeats to telomere ends [Greider and Blackburn 1985; Greider and Blackburn 1987; Kruk, Rampino et al. 1995; Schulz, Zakian et al. 1996; Wyllie, Jones et al. 2000]. Additional evidence

linking WRN to telomeres arose during development of the WS mouse model. WRN deficient mice have no discernable phenotype [Lombard, Beard et al. 2000], likely due to extremely long murine telomeres (40 kb). However, elimination of telomerase for several generations drastically shortens the mouse telomeres; late generation (G4-G6) $Tert^{-/-}WRN^{-/-}$ mice display a phenotype similar to human WS including a decreased lifespan, short stature, graying and loss of hair, osteoporosis, and cataracts [Chang, Multani et al. 2004; Du, Shen et al. 2004]. Cells derived from these mice had shorter telomeres when compared to age-matched telomerase-deficient mice [Chang, Multani et al. 2004], indicating WRN may prevent excessive telomere loss.

TELOMERE STRUCTURE AND FUNCTION

Telomeres are specialized structures found at linear chromosome ends [McClintock 1941; Szostak and Blackburn 1982]. Human telomeres consist of 5-15 kb of the non-coding repeating sequence, TTAGGG/AATCCC [Moyzis, Buckingham et al. 1988; de Lange, Shiue et al. 1990] and protect the important internal genetic code. Although the majority of telomeric sequence exists in double-stranded form, telomeres end in a 3' overhang of the G-rich strand [Greider and Blackburn 1987; Henderson and Blackburn 1989; McElligott and Wellinger 1997]. A proteinaceous structure normally protects telomere ends [van Steensel, Smogorzewska et al. 1998; Veldman, Etheridge et al. 2004]. These protective proteins involved are collectively termed shelterin, which includes the telomere-specific double-stranded DNA binding proteins TRF1 and

TRF2, the single-stranded G-rich telomere binding protein POT1, as well other interacting proteins (RAP1, TIN2, and TPP1) (Figure 1.1A) [Zhong, Shiue et al. 1992; Billaud, Brun et al. 1997; Broccoli, Smogorzewska et al. 1997; Baumann and Cech 2001; de Lange 2005]. The protective nature of shelterin proteins may stem from T-loops, a specialized telomere end structure identified in mammalian cells [Griffith, Comeau et al. 1999]. These structures, which also may represent recombination intermediates, are generated with assistance by TRF2 [Stansel, de Lange et al. 2001] by invasion of the 3' telomeric overhang into the double-stranded repeats (Figure 1.1B). By concealing the free telomere terminus, T-loops likely protect telomere ends from being recognized as a double-strand break by DNA repair proteins. The G-rich sequences of telomeres may also fold into additional structures, including G-quadruplexes, a secondary structure that readily forms *in vitro* in the presence of K⁺ or Na⁺ through Hoogsteen interactions [Wang and Patel 1993; Xu, Noguchi et al. 2006; Phan, Kuryavyi et al. 2007]. G-quadruplexes have been confirmed to exist within *Stylonychia lemnae* and *Saccharomyces cerevisiae* [Schaffitzel, Berger et al. 2001; Zhang, Tong et al. 2010]. Although G-quadruplexes have not been observed in human cells, more than 300,000 sites capable of forming G-quadruplexes have been identified within the human genome, with many of these located at telomeres [Huppert and Balasubramanian 2005; Huppert and Balasubramanian 2007]. These structures likely form in single-stranded G-rich regions generated during replication and/or recombination or at the 3' telomeric single-stranded overhang [Tang, Kan et al. 2008; Lipps and Rhodes 2009].

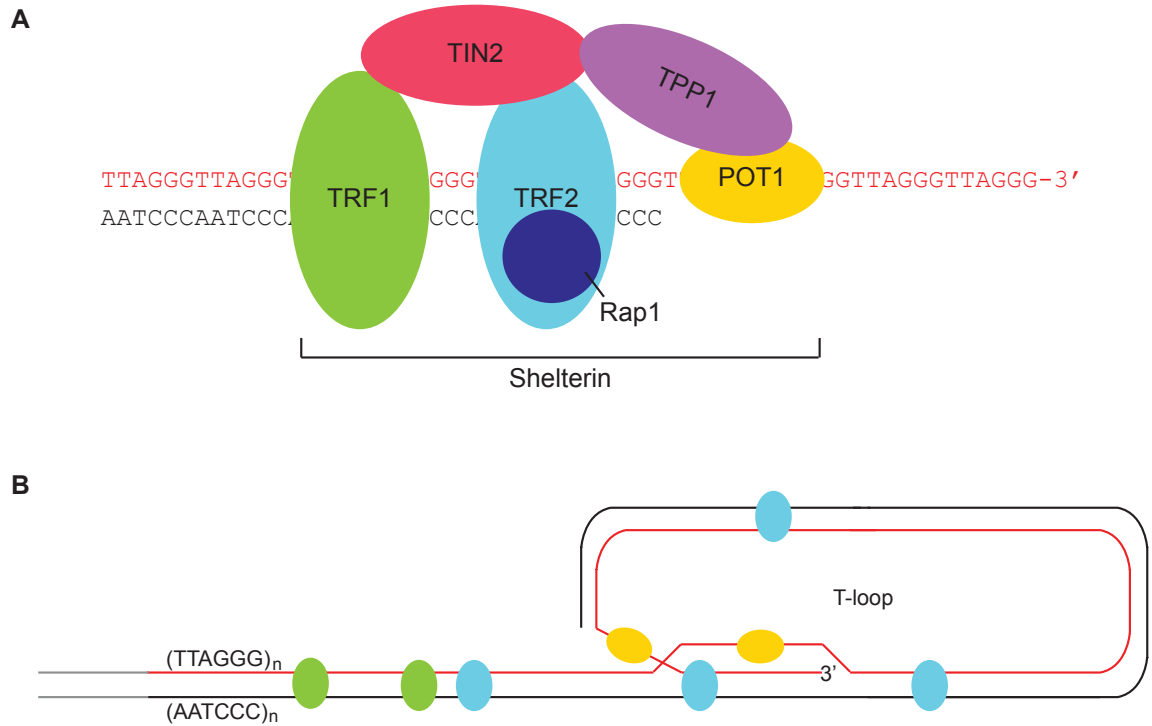


Figure 1.1 Protective telomere-specific proteins and structures. A) Shelterin proteins bound to telomeric sequence. The G-rich lagging strand is indicated in red, and the C-rich leading strand is indicated in black. **B)** T-loop structure with shelterin proteins. The G-rich lagging strand is indicated in red, and the C-rich leading strand is indicated in black.

TELOMERE LENGTH AND PROTECTION DETERMINES CELL FATE

Telomere length correlates with replicative capacity of human fibroblasts, and further correlations exist between *in vitro* replicative potential and donor age [Allsopp, Vaziri et al. 1992; Yang, Suwa et al. 2001]. Therefore, telomere length and functionality are believed to contribute to aging and cancer (Figure 1.2). Germ cells and most cancer cells possess an active form of telomerase, which adds additional repeats to the telomere ends [Greider and Blackburn 1985; Greider and Blackburn 1987], virtually immortalizing these cells [Greider and Blackburn 1985; Allsopp, Vaziri et al. 1992; Shay and Bacchetti 1997]. Conversely, somatic cells possess very low levels of telomerase and therefore, are unable to extend telomeres to a great extent [Harley, Futcher et al. 1990]. Along with insufficient telomerase activity, cells are unable to completely replicate the total length of the chromosome, also known as the “end replication problem,” and thus, telomeres shorten with each normal round of replication [Watson 1972; Harley, Futcher et al. 1990]. Following many rounds of replication, telomeres eventually shorten to a length at which chromosome end is no longer protected, perhaps due to the inability to form a protective structure, such as a T-loop. Once telomeres reach this limit, also known as the Hayflick limit, cells are unable to continue dividing [Hayflick 1965]. Telomeres are likely replicated unidirectionally [Gilson and Geli 2007], indicating fork stalling and collapse within telomeres may lead to large telomere deletions and accelerated telomere shortening. These shortened, unprotected chromosome ends are recognized by the cell as a double strand break, and through activation of ATM

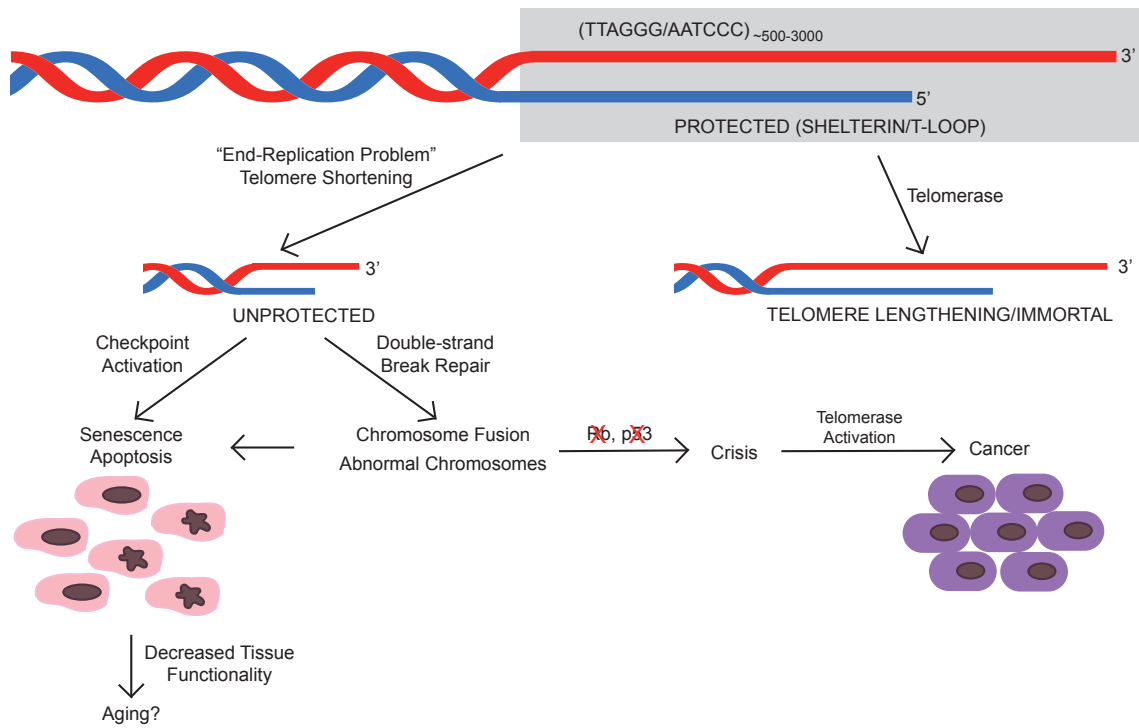


Figure 1.2 Telomere length hypothesis and aging/cancer.

and p53, cell cycle arrest occurs [Chin, Artandi et al. 1999; Denchi and de Lange 2007]. In a similar manner, TRF2 loss and subsequent telomere deprotection on long telomeres induces a DNA damage response [van Steensel, Smogorzewska et al. 1998; Takai, Smogorzewska et al. 2003; Veldman, Etheridge et al. 2004]. In many arrested cells, apoptosis results; however, fibroblasts undergo senescence, an irreversible state during which the cell is unable to divide or function in a normal capacity [Hayflick 1976]. Senescent (and apoptotic) cells accumulate in aging individuals [Dimri, Lee et al. 1995], suggesting these cells may reduce the capacity for tissues to function properly [Campisi 2005]. Therefore, the process of telomere erosion and subsequent loss of functional cells may lead to the development of aging characteristics.

Even though unprotected telomeres generally lead to cell cycle arrest, inactivation of p53 and Rb can allow cells to escape arrest and continue dividing (Figure 1.2) [Shay, Wright et al. 1991]. These cells enter crisis, a cellular state of extremely shortened telomeres and numerous telomere abnormalities including telomere-telomere chromosomal fusions [Wright and Shay 1992; Shay and Wright 2005]. Although the majority of cells in crisis undergo apoptosis, approximately 1 in every 10 million cells escape crisis by activating telomerase or other telomere-lengthening pathways to become immortal [Wright and Shay 1992; Shay, Van Der Haegen et al. 1993]. With these cells possessing a method for extending telomeres as well as inactivated tumor suppressors p53 and Rb, they are capable of becoming tumorigenic [Wright and Shay 1992].

In addition to the end-replication problem, difficulties encountered during telomere metabolism may contribute to the development of aging and/or cancer. In particular, problematic replication may lead to accelerated loss of telomere sequence. Especially when replicating repeating sequences, the replication machinery may “slip” by essentially losing its frame along the sequence, an event that may lead to a telomeric sequence deletion [Streisinger, Okada et al. 1966; Kunkel 1986]. However, more severe events of telomere loss may occur as a result of replication fork collapse at sites of fork-blocking DNA damage or secondary structures [Betous, Rey et al. 2009]. Without a converging fork at telomeres [Gilson and Geli 2007], fork collapse prevents synthesis of the entire telomere and thus can result in telomere loss [Chavez, Tsou et al. 2009]. Similar to replication, homologous recombination may contribute to sequence loss if homologous sequences are aligned in an incorrect frame. Excessive and stochastic telomere loss can accelerate telomere shortening and prematurely generate unprotected telomeres. However, even long telomeres can become dysfunctional as a consequence of T-loop loss [van Steensel, Smogorzewska et al. 1998; Takai, Smogorzewska et al. 2003; Veldman, Etheridge et al. 2004]. Regardless of the mechanism, unprotected telomeres lead to the activation of cell-cycle checkpoints and senescence or apoptosis, potentially contributing to aging (Figure 1.2). Further illegitimate recombination of these dysfunctional telomeres, in addition to inactivation of tumor suppressors, may lead to tumorigenesis (Figure 1.2). Since WRN is proposed to play a role in telomere metabolism, we propose WRN promotes proper replication, recombination,

and/or end protection as a mechanism to maintain telomere stability and protect against aging and cancer.

THE WERNER SYNDROME PROTEIN, WRN

On the molecular level, WS is an autosomal recessive disease caused by defects in a single gene product, WRN [Yu, Oshima et al. 1996]. Most of the WRN mutations identified generate mutant proteins that lack the nuclear localization signal; therefore, these mutant WRN proteins are degraded in the cytoplasm and do not enter the nucleus where their function is performed [Matsumoto, Shimamoto et al. 1997; Goto, Yamabe et al. 1999; Moser, Kamath-Loeb et al. 2000; von Kobbe and Bohr 2002]. This 162 kDa protein is a member of the RecQ helicase family, which includes proteins deficient in other premature aging and cancer-prone disorders such as BLM (deficient in Bloom syndrome) and RecQ4 (deficient in Rothmund-Thomson syndrome) (Figure 1.3) [Ellis, Groden et al. 1995; Yu, Oshima et al. 1996; Kitao, Shimamoto et al. 1999]. As opposed to humans, which possess five RecQ proteins, lower eukaryotes, such as *Saccharomyces pombe* (Rqh1) and *Saccharomyces cerevisiae* (Sgs1), only possess a single RecQ protein (Figure 1.3) [Watt, Louis et al. 1995; Stewart, Chapman et al. 1997].

All members of the RecQ family possess seven highly conserved amino acid sequence motifs (Figure 1.3) [Karow, Wu et al. 2000], and it is this region that binds and hydrolyzes ATP to drive a 3' to 5' helicase activity [Gray, Shen et

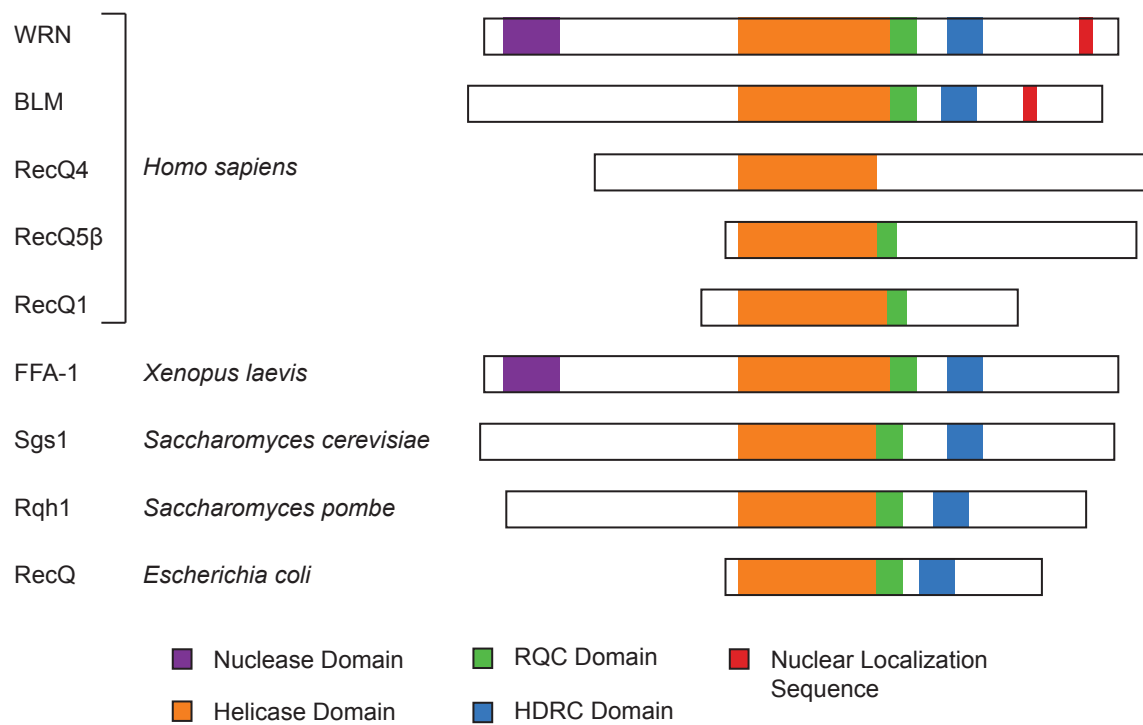


Figure 1.3 RecQ helicase family of proteins.

al. 1997]. Specifically, WRN unwinds duplex regions of complex structures such as D-loops, three-way junctions, Holliday junctions, replication forks, and flaps [Mohaghegh, Karow et al. 2001; Brosh, Waheed et al. 2002; Orren, Theodore et al. 2002; Opresko, Sowd et al. 2009], but the protein also disrupts the Hoogsteen interactions of G-quadruplexes [Fry and Loeb 1999; Mohaghegh, Karow et al. 2001]. Similar to WRN, BLM readily unwinds Holliday junctions, forks, and D-loops in addition to G-quadruplexes [Mohaghegh, Karow et al. 2001; Bachrati, Borts et al. 2006]. In contrast to unwinding, WRN promotes annealing of two complementary strands at a significantly faster rate than occurs in the absence of protein [Machwe, Xiao et al. 2005]. Even though it seems contradictory for a single protein to possess unwinding and strand annealing activities, WRN coordinates these activities to perform strand exchange and fork regression [Machwe, Xiao et al. 2005; Machwe, Xiao et al. 2006; Machwe, Xiao et al. 2007]. Regression, which involves concurrent annealing of homologous daughter strands and parental strands, is proposed to be the first response to stalled replication forks, allowing repair and replication restart [Machwe, Xiao et al. 2006; Machwe, Xiao et al. 2007]. In addition, WRN is the only human RecQ protein that possesses a nuclease domain that confers a 3' to 5' exonuclease activity [Shen, Gray et al. 1998]. Consistent with a role in telomere metabolism, WRN functionally interacts with the shelterin proteins, TRF2 and POT1 [Opresko, von Kobbe et al. 2002; Machwe, Xiao et al. 2004; Opresko, Mason et al. 2005]. WRN also interacts with the main lagging strand polymerase, pol δ [Kamath-Loeb, Loeb et al. 2001; Nick McElhinny, Gordenin et al. 2008].

Therefore, the evidence presented here is consistent with a WRN function in telomere metabolism.

RESEARCH OBJECTIVES

WS is characterized by genomic instability as well as sensitivity to DNA damaging agents that block replication, strongly supporting a WRN role in genomic maintenance. However, in recent years, much of the evidence points to WRN also functioning in telomere metabolism. Consistent with a role in telomere replication and/or recombination, WRN localizes to the telomeres during S phase, potentially through a functional interaction with the shelterin proteins TRF2 and POT1, which enhance WRN's helicase and/or exonuclease activity. Telomere loss, potentially resulting from inefficient replication in the absence of WRN, likely leads to the premature senescence of WS cells in culture since telomerase expression extends their replicative lifespan. The influence of telomeres on aging is also evident in the WS mouse model, which required several generations of murine telomere shortening to develop a WS phenotype. In addition to the telomere aspects of WRN deficiency, WRN possesses efficient catalytic activities on several replication or recombination-related structures, suggestive of a biochemical role in these processes. In the present study, I wished to more closely examine the role of the WRN protein in several aspects of telomere maintenance. The specific hypothesis of this work was that WRN helps maintain telomere stability by its involvement in the promotion of proper and efficient replication and/or recombination. Proper

telomere metabolism may be particularly valuable at telomeres, due to several unique elements of telomeric sequences. Telomeres are G-rich, and thus are capable of forming G-quadruplexes, while the repetitive nature allows for strand-slippage and misalignment during replication and/or recombination. Specialized T-loop structures and the binding of telomere-specific proteins may also act as barriers for replication. Furthermore, in the event of fork blockage due to DNA damage or one of these elements, the unidirectional nature of telomere replication may lead to telomere loss. Thus, I investigated potential roles of WRN in telomere replication and recombination, by primarily examining WRN's action on several telomere metabolism-related structures.

Telomeres are G-rich, and thus are capable of forming G-quadruplexes, particularly within single-stranded regions generated during replication and/or recombination. The lagging strand is likely to develop single-stranded regions between Okazaki fragments, making this G-rich strand particularly susceptible to intramolecular G-quadruplex formation. Different types of template modifications are known to have an impact on polymerase progression, with most studies examining DNA damage. While replicative polymerases are often blocked by DNA damage, the main function of translesion polymerases is to bypass these fork-blocking lesions. However, I investigated the possibility that compact secondary structures like G-quadruplexes may also block the progression of polymerases and thus replication. In this study, I initially determined conditions under which intramolecular G-quadruplexes are formed and stabilized.

Subsequently, I studied how these structures impacted polymerase progression and mutation formation.

WS cells are sensitive to DNA damaging agents that block or stall replication, suggesting WRN promotes proper replication. Consistent with a role in responding to blocked replication forks, WRN performs *in vitro* fork regression, the proposed initial response to blocked replication forks. During regression, WRN coordinates its helicase and annealing activities to simultaneously pair the newly synthesized complementary daughter strands while also annealing the parental strands, generating a Holliday junction (see Figure 3.4A), an event that allows repair and proper resumption of replication. Particularly due to the lack of bidirectional replication, telomeres may be particularly sensitive to fork blockage at DNA damage or G-quadruplexes, making proper replication especially critical to prevent sequence loss. Furthermore, repeating sequences such as telomeres may become misaligned during regression, potentially leading to insertions or deletions following additional processing. By properly aligning repeating sequences during replication fork regression, WRN may enhance replication efficiency. In this study, I analyzed the fidelity of WRN-mediated fork regression within telomeric and dinucleotide repeating sequences using multiple methods of detecting repeat alignment.

The genomic and telomere instability in WS cells also suggest WRN may suppress illegitimate recombination. Homologous recombination (HR) is often utilized as a high fidelity mechanism in the repair of collapsed replication forks,

double-strand breaks, or other replication errors. Genomic instability is also observed in diseases that result from HR defects [van Gent, Hoeijmakers et al. 2001], suggesting that HR may be deficient in WS. However, homology-based strand invasion also occurs in other areas of telomeres, including during T-loop formation. These specialized structures, which are generated by a recombination-like mechanism involving invasion of the G-rich 3' overhang into homologous duplex repeats, are proposed to protect the ends of linear chromosomes from being recognized as a double-strand break. WS cells exhibit signs of telomere dysfunction, indicating WRN may function in telomere-end protection. As mechanisms to prevent telomere dysfunction, WRN may suppress illegitimate recombination by promoting telomeric HR and T-loop development. In this study, I focused on WRN's role at a single recombination-related structure that mimics a strand invasion intermediate. Initially, I compared WRN's helicase activity on a model strand invasion intermediate to other similar structures at physiological salt concentrations. To directly study a telomeric role of WRN, I examined how inclusion and placement of telomeric sequences influenced WRN-mediated unwinding of these model strand invasion intermediates. Finally, since these studies were carried out in physiological conditions that favor formation of G-rich secondary structures, I investigated the impact G-quadruplexes and guanine hairpins have on WRN's helicase activity related to model strand invasion intermediates.

In this study, I addressed the following topics:

Chapter 2—The effect of G-quadruplexes on DNA polymerase progression

Chapter 3—Fidelity of WRN-mediated regression of model replication forks with repeating sequences

Chapter 4—Recombination-related structural preference of WRN at physiological salt concentrations

Chapter 5—Telomeric sequence specificity of recombinational intermediates of WRN at physiological salt concentrations

CHAPTER 2

THE EFFECT OF G-QUADRUPLEXES ON DNA POLYMERASE

PROGRESSION

INTRODUCTION

Telomeres as well as other G-rich sequences present numerous difficulties for the replication machinery. In addition to the repeating nature and unique structural aspects, mammalian telomeres are composed of G-rich TTAGGG repeats that possess the potential to form G-quadruplex structures. G-quadruplexes are highly compact secondary structures that can form by the interaction of four runs of at least three guanine bases. Specifically, Hoogsteen interactions between the N², N⁷, N¹ and O⁶ positions among four guanine bases form a G-quartet, a structure stabilized by a monovalent cation such as K⁺ or Na⁺ (Figure 2.1A), and stacking of at least three G-quartets forms a G-quadruplex (Figure 2.1B). Furthermore, G-quadruplexes exist in a variety of forms defined by the number of strands involved; intermolecular G-quadruplexes form from the interaction of two or more strands and intramolecular G-quadruplexes are formed by the interaction of a single strand, both of which are stable secondary structures (Figure 2.1C) [Lipps and Rhodes 2009].

Although G-quadruplexes are readily formed *in vitro* by a variety of G-rich sequences, including the Fragile X syndrome associated CGG repeats [Fry and

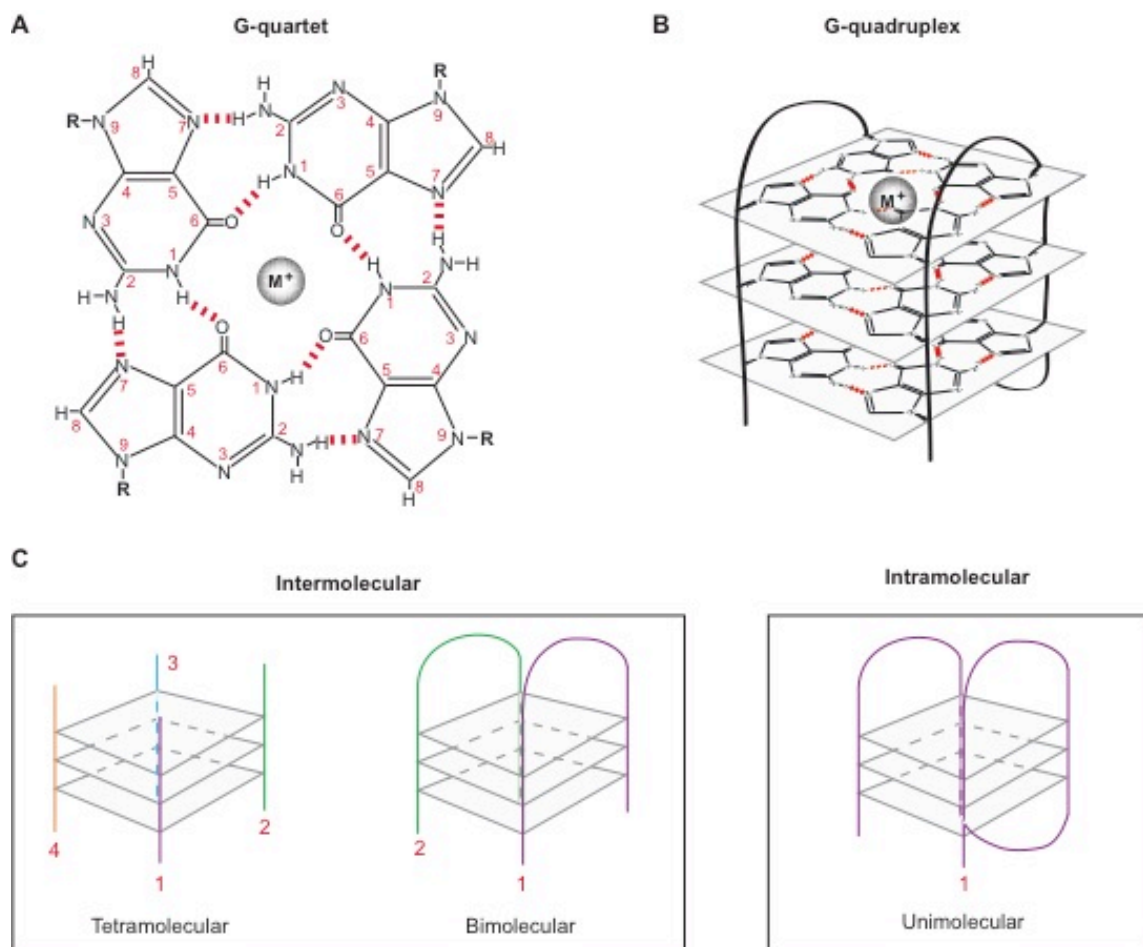


Figure 2.1 G-quadruplex structure. **A)** Structure of a G-quartet in the presence of a monovalent cation (M^+). Hydrogen-Hoogsteen bonding indicated by red dashes. **B)** Structure of an intramolecular G-quadruplex, consisting of three planar G-quartets. **C)** Classifications of G-quadruplexes based on the number of strands involved.

Loeb 1994; Kettani, Kumar et al. 1995], the c-myc promoter sequence [Searle, Williams et al. 2004], and the human telomeric sequence [Wang and Patel 1993; Phan, Kuryavyi et al. 2007; Xu, Ishizuka et al. 2009], these structures have not yet been proven to exist *in vivo* in human cells. However, evidence indicates that G-quadruplexes form in other organisms, including *Saccharomyces cerevisiae* [Zhang, Tong et al. 2010] and the macronuclear telomeres of the ciliated protozoan *Stylonychia lemnae* [Schaffitzel, Berger et al. 2001]. Importantly, researchers have identified more than 376,000 sites, concentrated in gene promoters and telomeres, within the human genome exhibiting the potential to form G-quadruplexes [Huppert and Balasubramanian 2005; Huppert and Balasubramanian 2007]. Since duplex DNA appears unlikely to spontaneously dissociate in favor of G-quadruplex formation, these structures are likely to form primarily within single stranded regions such as the 3' overhang at telomeres or those that form during transcription, replication, or recombination [Lipps and Rhodes 2009]. Importantly, within these single-stranded regions, intramolecular G-quadruplexes, as opposed to intermolecular, are the likely secondary structure to form [Tang, Kan et al. 2008; Lipps and Rhodes 2009].

Stable secondary structures, such as intramolecular G-quadruplexes, may impede replication. Strongly indicating replication difficulties at G-rich telomeric sequences, human telomeres develop double-strand breaks dependent upon replication, thus resembling fragile sites [Sfeir, Kosiyatrakul et al. 2009]. Specifically within telomeres, replication fork stalling by G-

quadruplexes may lead to telomere instability and subsequent apoptosis or senescence, similar to characteristics associated with WS. In fact, more double strand breaks occurred following treatment with a G-quadruplex stabilizing ligand in cells lacking the translesion polymerases pol η or pol κ , not only indirectly suggesting the existence of G-quadruplexes *in vivo*, but also implying these structures inhibit replication [Betous, Rey et al. 2009]. *In vitro* biochemical experiments showed a bimolecular G-quadruplex on the template strand inhibits pol δ , the main polymerase in lagging strand synthesis [Kamath-Loeb, Loeb et al. 2001]. Although these results are valid, an intramolecular G-quadruplex is considered to most likely form *in vivo* [Tang, Kan et al. 2008; Lipps and Rhodes 2009]. Therefore, in these studies, I set out to test what effect a unimolecular G-quadruplex formed from human telomeric sequence on the template strand would have on a wide range of human and non-human polymerases. In these experiments, I tested not only replicative DNA polymerases but also translesion DNA polymerases that are widely thought to function in response to stalled replication.

METHODS

Enzymes. T4 polynucleotide kinase and the polymerases Kexo⁺ and T4 DNA polymerase were purchased from New England Biolabs (Ipswich, MA). Human polymerase δ was provided as a gift from Guo-Min Li (University of Kentucky). All other polymerases used in this chapter, including human polymerase η , S.

cerevisiae polymerase η , human polymerase κ , human polymerase β , and polymerase μ were acquired from Enzymax (Lexington, KY).

DNA substrates. PAGE-purified DNA oligonucleotides were obtained from Integrated DNA Technologies (Coralville, IA). Sequences of all oligos are shown in Table 2.1. Importantly, the oligos 4xGGG and ext-4xGGG contain four human telomeric repeats, and thus, four runs of guanine bases. However, 3xGGG contains only three human telomeric repeats (three runs of guanine bases) and is not capable of forming an intramolecular G-quadruplex. The oligo 4xGGG²² containing most of the telomeric template region of 4xGGG and ext-4xGGG was a gift from Mike Fried (University of Kentucky). To generate the substrates used, 4xGGG²² and primer oligos P31 and P34 were 5' radiolabeled using ³²P- γ -ATP and T4 polynucleotide kinase. Radiolabeled strands were run through Mini Quick Spin Oligo Columns (Roche, Indianapolis, IN) to remove unincorporated ATP. Hereafter, radiolabeled strands are indicated by asterisks. Labeled primer/template substrates were produced by annealing 3xCCC, 3xGGG, 4xGGG, or ext-4xGGG to *P31 or *P34 (Figure 2.2) in 50 mM Tris (pH 8.0) and 10 mM MgCl₂ by heating to 90°C and slow cooling to room temperature. The substrates were then further purified by native PAGE (10%), excised, and eluted in 10 mM Tris (pH 8.0) containing 10 or 25 mM NaCl.

Dimethyl sulfate protection assay. In 0-75 mM KCl, *4xGGG²² (1.75 nM) was heat denatured at 90°C and slow cooled to room temperature to promote G-quadruplex formation. Samples were treated with 0.5% dimethyl sulfate (DMS)

Table 2.1 Oligonucleotides used to construct primer/template substrates.

Primers

P31

5'-CACTGACTCCAGGAACTGGAGGATGCCTAGG-3'

P34

5'-CACTGACTCCAGGAACTGGAGGATGCCTAGGTAA-3'

Templates

3xCCC

5'-TAACCCTAACCCTAACCCTAACCTAGGCATCCTCCAGTTCCTGGAGTCAGTG-3'

3xGGG

5'-TTAGGGTTAGGGTTAGGGTTACCTAGGCATCCTCCAGTTCCTGGAGTCAGTG-3'

4xGGG

5'-AGGGTTAGGGTTAGGGTTAGGGTTACCTAGGCATCCTCCAGTTCCTGGAGTCAGTG-3'

ext-4xGGG

5'-CATTTCAATTTTAGGGTTAGGGTTAGGGTTAGGGTTACCTAGGCATCCTCCAGTTCCTGGAGTCAGTG-3'

Other

4xGGG²²

5'-AGGGTTAGGGTTAGGGTTAGGG-3'

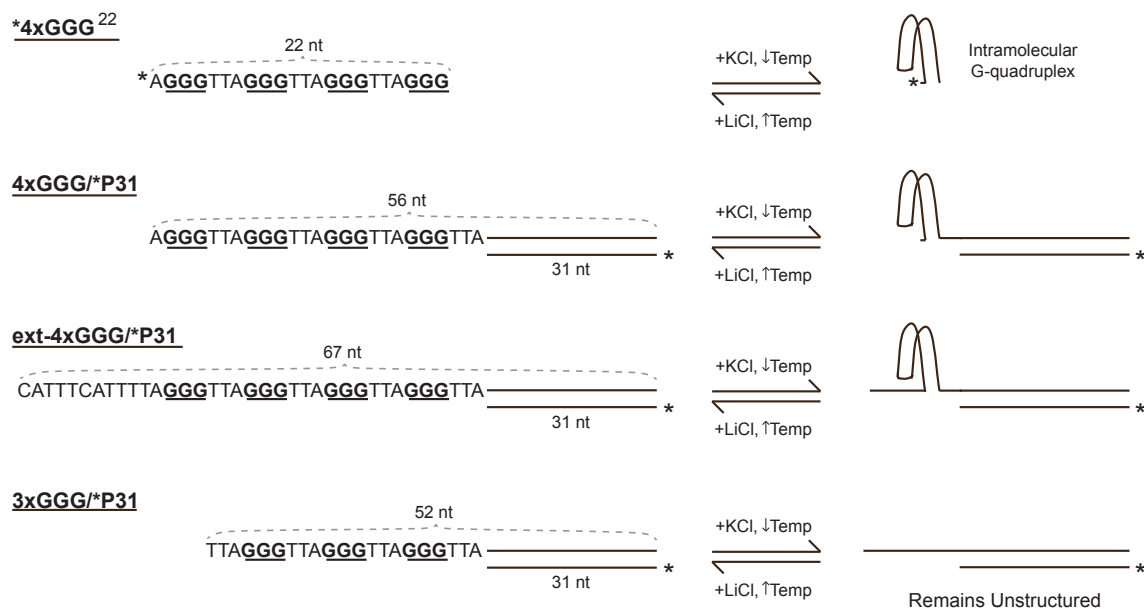


Figure 2.2 Primer/template substrates. To generate primer/template substrates, a template strand (4xGGG, ext-4xGGG, or 3xGGG) is annealed to a *P31 or *P34 (not shown) 5' radiolabeled primer strand. The sequence of 4xGGG²² (top), which is capable of forming an intramolecular G-quadruplex, was used as a model for the single-stranded template of 4xGGG/*P31 and ext-4xGGG/*P31. Conditions that favor (or disfavor) G-quadruplex formation are indicated. These conditions do not significantly alter the structure of the control 3xGGG/*P31 and 3xCCC/*P31 (not shown) templates (also see Figure 2.4A-B).

(Sigma-Aldrich; St. Louis, MO) in extension buffer (40 mM Tris-HCl (pH 8.0), 1 mM MgCl₂, 5 mM dithiothreitol, 100 µg/mL bovine serum albumin (BSA), 0.1% NP40, and 250 µM ATP) in 0-75 mM KCl at room temperature for 10 min, and the reaction was stopped by addition of 250 mM β-mercaptoethanol and 375 mM sodium acetate (pH 7.0). DNA from each sample was collected by standard ethanol precipitation using yeast tRNA (10 µg) as a carrier. The resulting pellet was resuspended in 10% piperidine (Sigma), incubated at 90°C for 30 min, and the liquid was removed using vacuum evaporation. The samples were resuspended in 10 mM Tris (pH 8.0) and an equal volume of formamide loading buffer (95% formamide, 20 mM EDTA, 0.05% bromophenol blue, and 0.05% xylene cyanol) was added. To facilitate comparison between samples, equal amounts of radioactivity in individual samples were electrophoresed on a denaturing polyacrylamide (14%) gel. DNA fragments were visualized using Storm 860 Phosphorimager and ImageQuant software (GE Healthcare).

DNA structure assessment by native PAGE. 3xCCC/*P31, 4xGGG/*P31, and 3xGGG/*P31 (200 pM) were incubated in 75 mM KCl or LiCl at 25°C for 1 h to allow for secondary structure formation and 1/6 volume of acrylamide running dyes (30% glycerol, 0.25% xylene cyanol, 0.25% bromophenol blue) was added. DNA structures were electrophoresed by native PAGE (15% acrylamide, 37.5:1) at room temperature in 1x TBE (0.45 M Tris, 0.45 M boric acid, 10 mM EDTA) containing either 75 mM KCl or LiCl in both the gel and running buffer. Labeled DNA products were visualized as described above.

Primer extension assay. Primer/template substrates (3xCCC/*P31, 4xGGG/*P31, ext-4xGGG/*P31, 3xGGG/*P31, 3xGGG/*P34, or ext-4xGGG/*P34) (0.2-0.4 nM) were treated with a polymerase (Kexo⁻, T4 DNA polymerase, human polymerase δ , human polymerase η , *S. cerevisiae* polymerase η , human polymerase κ , human polymerase μ , or human polymerase β) at the concentrations indicated in extension buffer with 75 mM KCl or LiCl and 100 μ M dNTP's. Reactions were incubated for 5-30 min at 18-37°C with one or more dNTP's and/or in a stepwise manner as specified in the Results. An equal volume of formamide loading buffer was added to stop reactions. Samples were heat denatured and analyzed by denaturing PAGE (14%). Products resulting from extension of the radiolabeled primer strand were visualized as indicated above.

RESULTS

Formation and stability of telomeric intramolecular G-quadruplex structures. G-quadruplexes are formed by the interactions of four runs of three or more guanines by weak Hoogsteen bonding in the presence of K⁺ or Na⁺ (Figure 2.1; Figure 2.3A). These compact secondary structures are capable of forming from telomeric repeats or other G-rich sequences and may block polymerases during DNA replication. In fact, a bimolecular G-quadruplex involving the template strand inhibits human DNA polymerase δ *in vitro* [Kamath-Loeb, Loeb et al. 2001]. However, without a second G-rich single-stranded DNA molecule, intermolecular G-quadruplexes are unlikely to form during replication,

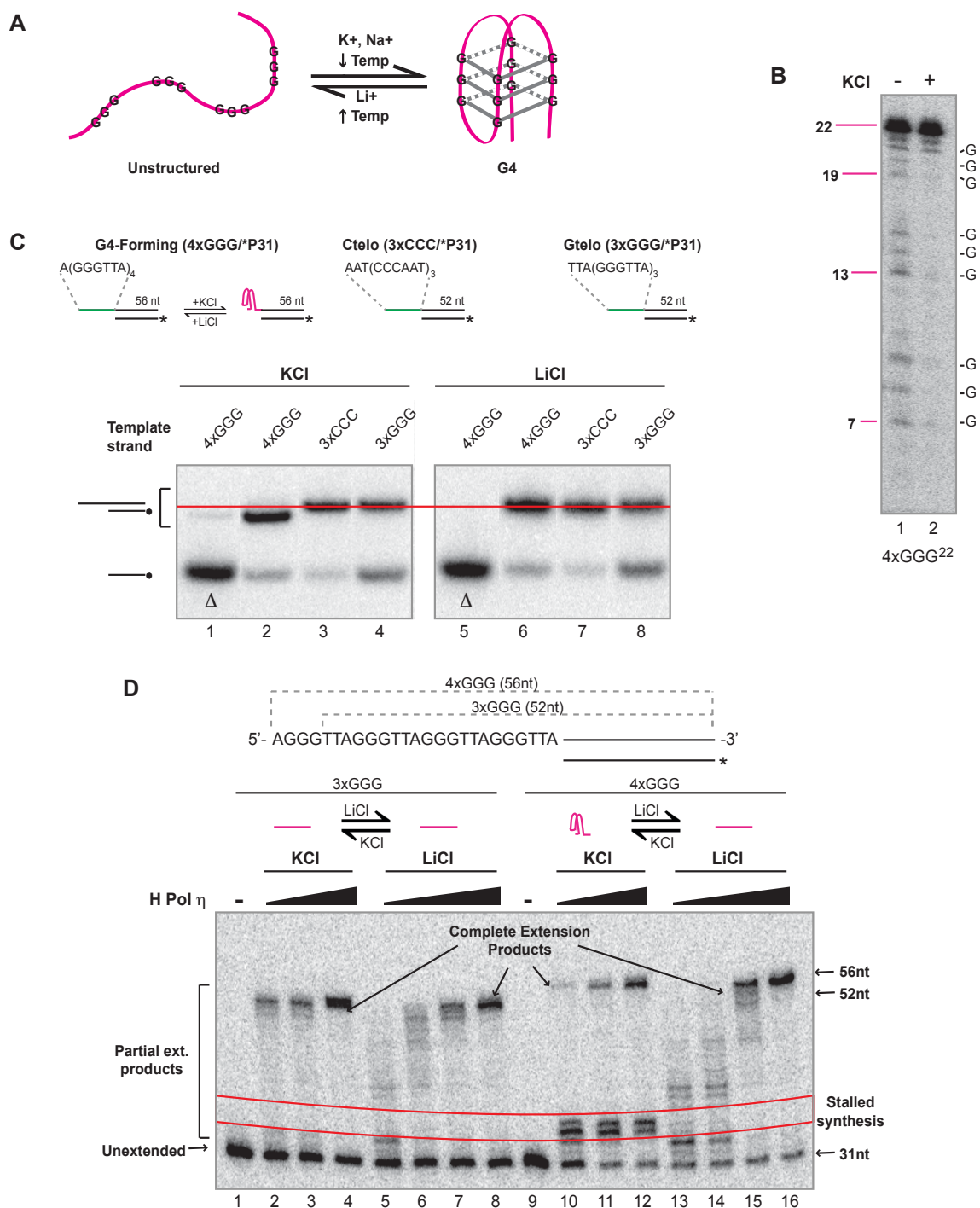


Figure 2.3 Template sequence of 4xGGG/*P31 forms an intramolecular G-quadruplex. **A)** Formation of an intramolecular G-quadruplex from single-stranded DNA containing four GGG runs. Conditions that impact formation and dissociation of G-quadruplexes are indicated. **B)** To detect G-quadruplex formation, a DMS protection assay was performed on *4xGGG²², in extension buffer conditions containing 0 or 75 mM KCl. Products resulting from cleavage

at unmethylated guanine bases are analyzed by denaturing PAGE. Length of resulting DNA fragments are indicated on the left. **C)** Control (3xCCC/*P31 and 3xGGG/*P31) or test (4xGGG/*P31) primer/template substrates were incubated in 75 mM KCl or LiCl for 1 hr at 25°C. Migration of these substrates was analyzed on native PAGE (15%) containing 75 mM KCl or LiCl in the gel matrix and running buffer. The red line indicates migration of primer/template substrates with an unstructured template. **D)** Primer extension assays were performed by incubating human pol η (0.05-0.26 nM in KCl or 0.10-1.0 nM in LiCl) with 3xGGG/*P31 or 4xGGG/*P31 (0.3 nM) in extension buffer containing 75 mM KCl or LiCl at 37°C for 5 min. Heat-denatured primer strands were separated and visualized after denaturing PAGE. Positions of partial extension products indicating polymerase blockage are highlighted (between red lines).

while intramolecular G-quadruplexes can easily form by self-association within these regions. During lagging strand synthesis, numerous single-stranded regions are generated between Okazaki fragments, making the lagging strand particularly susceptible to secondary structures. Importantly, the telomeric lagging strand is G-rich, providing the potential for intramolecular G-quadruplex formation during replication. Here, the effect of an intramolecular G-quadruplex on the template strand during synthesis using a variety of DNA polymerases was examined.

It was first necessary to confirm that the template strand of these primer/template substrates formed an intramolecular G-quadruplex. A variety of methods historically used to detect G-quadruplex formation were utilized here, including the dimethyl sulfate (DMS) protection assay, PAGE analysis using primer/template substrates, and polymerase extension assays in conditions that favor G-quadruplex formation versus conditions that disfavor G-quadruplexes.

The DMS protection assay is based on the Maxam-Gilbert sequencing protocol. DMS methylates the N⁷ position of guanine bases, but not guanines involved in a G-quadruplex structure [Sen and Gilbert 1988; Balagurumoorthy and Brahmachari 1994] (see Figure 2.1A). The DNA backbone is randomly cleaved by piperidine at methylated guanines generating a ladder-like pattern of radiolabeled DNA fragments when analyzed on a denaturing gel [Maxam and Gilbert 1980]. Thus, guanines involved in a G-quadruplex structure remain unmethylated and no backbone cleavage occurs at those positions [Williamson,

Raghuraman et al. 1989]. The oligonucleotide *4xGGG²² is capable of forming a G-quadruplex in the presence of K⁺ since it contains four runs of three guanine bases. Therefore, the DMS assay was performed on *4xGGG²² at 25°C in extension buffer without KCl or with 75 mM KCl, and the resulting patterns of DNA fragments were compared. In the absence of KCl, bands corresponding to DNA fragments cleaved at each guanine base were generated, indicating all guanine bases were methylated and no G-quadruplex structure was formed under these conditions (Figure 2.3B, lane 1). Conversely, these bands were dramatically reduced in the presence of K⁺ (lane 2), clearly indicating a loss of DMS methylation at these guanines and suggesting telomeric sequence containing four G runs forms a G-quadruplex structure in the presence of 75 mM KCl, a concentration even lower than the physiological K⁺ concentration (140-150 mM) [Thier 1986]. Although this sequence has the potential to form an intramolecular G-quadruplex, it is notable that this assay cannot differentiate between inter- and intramolecular G-quadruplexes. Analysis by circular dichroism (CD) revealed this oligonucleotide forms an intramolecular G-quadruplex in 100 mM KCl (Figure 5.6C) (also see Chapter 5 for more details).

In addition to the DMS protection assay, other methods to examine potential G-quadruplex formation were also used. DNA structure analysis using native PAGE allows differentiation of intra- and intermolecular G-quadruplexes. Intramolecular G-quadruplexes materialize from interaction of a single molecule, generating a more compact structure that migrates faster in a native polyacrylamide gel than single-stranded DNA [Henderson, Hardin et al. 1987;

Williamson, Raghuraman et al. 1989]. Intermolecular G-quadruplexes also form a compact structure, but are composed of two or more strands and thus migrate at a slower rate compared to single-stranded DNA [Sen and Gilbert 1988; Sundquist and Klug 1989]. Therefore, to determine the nature of the G-quadruplex I was working with, the migration of several primer/template substrates was analyzed on native PAGE using differing monovalent cation buffer conditions in both the sample and electrophoresis buffers. I used buffers containing KCl, which promotes and stabilizes G-quadruplexes, or LiCl, which favors unstructured DNA (Figure 2.3A) [Williamson, Raghuraman et al. 1989]. Although the duplex regions of all primer-template substrates were identical in length and sequence, the single-stranded template region of the test substrate 4xGGG/*P31 contains four runs of guanines (as for *4xGGG²²) and maintains the potential to form an intra- or intermolecular G-quadruplex in buffers containing K⁺ (Figure 2.3A). Conversely, the substrate 3xCCC/*P31 entirely lacks guanines within the single-stranded template, ruling out the formation of any type of G-quadruplex, and also lacks self-complementarity, excluding development of other Watson-Crick secondary structures. Another comparative control, the 3xGGG/*P31 substrate, contains three guanine runs in the single-stranded template; this design eliminates the possibility of an intramolecular G-quadruplex, although the multiple template strands could potentially associate to form an intermolecular G-quadruplex. Therefore, primer-template substrates were incubated and electrophoresed by native PAGE in buffers containing either 75 mM KCl or LiCl to observe changes in electrophoretic mobility that would indicate formation of a G-quadruplex (Figure 2.3C). The relative migration

positions of both partial duplex control substrates, 3xCCC/*P31 (lanes 3, 7) and 3xGGG/*P31 (lanes 4, 8), were essentially identical to one another and unchanged in KCl versus LiCl. The substrate 4xGGG/*P31 migrated to a similar position as the control substrates in the presence of LiCl (lane 6), strongly indicating the template exists in single-stranded form under these conditions. However, in KCl, the 4xGGG/*P31 substrate migrated at a faster rate than either of the control substrates (compare lanes 2-4), suggesting that its single-stranded template region, which is actually 4 nt longer than either control template, forms a compact structure. The faster migration of the 4xGGG/*P31 substrate specifically in KCl, along with use of low DNA concentrations that disfavor intermolecular interactions [Williamson, Raghuraman et al. 1989], strongly suggests that the sequence forming the template strand folds into an intramolecular G-quadruplex. These results also suggest the G-quadruplex detected in Figure 2.3B likely existed in a unimolecular form.

To further examine the secondary structure of the 4xGGG/*P31 template, which is capable of forming an intramolecular G-quadruplex, polymerase extension of the template sequence was examined. Using a range of human pol η concentrations, I performed the primer extension assay at 37°C on the control substrate 3xGGG/*P31 or 4xGGG/*P31 in 75 mM KCl or LiCl (Figure 2.3D). Extension of the labeled primer strand (31 nt) by human pol η was examined by denaturing PAGE. In KCl (lanes 2-4), human pol η fully extended (52 nt) the control template 3xGGG/*P31 (lanes 2-4), a result that is indicative of an unstructured, single-stranded template. In LiCl, the control template,

3xGGG/*P31, was only partially extended (31-51 nt) at lower human pol η concentrations (lanes 5-6), but full extension (52 nt) was observed at greater polymerase concentrations (lanes 7-8). However, considering LiCl disfavors G-quadruplex formation, incomplete extension of the control template was likely a result of reduced polymerase activity in LiCl rather than polymerase blockage. In a similar manner to the control template, 4xGGG/*P31 was extended to completion (56 nt) in LiCl at the greatest human pol η concentration (lane 16), while production of partial extension products (32-55) correlated with reduced polymerase activity (lanes 13-15). However, the extension pattern was drastically different in KCl, conditions that favor G-quadruplex formation (lanes 10-12). Specifically, the most prominent bands observed are 34 and 35 nt in length, corresponding to extension of the primer by 3 and 4 nt, respectively, up to the first GGG run that would be involved in a presumed intramolecular G-quadruplex structure. Notably, some full extension (56 nt) was observed especially with increasing polymerase concentrations. Taken together with previous DMS and native PAGE analyses (Figure 2.3B-C), these results further confirm that the single-stranded region of the template strand of 4xGGG/*P31 folds into an intramolecular G-quadruplex in KCl, while the template of 3xGGG/*P31 that contains only three GGG runs, remains in single-stranded form under either buffer condition.

The presence of both truncated and fully extended products in primer extension assays performed on the 4xGGG/*P31 substrate with higher pol η concentrations at 37°C in 75 mM KCl (Fig. 2.3D, lanes 11 and 12) suggested

that its template region might exist in dynamic equilibrium between intramolecular G-quadruplex and unfolded states. To better understand formation and stability of these intramolecular G-quadruplexes before continuing these studies with DNA polymerases, I investigated the effects of two parameters known to affect G-quadruplex stability--i.e., temperature and monovalent cation (K^+) concentration [Lee, Okumus et al. 2005]. First, the effect of temperature (18°C vs. 37°C) on human pol η extension of the G-quadruplex-forming substrate, 4xGGG/*P31, was compared with the control substrate, 3xGGG/*P31 (Figure 2.4A). Human pol η completely extended 3xGGG/*P31 (52 nt) at 18°C (lanes 2-3) and 37°C (lanes 4-5), with temperature having little effect on polymerase activity. Assays with G-quadruplex forming 4xGGG/*P31 substrate (lanes 6-10) exhibited a markedly different pattern and a pronounced temperature effect. At 37°C , 4xGGG/*P31 was extended 1-4 nt (32-36 nt), indicating polymerase blockage at an intramolecular G-quadruplex (lanes 9-10). However, particularly at the greatest human pol η concentration, a large percentage (54%) of fully extended product (56 nt) was also generated (lane 10). At a G-quadruplex stabilizing temperature (18°C), a greater percentage of 4xGGG/*P31 indicated G-quadruplex blockage (32-35 nt) (lanes 7-8), and less full extension (56 nt) was observed (18%) (lane 8). These results strongly suggest that the template region of the 4xGGG/*P31 substrate is in dynamic equilibrium between its unfolded single-stranded state and an intramolecular G-quadruplex structure, with the latter being much more favored at 18°C compared to 37°C . With very little extension occurring at temperatures that favor G-

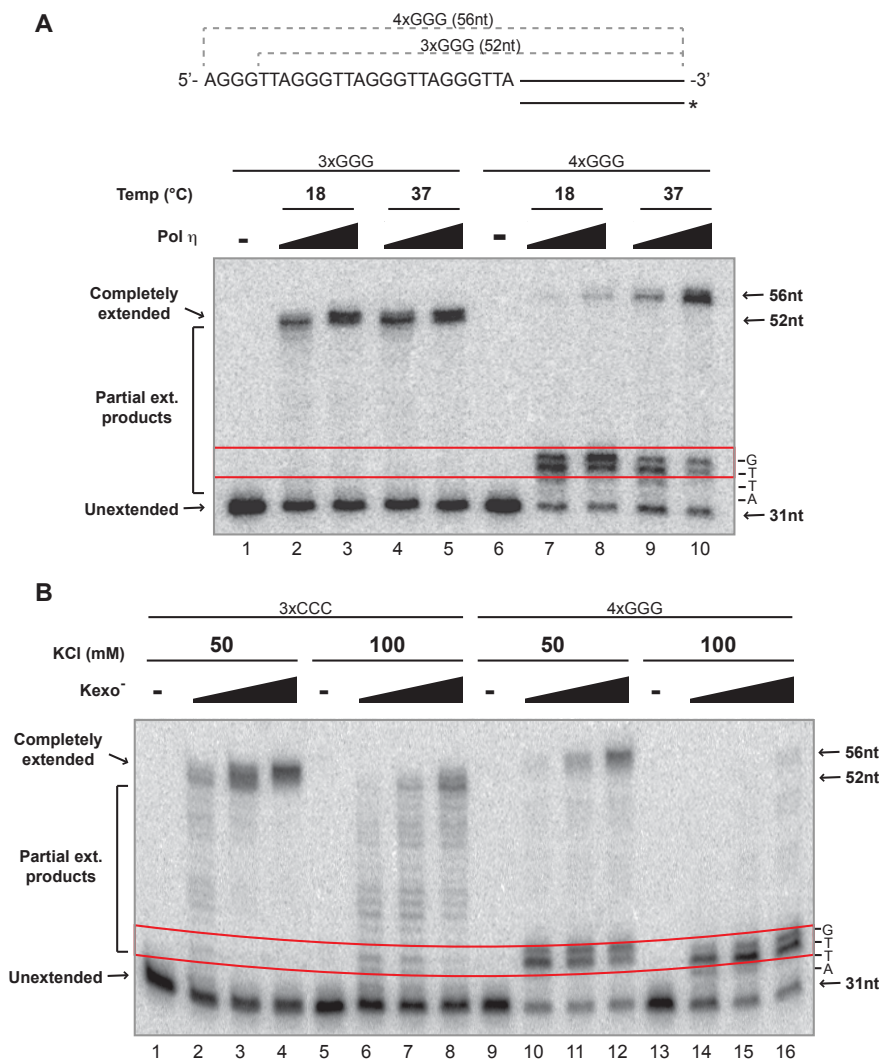


Figure 2.4 Effect of temperature and KCl concentration on G-quadruplex stability. **A)** To determine the effect of temperature on G-quadruplex stability, primer extension assays were performed at 18°C and 37°C. Human pol η (0.26-0.51 nM at 18°C or 0.10-0.26 nM at 37°C) was incubated with 3xGGG/*P31 or 4xGGG/*P31 (0.3 nM) each in extension buffer with 75 mM KCl for 5 min. **B)** To examine G-quadruplex stability in KCl, Kexo⁻ (2.5-25 U/L) was incubated with 3xCCC/*P31 or 4xGGG/*P31 (0.2 nM) each in extension buffer with and 50 or 100 mM KCl at 37°C for 5 min. For both panels, positions of partial extension products indicating polymerase blockage are highlighted (between red lines) and the first four nucleotides of the template and relevant product sizes are indicated at right.

quadruplex formation (18°C), these results indicate that polymerization by human pol η is essentially blocked at intramolecular G-quadruplexes.

To further examine G-quadruplex stability, polymerase extension at a range of K^+ concentrations was also studied. Similar to lower temperatures, greater KCl concentrations support stable G-quadruplex structure [Lee, Okumus et al. 2005]. To evaluate the effect of K^+ concentration on the template structure, extension of 4xGGG/*P31 and the unstructured substrate 3xCCC/*P31 was compared at 37°C in 50 mM or 100 mM KCl by Kexo⁻, a more processive polymerase than human pol η (Figure 2.4B). The control 3xCCC/*P31 primer was readily extended in 50 (lanes 2-4) and 100 mM KCl (lanes 6-8), with higher levels of fully extended products (52 nt) occurring as Kexo⁻ concentrations increased, although polymerase activity was somewhat reduced at the higher KCl concentration. In contrast, on the 4xGGG/*P31 substrate, there was evidence of G-quadruplex-mediated blockage of Kexo⁻ (across the range of enzyme concentrations) as well as a substantial effect of KCl concentration on this blockage (lanes 10-12, 14-16). In 50 mM KCl at the highest Kexo⁻ concentration, a large percentage (46%) of 4xGGG/*P31 was extended to completion (56 nt) although a substantial fraction (37%) of blocked products (34-35 nt) was observed (lane 12). However, at the same Kexo⁻ concentration in 100 mM NaCl, a much higher level (68%) of blockage was evident (lane 16). While the decrease in complete extension at greater KCl concentrations may, in part, result as a consequence of a reduced polymerase activity under these conditions, previously reported evidence regarding the

stability of G-quadruplexes in K^+ [Lee, Okumus et al. 2005] along with the primer extension results presented in Figure 2.4B support the view that intramolecular G-quadruplexes formed by 4xGGG/*P31 are more favored in 100 mM KCl compared to 50 mM KCl. Along with the evidence presented in Figure 2.4A, these results suggest the template region of 4xGGG/*P31 exists in a dynamic equilibrium between an unstructured single strand and an intramolecular G-quadruplex. Lower temperatures and greater KCl concentrations shift that equilibrium towards G-quadruplex formation and stability. Furthermore, the results presented here indicate not only human pol η , but also the more processive Kex ω^- , fully extend unstructured templates but strongly pause at an intramolecular G-quadruplex on the template strand.

Intramolecular G-quadruplex blockage not limited to human pol η .

Although the previous results with human pol η (and Kex ω^-) were significant, organisms possess a variety of DNA polymerases that may be capable of bypassing intramolecular G-quadruplexes. These include polymerases involved in processive synthesis of long DNA tracts (such as Kex ω^- , T4 DNA polymerase, and human pol δ) or more distributive DNA polymerases involved in bypass of damaged DNA or DNA repair (including pol η , pol κ , pol μ , and pol β) (Table 2.2). Therefore, in addition to human pol η , the effect of an intramolecular G-quadruplex in the template on extension by other polymerases was also investigated. Here, I used the G-quadruplex-forming 4xGGG/*P31 (template strand 56nt in length) as well as a new substrate, ext-4xGGG/*P31 (template strand 67nt in length), which is identical to 4xGGG/*P31 except for an 11 nt 5'

Table 2.2 Description of polymerases used.

Processive		Klenow exo ⁻	Fragment of <i>E. coli</i> DNA Pol I; DNA repair polymerase; lacks exo
		T4 DNA Polymerase	T4 phage replicative polymerase; possesses 3' to 5' exo activity
		Human Pol δ	Lagging strand replicative polymerase; 3' to 5' exo activity ^a
Distributive	Translesion	Human Pol η	Y-family translesion polymerase; responsible for bypass of CPDs ^a
		<i>S. cerevisiae</i> Pol η	Y-family translesion polymerase; responsible for bypass of CPDs ^b
		Human Pol κ	Acts at abasic sites; low fidelity ^a
		Human Pol μ	Located in peripheral lymphoid tissues; potential hypermutase ^a
	Other	Human Pol β	Gap filling polymerase; involved in base excision repair ^a

^a Reviewed in Hubscher, U., et al. (2002)

^b Johnson, R.E., et. al. (1999)

extension of random sequence on the template strand. Extension on the control 3xGGG/*P31 substrate compared to a G-quadruplex-forming substrate, either 4xGGG/*P31 or ext-4x-GGG/*P31, was examined using increasing polymerase concentrations in 75 mM KCl (Figure 2.5). The reaction temperature (25-37°C) and times (5-60 min) were varied (as indicated in Figure 2.5) to optimize extension for each polymerase. The reaction conditions (5-10 min at 37°C) were similar for all polymerases except human pol μ and human pol β . As expected from earlier experiments, Kexo⁻ extended the control template, 3xGGG/*P31, to completion (52 nt) in a manner related to enzyme concentration (lanes 7-8). In contrast, when ext-4xGGG/*P31 substrate was utilized, the major products observed (34-35 nt) suggested blockage of Kexo⁻ by the G-quadruplex, even though low amounts of longer and fully extended (67 nt) products were observed with their levels and lengths correlating to polymerase concentration (lanes 2-3). When the replicative T4 DNA polymerase was employed, I mainly observed full extension of the control primer but also some shorter (<31 nt) products reflecting degradation of the primer strand (lanes 13-14) by the established 3' to 5' exonuclease activity of T4 DNA polymerase [Doetsch, Chan et al. 1985]. However, with the G-quadruplex-forming substrate, 4xGGG/*P31, the primary products observed with T4 DNA polymerase were between 32-34 nt in length with minor amounts of fully extended (56 nt) products (lanes 10-11). Similar to T4 DNA polymerase, human pol δ , the main lagging strand replicative DNA polymerase [Burgers 2009], fully extended the control substrate (lanes 22-24) and generated primarily 32-34 nt products using the ext-4xGGG/*P31 substrate with some full extension (67 nt) occurring as polymerase concentrations

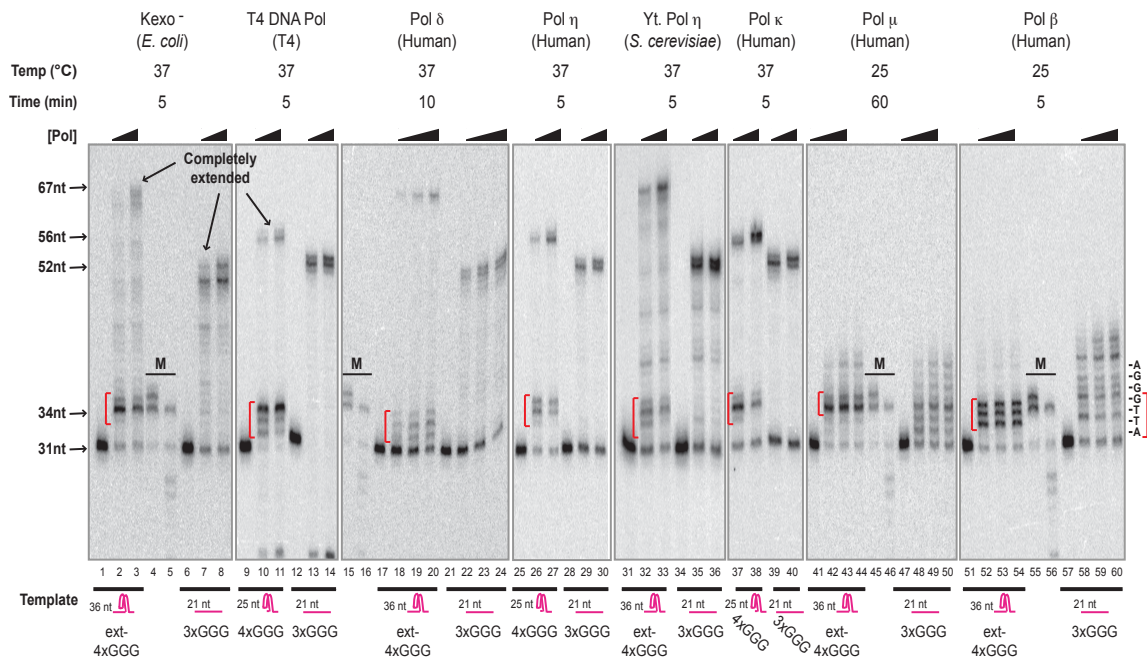


Figure 2.5 Replicative and translesion polymerases are blocked by an intramolecular G-quadruplex. In standard primer extension assays, control (3xGGG/*P31) or G-quadruplex-forming (4xGGG/*P31 or ext-4xGGG/*P31) (0.2-0.3 nM) was incubated with increasing concentrations of the following polymerases: Kexo⁻ (10-20 U/L), T4 polymerase (50-100 U/L), pol δ (3.4-17.1 nM), human pol η (0.10-0.26 nM), *S. cerevisiae* pol η (2.1-4.2 nM), pol κ (1.3-2.5 nM), pol μ (5.5-27.3 nM), or pol β (11.6-46.3 nM). Incubation temperature and time for each polymerase is indicated (top). Markers (M) generated by 4xGGG/*P31 extension using Kexo⁻ (lanes 4, 15, 45, and 55) or T4 polymerase (lanes 5, 16, 46, and 56) are denoted. Positions of partial extension products indicating polymerase blockage are highlighted (red brackets).

increased (lanes 18-20). Compared to the 34 and 35 nt products generated by Kexo- on the intramolecular G-quadruplex containing templates, the slightly shorter 32-34 nt products observed with both T4 DNA polymerase and human pol δ were likely the result of some degradation or “proofreading” by the 3’ to 5’ exonuclease activities inherent to these polymerases. Among the translesion polymerases tested, the human and yeast pol η enzymes were compared. As anticipated from earlier results, human pol η extended the control substrate to completion (52 nt) (lanes 29-30), but generated mainly 34 and 35 nt products as well as some completely extended products (56 nt) on the ext-4xGGG/*P31 substrate (lanes 26-27). Yeast pol η showed similarities and minor differences with its human counterpart, generating primarily fully extended products with 3xGGG/*P31 substrate (lanes 35-36) and prominent bands of 33-35 nt using ext-4xGGG/*P31 that reflect blockage of synthesis by the intramolecular G-quadruplex. In contrast to human pol η , yeast pol η generated higher levels of products reflecting polymerization past the point at which the putative intramolecular G-quadruplex forms including both fully (67 nt) and incompletely (between ~40-66 nt) extended products (lanes 32-33); notably, many of the incompletely extended products were also detectable in reactions performed with control 3xGGG/*P31 substrate, suggesting that these products were natural, sequence-specific pause sites and not related to G-quadruplex formation. Another translesion polymerase, human pol κ , showed extension patterns most similar to human pol η --i.e., it fully extended the control substrate (lanes 39-40) and a substantial fraction of the 4xGGG/*P31 substrate but was also frequently blocked (by G-quadruplex formation) on the latter, as evidenced

by the prominent 33 nt bands (lanes 37-38). The DNA synthesis characteristics of both pol μ and pol β (on both control and test substrates) were markedly different than the other polymerases tested, such that substantial changes to reaction conditions were necessary. Unlike the previous polymerases tested, pol μ (60 min at 25°C) only extended the control substrate between 1-8 nt (32-39 nt), with a major pause site at 34 nt (lanes 48-50). However, on the ext-4xGGG substrate, pol μ was primarily blocked after adding 3-4 nt (34-35 nt) (lanes 42-44). In a similar manner, pol β (5 min at 25°C) only extended the control substrate 1-11 nt (32-42 nt) (lanes 58-60) and the ext-4xGGG/*P31 2-4 nt (33-35 nt) (lanes 52-54).

In summarizing the results above, the activity of several DNA polymerases was examined under conditions (75 mM KCl) in which the template of the test substrate has been demonstrated (see Figures 2.3 and 2.4) to fold into an intramolecular G-quadruplex. Importantly, synthesis by all processive, translesion, and other distributive polymerases examined in this study was stalled precisely opposite the position corresponding to where an intramolecular G-quadruplex would be formed on the template strand of 4xGGG/*P31 and ext-4xGGG/*P31. Because of earlier results on the effects of temperature on the dynamics of these specific intramolecular G-quadruplexes and synthesis by human pol η (Fig. 2.4A, lanes 6-10), these results indicate that stable intramolecular G-quadruplexes in the template of these substrates completely block DNA synthesis by all polymerases tested here. Note the enzymes lacking exonuclease activity, including Kexo⁻, pol η , *S. cerevisiae* pol η , pol κ , pol μ , and

pol β , generate a 35 nt product corresponding to incorporation of nucleotide opposite the initial guanine base presumably involved in the intramolecular G-quadruplex. The lack of this product (as well as the prominence of 32-33 nt products) in reactions with T4 DNA polymerase and pol δ was probably due to the exonuclease activity associated with these enzymes. These results suggest a wide range of polymerases, including translesion polymerases that bypass bulky DNA lesions, are dramatically inhibited by an intramolecular G-quadruplex on the template strand.

Pol η may promote mutagenesis at G-quadruplexes. The previous results show the 4xGGG/*P31 and ext-4xGGG/*P31 templates forms an intramolecular G-quadruplex (in 75 mM KCl) that inhibits synthesis by human pol η (and other polymerases) (Figures 2.3-2.5). Although this single-stranded telomeric template consists of four runs of guanine bases that fold into the intramolecular G-quadruplex, the 3'-ATT-5' sequence adjacent to the primer/template junction is not involved in the secondary structure (Figure 2.6A, top panel). Under conditions that favor G-quadruplex formation and include all dNTPs, products up to 34 nt in length are likely generated from proper adenine and thymine incorporation opposite these initial three bases. As mentioned above, the 35 nt product reflects addition of an extra nucleotide, putatively opposite the initial guanine within the first GGG run involved in the G-quadruplex structure. Due to the potential for polymerase misincorporation and subsequent mutagenesis, the fidelity of human pol η incorporation upon encountering an intramolecular G-quadruplex was assessed, initially by limiting the nucleotide availability (Figure

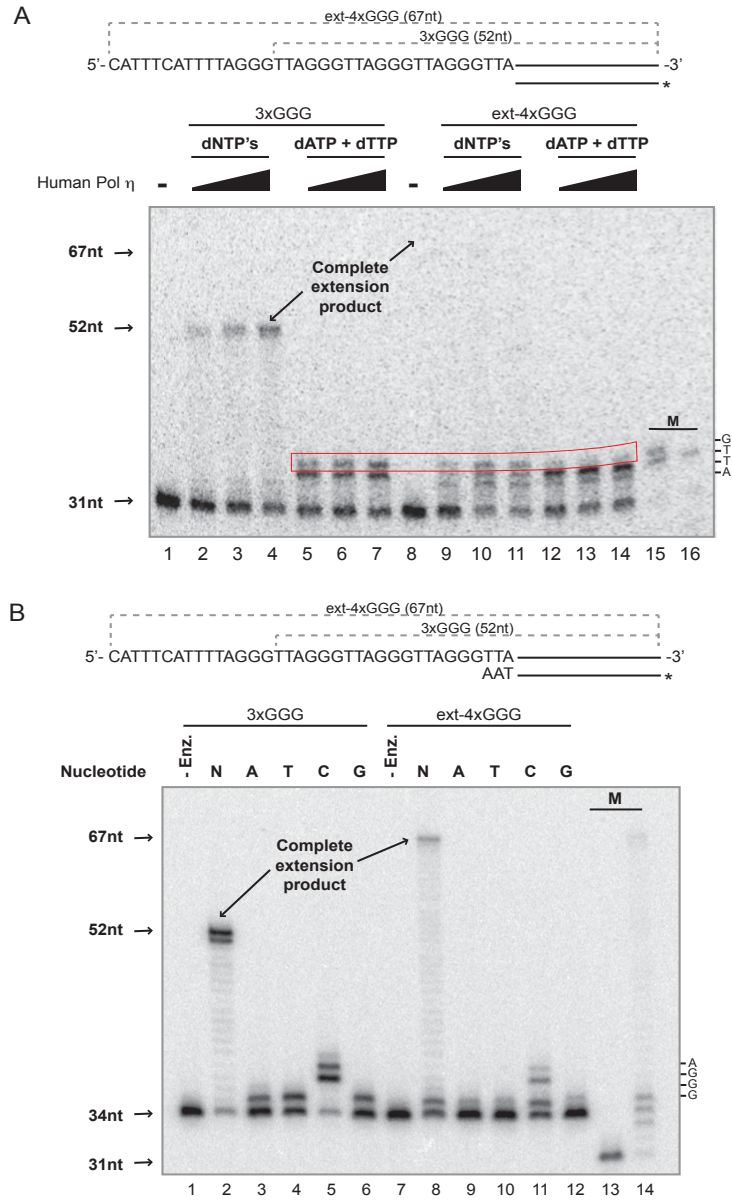


Figure 2.6 Human pol η is capable of misincorporation upon encountering an intramolecular G-quadruplex. **A)** Primer extension was performed on 3xGGG/*P31 or ext-4xGGG/*P31 (0.4 nM) each using human pol η (0.51-2.1 nM) in extension buffer containing 75 mM KCl with dNTPs or dATP + dTTP (100 μM each) at 18°C for 5 min. The red box highlights products generated by incorporation related to the first guanine in the 3XGGG and 4XGGG template strands. Markers (M) were generated as described in Figure 2.5. **B)** In the presence of all dNTPs or individual nucleotides (100 μM) each, primer extension was performed on 3xGGG/*P34 or ext-4xGGG/*P34 (0.4 nM) using human pol η (1.03 nM) in extension buffer with 75 mM KCl at 18°C for 5 min. Markers (M) were generated as described in Figure 2.5.

2.6A). For the substrates 3xGGG/*P31 and ext-4xGGG/*P31, only dATP and dTTP are required to extend the primer strand up to the initial run of guanines (34 nt). Therefore, for the experimental design, 3xGGG/*P31 and ext-4xGGG/*P31 substrates were incubated with increasing concentrations of human pol η in the presence of all dNTP's or dATP + dTTP only; importantly, these reactions were performed at 18°C (and in 75 mM KCl) to further promote formation and stabilization of G-quadruplexes. As expected, the control substrate, 3xGGG/*P31, was extended to completion (52 nt) (lanes 2-4) in the presence of all nucleotides, similar to Figure 2.3-2.4. Also consistent with previous results, in the presence of all dNTPs, ext-4xGGG/*P31 was extended by 3 nt (34 nt product) up to the intramolecular G-quadruplex with some incorporation of an additional nucleotide (lanes 9-11). However, in the presence of only dATP and dTTP, incorporation of 3 nt was observed on the control (unfolded) substrate to generate a 34 nt product and significant levels of 35 nt product (lanes 5-7), reflecting misincorporation of either dATP or dTTP opposite the first guanine base. Importantly, in reactions with 4xGGG/*P31 and only dATP and dTTP, the primary products were 34 nt or less with detectable but low amounts of 35 nt product (lanes 12-14). The amount of incorporation opposite the first run of guanine bases was substantially reduced when an intramolecular G-quadruplex was present in the template compared to an unstructured template. Therefore, these results suggest that human pol η may misincorporate opposite an intramolecular G-quadruplex, but not to the same frequency that it misincorporates opposite undamaged and unstructured templates.

To more closely examine incorporation when an intramolecular G-quadruplex is present in the template, substrates with the same template strand but using a primer strand that is three nucleotides longer (34 nt total length) were generated. This longer primer strand ends just before the first guanine in the template strands of the control 3xGGG/*P34 substrate and the intramolecular G-quadruplex-forming ext-4xGGG/*P34 substrate (Figure 2.6B, top). To determine which nucleotide is preferentially incorporated opposite the first guanine base, I studied primer extension at 18°C in 75 mM KCl by human pol η using all dNTPs or dATP, dTTP, dCTP, or dGTP individually (Figure 2.6). On the control substrate 3xGGG/*P34 with the unfolded template strand, human pol η fully extends nearly all (88%) of the primer strand in the presence of all dNTPs (lane 2), similar to earlier results using the 3xGGG/*P31 substrate. Consistent with the previously reported low fidelity of pol η on undamaged templates [Johnson, Washington et al. 2000], I observed misincorporation opposite guanine when only dATP, dTTP, or dGTP was supplied. The control substrate, 3xGGG/*P31, was extended one nucleotide (35 nt) in the presence of only dATP (31%, lane 3), dTTP (44%, lane 4), or dGTP (34%, lane 6). Conversely, dCTP is correctly incorporated opposite the first three guanines forming a 37 nt product with some further extension to form a 38 nt and even detectable levels of 39 nt products (lane 5). On the G-quadruplex forming ext-4xGGG/*P34 substrate, human pol η in the presence of all dNTPs generated products reflecting unblocked extension (40%) (36-67 nt) and those from addition of only one nucleotide (25%), although a large fraction (35%) of the

substrate was not extended at all (lane 8). With only dATP available, a small percentage of ext-4xGGG/*P34 was extended one nucleotide (17%) (35 nt) (lane 9). Likewise, an almost identical percentage of the substrate was extended one nucleotide (34 nt) in the presence of dTTP (16%) (lane 10) or dGTP alone (15%) (lane 12). However, a more complicated pattern was observed on ext-4xGGG/*P34 in the presence of dCTP alone. Extension under these conditions occurred with greater frequency, and produced substantial levels of products reflecting incorporation of only one nucleotide (35 nt, 31%) or three or more nucleotides (36-38 nt, 30%) (lane 11). The longer products (37-38 nt) were attributed to correct incorporation of three cytosines opposite the initial GGG run (plus some misincorporation of dCTP opposite adenine at the fourth position) in templates in an unfolded state before or during the course of the reaction. On the other hand, generation of the 35 nt product is more challenging to interpret. However, its prominence and the lack of a 36 nt band suggests that the 35 nt product results from incorporation of a single dCTP when the intramolecular G quadruplex is present in the template; the frequency of this event (31%) compared to incorporation of other nucleotides (15-17%) also suggests some preference for incorporation of dCTP by pol η upon encountering an intramolecular G-quadruplex in the template. Additionally, I did not observe any prominent products in the 40-50 nt range that might be generated by “skipping” over the G-quadruplex (21 nt folded into a compact structure) followed by extension of the remaining sequence (11 nt) (lane 8). Similarly, *S. cerevisiae* pol η , human pol μ , and human pol β all preferentially incorporated cytosine at an intramolecular G-quadruplex, while low levels of misincorporation of A, T, or

G was observed on unstructured as well as G-quadruplex-forming templates. However, human pol κ incorporated little dCTP opposite the initial guanine, but some incorporation producing a 37 nt product was observed, potentially opposite unstructured templates. Little misincorporation occurred opposite an intramolecular G-quadruplex, although human pol κ readily misincorporated A, T, and G opposite the first guanine of the control template (data not shown). Therefore, these results indicated human pol η , as well as *S. cerevisiae* pol η , pol μ , and pol β , preferentially incorporated cytosine upon encountering an intramolecular G-quadruplex.

Although human pol η misincorporation at an intramolecular G-quadruplex occurs at a low frequency, any misincorporation followed by continued extension by a polymerase may lead to mutagenesis. Therefore, to determine if pol η could promote mutagenesis at G-quadruplexes, a protocol was developed (Figure 2.7A) to determine if human pol η could extend from a nucleotide misincorporated due to encountering an intramolecular G-quadruplex in the template. In step 1, misincorporation of a single nucleotide opposite a stable intramolecular G-quadruplex was promoted by incubation of 4xGGG/*P34 (or as control, the unfolded 3xGGG/*P34 substrate) with dATP, dTTP, and dGTP and human pol η at 18°C, a temperature that stabilizes G-quadruplexes but still permits synthesis by pol η . Then, in step 2, further extension was encouraged by simultaneously introducing dCTP and increasing the temperature to 37°C to destabilize the G-quadruplex to some extent (Figure 2.7A). As a separate control, each step was performed in the presence of all dNTPs. A small amount

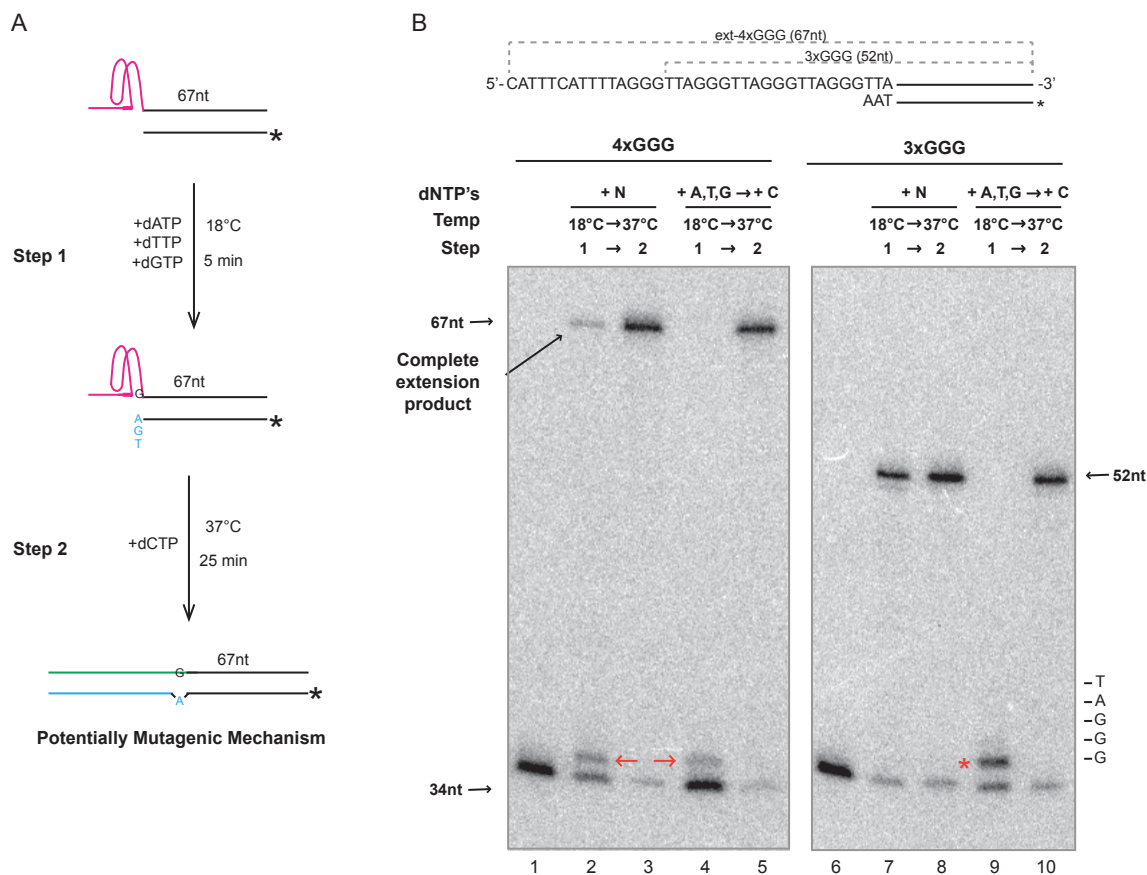


Figure 2.7 Human pol η extends from a misincorporated nucleotide. A) Protocol for determining ability of human pol η to promote mutagenesis when encountering an intramolecular G-quadruplex. **B)** A primer extension assay was performed in two steps. Initially, 4xGGG/*P34 or 3xGGG/*P34 (0.4 nM) was incubated with human pol η (1.03 nM) with all dNTPs (N) or dATP (A), dTTP (T), and dGTP (G) (100 μ M each) at 18°C for 5 min. Upon completion of step 1, the reaction was supplemented with dCTP (100 μ M) and incubated at 37°C for 25 min. Aliquots (4 μ L) of the reaction were removed immediately after completion of each step for analysis by denaturing PAGE. The red arrows highlight products generated by incorporation by human pol η upon encountering the intramolecular G-quadruplex. The red asterisk (*) highlights products generated opposite the first guanine on an unstructured template.

of these reactions was removed following each step for analysis of extension of the primer strand by denaturing PAGE (Figure 2.7B). As expected, the primer strand of the unfolded 3xGGG/*P34 substrate was fully extended (52 nt) in the presence of all dNTPs following step 1 with essentially no change occurring during step 2 (Figure 2.7B, lanes 7-8). When no dCTP is present during step 1, most of the primer strand is extended by only 1 nt (35 nt) (lane 9), a misincorporated nucleotide, with full extension occurring when dCTP is added in step 2 (lane 10). Therefore, on a normal template human pol η can both misincorporate and extend from the 3' mismatch, as previously reported [Washington, Johnson et al. 2001]. Rather than complete extension as observed with the control substrate (lane 7), in all dNTPs, the G-quadruplex forming ext-4xGGG/*P34 is extended only one nucleotide (35 nt) following step 1 (G-quadruplex stabilizing conditions) (lane 2). However, full extension (67 nt) of this product and the remaining substrate is achieved following heating and destabilization of the G-quadruplex in step 2 (lane 3). Limiting the available nucleotides to dATP, dTTP, and dGTP leads to a 35 nt product, indicating some misincorporation by pol η when the intramolecular G-quadruplex is present in the template (Fig. 2.7B, lane 4), as previously demonstrated (Figure 2.6B, lanes 9, 10, and 12). Following heat destabilization of the G-quadruplex along with introduction of dCTP (step 2), I observed disappearance of both this product and the remainder of the original substrate concomitant with appearance of fully extended (67 nt) product (lane 5). Thus, human pol η fully extends not only the original unextended substrate but also those singly misincorporated products that form 3' mismatches with template. Although human pol η possesses a low

rate of misincorporation at intramolecular G-quadruplexes, these results suggest pol η may promote mutagenesis on templates that form intramolecular G-quadruplexes as well as on normal, undamaged templates.

DISCUSSION

Numerous G-rich regions of the genome, including long stretches of the telomeric repeat sequence TTAGGG found at both ends of each human chromosome, have the potential to form G-quadruplex structures [Huppert and Balasubramanian 2005]. Single-stranded G-rich regions on telomeric 3' overhangs or exposed during DNA replication (particularly lagging strand replication) can assemble into these structures, with intramolecular G-quadruplex formation presumably being favored in these situations [Tang, Kan et al. 2008; Lipps and Rhodes 2009]. Importantly, G-rich telomeric repeat sequences are specifically subject to lagging strand replication, likely increasing the propensity for formation of these compact but bulky secondary structures that may impact DNA polymerase function and/or fidelity. Here, telomeric substrates with the potential to form G-quadruplex structures were designed, and their effects were examined on DNA synthesis *in vitro* using various DNA polymerases. The template strand of model primer-template substrate possessing four guanine runs was confirmed to form an intramolecular G-quadruplex, and I determined conditions that favor greater G-quadruplex stability. A range of polymerases, including those classified as processive (Kexo⁺, T4 polymerase, and pol δ) and distributive (*S. cerevisiae* pol η , human

pol η , pol κ , pol μ and pol β), were blocked by an intramolecular G-quadruplex on the template strand. Further analysis of human pol η , as well as *S. cerevisiae* pol η , human pol κ , human pol β , and human pol μ , revealed the potential for misincorporation and mutagenesis at intramolecular G-quadruplexes, although cytosine was preferred in most cases.

Telomeres resemble fragile sites indicating frequent replication stress [Sfeir, Kosiyatrakul et al. 2009]. One source of replication stress within this G-rich sequence may result from G-quadruplex formation. To assess the affect telomeric G-quadruplexes have on DNA synthesis, primer/template substrates with single-stranded templates were designed to contain human telomeric repeats including 3 or 4 GGG runs; only those with 4 GGG runs are capable of forming intramolecular G-quadruplexes. A DMS protection assay indicated that a 22 nt telomeric sequence (4xGGG²²) containing 4 GGG runs forms a G-quadruplex in 75 mM KCl. Native gel analysis indicated that a (longer) primer-template substrate containing 4 GGG runs (4xGGG/*P31) migrated faster than (shorter) primer-template substrates (3xGGG/*P31 and 3xCCC/*P31, containing 3 GGG and 3 CCC runs, respectively) in the presence of KCl; in contrast, the migration of these three substrates in LiCl was essentially identical. Since KCl favors G-quadruplex formation while LiCl favors unstructured DNA, these results indicate that G-quadruplexes formed from telomeric single-stranded regions containing 4 GGG runs were unimolecular in nature. Furthermore, synthesis by human pol η on 4xGGG/*P31 was largely blocked in KCl but not in LiCl, again suggesting that the single-stranded template region folds into an intramolecular

G-quadruplex in the presence of KCl. These results also indicate that a dynamic equilibrium exists between unfolded DNA and this intramolecular G-quadruplex structure, with certain conditions (higher K^+ concentrations and lower temperatures) favoring G-quadruplex formation and stability, in accord with previous findings [Lee, Okumus et al. 2005]. When primer extension assays are performed with 4xGGG/*P31 under more favorable conditions for G-quadruplex formation (100 mM KCl or 18°C), full length extension products are reduced while polymerase stalling opposite the point of G-quadruplex formation is increased, suggesting that DNA synthesis is completely blocked upon encountering stable intramolecular G-quadruplexes in the template.

Human cells possess many DNA polymerases, including not only polymerases used in DNA replication and repair but also translesion polymerases capable of bypassing large, bulky DNA lesions. Using primer extension assays, I found a wide variety of DNA polymerases are blocked by an intramolecular G-quadruplex on the template strand. The processive polymerases Kex ω ⁻, T4 polymerase, and human pol δ , which are primarily involved in synthesizing undamaged templates, were all blocked while extending the G-quadruplex forming substrates (4xGGG/*P31 or ext-4xGGG/*P31). However, intramolecular G-quadruplexes might be somewhat comparable to sites of bulky DNA damage that frequently inhibit processive polymerases. Some replication-inhibiting DNA lesions can be bypassed by damage-specific, distributive translesion polymerases that are widely thought to be implemented subsequent to replication blockage. However, none of the translesion

polymerases included in this study (*S. cerevisiae* pol η , human pol η , human pol κ , and human pol μ) was able to extend through or even skip over the intramolecular G-quadruplex. Human pol β , a distributive polymerase involved in base excision repair, was also blocked by an intramolecular G-quadruplex. Although human pol η and human pol κ have previously been reported to aid in replication through G-quadruplexes [Betous, Rey et al. 2009], the results presented here suggest these polymerases may not directly act to bypass the G-quadruplex structure. Since replicative, repair, and bypass polymerases were examined in this study, DNA polymerases are unlikely, without aid from other proteins, to replicate through or bypass intramolecular G-quadruplexes. Thus, the ability of G-quadruplexes to block both replicative and translesion DNA polymerase may further exacerbate replication difficulties and result in replication collapse and double-strand break formation. Indeed, telomeres are fragile in response to replication stress [Sfeir, Kosiyatrakul et al. 2009]. Discontinuous lagging strand synthesis generates regions of single-stranded DNA, increasing the potential for intramolecular G-quadruplex formation when this strand is guanine-rich, as is always the case for replication through telomeric DNA. Upon encountering a G-quadruplex on the lagging strand, these results indicate human pol δ , the primary polymerase for lagging strand synthesis, would be blocked resulting in incomplete synthesis of the Okazaki fragment. These results also suggest that recruitment of translesion polymerases to these sites would be ineffective for bypassing G-quadruplexes. Although downstream leading and lagging strand synthesis likely continues, polymerase blockage by

G-quadruplexes could generate persistent single-strand gaps eventually leading to double-strand breaks, a hallmark of DNA fragility.

Although these results indicate that an intramolecular G-quadruplex presents a strong if not complete barrier to passage by most polymerases, a DNA polymerase may misincorporate a nucleotide upon encountering these secondary structures, generating a potential for mutagenesis. Analysis of these range of polymerases revealed those lacking 3' to 5' exonuclease activity, including Kex^o-, human pol η , *S. cerevisiae* pol η , pol κ , pol μ , and pol β inserted an additional nucleotide corresponding to the first guanine run involved in the G-quadruplex structure. Primer extension assays were carried out in the presence of limited or individual nucleotides to examine possible misincorporation by polymerases upon encountering an intramolecular G-quadruplex in the template. Human pol η (as well as yeast pol η , human pol μ and human pol β) favored incorporation of cytosine at a position corresponding to initial guanine involved in the G-quadruplex in the template, although significant but lower levels of misincorporation of adenine, thymine, or guanine were observed. This was somewhat surprising, but may suggest that the 3'-most guanine in this intramolecular G-quadruplex is partially accessible to be "read" by these polymerases. Further extension of the primer appears completely blocked by stable G-quadruplex structures, although dynamic unfolding of these structures would permit resumption of synthesis. Even though misincorporation might occur at a low frequency upon encountering an intramolecular G-quadruplex, subsequent dissociation of a G-quadruplex along with continued extension from

the 3' mismatch would result in mutagenesis. Such a mutagenic process was modeled using a two-step protocol (Fig. 2.7). Indeed, the results indicated that adenine, thymine, or guanine misincorporated upon encountering an intramolecular G-quadruplex (stabilized at 18°C) was subject to further extension upon raising the temperature (to 37°C), which destabilizes the G-quadruplex. At physiological temperatures, intramolecular G-quadruplexes likely exist in a dynamic equilibrium with unstructured single-stranded DNA [Lee, Okumus et al. 2005]. Thus, this two-step protocol mimics misincorporation at an intramolecular G-quadruplex followed by a dynamic shift to an unstructured template. Taken together, these results suggest that, upon encountering an intramolecular G-quadruplex, misincorporation by pol η or another translesion polymerase may occur. Subsequent template unfolding, occurring either spontaneously or enzymatically, would generate a mismatch that is subject to further extension, thus promoting mutagenesis within G-quadruplex-forming sequences.

Although not every DNA polymerase found in humans was examined in this study, the wide range of polymerases tested, including translesion polymerases that bypass bulky single-nucleotide lesions, suggested polymerases alone could not appropriately deal with intramolecular G-quadruplexes during replication. Since the inability to properly deal with these structures might result in rampant genomic and telomeric instability, another pathway may exist within human cells to resolve these potentially problematic structures. A number of helicases have been shown to disrupt G-quadruplexes, including Pif1 [Ribeyre, Lopes et al. 2009] and Sgs1 [Sun, Bennett et al. 1999] in

S. cerevisiae and FANCI [London, Barber et al. 2008; Wu, Shin-ya et al. 2008], BLM [Sun, Karow et al. 1998], and WRN [Fry and Loeb 1999; Mohaghegh, Karow et al. 2001] in humans. Importantly, the human diseases resulting from deficiency of FANCI, BLM, and WRN (Fanconi anemia, BS, and WS respectively) all exhibit genomic instability [Wu and Brosh 2010]. Additionally, RPA [Salas, Petruseva et al. 2006] and POT1 (with telomeric sequences) [Zaug, Podell et al. 2005] have been shown to disrupt these structures, although not enzymatically. Disruption of these structures during replication (particularly of the lagging strand) by one or more of these factors would permit unperturbed DNA synthesis and diminish their capacity to induce genetic change.

Although several other enzymes have been implicated in unwinding G-quadruplexes, evidence exists supporting a role for WRN in promoting replication through G-quadruplexes. *In vitro* biochemical studies showed that WRN interacts with pol δ and its helicase activity facilitates synthesis by pol δ through a bimolecular G-quadruplex-forming template [Kamath-Loeb, Loeb et al. 2001]. Pol δ is the main polymerase involved in lagging strand synthesis [Nick McElhinny, Gordenin et al. 2008], an important aspect to consider due to the inherent capability of the guanine-rich telomeric lagging strand to form G-quadruplexes. WRN-deficient cells exhibit chromosomal and telomere instability [Goto, Miller et al. 1996; Pirzio, Pichierri et al. 2008], suggesting WRN plays a role in telomere maintenance. In fact, WRN has been implicated in promoting proper synthesis of the G-rich lagging telomeric strand [Crabbe, Verdun et al. 2004]. By resolving intramolecular G-quadruplexes that block lagging strand

synthesis of telomeres, WRN may act to promote telomere replication and stability. Without proper G-quadruplex resolution in the absence of WRN, these secondary structures persist and create more extensive replication difficulties (as alluded to above), thus generating telomere fragility, double strand breaks, and subsequent stochastic telomere loss. Therefore, WRN may play a major role in promoting efficient replication of telomeres (and perhaps other G-rich sequences) by actively resolving intramolecular G-quadruplex structures that form in single-stranded regions of the G-rich lagging strand.

CHAPTER 3

FIDELITY OF WRN-MEDIATED REGRESSION OF MODEL REPLICATION FORKS WITH REPEATING SEQUENCES

INTRODUCTION

One of the many proposed roles of WRN, as well as other RecQ helicases, is acting at blocked replication forks caused by bulky DNA lesions or stalled replication forks resulting from hydroxyurea, topoisomerase inhibitors, and interstrand crosslinking agents to which WRN-deficient cells are sensitive [Lebel and Leder 1998; Pichierri, Franchitto et al. 2001; Poot, Yom et al. 2001]. Following depletion of nucleotide pools by hydroxyurea, WRN becomes phosphorylated by ATR [Pichierri, Rosselli et al. 2003] and subsequently translocates to nuclear foci corresponding to sites of stalled replication [Constantinou, Tarsounas et al. 2000]. However, even in the absence of exogenous DNA damaging agents, asymmetric replication fork progression is observed in WS primary fibroblasts [Rodriguez-Lopez, Jackson et al. 2002]. Together, along with greater chromosomal instability associated with WRN deficiency [Goto, Miller et al. 1996], these observations indicate WRN plays a role in the resolution of stalled or blocked replication forks, and the absence of WRN may lead to initiation of error-prone and/or illegitimate recombination leading to chromosomal abnormalities.

Compared to random, non-repeating regions of the genome, repetitive sequences are inherently more difficult to replicate and exhibit greater instability. “Strand slippage” at repeating sequences during replication leads to insertions and deletions [Streisinger, Okada et al. 1966; Kunkel 1986]. Additionally, homologous recombination between chromatids/chromosomes of large regions of repeating sequences may result in incorrect frame pairing. One such repetitive sequence, telomeres are the protective structures found at the ends of all linear chromosomes. Telomeres have recently been identified as fragile sites induced by replication stress [Sfeir, Kosiyatrakul et al. 2009], with WRN loss exacerbating fragile site instability [Pirzio, Pichierri et al. 2008]. Therefore, telomeric instability found within WRN-deficient cells may stem from replication stress along with the innate instability at telomeres.

Recently, our lab determined WRN performs regression of a model replication fork [Machwe, Xiao et al. 2006]. Regression involves coordination of WRN’s helicase and annealing activities, while the exonuclease activity acts to degrade the leading daughter strand in a limited manner that optimizes regression efficiency [Machwe, Xiao et al. 2007]. Due to this *in vitro* activity, WRN may limit genomic instability by regressing stalled or blocked replication forks, which would allow subsequent repair of the damage and continued replication. These previous studies identified regression activity using model replication forks containing random sequence; however, repeating sequences such as telomeric sequences may become misaligned during regression. “Looping out” of repeats during fork regression may lead to a loss of sequence.

Since WRN has been implicated as a telomere stabilizing protein, I examined the alignment of daughter duplexes following WRN-mediated regression of two different model replication forks containing either telomeric or dinucleotide repeats within the parental-daughter arms.

METHODS

Enzymes. The point mutation of WRN-E84A eliminates the 3' to 5' exonuclease activity [Huang, Li et al. 1998] while maintaining the helicase and annealing activities of WRN [Machwe, Xiao et al. 2005; Machwe, Lozada et al. 2006]. WRN-E84A was overexpressed in insect cells and purified as described in [Orren, Brosh et al. 1999] except with inclusion of 0.1% Nonidet P40 in all liquid chromatography buffers. Robert Lloyd (University of Nottingham) provided RecG, which was purified according to Mahdi et al. [Mahdi, Briggs et al. 2003]. T4 polynucleotide kinase, Klenow fragment (3' to 5' exo^- , referred to hereafter as Kexo $^-$), as well as all restriction enzymes were purchased from New England Biolabs (Ipswich, MA).

DNA substrates. All PAGE-purified oligonucleotides used for these experiments were purchased from Integrated DNA Technologies, Inc (Coralville, IA) (Table 3.1). As specified, “daughter” strand oligonucleotides (LagD50telo, LeadD38telo, LagD50AC, LeadD38AC, LagD54AC, and LeadD42AC) were 5' radiolabeled using ^{32}P - γ -ATP and T4 polynucleotide kinase, and unincorporated ATP was removed using Mini Quick Spin Oligo Columns (Roche, Indianapolis,

Table 3.1 Oligos used to construct model replication forks and daughter duplexes

LagD50telo

5'-CCCTAACCTAACCTAACCCAGTCTTCAGATGGCTTCAGAAGCTTGAGG-3'

LeadD38telo

5'-CCTCAAGCTTCTGAAGCCATCTGAAGACTGGGTTAGGG-3'

LeadP88telo

5'-GCTGTACGACTGATACTGTGACAAGTTCTGTGCGCTGAAGAATACCCTAACCCTAACCCAGTCTTCAGATGGCTTCAGAAGCTTGAGG-3'

LagP88telo

5'-CCTCAAGCTTCTGAAGCCATCTGAAGACTGGGTTAGGGTTAGGGTTAGGGTCAGCGCACAGAACTTGTCACAGTATCAGTCGTACAGC-3'

LagD50AC

5'-ACACACACACACACACACATGCCCAGTTCTTCAGTCGGAAGCTTGAGG-3'

LeadD38AC

5'-CCTCAAGCTTCCGACTGAAGAACTGGGCATGTGTGTGT-3'

LagP88AC

5'-CCTCAAGCTTCCGACTGAAGAACTGGGCATGTGTGTGTGTGTGTGTGTTCAGCGCACAGAACTTGTCACAGTATCAGTCGTACAGC-3'

LeadP88AC

5'-GCTGTACGACTGATACTGTGACAAGTTCTGTGCGCTGATGTGTCACACACACACACATGCCCAGTTCTTCAGTCGGAAGCTTGAGG-3'

LeadD42AC

5'-CCTCAAGCTTCCGACTGAAGAACTGGGCATGTGTGACACTGT-3'

LagD54AC

5'-ACACACACACACACAGTGTACACATGCCCAGTTCTTCAGTCGGAAGCTTGAGG-3'

IN). Four-stranded replication forks were formed using a two-step annealing process. Initially, in 50 mM Tris (pH 8.0) and 10 mM MgCl₂, excess daughter strands are annealed to their complementary parental strands by heating at 90°C and slow cooling in a stepwise manner (decreasing the temperature in 5°C increments and holding at each temperature 2-5x longer than slow cooling (5-15 min)). Our lab has found this stepwise annealing procedure promotes proper alignment of repeating sequences, provided the annealed strands contain a region of complementary non-repeating sequence. Proper annealing of the resulting leading and lagging parental/daughter partial duplexes containing either human telomeric or dinucleotide repeats created from the primary annealing step was supported via native PAGE analysis. In the secondary annealing step, leading parental/daughter partial duplexes are annealed to their corresponding lagging parental/daughter partial duplex at 25°C overnight to form four-stranded replication forks. The partial duplexes LagP88telo/LagD50telo and LeadP88telo/LeadD38telo were annealed to form the telomeric replication forks *LagD50Fork-telo and *LeadD38Fork-telo (Figure 3.1); the substrate names and asterisks indicate the labeled strand in each substrate here and below. Similarly, LagP88AC/LagD50AC and LeadP88AC/LeadD38AC were annealed to form the dinucleotide replication forks, *LagD50Fork-AC and *LeadD38Fork-AC (Figure 3.1). Preformed daughter duplexes used throughout this chapter, *LagD50telo/LeadD38telo, LagD50telo/*LeadD38telo, *LagD50AC/LeadD38AC, and LagD50AC/*LeadD38AC, were annealed using the step-wise slow-cooling protocol described previously. Likewise, single-stranded loop-containing daughter duplexes, *LagD54AC/LeadD38AC,

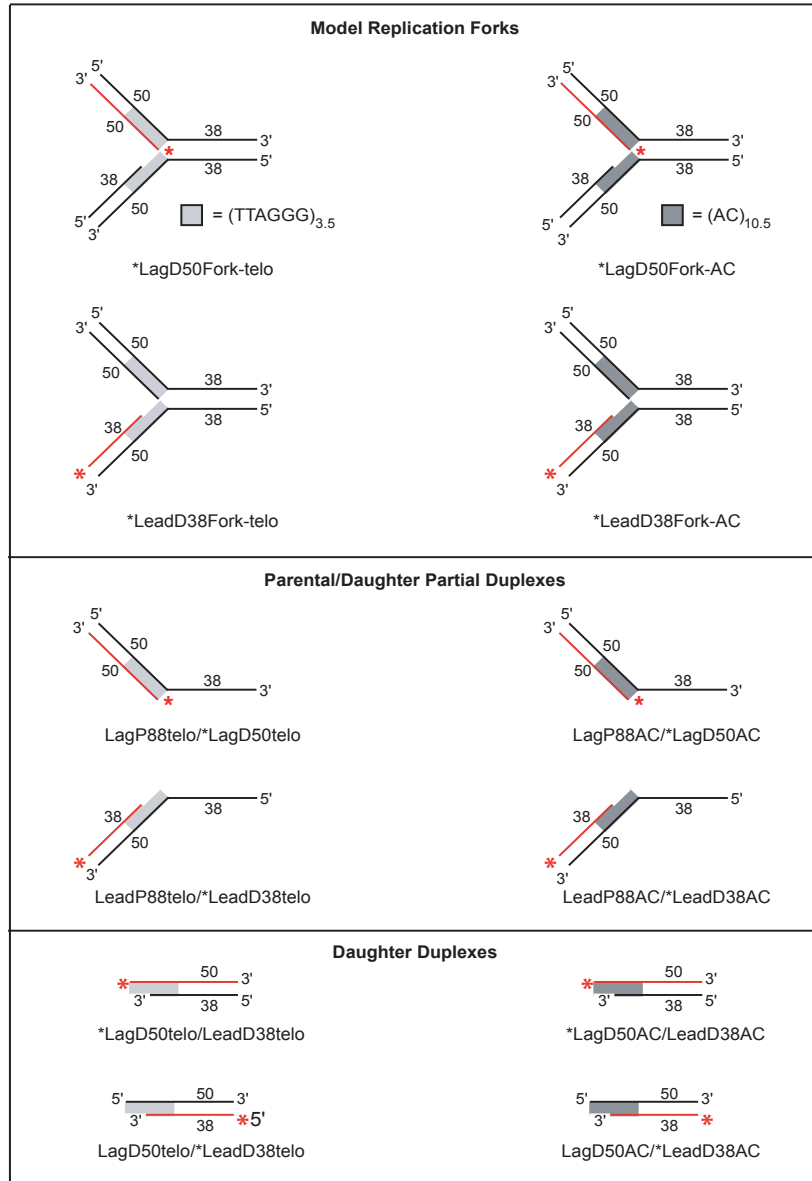


Figure 3.1 Model replication fork and partial duplex substrates. Model replication forks (top) were generated by a two-step annealing process (see “Methods”). One daughter strand was 5’ radiolabeled, as indicated by asterisk (*). Parental/daughter duplexes (middle) or daughter duplexes (bottom) were generated by annealing the indicated oligonucleotides. Daughter duplexes containing either a radiolabeled lagging strand (*50) or leading strand (*38) were also created.

LagD54AC/*LeadD38AC, *LagD50AC/LeadD42AC, and LagD50AC/*LeadD42AC, were annealed in a similar manner (Figure 3.1). All annealed products were electrophoresed on an 8% polyacrylamide native gel with excision of bands corresponding to particular substrates followed by elution in 10 mM Tris, pH 8.0, and 10 mM NaCl buffer.

Fork regression assay. Fork regression assays were carried out in 10-50 μ L WRN reaction buffer (40 mM Tris-HCl [pH 8.0], 4 mM $MgCl_2$, 5 mM dithiothreitol, 100 μ g/mL bovine serum albumin [BSA], 0.1% NP40, and 1 mM ATP) containing labeled replication fork substrate (0.05 nM) and WRN-E84A (0.1-1.0 nM) or RecG (0.5 nM). Reaction samples were incubated at 4°C for 5 min followed by incubation at 37°C for the times indicated. To halt the enzymatic reaction, 1/6 volume of helicase dyes (30% glycerol, 0.9% SDS, 50 mM EDTA, 0.25% bromophenol blue, and 0.25% xylene cyanol) was added and the resulting DNA products were electrophoresed on a native polyacrylamide (8%) gel. Following gel drying, labeled products were viewed and quantitated using the Storm 860 Phosphoimager and ImageQuant software (GE Healthcare).

Restriction digestion analysis. Fork regression was performed as described above in 50 μ L WRN reaction buffer with 0.05 nM labeled fork substrate (*LagD50Fork-telo, *LeadD38Fork-telo, *LagD50Fork-AC, or *LeadD38Fork-AC) incubated with 0.3-1.2 nM WRN-E84A or 0.5 nM RecG at 4°C for 5 min and 37°C for 30 min. Subsequently, 7.5-8.5 μ L aliquots were removed and additional components were included to meet the specific conditions required for each

restriction enzyme. Some experiments included a 50°C incubation step to ensure WRN inactivation prior to restriction enzyme digestion. To examine, repeat alignment following fork regression, these reactions (0.2 nM *DNA) were incubated with the appropriate restriction enzymes (Bmr I, Bbs I, Xcm I, Acu I, Nsp I, or Msl I) (Table 3.2) at 37°C for 2 h. In parallel, 0.02 nM of control preformed daughter duplexes or looped daughter duplexes were digested with the same restriction enzymes in suitable buffers as described above. Reactions were halted by addition of equal volume of formamide loading buffer (95% formamide, 20 mM EDTA, 0.05% xylene cyanol, and 0.05% bromophenol blue) or 1/6 volume of native gel dyes (30% glycerol, 0.9% SDS, 50 mM EDTA, 0.25% bromophenol blue, and 0.25% xylene cyanol). All resulting products were electrophoresed on denaturing (14%) or native (8%) polyacrylamide gels. Radiolabeled DNA species were viewed and quantitated as previously described.

Primer extension analysis. Subsequent to some fork regression assays performed on *LeadD38Fork-telo or *LeadD38Fork-AC (as previously described), 8.5 µL aliquots were removed and additional components were added along with 500 µM of each dGTP, dATP, and dTTP. To examine repeat alignment following fork regression, these samples (0.04 nM *DNA) (10 µL) were incubated with 0.025 U Kexo⁺ at 37°C for 30 min. Preformed daughter duplex (0.4 nM) was extended in the same manner. Samples were heated at 90°C for 5 min, electrophoresed on denaturing (14%) polyacrylamide gels. Labeled extension products were viewed and quantitated as indicated above.

Table 3.2 Restriction enzymes used to test repeat alignment.

Enzyme	Units (per 20 μ L)	Buffer Conditions
Telomeric Forks		
Bmr I	0.025 U	10 mM $MgCl_2$, 50 mM NaCl
Bbs I	0.5 U	10 mM $MgCl_2$, 20 mM NaCl
Xcm I	0.5 U	10 mM $MgCl_2$, 50 mM NaCl
Dinucleotide Forks		
Acu I	2.5 U	10 mM $MgCl_2$, 50 mM NaCl, 0.1 μ M S-adenosylmethionine
Bmrl	0.05 U	10 mM $MgCl_2$, 50 mM NaCl
Msl I	2.5 U	10 mM $MgCl_2$
Nsp I	5 U	10 mM $MgCl_2$, 50 mM NaCl, 250 μ g/mL BSA

RESULTS

WRN regresses model replication forks [Machwe, Xiao et al. 2006; Machwe, Xiao et al. 2007]. Fork regression, the proposed first step in response to stalled or blocked replication forks, involves concurrent pairing of the two complementary daughter strands and reannealing of the parental strands to generate a Holliday junction/chicken foot intermediate [Machwe, Xiao et al. 2007]. However, in our standard fork regression assays using oligomeric substrates, the end product used to detect fork regression activity is a “daughter duplex” containing only the annealed daughter strands. In this previous work, the complementary regions of the replication fork consisted of random sequence, essentially dictating proper alignment of the daughter duplex during regression. However, within regions of the genome containing repeating sequences, such as telomeres, correct alignment during fork regression would be crucial to avoid deletions and insertions from resulting after further processing. Since WRN is associated with telomere maintenance, I investigated the fidelity of WRN-mediated replication fork regression of telomeric and other repeating sequences. Here, following regression of a model replication fork by WRN, alignment of repeating sequences will be tested via two methods: restriction enzyme digestion and primer extension (Figure 3.2).

Restriction enzyme action on fully complementary versus loop-containing duplexes. To analyze alignment of daughter duplexes formed from replication fork regression, model replication forks were designed to contain either telomeric

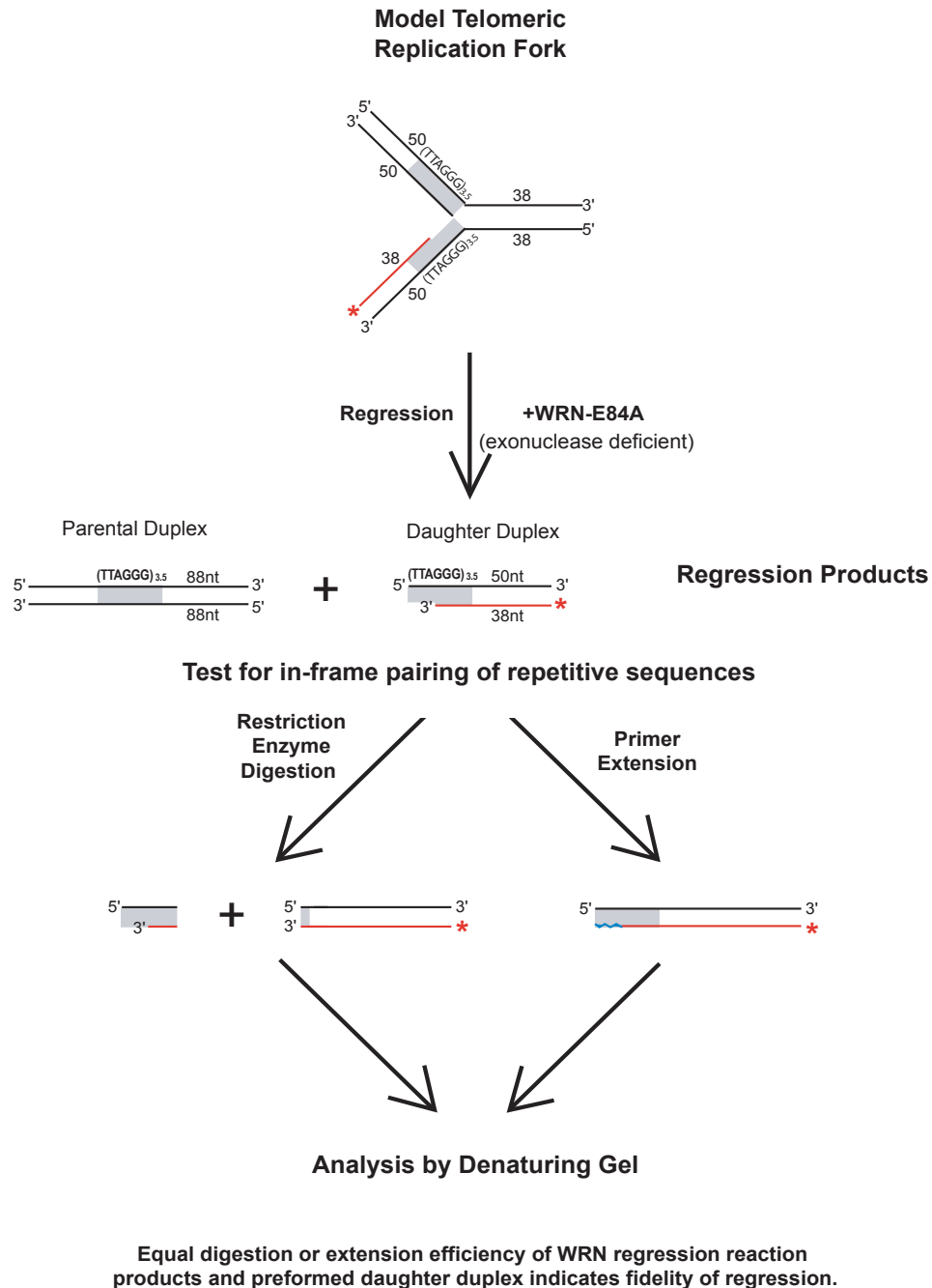


Figure 3.2 Protocol for WRN-mediated fork regression repeat alignment analysis. Following WRN-E84A-mediated fork regression, alignment of the repeating sequences on the daughter duplex was analyzed by restriction enzyme digestion (left) or primer extension (right). The resulting products were analyzed by denaturing (shown) and native (not shown) PAGE. Equal digestion or extension efficiency of a daughter duplex generated by WRN-mediated regression and a control, preformed daughter duplex suggests proper alignment of repeats.

or dinucleotide repeats on the daughter/parental arms proximal to the fork junction (Figure 3.1, top). Misalignment of these repeats during WRN-mediated regression would result in some repeats “looping out,” —i.e., generation of unpaired single-stranded loops. Within the duplex repeating sequence, restriction enzyme cleavage or recognition sites that would potentially be disrupted by misalignment and loop formation were included. Theoretically, properly aligned daughter duplexes would be cut by restriction enzymes. In contrast, these same restriction enzymes would not cut daughter duplexes containing a loop. To test the validity of this assay, I generated three preformed daughter duplexes using a slow-cooling protocol. A control daughter duplex (LagD50AC/LeadD38AC) contains properly aligned repeats and no unpaired loops (Figure 3.3A). One series of daughter duplexes (LagD54AC/LeadD38AC) forms a 4 nt unpaired loop (designated by the triangle, Figure 3.3A) within the Msl I recognition site (denoted by green box, Figure 3.3A) on the lagging strand (top) within the AC dinucleotide repeating region, and the other series of daughter duplexes (LagD50AC/LeadD42AC) forms a 4 nt unpaired loop within the Msl I recognition site of the repeating region on the leading strand (bottom, Figure 3.3A). Daughter duplexes were treated with Msl I, and the resulting products were analyzed by denaturing PAGE by examining changes in migration of the labeled strand. Properly aligned daughter duplexes were cleaved efficiently by Msl I, as shown by the appearance of shorter and expected 18 and 32 nt products (Figure 3.3B, lanes 6 and 12); by comparison, little or no cutting was seen on the daughter duplexes possessing unpaired loops (lanes 2, 4, 8, and 10). In fact, these “looped” substrates remained intact following Msl I

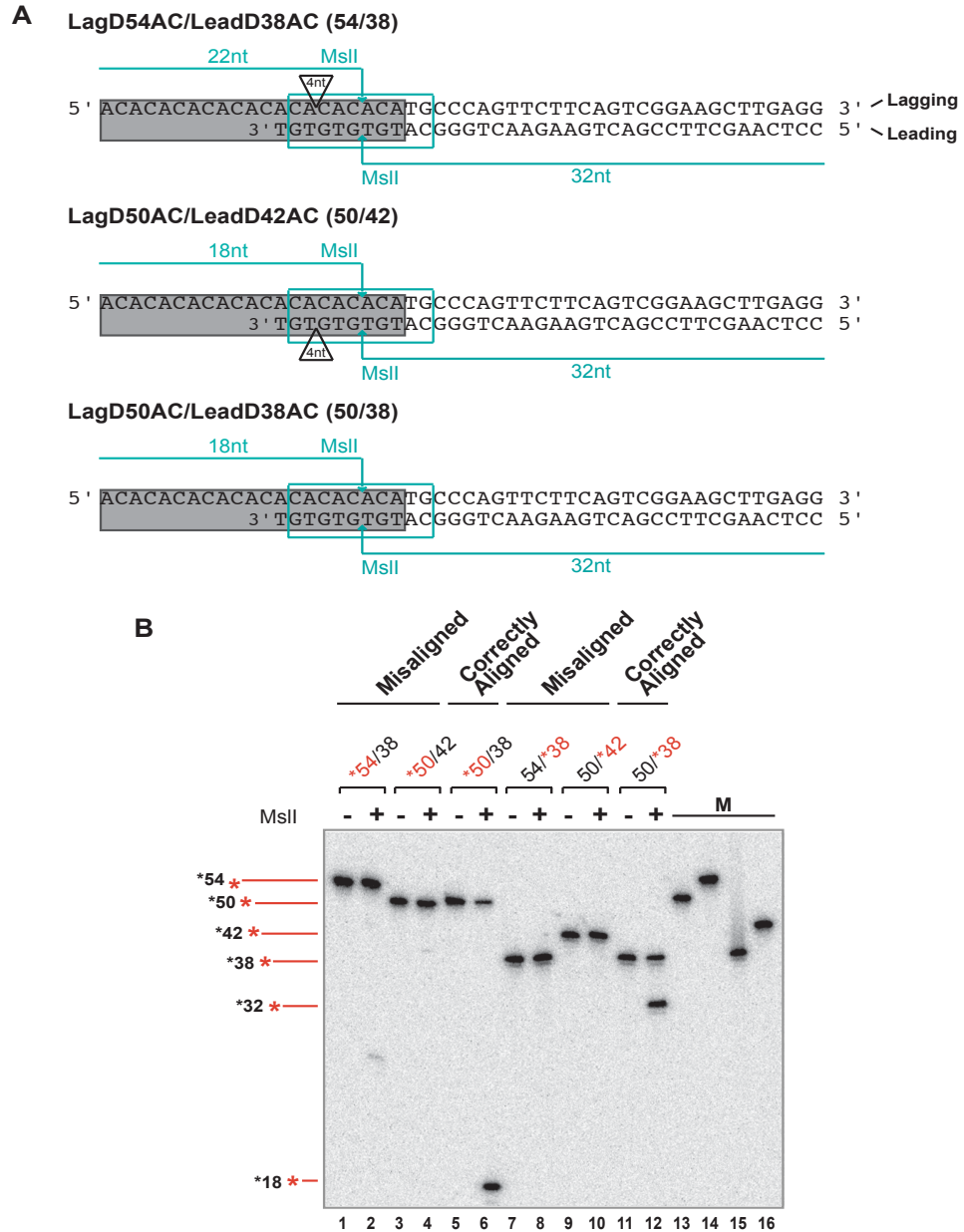


Figure 3.3 Analysis of experimental approach on dinucleotide repeat substrates. **A**) Daughter duplex with (AC)_{10.5} sequence. Control (50/38), looped lagging strand (54/38), and looped leading strand (50/42) daughter duplexes were used. Location of unpaired loops are indicated (triangle). Msi I recognition sequence (box), cut sites (arrows), and expected product lengths are shown. Lagging (top) and leading (bottom) strand lengths are indicated. **B**) Control (50/38) and looped (54/38 or 50/42) daughter duplexes (0.03 nM) with labeled lagging or leading strands (indicated by asterisk (*)) were digested by Msi I (0.125 U/ μ L) and the resulting products were analyzed by denaturing PAGE (14%). Lengths of labeled strand products are indicated (left). Markers for 38, 42, 50, 54 nt products were used (lanes 13-16).

treatment as determined by native PAGE (data not shown), indicating neither strand was cut by Msl I. Conversely, the unpaired loop does not destroy the recognition sequence or cleavage site of Bmr I, which efficiently cuts the properly aligned as well as the loop-containing daughter duplexes (data not shown). Thus, these results indicate formation of a single-stranded, unpaired loop within the recognition sequence (and likely the cut site) on the daughter duplex would prevent cleavage by restriction enzymes, suggesting this assay would be effective for detecting correct and incorrect repeat alignment during replication fork regression.

WRN properly aligns telomeric repeats during replication fork regression.

Following validation of this strategy using restriction enzymes to test alignment of repeated sequences, I wanted to determine if repeats are properly aligned during WRN-mediated replication fork regression. The exonuclease-deficient WRN mutant, WRN-E84A, was used throughout this chapter to prevent possible degradation of the DNA substrates. Model replication forks were designed with repeating sequence on the parental-daughter arms next to the fork junction (Figure 3.1). These substrates contained a 12 nt single-stranded gap on the leading arms (with fewer double-stranded repeats) to provide a better structure for regression by WRN [Machwe, Xiao et al. 2007]. Replication forks with a 5' radiolabeled lagging or leading daughter strand were generated, and WRN-mediated regression would convert these forks into daughter duplexes containing the respective labeled daughter strand. Thus, the model replication fork consisting of a labeled lagging strand was utilized to examine repeat

alignment of the lagging daughter strand. Likewise, the model replication fork with a labeled leading strand was used to inspect leading strand repeat alignment.

Due to the implication of WRN in telomere maintenance, I first focused on WRN's ability to properly align 3.5 telomeric repeats during fork regression (Figure 3.4A). Using native PAGE to separate the replication fork from WRN-E84A-dependent formation of daughter duplex, the ability of the WRN to regress a model replication fork with telomeric repeats was determined. Since restriction digestion of the replication fork would produce the same shorter labeled product on denaturing PAGE as cleavage of the daughter duplex, it was critical to determine the conditions required for complete regression. WRN-E84A was titrated on *LagD50Fork-telo, and daughter duplex was produced in a concentration-dependent manner, with 62% converted after 10 min at 0.72 nM (Figure 3.4B, lane 5). Using 0.34 nM WRN-E84A, the kinetics of fork regression of the telomeric fork were examined, with 90% converted to daughter duplex following 30 min (Figure 3.4C, lane 6). These latter conditions were used to achieve essentially complete fork regression in subsequent experiments.

Having established conditions that allow near complete regression of a replication fork substrate containing telomeric repeats, I next analyzed the ability of WRN to properly align telomeric repeats during fork regression. Based on the previous results using daughter duplexes with unpaired loops (Figure 3.3), misalignment and "looping out" of repeats within the recognition (or cut) site

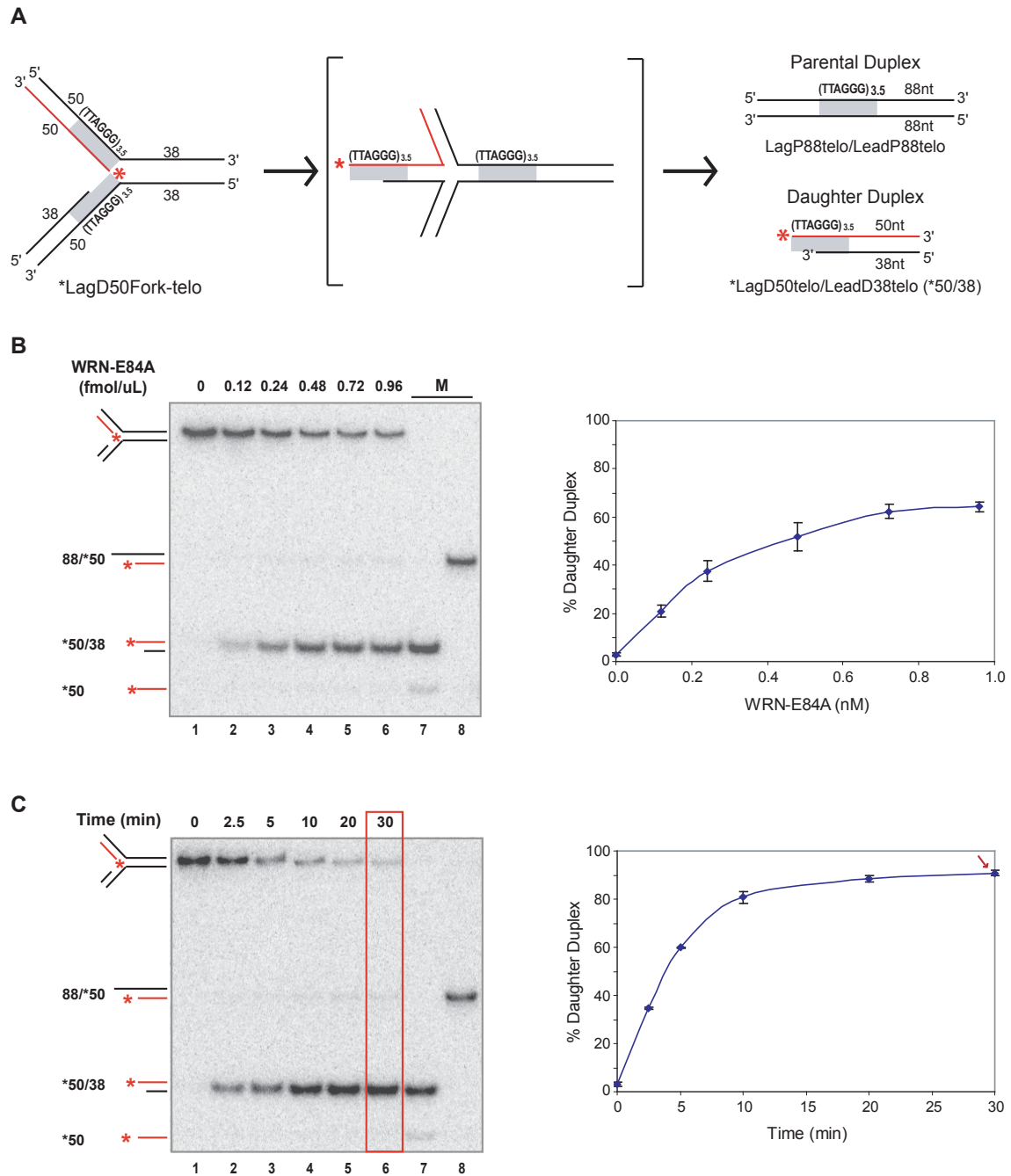


Figure 3.4 Regression of model replication fork with (TTAGGG)_{3.5}. A) *LagD50Fork-telo contains (TTAGGG)_{3.5} repeats (indicated by grey box) on the daughter-parental strands, adjacent to 5 nt of unique sequence at the fork junction (not shown). A single daughter strand (here, lagging) is radiolabeled (asterisk (*)). A 12 nt single-stranded gap was included on the leading strand for optimal regression activity. Through a chicken-foot intermediate, WRN converts the model fork to an unlabeled parental duplex (LagP88telo/LeadP88telo) and a labeled daughter duplex (*LagD50telo/LeadD38telo). **B)** WRN-E84A (0-0.96 nM) was incubated with *LagD50Fork-telo (0.05 nM) at 37°C for 10 min.

Regression products were analyzed by native PAGE (8%). Markers for the *50/38 daughter duplex and 88/*50 parental/daughter duplex are indicated. Percentage of fork converted to daughter duplex (mean \pm SE) was quantitated from four independent experiments (right). **C)** WRN-E84A (0.34 nM) was incubated with *LagD50Fork-telo (0.05 nM) at 37°C for 0-30 min. Regression products were analyzed by native PAGE (8%). Markers for the *50/38 daughter duplex and 88/*50 parental/daughter duplex are shown. Percentage of fork converted to daughter duplex (mean \pm SE) was quantitated from four independent experiments (right). Red arrow denotes conditions used for subsequent regression experiments (0.34 nM WRN-E84A for 30 min).

would likely eliminate restriction enzyme cleavage. Following near complete regression of *LagD50Fork-telo or *LeadD38Fork-telo by WRN (78-89%, data not shown), the reaction volume was split into aliquots, each treated with different restriction enzymes. Restriction enzymes were chosen that have a recognition sequence (Bmr I, Xcm I, denoted by lines) and/or cut site (Bmr I, Bbs I, denoted by arrows) within the repeating sequence (Figure 3.5A). In parallel, preformed daughter duplex substrates were treated under the same conditions to serve as markers for proper alignment and controls for efficiency of restriction digestion. The lengths of the expected *DNA fragments generated by restriction digestion of a properly aligned daughter duplex are indicated for each restriction enzyme (Figure 3.5A). The restriction products were analyzed on both native (data not shown) and denaturing polyacrylamide gels. Bmr I (14 nt) and Xcm I (27 nt) both cut the labeled lagging strand of the *LagD50telo/LeadD38telo daughter duplex formed by WRN-mediated regression almost to completion (>90%, at essentially the same efficiency as the preformed daughter duplex) (Figure 3.5B, compare lanes 3-6), indicating that daughter duplexes formed during regression did not contain unpaired loops due to misalignment of telomeric repeats. Likewise, analysis of cutting on the leading daughter strand (*LeadD38telo) shows both Xcm I (24 nt) and Bbs I (30 nt) cut the daughter duplex (LagD50telo/*LeadD38telo) formed from WRN-mediated regression to near completion (82-91%), again at a similar efficiency as preformed daughter duplex (Figure 3.5C, compare lanes 10,11,13,14). These results were confirmed by native PAGE analysis (data not shown). Results with Bmr I on LagD50telo/*LeadD38telo and Bbs I on *LagD50telo/LeadD38telo were not

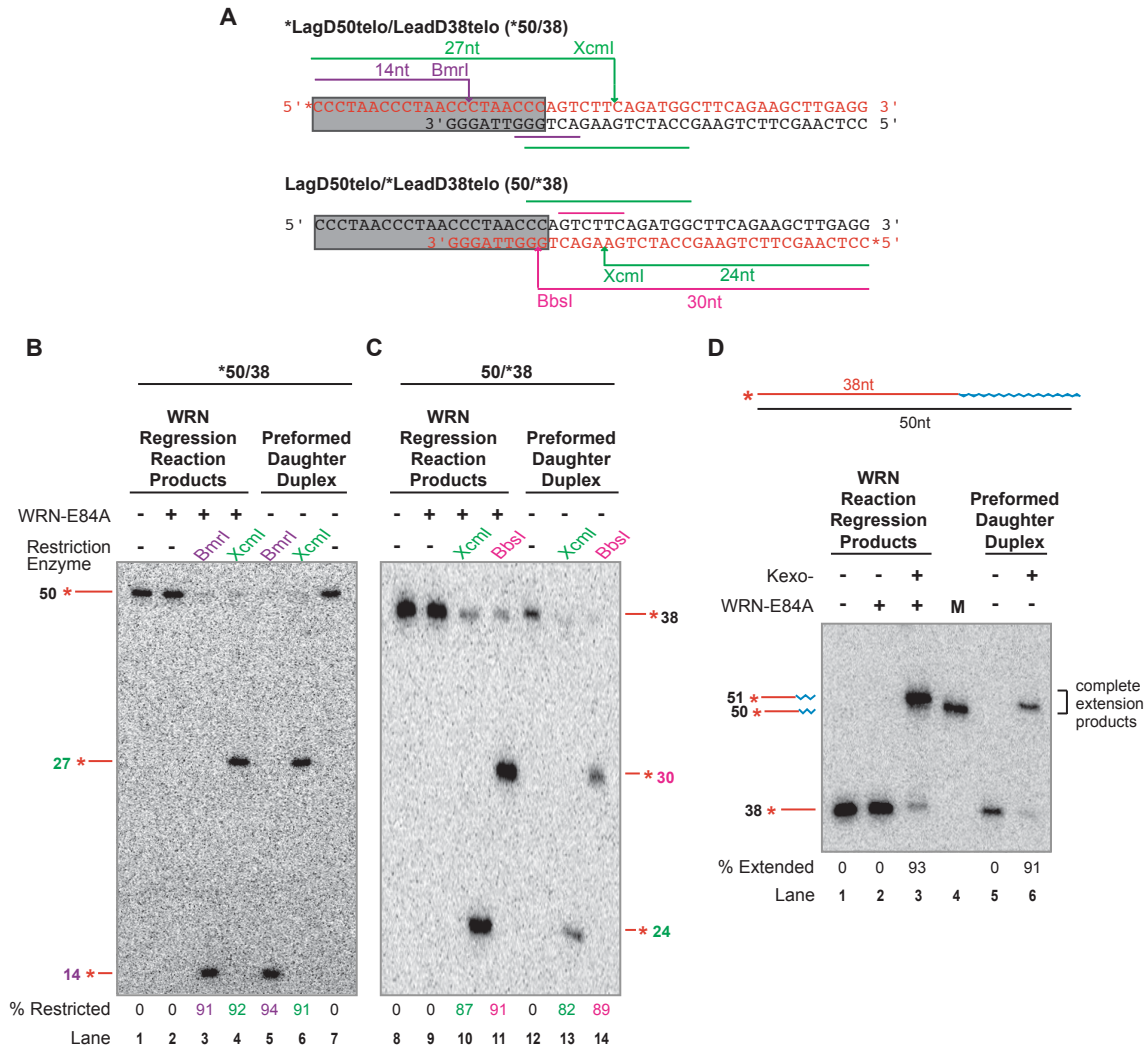


Figure 3.5 Alignment analysis of (TTAGGG)_{3.5} repeats. A) Daughter duplex with (TTAGGG)_{3.5} repeats (gray box) with labeled lagging strand (top, *50/38) or leading strand (bottom, 50/*38). Restriction enzyme recognition sequence (line) and cut sites (arrow) are denoted. Product lengths from restriction enzyme digestion of the respective labeled strands are indicated. **B)** Restriction analysis of telomeric repeats. Fork regression of *LagD50Fork-telo (0.05 nM) was performed using WRN-E84A (0.34 nM) at 37°C for 30 min. The *50/38 daughter duplex (0.02 nM) was digested by Bmr I (0.001 U/μL) (purple) or Xcm I (0.025 U/μL) (green). Preformed daughter duplexes (0.02 nM) were used as a control. Restriction digestion products were analyzed by denaturing (14%) (shown) or native (8%) (not shown) PAGE. Product sizes are indicated. Percent of labeled strand converted to restriction product is indicated below each lane. **C)** Fork regression of *LeadD38Fork-telo (0.05 nM) was performed using WRN-E84A (0.34 nM) at 37°C for 30 min. The 50/*38 daughter duplex (0.02) was digested by Xcm I (0.025 U/μL) (green) or Bbs I (0.025 U/μL) (pink). Preformed daughter duplexes (0.02 nM) were used as a control. Restriction digestion products were analyzed by denaturing (14%) (shown) or native (8%) (not shown) PAGE.

Product sizes are indicated. Percent of labeled strand converted to restriction product is indicated below each lane. **D)** Primer extension analysis of telomeric repeats. Following fork regression of *LeadD38Fork-telo (see above), daughter duplex product (0.04 nM) was treated with Kexo⁻ (0.0025 U/μL) at 37°C for 30 min. Preformed daughter duplex (50/*38) (0.048 nM) was used as a control. Extension products were analyzed by denaturing PAGE (14%). Product sizes are indicated (left). Percentage of labeled strand converted to full length product is indicated below each lane.

shown due to a lack of efficient cutting on the indicated labeled strand on the respective preformed, fully paired daughter duplexes (data not shown), suggesting difficulties with the enzymes and not misalignment of the daughter duplex. Although ideally each restriction enzyme would efficiently cleave both daughter strands in every instance, these results are consistent with the results presented here (Figure 3.5B,C). Thus, this analysis using restriction enzymes indicates WRN properly aligns telomeric repeats during replication fork regression.

In addition to restriction enzyme analysis, I also employed DNA polymerase extension to examine proper alignment of repeated sequences during replication fork regression. Correctly aligned daughter duplexes generated by WRN-E84A-mediated fork regression contain 12 nt 5' overhangs (Fig. 3.5A) of the lagging daughter strand that can be utilized as templates for extension of the shorter radiolabeled leading strand using Kexo⁻. If the daughter duplex is properly aligned, Kexo⁻ will fully extend the 38 nt leading strand to the end of the template (Fig. 3.5D, top), generating 50-52 nt length products (note that Kexo⁻ can add 1-2 untemplated nucleotides [Clark, Joyce et al. 1987]) when analyzed using denaturing PAGE. However, Kexo⁻ extension of a daughter duplex possessing a loop due to misalignment would result in longer or shorter products depending on whether loops were present in the leading or lagging strands, respectively. In a similar manner as the restriction enzyme assays, a model replication fork with 3.5 telomeric repeats and a labeled leading daughter strand, *LeadD38Fork-telo, was regressed by WRN-E84A to near completion to

form daughter duplex (75%, data not shown) following a 30 min incubation. Immediate addition of Kexo⁻ to these reactions leads to extension of the leading daughter strand (38-mer) to primarily produce a 51 nt product (93%) (Figure 3.5D, lane 3), demonstrating proper alignment of the daughter duplex by WRN. Notably, no additional products were detected other than the unextended 38-mer leading strand, suggesting that there was no misalignment of telomeric repeats during WRN-mediated regression to form the daughter duplex. At a similar efficiency, Kexo⁻ extended the preformed daughter duplex to produce a 51 nt product (Figure 3.5D, compare lanes 3 and 6). Combined with the previous restriction enzyme analysis, these results suggest WRN properly aligns telomeric repeats during replication fork regression of model replication forks.

WRN aligns dinucleotide repeats during fork replication fork regression.

Given that WRN correctly aligns telomeric repeats during replication fork regression, I also wanted to test WRN's fidelity on a considerably shorter repeating unit with a greater potential for misalignment. Therefore, dinucleotide repeats provide a more stringent evaluation of WRN's fidelity during fork regression than telomeric repeats. I constructed a model replication fork with 10.5 dinucleotide (AC) repeats (on the lagging daughter strand) within the parental-daughter arms near the fork junction; however, all other structural aspects are the same as the telomeric fork (Figure 3.6A). As with the telomeric fork, I initially analyzed the extent of WRN-mediated fork regression using a model replication fork with dinucleotide repeats, *LagD50Fork-AC (Figure 3.6). Although 80% regression was achieved with 0.4 nM WRN-E84A following 10

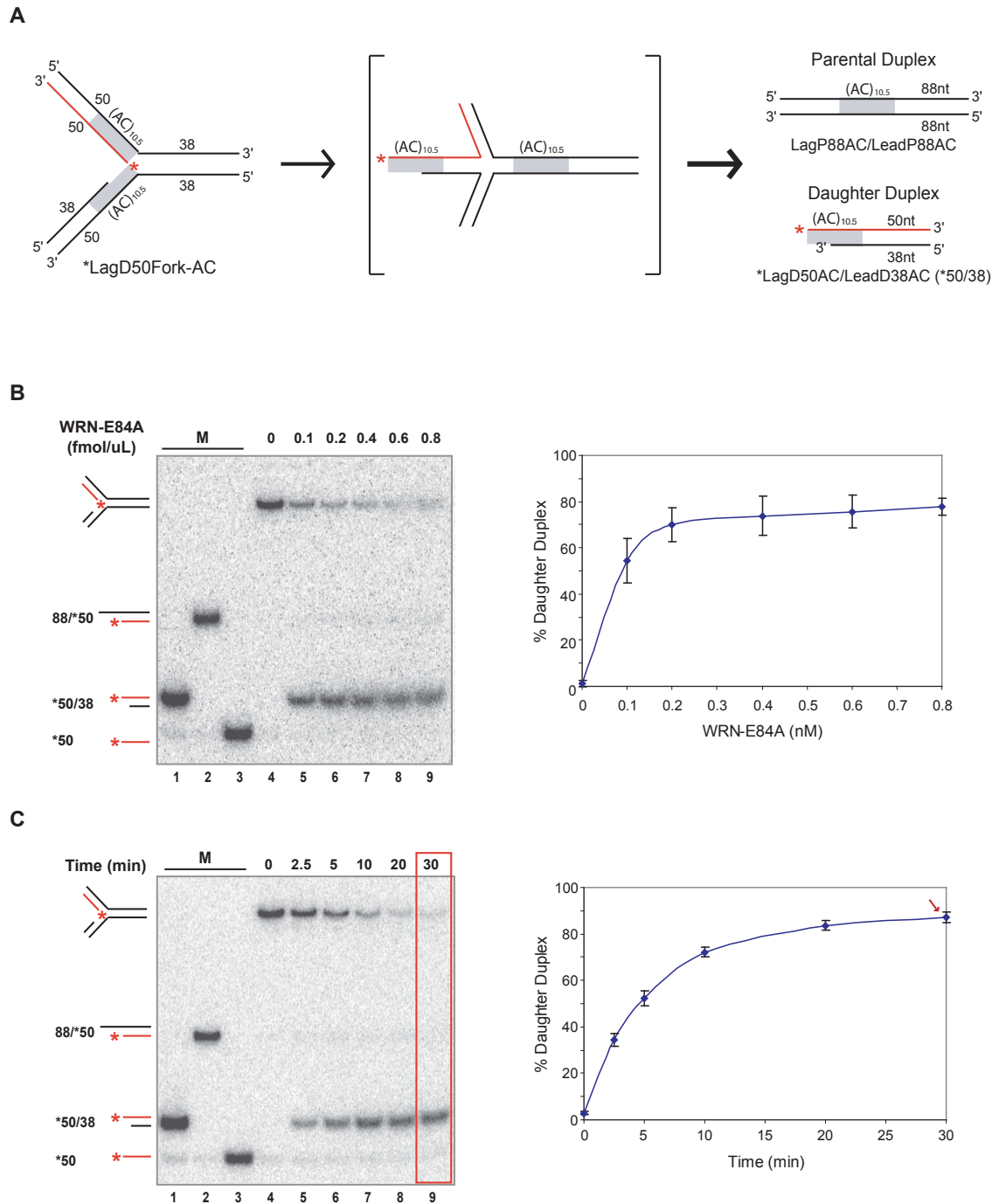


Figure 3.6 Regression of model replication fork with (AC)_{10.5}. **A)** Regression of *LagD50Fork-AC produces a non-labeled parental duplex (LagP88AC/LeadP88AC) and a radiolabeled daughter duplex (*LagD50AC/LeadD38AC). Location of (AC)_{10.5} repeats are indicated by grey box. **B)** Regression was performed by incubating *LagD50Fork-AC (0.05 nM) with WRN-E84A (0-0.8 nM) at 37°C for 10 min. Regression products were analyzed by native PAGE (8%). Percentage of fork converted to daughter duplex (mean \pm SE) was calculated from three independent experiments (right).

C) To perform regression, *LagD50Fork-AC (0.05 nM) was incubated with WRN-E84A (0.36 nM) at 37°C for 0-30 min. Regression products were analyzed by native PAGE (8%). Percentage of fork converted to daughter duplex (mean \pm SE) was calculated using three independent experiments. Red arrow denotes conditions used for some subsequent regression experiments (0.36 nM WRN-E84A for 30 min).

min (lane 7, Figure 3.6B), further conversion (87%) was achieved after 30 min (lane 9, Figure 3.6C), a level that is comparable to the telomeric fork (Figure 3.4C, lane 6). These optimal conditions were used for regression of the dinucleotide repeat fork in subsequent reactions.

Initially, alignment of dinucleotide repeats in the daughter duplexes formed from WRN-mediated regression of the dinucleotide fork was tested using restriction enzymes (Figure 3.7A). Preformed daughter duplexes were examined in parallel as positive controls. Once again, forks (and preformed daughter duplexes) were constructed with either the lagging (*LagD50AC) or leading (*LeadD38AC) daughter strand labeled. Restriction enzymes were chosen that have recognition sites (Msl I or Nsp I) and/or cut sites (Bmr I, Msl I, Acu I, and Nsp I) within the repeating sequences (Figure 3.7A). Lengths of the expected *DNA fragments formed from restriction digestion of a properly aligned daughter duplex are indicated for each individual enzyme (Figure 3.7A). Following near complete regression by WRN-E84A (67-92%, data not shown), restriction products were analyzed on native (data not shown) and denaturing polyacrylamide gels. The *LagD50AC/LeadD38AC daughter duplex formed from WRN-mediated regression was cut by Acu I (16 nt, 71%), Bmr I (19 nt, 82%), and Msl I (18 nt, 79%) with similar efficiency as the preformed *LagD50AC/LeadD38AC daughter duplex (70%, 85%, and 73% respectively) (Figure 3.7B, compare lanes 3, 4, 5 with 7, 8, 9). Likewise, Msl I (32 nt, 67%) and Nsp I (31 nt, 90%) cleaved the WRN-generated LagD50AC/*LeadD38AC daughter duplex to a similar degree as the preformed 50/*38 daughter duplex

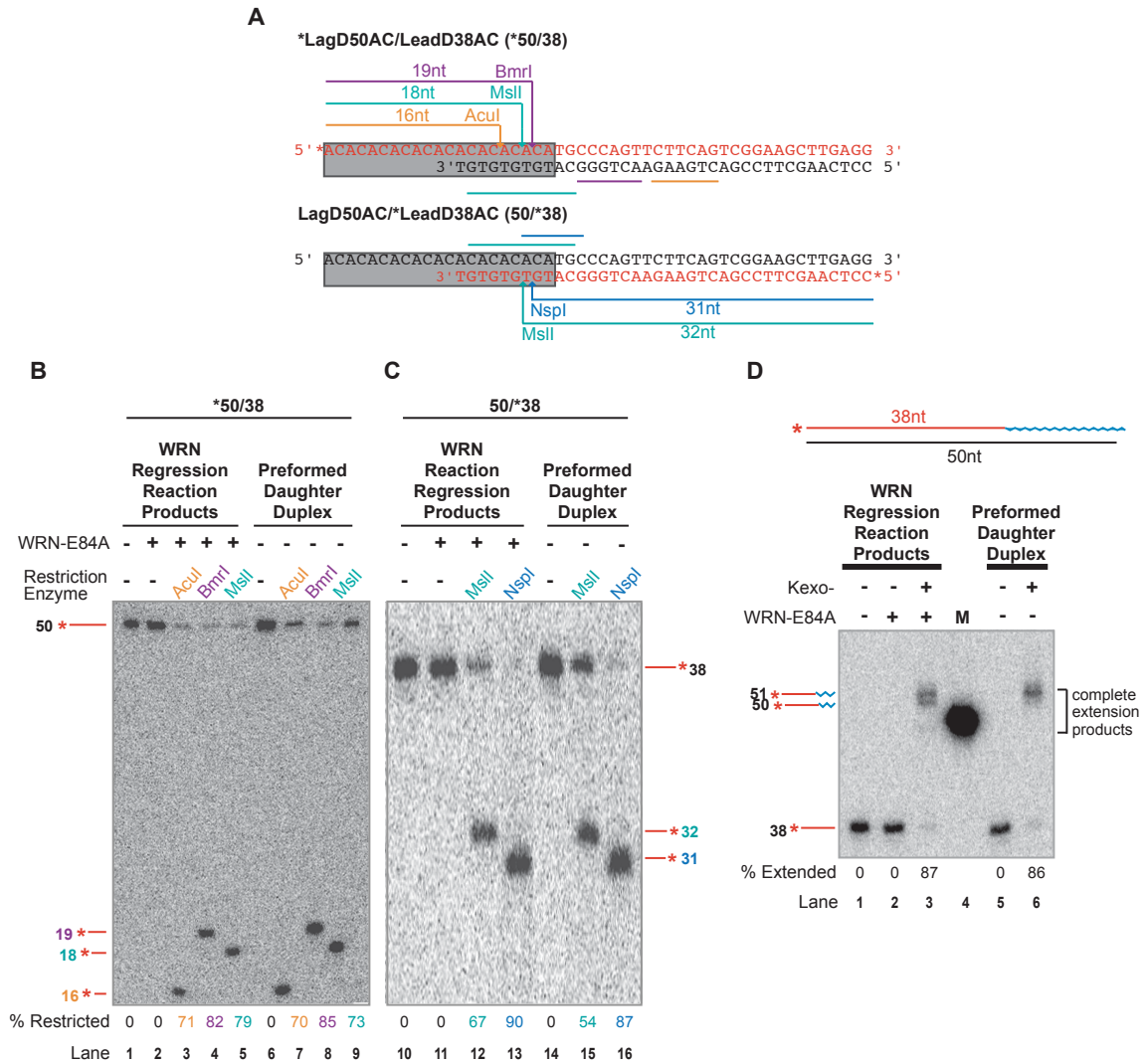


Figure 3.7 Alignment analysis of (AC)_{10.5} repeats. A) Daughter duplex with (AC)_{10.5} repeats (gray box) with labeled lagging strand (top, *50/38) or leading strand (bottom, 50/*38). Restriction enzyme recognition sequence (line) and cut sites (arrow) are denoted. Product lengths from restriction enzyme digestion of the respective labeled strands are indicated. **B)** Restriction analysis of dinucleotide repeats. Fork regression of *LagD50Fork-AC (0.05 nM) was performed using WRN-E84A (0.36 nM) at 37°C for 30 min. The *50/38 daughter duplex (0.019 nM) was digested by Acu I (0.125 U/μL) (orange), Bmr I (0.0025 U/μL) (purple), or Msl I (0.125 U/μL) (teal). Preformed daughter duplexes (0.02 nM) were used as a control. Restriction digestion products were analyzed by denaturing (14%) (shown) and native (8%) (not shown) PAGE. Product sizes are indicated. Percent of labeled strand converted to restriction product is indicated below each lane. **C)** Fork regression of *LeadD38Fork-AC (0.05 nM) was performed using WRN-E84A (1.17 nM) at 37°C for 30 min. The 50/*38 daughter duplex (0.02 nM) was digested by Msl I (0.125 U/μL) (teal) or Nsp I (0.25 U/μL) (blue). Preformed daughter duplexes (0.02 nM) were used as a

control. Restriction digestion products were analyzed by denaturing (14%) (shown) and native (8%) (not shown) PAGE. Product sizes are indicated. Percent of labeled strand converted to restriction product is indicated below each lane. **D)** Primer extension analysis of dinucleotide repeats. Following fork regression of *LeadD38Fork-AC (see above), daughter duplex product (0.04 nM) was treated with Kexo⁻ (0.0025 U/μL) at 37°C for 30 min. Preformed daughter duplex (50/*38) (0.048 nM) was used as a control. Product sizes are indicated (left). Percentage of labeled strand converted to full length product is indicated below each lane.

(54% and 87% respectively) (Figure 3.7C, compare lanes 12, 13 with 15, 16). Restriction enzyme cleavage was also observed by native PAGE analysis (data not shown). Like restriction enzyme analysis on the telomeric daughter duplexes, some restriction enzymes (Acl I, Bmr I, and Nsp I) did not cleave both daughter strands. Importantly, these enzymes did not cut the properly aligned daughter duplexes indicating a limitation of the enzyme and not misalignment. Therefore, these results obtained using restriction enzymes suggest the shorter dinucleotide repeats are properly aligned by WRN during replication fork regression.

Alignment of daughter duplexes containing dinucleotide repeats was also determined using primer extension. Following fork regression by WRN to form a daughter duplex, Kex^o can use the 12 nt 5' overhang of the 50 nt lagging strand (Fig. 3.7A) as a template to extend the 38 nt labeled leading strand (Fig. 3.7D, top). Following near complete regression of *LeadD38Fork-AC by WRN (90%, data not shown), Kex^o extends the leading strand, generating a fully extended product (50 nt) and occasionally adds one additional untemplated nucleotide (51 nt) (87%) (Figure 3.7D, lane 3) [Clark, Joyce et al. 1987]. Importantly, these extension products comigrate with those formed from the preformed daughter duplex and are generated with similar efficiency (86%) (lane 6); furthermore, no shorter or longer extension products that would indicate misalignment are formed. The 50 nt marker, which is made up of the sequence complementary to the extension product, does not migrate to the same location as the extended leading strand likely due to differing sequences. Therefore, even in the absence

of a proper 50 nt marker, these results are supportive of proper repeat alignment of the WRN-produced daughter duplex. Along with the previous results using restriction enzymes, these findings suggest that WRN properly aligns both short repeats, such as dinucleotide repeats, and longer repeats during fork regression.

The non-RecQ helicase, RecG, aligns telomeric repeats during replication fork regression. In addition to WRN, a few other enzymes have been demonstrated to perform fork regression. Among those enzymes, it is unknown whether repeat alignment during regression is limited to WRN. Therefore, I examined the alignment of telomeric repeats of the daughter duplex formed from regression of the *LeadD38Fork-telo by RecG (Figure 3.8), an *Escherichia coli* ATP-dependent helicase that performs fork regression [Whitby and Lloyd 1998]. Like the previous WRN experiments, following near complete regression by RecG (80.5%) (Figure 3.8A, lane 2), the resulting daughter duplex, LagD50telo/*LeadD38telo, was treated with restriction enzymes with a recognition site (Xcm I) or a cut site (Bbs I) within the telomeric repeats (Figure 3.8B, top). Xcm I (24 nt, 85%) and Bbs I (30 nt, 90%) cut the daughter duplex formed from regression with similar efficiency as the preformed daughter duplex (77% and 85% respectively) (Figure 3.8B, compare lanes 3, 4 with 6, 7). Therefore, use of restriction enzymes indicates RecG properly aligns telomeric repeats during regression.

In parallel, I also performed primer extension assays on the products of regression reactions carried out by RecG on the *LeadD38Fork-telo substrate

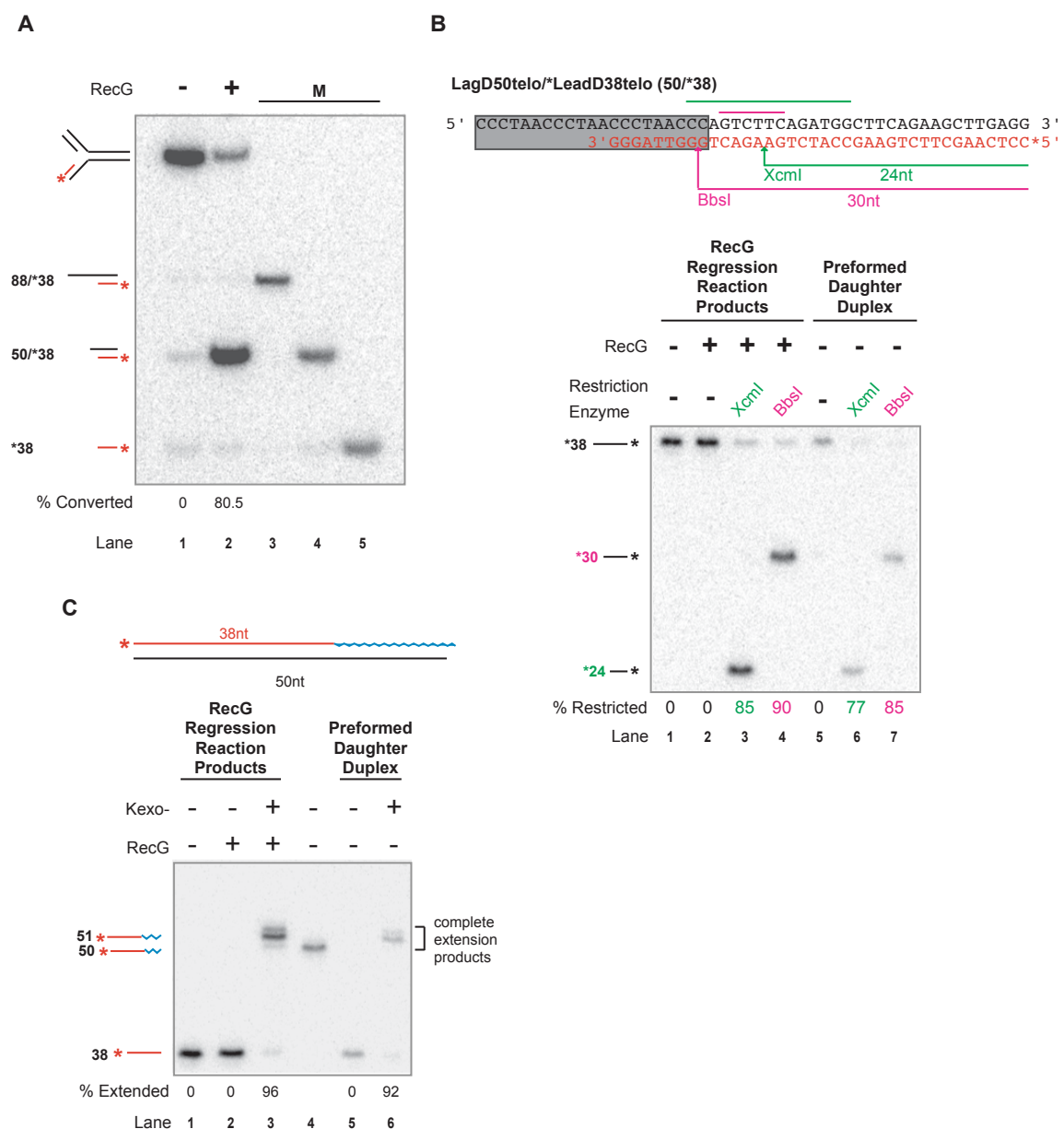


Figure 3.8 Alignment analysis of (TTAGGG)_{3.5} repeats following RecG-mediated regression. **A)** Regression was performed by incubated *LeadD38Fork-telo (0.05 nM) with RecG (0.5 nM) at 37°C for 30 min. Regression products were analyzed by native PAGE (8%). Markers of the parental/daughter duplex (88/*38), daughter duplex (50/*38), and single strand (*38) are shown. Percentage of fork converted to daughter duplex is indicated below (lane 2). **B)** Restriction analysis of telomeric fork following regression by RecG. Daughter duplex with (TTAGGG)_{3.5} repeats (gray box) with labeled leading strand (50/*38) (top). Restriction enzyme recognition sequence (line) and cut sites (arrow) are denoted. Product lengths from restriction enzyme digestion of the respective labeled strands are indicated. Following fork regression of *LeadD38Fork-telo (see above), the 50/*38 daughter duplex (0.02

nM) was digested by Xcm I (0.025 U/ μ L) (green) or Bbs I (0.025 U/ μ L) (pink). Preformed daughter duplexes (0.02 nM) were used as a control. Restriction digestion products were analyzed by denaturing (14%) (shown) and native (8%) (not shown) PAGE. Product sizes are indicated. Percent of labeled strand converted to restriction product is indicated below each lane. **C)** Primer extension analysis of dinucleotide repeats. Following fork regression of *LeadD38Fork-AC (see above), daughter duplex product (0.04 nM) was treated with Kexo⁻ (0.0025 U/ μ L) at 37°C for 30 min. Preformed daughter duplex (50/*38) (0.048 nM) was used as a control. Extension products were analyzed by denaturing PAGE (14%). Product sizes are indicated (left). Percentage of labeled strand converted to full-length product is indicated below each lane.

containing telomeric repeats. In these assays, Kexo⁻ predominately generated a 51 nt extension product (with some 50 and 52-mers produced) (96%) from the daughter duplex generated from RecG regression, LagD50telo/*LeadD38telo (Figure 3.8C, lane 3). Notably, no shorter or longer products were detected, suggesting no unpaired loops were formed. When the preformed daughter duplex was used as substrate for extension by Kexo⁻ (lane 6), similar results were obtained (92% extended). These results indicate that both WRN and RecG, properly align repeated sequences during fork regression.

DISCUSSION

As an initial response to blocked replication, WRN is proposed to regress replication forks, a mechanism that allows for lesion bypass or repair as a method of genome maintenance and stability. WRN unwinds the daughter strands from the respective parental strands and in concert, anneals the homologous daughter strands as well as the homologous parental arms, forming a chicken-foot intermediate [Machwe, Xiao et al. 2007]. Our lab previously reported WRN regresses model replication forks with random sequence producing a daughter duplex and a parental duplex in the *in vitro* model system [Machwe, Xiao et al. 2006]. Unlike random sequences, the potential exists for misalignment of repeating sequences during regression. In particular, misalignment of telomeric sequence may lead to telomere deletions. Due to the strong evidence linking WRN to telomeres, I investigated the alignment of repeating sequences within the daughter duplex following WRN-mediated

regression. The results presented here indicate WRN mediates correct “in-frame” alignment of both telomeric (TTAGGG) and dinucleotide (AC) repeats during replication fork regression, as demonstrated using both restriction enzyme and primer extension assays, supporting a role for WRN in promotion of efficient telomere replication.

Initially, and most relevant to WRN, alignment of telomeric repeats was examined. Model replication forks containing 3.5 telomeric repeats with either the lagging strand (*LagD50Fork-telo) or leading strand (*LeadD38Fork-telo) were efficiently regressed by WRN, producing a radiolabeled daughter duplex. Using restriction enzymes with cut or recognition sites within the telomeric repeats, I examined the alignment of the daughter duplex repeats. Unpaired loops that destroy the recognition site, similar to those that may occur during repeat misalignment, eliminated restriction enzyme cleavage of both the leading and lagging strands, confirming the validity of this restriction enzyme analysis. However, following near complete WRN-mediated regression, restriction enzymes cleaved both the leading and lagging strand of the daughter duplex product, as determined by native and denaturing PAGE. Importantly, restriction enzyme analysis of control preformed daughter duplexes produced identical ³²P-DNA products with a similar cleavage efficiency, indicating proper telomeric repeat alignment during WRN-mediated fork regression. To further examine telomeric repeat alignment, I utilized a primer extension assay on daughter duplexes produced by WRN-mediated regression. Primer extension of misaligned daughter duplexes with “looped out” repeats would result in shorter

or longer extension products. Primer extension generated full-length extension products of regression-generated and control preformed daughter duplexes at similar efficiencies, again supporting proper telomeric repeat alignment by WRN during regression. These results were not limited to WRN as RecG, a non-RecQ helicase that has also been demonstrated to perform fork regression [Whitby and Lloyd 1998], correctly aligned telomeric repeats.

Although WRN properly aligns telomeric repeats, shorter repeats possess a greater probability of misalignment. Therefore, I examined the alignment of dinucleotide (AC) repeats during fork regression using restriction enzyme analysis and primer extension analysis. Following complete fork regression of *LagD50Fork-AC or *LeadD38Fork-AC, restriction enzyme cleavage was observed on both the lagging and leading strands of the resulting daughter duplex. Importantly, restriction digestion of control preformed daughter duplexes generated identical products at similar efficiencies, suggesting WRN properly aligned dinucleotide repeats during fork regression. Polymerase extension of regression-generated daughter duplexes produced full-length products, and no shorter or longer products were observed. These products were generated at similar levels and comigrated with control preformed daughter duplex extension products. Therefore, the results presented here indicate WRN correctly aligns not only telomeric repeats but also shorter dinucleotide repeats of daughter duplexes, revealing the precise nature of WRN regression, particularly at repeating sequences. The impressive ability of the enzyme to properly align much shorter repeats provides greater support for a strong proficiency of WRN

for proper alignment of telomeric sequence. These daughter duplex products are generated by annealing, either following WRN-mediated unwinding of parental/daughter strands or in coordination with unwinding. Proper alignment of telomeric and dinucleotide repeats during WRN-mediated fork regression support an active mechanism, with coordination of helicase and annealing activities, as previously reported [Machwe, Xiao et al. 2007].

Loss of WRN leads to hypersensitivity to chemical agents that stall or block replication [Lebel and Leder 1998; Pichierri, Franchitto et al. 2001; Poot, Yom et al. 2001], indicating the WRN protein may play a role in replication. Even in the absence of exogenous agents, WS cells undergo asymmetric replication [Rodriguez-Lopez, Jackson et al. 2002] and are more prone to developing double-strand breaks at fragile sites [Pirzio, Pichierri et al. 2008], indicating replication difficulties. In particular, WS cells specifically undergo elevated recombination at telomeres [Laud, Multani et al. 2005], a repeating sequence that also resemble fragile sites [Sfeir, Kosiyatrakul et al. 2009], likely suggesting frequent telomere replication fork stalling in the absence of WRN. Particularly at telomeres, WRN may perform fork regression as a high-fidelity mechanism to repair or resolve DNA damage or secondary structures that block replication, thus promoting complete telomere synthesis and maintenance of functional telomeres. Even in the presence of WRN, telomeres possess unique features that may render these sequences more susceptible to replication fork blockage than other regions of the genome. Telomeres are likely replicated unidirectionally [Gilson and Geli 2007], meaning a converging fork will not

rescue blocked forks located at the chromosome ends. Unique telomeric structures (T-loops) [Griffith, Comeau et al. 1999], and telomere-specific binding proteins (TRF1, TRF2, and POT1) [Zhong, Shiue et al. 1992; Billaud, Brun et al. 1997; Broccoli, Smogorzewska et al. 1997; Baumann and Cech 2001] likely need to be resolved or displaced prior to arrival of the replication fork. Additionally, due their repetitive, G-rich nature, the lagging strands of telomeres are capable of forming bulky and compact secondary structures within single-stranded regions generated during replication such as G-quadruplexes or guanine hairpins (Chapter 2) [Lipps and Rhodes 2009]. I reported intramolecular G-quadruplexes block a wide range of polymerases (Chapter 2), suggesting these structures may contribute to the replication stress observed at telomeres. WRN, which colocalizes with sites of stalled replication [Constantinou, Tarsounas et al. 2000], functionally interacts with several members of the replication machinery, including pol δ , PCNA, and RPA [Brosh, Orren et al. 1999; Lebel, Spillare et al. 1999; Kamath-Loeb, Johansson et al. 2000; Rodriguez-Lopez, Jackson et al. 2003]. WRN interacts with telomeres during synthesis [Crabbe, Verdun et al. 2004; Opresko, Otterlei et al. 2004] and may be specifically recruited to stalled replication forks at telomeres through a functional interaction with the telomere-binding proteins TRF2 and/or POT1 [Opresko, von Kobbe et al. 2002; Machwe, Xiao et al. 2004; Opresko, Mason et al. 2005], which may be associated with the telomeric replication fork [Arnoult, Saintome et al. 2009]. In the absence of WRN, stalled telomeric replication forks may collapse and/or undergo recombination, potentially leading to significant telomere loss and telomere instability, similar to the molecular characteristics of

WS [Bai and Murnane 2003; Chang, Multani et al. 2004; Crabbe, Jauch et al. 2007]. By performing high-fidelity fork regression in telomeric repeating sequences, WRN may help maintain telomere sequence and structural integrity in the event of replication difficulties, thereby evading the telomere dysfunction and premature aging observed in human WS.

CHAPTER 4

RECOMBINATION-RELATED STRUCTURAL PREFERENCE OF WRN AT PHYSIOLOGICAL SALT CONCENTRATIONS

INTRODUCTION

In response to stalled or blocked replication forks, various mechanisms are often employed to maintain genomic stability. Bulky DNA damage or secondary structures on the leading or lagging strands that block replication may be bypassed by translesion polymerases or be repaired following regression. However, homologous recombination (HR) may also be employed under these circumstances as an error-free mechanism to allow replication to continue past a blockage [Wu and Hickson 2006]. In addition, HR is the preferred pathway of double-strand break repair at stalled replication sites [Arnaudeau, Lundin et al. 2001]. Regardless of the specific mechanism, proper HR requires efficient completion of strand invasion, branch migration, and resolution [Hiom 2001]. Diseases resulting from a deficiency in any of these HR steps are characterized by genomic instability and a predisposition for cancer [van Gent, Hoeijmakers et al. 2001], similar to RecQ-related syndromes such as WS [Salk, Au et al. 1981; Goto, Miller et al. 1996], suggesting WRN may play a role in HR. WRN homologs in both *E. coli* (RecQ) and *S. cerevisiae* (Sgs1) suppress illegitimate recombination [Harmon and Kowalczykowski 1998; Yamagata, Kato et al. 1998; Myung, Datta et al. 2001], while WRN depletion in *Xenopus laevis* egg extracts

reduces homology-based repair [Yan, McCane et al. 2005], suggesting a role in recombination may be conserved in humans. Cells derived from patients with WS are sensitive to agents that block or stall replication, including interstrand crosslinkers, topoisomerase inhibitors, and hydroxyurea [Lebel and Leder 1998; Pichierri, Franchitto et al. 2001; Poot, Yom et al. 2001], suggesting WRN plays a role in the repair of replication fork stalling potentially through a HR pathway.

In addition to WRN's preference for substrates that resemble recombination intermediates [Bohr 2008], WRN also exhibits several activities that together could suggest a role in recombination. WRN possesses a 3' to 5' helicase activity that has been demonstrated to play an important role in genomic stability at common fragile sites [Pirzio, Pichierri et al. 2008], which may be repaired by HR [Schwartz, Zlotorynski et al. 2005]. WRN can also anneal two complementary strands, an activity that seems contradictory to unwinding [Machwe, Xiao et al. 2005]. However, WRN coordinates its helicase and annealing activities to perform strand exchange *in vitro* [Machwe, Xiao et al. 2005]. During strand exchange, WRN cooperatively unwinds duplex DNA and anneals the complementary invading strand through a strand invasion intermediate. The mechanism of strand invasion is similar to branch migration, suggesting WRN may resolve recombination intermediates *in vivo*. Therefore, in response to replication fork blockage or stalling, WRN may perform branch migration and potentially resolve recombination intermediates to promote genomic stability.

Although recombination intermediates are formed throughout the genome, WRN is likely to play a more significant role in telomere HR as the genomic instability observed in WS has been linked to telomere dysfunction [Crabbe, Jauch et al. 2007]. Loss of WRN's helicase activity in murine cells leads to elevated telomeric sister chromatid exchange (T-SCE), suggesting this activity of WRN normally represses illegitimate telomere recombination [Laud, Multani et al. 2005]. Telomeric HR may be more inherently difficult since thousands of repeating units may misalign during recombination. Telomeres in mammalian cells also form a unique structure that protects the ends of linear chromosomes from double-strand break recognition and checkpoint activation [Chin, Artandi et al. 1999; Griffith, Comeau et al. 1999; Denchi and de Lange 2007]. T-loops are formed by invasion of the 3' single strand overhang into the telomeric duplex, a similar strand invasion event that occurs during HR. The 3' lagging strand overhang of telomeres invades the telomeric duplex forming a large loop structure. WS primary fibroblasts senesce with longer telomeres on average than normal controls [Schulz, Zakian et al. 1996], suggesting the premature senescence observed in WS may be due to a single critically short and/or dysfunctional telomere [Wyllie, Jones et al. 2000; Hemann, Strong et al. 2001]. Therefore, WRN may protect against telomere stability by promoting proper recombination and T-loop formation while suppressing illegitimate telomeric recombination. Specifically, I examined WRN's role at a strand invasion intermediate while focusing on the telomeric aspects of this structure. Here, I performed helicase and binding assays to investigate WRN's structural preferences of recombination intermediates, especially at physiological

intracellular salt concentrations. Telomeric sequence characteristics are considered in Chapter 5.

METHODS

Enzymes. WRN-E84A has a point mutation that eliminates the exonuclease activity [Huang, Li et al. 1998] but retains the 3' to 5' helicase activity. The enzyme was overexpressed as described in Chapter 3. DNase I and T4 polynucleotide kinase (PNK) were purchased from New England Biolabs (Ipswich, MA). BLM was overexpressed as described in [Karow, Chakraverty et al. 1997] and provided as a gift by Joanna Groden (Ohio State University). UvrD was provided as a gift by Steven Matson (University of North Carolina).

DNA substrates. All oligonucleotides used were PAGE-purified and purchased from Integrated DNA Technologies, Inc (Coralville, IA) (Table 4.1). The oligo "base" was 5' radiolabeled using ^{32}P - γ -ATP and T4 polynucleotide kinase as described in Chapter 2. To form three-way junctions, single-flap substrates, and two-stranded forks (Figure 4.1), an excess of the appropriate cold oligonucleotides (5' flap and/or 3' flap) were annealed to *base in 50 mM Tris (pH 8.0) and 10 mM MgCl_2 by heating to 90°C and slow cooling in a step-wise manner as described in Chapter 2. Three-way junction substrates, 3-way(5'-comp) and 3-way(3'-comp), were generated using a two-step annealing process. An excess of the non-complementary 3'flap(21nt) or 5'flap(21nt) were initially annealed to *base as described above. A slight excess of the flap strand

Table 4.1 Oligonucleotides used to construct HR-related substrates.

Base Oligos

***Base**

5'-CACTGACTCCAGGAAGTGGAGGATGCCTAGGTGGCCAGCTGCCGTCCAGACTCAGAGGAGTG-3'

5' Flap Oligos

5'flap(0nt)

5'-CCTAGGCATCCTCCAGTTCCTGGAGTCAGTG-3'

5'flap(5nt)

5'-CTAGTCCTAGGCATCCTCCAGTTCCTGGAGTCAGTG-3'

5'flap(21nt)

5'-TCACCTTGACAAGTGACTGTGACCTAGGCATCCTCCAGTTCCTGGAGTCAGTG-3'

5'flap(21nt)comp

5'-AGTCTGGACGGCAGCTTGTGACCTAGGCATCCTCCAGTTCCTGGAGTCAGTG-3'

5'flap(31nt)

5'-CACTTGGACCTCAAGTCCGACTCAGGCTAGTCCTAGGCATCCTCCAGTTCCTGGAGTCAGTG-3'

3' Flap Oligos

3'flap(0nt)

5'-CACTCCTCTGAGTCTGGACGGCAGCTGGCCA-3'

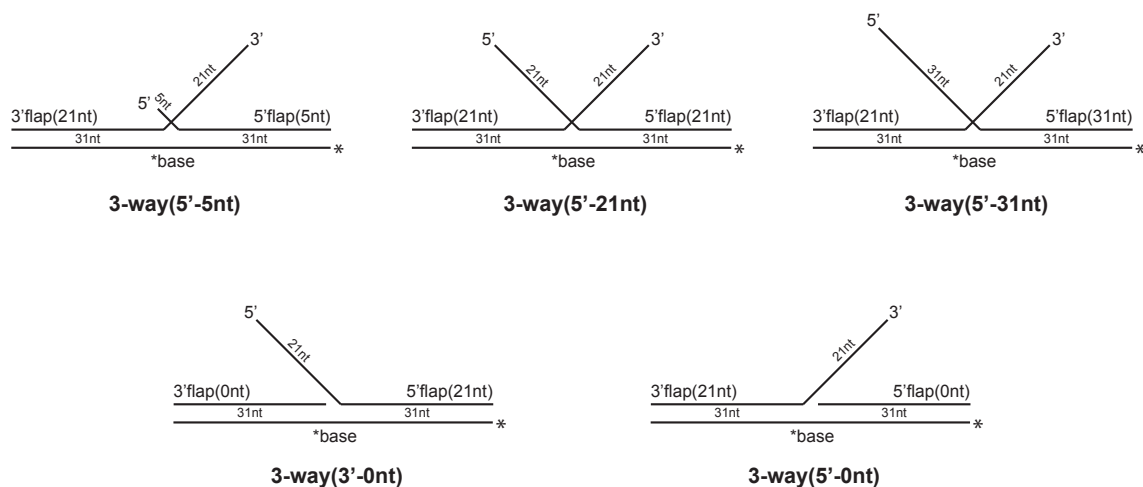
3'flap(21nt)

5'-CACTCCTCTGAGTCTGGACGGCAGCTGGCCAAGTGTGAGTGTGAGTGTGAGT-3'

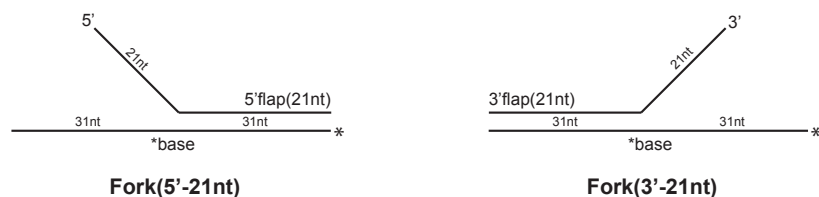
3'flap(21nt)comp

5'-CACTCCTCTGAGTCTGGACGGCAGCTGGCCAAGTGTGCATCCTCCAGTTCCT-3'

3-Way Junction Substrates



Fork Substrates



Complementary 3-Way Junction Substrates

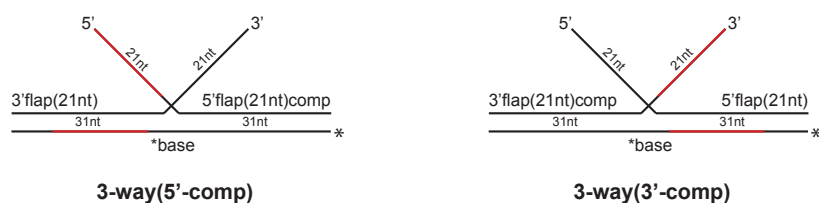


Figure 4.1 HR-related substrates. Three-way junction (top) and fork (middle) substrates were generated by annealing the indicated oligonucleotides. Complementary three-way junction substrates were annealed using a two-step process (see Methods).

containing base complementarity (5'flap(21nt)comp or 3'flap(21nt)comp) were then annealed to the respective fork at room temperature overnight. To remove unannealed strands, the substrates were electrophoresed on a 6% (19:1 unless otherwise stated) polyacrylamide native gel. The bands corresponding to each substrate were eluted in 10 mM Tris (pH 8.0) and 10 mM NaCl.

Helicase assay. Unwinding assays were performed in 10 μ L WRN reaction buffer (40 mM Tris-HCl (pH 8.0), 1 mM $MgCl_2$, 5 mM dithiothreitol, 100 μ g/mL BSA, 0.1% NP40, and 250 μ M ATP) with labeled substrate (0.2 nM), as specified in Results, and 0-100 mM NaCl. Reactions were carried out at 37°C with WRN-E84A (0.45-2.5 nM), BLM (0.31 nM), or UvrD (0.8 nM) for 0-15 min. Enzymatic reactions were stopped by addition of 0-0.16% SDS and 4 mM EDTA. Enzymes were digested using 0.4 mg/mL proteinase K at 37°C for 10 min and 1/6 volume of dyes (30% glycerol, 50 mM EDTA, 0.25% bromophenol blue, and 0.25% xylene cyanol) was added. The resulting DNA products were separated by native PAGE (6-8%). Labeled products were visualized and quantitated using the Storm 860 Phosphoimager and ImageQuant software (GE Healthcare).

Electrophoretic mobility shift assay (EMSA). To examine protein-DNA binding, EMSA was performed in 20 μ L WRN reaction buffer, except ATP was substituted with 250 μ M ATP γ S, the non-hydrolyzable ATP analog, along with 50 mM NaCl. Labeled substrate (0.1 nM), as specified in Results, and WRN-E84A (0.03-0.15 nM) were incubated at 37°C for 10 min. Either 1/6 volume of

glycerol (30%) or dyes, as indicated, was added to the reaction volume. DNA/enzyme complexes were separated from unbound substrate by electrophoresis at room temperature on 3.5% (37.5:1) native polyacrylamide gels in 1xTBE (90 mM Tris pH 8.0, 90 mM boric acid, 2 mM EDTA) without NaCl. Labeled DNA products were visualized as previously described.

DNase I footprinting. Footprinting was performed in 10 μ L WRN reaction buffer without NaCl to examine the location of WRN binding on the substrate. Radiolabeled *3-way(5'-21nt) (2.1 nM) was pre-incubated with WRN-E84A (0-5.76 nM) at 4°C for 5 min. Following WRN binding, DNase I (1 U/mL) was incubated with the DNA/WRN complexes at 25°C for 10 min. An equal volume of formamide loading buffer (95% formamide, 20 mM EDTA, 0.05% xylene cyanol, and 0.05% bromophenol blue) was added to stop the reaction. The resulting DNA fragments were heat denatured at 90°C for 5 min and electrophoresed on a 12% polyacrylamide denaturing gel. Labeled products were visualized as previously described.

RESULTS

Strand invasion intermediates are a preferred substrate for WRN in physiological salt. WRN prefers substrates that consist of complex single-strand/double-strand intersections, including structures found during recombination [Opresko, Cheng et al. 2004]. This study focused on WRN's activity on a HR-related strand invasion intermediate, a three-way junction

generated by invasion of a homologous single strand into a double-stranded region. Since the three-way junction is a predominant feature of T-loops, the protective structures found at the ends of mammalian telomeres [Griffith, Comeau et al. 1999], this recombination intermediate may provide greater insight into WRN's role in telomeric recombination. Furthermore, a three-way junction is generated during WRN-mediated strand exchange [Machwe, Xiao et al. 2005], suggesting WRN may combine its helicase and annealing activities to enhance branch migration of a similar structure during recombination. In the present chapter, I focus on the structural requirements for efficient WRN helicase activity.

To examine the structural preference of WRN as it relates to HR, I examined several structural variations of strand invasion intermediate. The three-way junction, which directly mimics a HR strand-invasion intermediate, consists of two single-stranded flaps, a 5' flap that mimics the invading strand and a non-invading 3' flap strand. These substrates consisted of a double stranded region on each side of the junction consisting of similar nucleotide composition, preventing unwinding bias. Single flap structures, *3-way(5'-0nt) and *3-way(3'-0nt) lack the 5' or 3' single-stranded flap, respectively. The two-stranded forks, *Fork(3'-21nt) and *Fork(5'-21nt) lack the strand forming the 5' flap or 3' flap, respectively (Figure 4.1). Using a WRN concentration previously determined to permit moderate but sub-saturating unwinding of 3-way (5'-21nt) substrate (data not shown), a helicase assay was performed on *3-way(5'-21nt), *3-way(5'-0nt), *3-way(3'-0nt), *Fork(3'-21nt), and *Fork(5'-21nt) in 50-200 mM

NaCl (Figure 4.2). The exonuclease-deficient WRN mutant, WRN-E84A, was used in these experiments for direct evaluation of WRN's helicase activity. Each product generated in this assay reflects displacement of one or more strands, as represented by faster migration on a native polyacrylamide gel. In the presence of ATP, WRN primarily displaced a single flap strand of $\ast 3$ -way(5'-21nt) generating a two-stranded fork product (Figure 4.2A, lane 2). A small amount of single-stranded \ast base was also generated by release of both flap strands (lane 2). While the two-stranded forks and single-flap substrates were unwound at similar levels in 50 mM NaCl, the model strand invasion intermediate $\ast 3$ -way(5'-21nt) was more efficiently unwound (Figure 4.2B). WRN-mediated unwinding of the two-stranded forks and single-flap substrates was reduced at 100 mM NaCl, while unwinding of the model strand invasion intermediate was unaffected (Figure 4.2B). WRN's preference for the model strand invasion intermediate was enhanced at 100-150 mM NaCl, but overall unwinding was significantly reduced at 200 mM NaCl (Figure 4.2B). To determine if the differing product amounts were due to WRN annealing activity, I examined the rate of unwinding of the dual-flap, $\ast 3$ -way(5'-21nt), single-flap, $\ast 3$ -way(5'-0nt), and two-stranded fork, \ast Fork(3'-21nt) substrates in 100 mM NaCl for 0-10 min (Figure 4.2C). A similar pattern of structural preference was observed even after short time points, suggesting these products resulted from structure-specific WRN helicase activity and not due to differential annealing (Figure 4.2C). Taken, together, these results indicate WRN preferentially unwinds a three-way junction structure resembling HR intermediates.

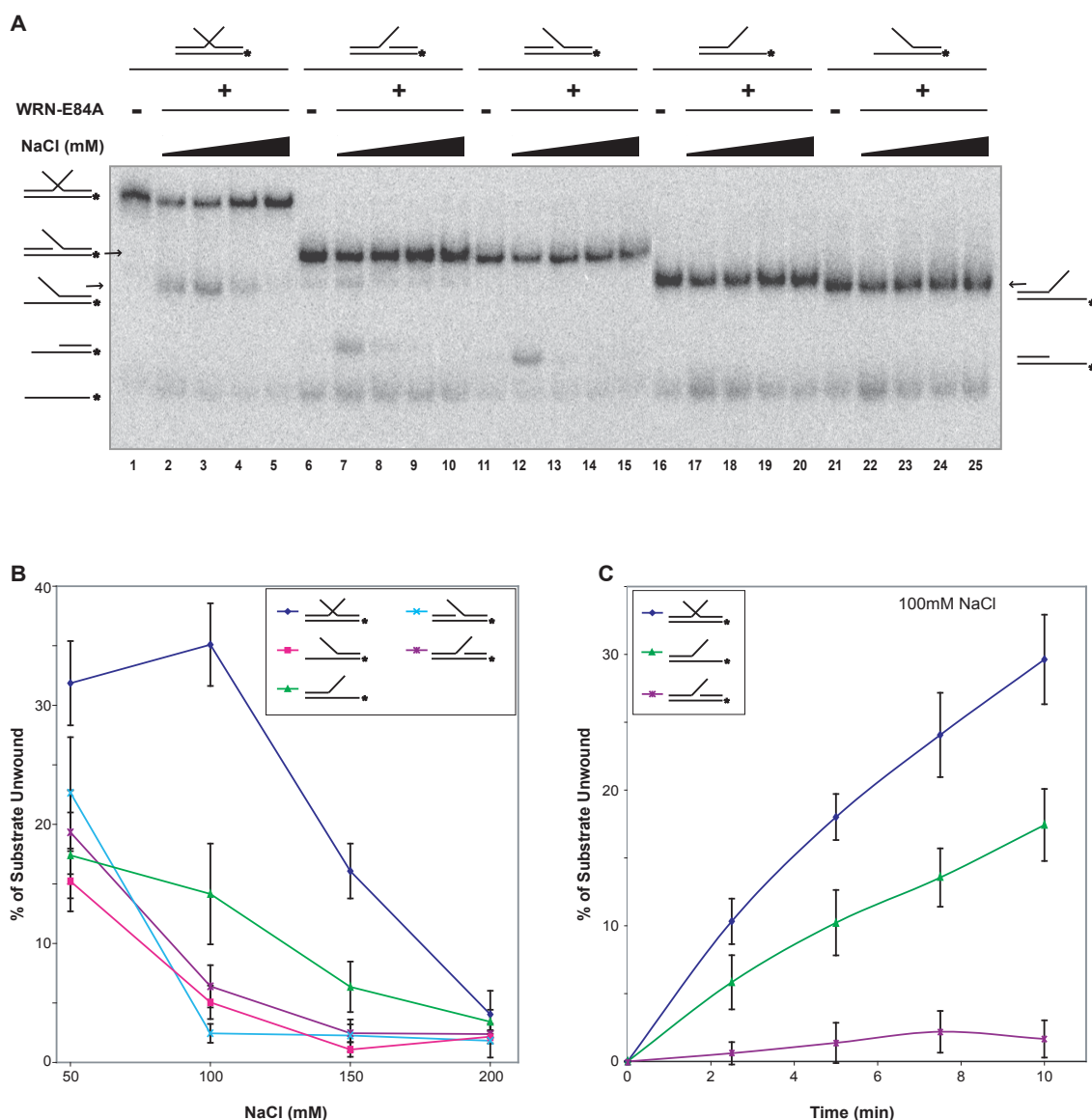


Figure 4.2 WRN preferentially unwinds model strand invasion intermediates. **A)** Helicase assays were performed on *3-way(5'-21nt) (lanes 1-5), *3-way(5'-0nt) (lanes 6-10), *3-way(3'-0nt) (lanes 11-15), *Fork(3'-21nt) (lanes 16-20), and *Fork(5'-21nt) (lanes 21-25) (0.2 nM) in 50-100 mM NaCl using WRN-E84A (0.45 nM) at 37°C for 10 min. Unwinding products were analyzed by native PAGE (6%). Structures of resulting DNA products are indicated. **B)** Calculations of percentage of original substrate converted to shorter products (mean \pm SE) using four independent experiments. Single-stranded DNA was not included in unwinding calculations of dual- or single-flap substrates. **C)** Helicase assays were performed on *3-way(5'-21nt), *Fork(3'-21nt), and *3-way(5'-0nt) (0.2 nM) in 100 mM NaCl using WRN-E84A (0.45 nM) at 37°C for 0-10 min. Unwinding products were analyzed by native PAGE (6%) (not shown). Percentage of the original substrate unwound (mean \pm SE) was calculated using five independent experiments.

Previous results indicated WRN preferentially unwound a model strand invasion intermediate compared to other related structures. To determine if greater helicase activity was a consequence of enhanced DNA binding, I examined binding of WRN-E84A protein over a range of concentration (0-200 nM) to *3-way(5'-21nt), *Fork(5'-21nt), *Fork(3'-21nt), *3-way(3'-0nt), *3-way(5'-0nt), and *base in 50 mM NaCl at 37°C for 10 min using EMSA (Figure 4.3). Discrete slower-migrating WRN-DNA complexes were generated in a WRN concentration-dependent manner, but WRN affinity varied with different structures (Figure 4.3A). WRN bound a greater percentage of the model strand invasion intermediate and *Fork(3'-21nt) compared to *Fork(5'-21nt), the single-flap substrates, or single-stranded *base. The pattern of structural discrimination observed here was mostly similar to the unwinding results. However, the helicase studies suggested the two-stranded fork *Fork(3'-21nt) was a poorer substrate than the model strand invasion intermediate.

In our experience, WRN-DNA binding is impacted by the presence of bromophenol blue (BPB) and xylene cyanol (XC), dyes used in gel electrophoresis. Since WRN bound the model strand invasion intermediate at similar levels as a two-stranded fork (Figure 4.3A-B), I examined binding of these structures under these conditions. Increasing WRN concentrations were incubated with *3-way(5'-21nt) and *Fork(3'-21nt) in 50 mM NaCl at 37°C. Following conclusion of the binding reaction, BPB and XC were added (Figure 4.3C). Under these more stringent conditions, WRN bound to the model strand invasion intermediate *3-way(5'-21nt) in a WRN-concentration dependent

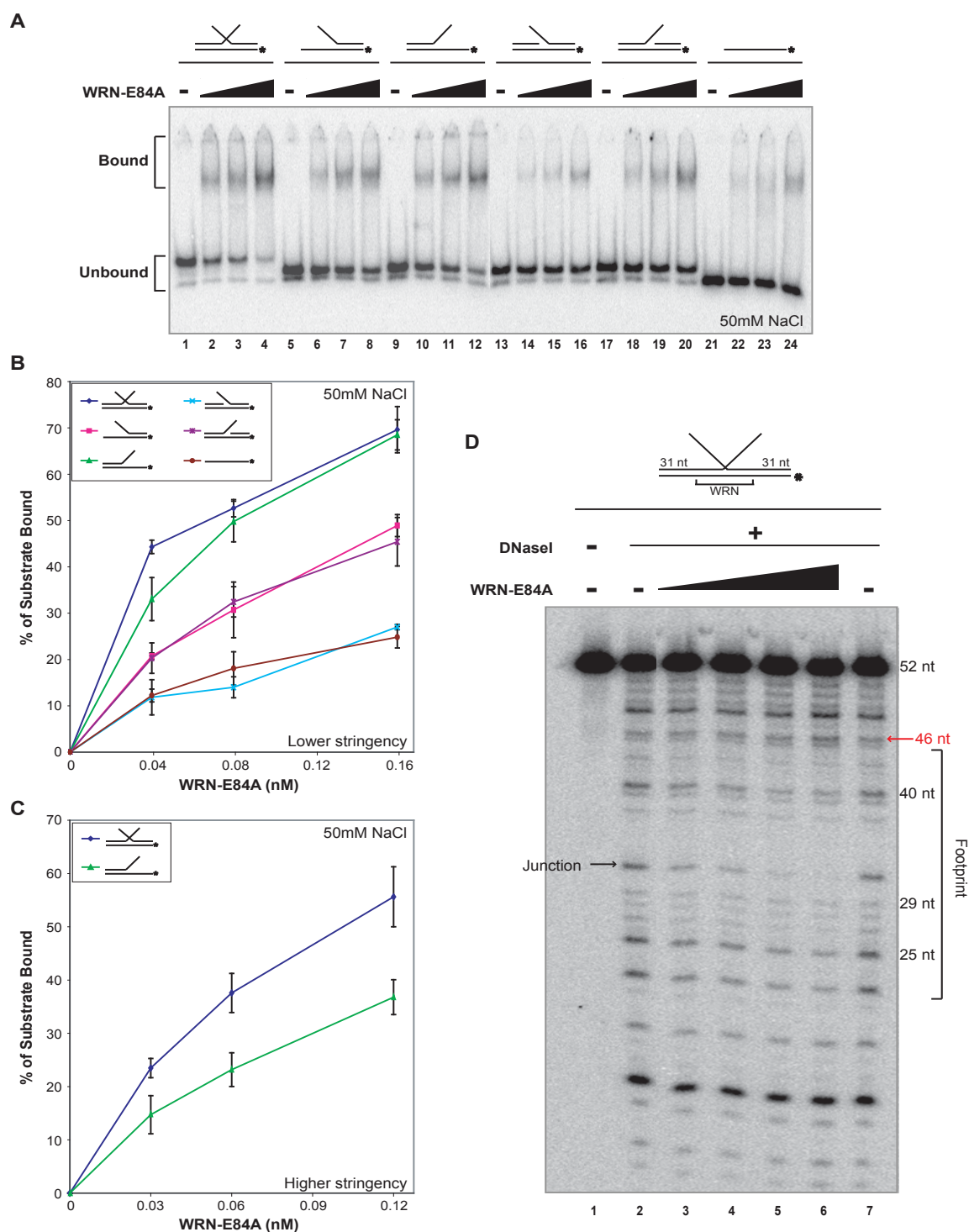


Figure 4.3 WRN more stably binds model strand invasion intermediates near the single-stranded/double-stranded junction. A) WRN preferentially binds a model strand invasion intermediate as determined by EMSA. WRN-E84A (0.038-0.15 nM) was incubated with *3-way(5'-21nt) (lanes 1-4), *Fork(5'-21nt) (lanes 5-8), *Fork(3'-21nt) (lanes 9-12), *3-way(3'-0nt) (lanes 13-16), *3-way(5'-0nt) (lanes 17-20), and *base (lanes 21-24) (0.1 nM) in 50 mM NaCl at

37°C for 10 min. Glycerol (30%) was added following the binding reaction. Binding was analyzed by native PAGE (3.5%, 37.5:1) at room temperature. **B)** Binding was quantitated as percentage of original substrate bound (mean \pm SE) using four independent experiments. **C)** WRN more stably binds a model strand invasion intermediate as determined by EMSA. WRN-E84A (0.03-0.12) was incubated with *3-way(5'-21nt) or *Fork(3'-21nt) (0.1 nM) in 50 mM NaCl at 37°C for 10 min. Glycerol (30%) with dyes (BPB and XC, 0.25% each) was added following the binding reaction. Binding was analyzed using native PAGE (3.5%, 37.5:1) (not shown). Binding was calculated as percentage of original substrate bound by WRN (mean \pm SE) using five independent experiments. **D)** WRN binds near the junction as determined by DNase I footprinting. WRN-E84A (0-5.8 nM) was incubated with *3-way(5'-21nt) (2.1 nM) at 4°C for 5 min. Subsequently, bound (and unbound) *3-way(5'-21nt) was incubated with DNase I (1.0 U/mL) at 37°C for 10 min. Labeled products were analyzed by denaturing PAGE (12%). Fragment sizes (right) and location of the junction (arrow, left) are indicated.

manner (Figure 4.3C). Overall, binding was reduced compared to Figure 4.2A-B, indicating the destabilizing nature of these conditions. However, WRN bound a greater percentage of the model strand invasion intermediate compared to the two-stranded fork ^{*}Fork(3'-21nt). Therefore, greater WRN-DNA complex stability is the likely the origin of enhanced unwinding efficiency observed by WRN on a model strand invasion intermediate.

Although gel-shift assays indicated a stable WRN interaction with a model strand invasion intermediate, the exact location of WRN binding on the 3-way junction (strand invasion intermediate) structure was determined by performing DNase I footprinting. In the absence of protein, treatment with DNase I generates a reproducible ladder of DNA fragments, as observed in lanes 2 and 7 (Figure 4.3D). When a DNA binding protein binds to the DNA, the protein protects from DNase I cleavage. Since the base strand of ^{*}3-way(5'-21nt) is radiolabeled, I examined WRN binding to the duplex region of a strand invasion intermediate, including the region near the junction of the three strands. First, to allow WRN binding to the substrate, increasing concentrations of WRN incubated with ^{*}3-way(5'-21nt) at 4°C for 5 min. Subsequently, the WRN-DNA complex was incubated with DNase I at 25°C for 10 min (Figure 4.3D). In the absence of WRN, a characteristic ladder of DNA fragments was generated, including a prominent band that was generated near the junction (31 nt) (Figure 4.3D, lanes 2, 7). However, weak cutting occurred immediately 3' to the junction limited (lanes 2 and 7). With increasing concentrations of WRN, the 31 nt band corresponding to the junction disappeared (lanes 3-6). Although to a lesser

extent, bands in the range of 22-40 nt also decreased in intensity (lanes 3-6). Furthermore, production of a 46 nt fragment was moderately increased, especially at the highest WRN concentration (lane 6), indicative of a hypersensitive site (indicated by red arrow), which highlights the 3' boundary of the WRN protein bound to the model strand invasion intermediate. Production of a hypersensitive site and protection of DNase I cleavage indicates WRN symmetrically binds to a 23 nt region of the duplex of *3-way(5'-21nt), mostly centered at the complex single/double-stranded junction, from which it mediates efficient unwinding of a model strand invasion intermediate.

WRN helicase selectively unwinds the non-invading strand of a model strand invasion intermediate. Depending on the directionality of strand invasion intermediate branch migration, WRN may promote or disrupt HR. Previous results indicated WRN unwinds a single flap strand from a model strand invasion intermediate, generating a fork product. However, the two possible fork products formed from WRN-mediated unwinding of the symmetric *3-way(5'-21nt) substrate are structurally identical and essentially co-migrated (Figure 4.2A), making it extremely difficult to determine the unwinding directionality of a strand invasion intermediate. Here, to effectively resolve the resulting fork products generated by WRN, I utilized a different model strand invasion substrate, *3-way(5'-31nt) that is identical to *3-way(5'-21nt) in the vicinity of the junction but possesses a longer 5' flap (31 nt vs. 21 nt) (Figure 4.1). On this modified substrate, displacement of the non-invading 3' flap strand produces a fork with two 31 nt single-stranded arms (Figure 4.4A, center to left).

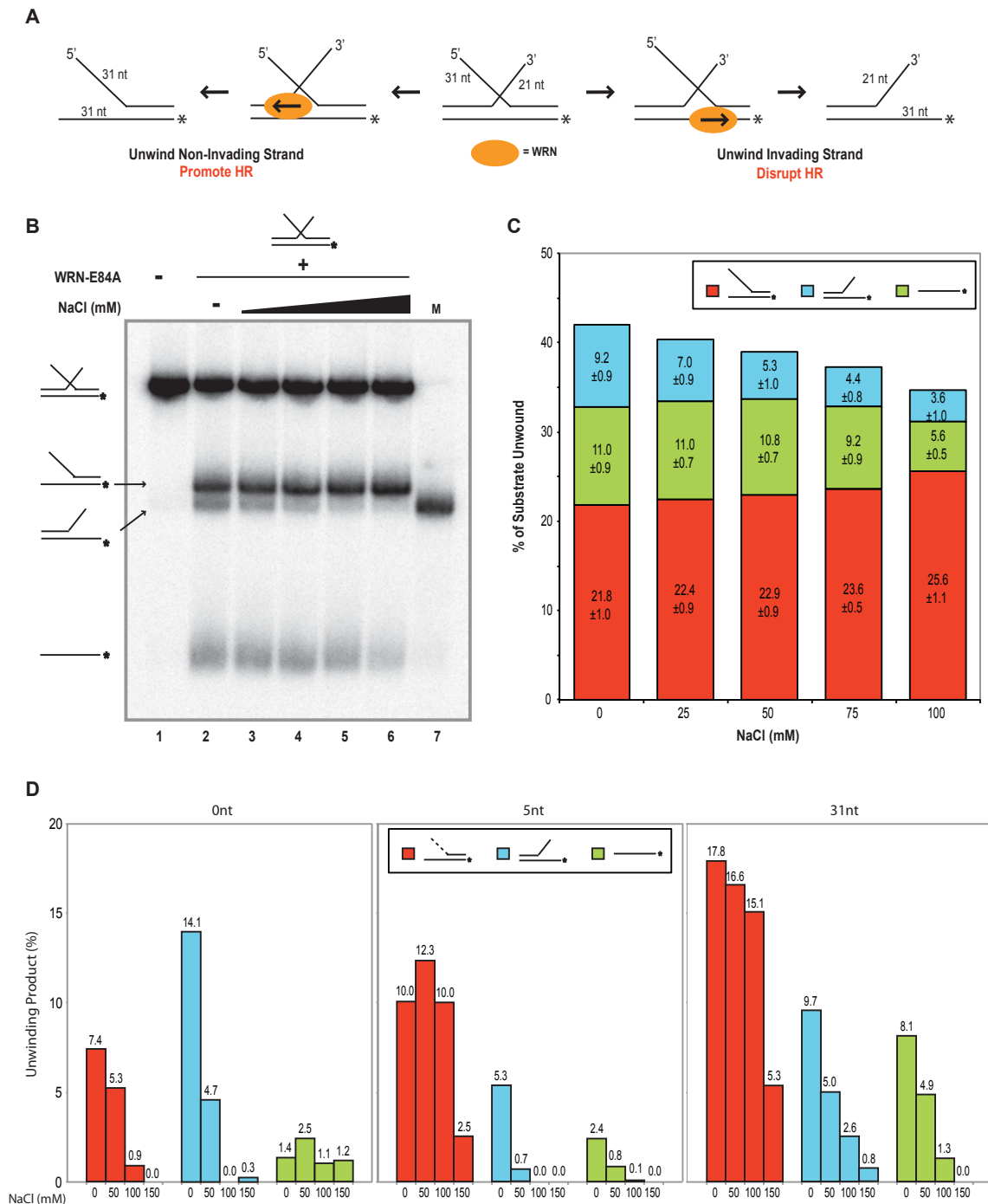


Figure 4.4 WRN unwinds the non-invading strand of a model strand invasion intermediate. **A)** Unwinding directionality may suggest a role for WRN in recombination. WRN (yellow oval) binds near the junction. Displacement of the non-invading strand (3' flap strand) results in promotion of HR (left). Displacement of the invading strand (5' flap strand) results in disruption of HR (right). **B)** Helicase assay to determine directionality. WRN-E84A (2.5 nM) was incubated with *3-way(5'-31nt) (0.2 nM) in 0-100 mM NaCl at 37°C for 15 min. Labeled unwinding products were analyzed by native PAGE

(8%). A marker for the faster migrating fork is shown. **C)** Bar graph of each individual unwinding product (mean \pm SE) using three independent experiments. **D)** A 5' single-stranded flap is required for proper directionality. Helicase assays were performed by incubating *3-way(5'-31nt), *3-way(5'-5nt), or *3-way(5'-0nt) (0.2 nM) with WRN-E84A (0.6 nM) in 0-150 mM NaCl at 37°C for 15 min. Labeled unwinding products were analyzed by native PAGE (6%) (not shown). Unwinding values are indicated above bars.

Conversely, WRN-mediated unwinding of the invading 5' flap strand generates a fork with a 31 nt 5' arm and a shorter 21 nt 3' arm that should migrate faster by native PAGE (Figure 4.4A, center to right). To determine the preferred directionality of WRN unwinding of a model strand invasion intermediate, I performed helicase assays by incubating WRN-E84A and *3-way(5'-31nt) at 37°C for 15 min; notably, these assays were performed at different NaCl concentrations ranging from 0-100 mM (Figure 4.4B-C). In the absence of NaCl, WRN unwound *3-way(5'-31nt) producing two different fork products and some single stranded *base (Figure 4.4B, lane 2). Displacement of the shorter, non-invading strand produced a larger fork product, while the smaller fork product, as confirmed by the marker (lane 7), migrated faster. Without NaCl, the primary fork product was generated by displacement of the non-invading strand (21.8%, Figure 4.4C), although a considerable percentage of the smaller fork (9.2%) and single strands (11.0%) were also produced (lane 2). Increasing the NaCl concentration reduced the amount of the smaller fork product (3.6% at 100 mM NaCl) and the single-stranded species (5.6%) while the larger fork product (25.6%) was unaffected (Figure 4.4C). These results indicate WRN preferentially unwinds the non-invading strand of a model strand invasion intermediate especially in high NaCl concentrations, a directionality that would promote HR.

These results thus far indicate WRN preferentially unwinds a model strand invasion intermediate compared to similar substrates, by almost exclusively displacing the non-invading strand (Figure 4.2, 4.4B-C). To examine

the effect of 5' flap length on unwinding and directionality, I compared unwinding of model strand invasion intermediates with 5' flap lengths of 0 nt, 5 nt, or 31 nt. The substrates *3-way(5'-0nt), *3-way(5'-5nt), and *3-way(5'-31nt) were unwound by WRN-E84A at a range of NaCl concentrations (0-150 mM) at 37°C for 15 min (Figure 4.4D). Although other products are generated, WRN primarily unwound the non-invading strand of *3-way(5'-31nt), especially in 100 mM NaCl (15.1%) (right panel), a result similar to Figure 4.4B-C. Shortening the length of the 5' flap to 5nt (*3-way(5'-5nt)) did not alter the preferred directionality, although the extent of unwinding was reduced at all NaCl concentrations (10% at 100 mM NaCl) with respect to the substrate with the longer 5' flap substrate (middle panel). However, results on the substrate without a 5' flap, *3-way(5'-0nt) were markedly different. In the absence of NaCl, WRN primarily unwound the invading strand, producing more of the shorter fork product (14.1%) compared to the larger fork (7.4%) (left panel). Production of all unwinding products of *3-way(5'-0nt) was reduced at greater NaCl concentrations. These results indicate that a 5' flap, even those that are extremely short in length, is a structural requirement for efficient unwinding by WRN. Although the invading strand (5' flap strand) was largely unaffected by the WRN helicase, the 5' flap promoted displacement of the non-invading strand, a directionality that favors additional HR.

Invading strand complementarity enhances WRN-mediated unwinding of the non-invading strand. The strand invasion intermediate substrates used in Figures 4.2-4.4 contained all unique, non-homologous sequences. However,

during HR, both the invading and non-invading strands would be completely homologous to the double-stranded DNA to which they anneal. Therefore, I examined the effect of sequence complementarity within a model strand invasion intermediate on WRN-mediated unwinding. Two new three-way junction substrates, *3-way(5'-comp) and *3-way(3'-comp), were designed with 5' or 3' single-stranded flaps that, for the 16 nt distal to the junction point, are complementary to the sequence on the labeled base strand (Figure 4.1, complementary sequences indicated in red). On each of these flaps, 5 nt regions of non-complementary sequence was included proximal to the junction to prevent spontaneous branch migration. The *3-way(5'-21nt) substrate used in previous experiments that lacks complementary sequence on both flaps was utilized as a comparative control. Helicase assays were performed by incubating WRN-E84A with *3-way(5'-comp), *3-way(3'-comp), or *3-way(5'-21nt) in 50-200 mM NaCl at 37°C for 15 min (Figure 4.5A-B). WRN unwound *3-way(5'-21nt), which lacks complementary sequence, at 50 mM NaCl (Figure 4.5A, lane 8), but unwinding was reduced at greater NaCl concentrations (lanes 9-11) since lower WRN concentrations were used compared to Figure 4.4. Compared to *3-way(5'-21nt), overall unwinding of *3-way(3'-comp), which possesses homology on the 3' flap, was slightly enhanced at 50 mM NaCl, but little unwinding was observed in 150-200 mM NaCl (Figure 4.5B). Sequence homology of the non-invading strand promoted essentially equal unwinding in both directionalities (Figure 4.5A, lane 13). However, unwinding of *3-way(5'-comp) was dramatically enhanced across the range of NaCl concentrations (Figure 4.5B). Importantly, WRN almost exclusively displaced the non-invading

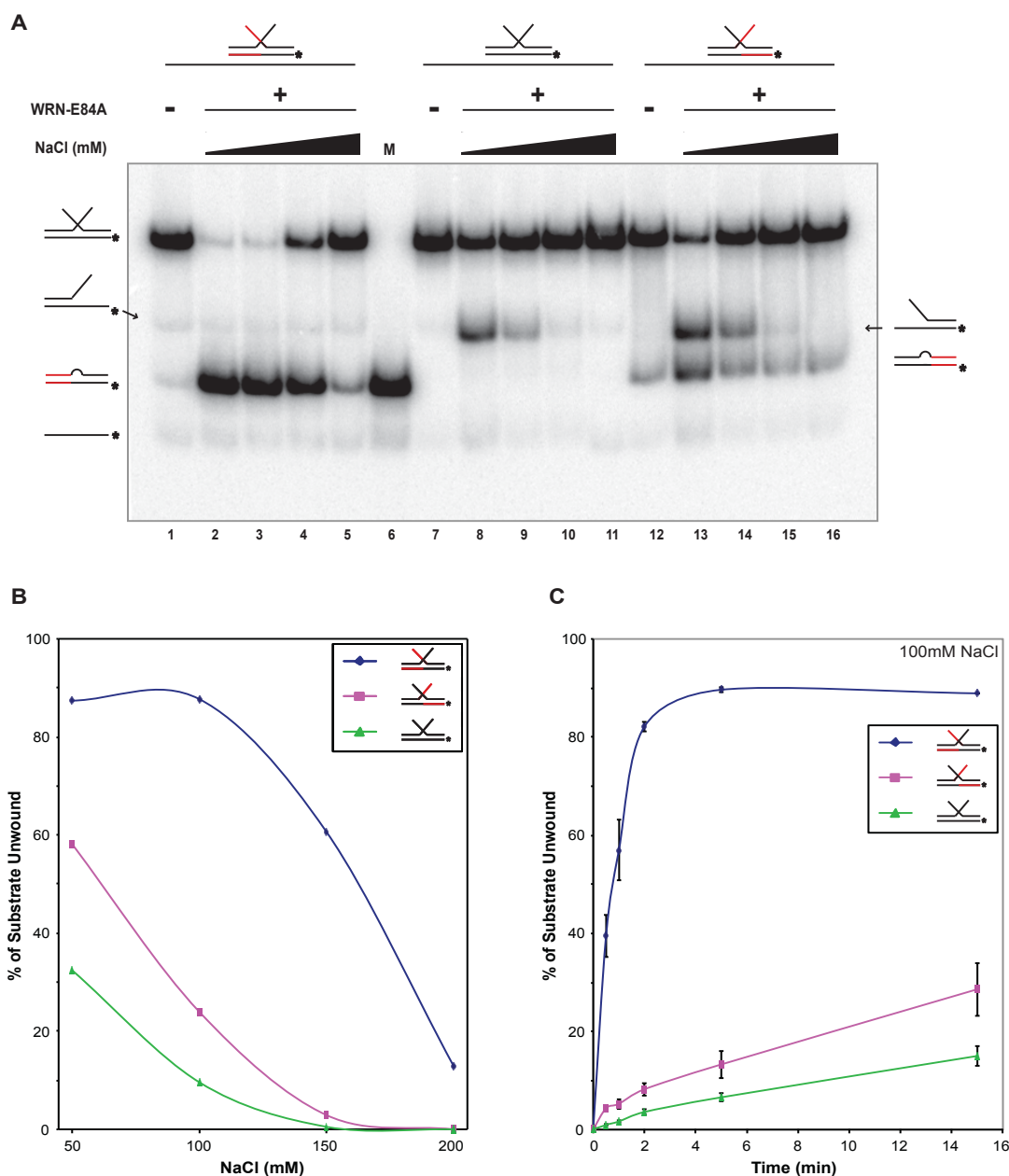


Figure 4.5 Invading strand complementarity enhances WRN-mediated unwinding. **A)** Helicase assay to examine effects of single-strand flap sequence complementarity on WRN-mediated unwinding. WRN-E84A (0.48 nM) was incubated with *3-way(5'-comp) (lanes 1-5), *3-way(5'-21nt) (lanes 7-11), or *3-way(3'-comp) (lanes 12-16) (0.2 nM) in 50-200 mM NaCl at 37°C for 15 min. Unwinding products were analyzed by native PAGE (6%). A bubble marker (M) is shown. **B)** Total unwinding was determined at each NaCl concentration. **C)** Time course of WRN-mediated unwinding of complementary substrates. In 100 mM NaCl, helicase assays were performed as above for 0-15 min. Unwinding products were analyzed by native PAGE (6%) (not shown). Total unwinding (mean \pm SE) was calculated from three independent experiments.

strand of *3-way(5'-comp) (Figure 4.5A, lanes 2-5). This result suggests invading strand sequence homology enhances WRN-mediated unwinding of the non-invading strand on a model strand invasion intermediate, especially in physiological salt concentrations.

To further investigate the impact homologous sequences have on WRN-mediated unwinding of a strand invasion intermediate, the rate of unwinding was examined at a physiologically relevant salt concentration. In 100 mM NaCl, *3-way(5'-comp), *3-way(5'-21nt), and *3-way(3'-comp) were incubated with WRN for 0-15 min at 37°C (Figure 4.5C). Compared to *3-way(5'-21nt), which lacks complementarity, 3' flap homology slightly enhanced unwinding at all time points (Figure 4.5C). Even after 0.5 min, with 5' flap homology, *3-way(5'-comp) unwinding was dramatically enhanced while unwinding was essentially complete by 5 min (89.6%). Therefore, WRN-mediated unwinding of the model strand invasion intermediate with 5' flap complementarity exhibited a dramatically accelerated reaction rate compare to other substrates. These results suggest the homology of the invading strand enhances WRN's helicase activity, especially in physiological salt conditions. The directionality at strand invasion intermediates observed in these and other experiments suggest WRN may promote HR.

Other helicases do not exhibit the same structural requirements as WRN.

The previous results indicate WRN may preferentially act at HR-related D-loops to promote proper recombination or telomere protection. However, other

helicases may possess similar structural requirements as WRN. Therefore, to determine WRN's specificity for strand invasion intermediates, the unwinding activity of other helicases with 3' to 5' directionality, including BLM and *E. coli* UvrD, was examined. The RecQ helicase, BLM, is deficient in the cancer predisposition disorder, Bloom's syndrome (BS) [Ellis, Groden et al. 1995; German 1997]. Like WRN, BLM possesses a 3' to 5' helicase, annealing, strand exchange, and fork regression activities [Karow, Chakraverty et al. 1997; Machwe, Xiao et al. 2005; Machwe, Xiao et al. 2006], indicating a potential for similar roles in the cell; unlike WRN, BLM lacks an exonuclease activity. Initially, I examined BLM's helicase activity on a model strand invasion intermediate. A helicase assay was performed by incubating BLM with *3-way(5'-31nt), which consists of a longer 5' flap (31 nt), in 0-100 mM NaCl at 37°C for 10 min (Figure 4.6A-B). Like WRN, BLM efficiently unwound *3-way(5'-31nt), by almost exclusively displacing the non-invading strand producing only the larger fork product (Figure 4.6A, lane 2), a directionality that was observed across the range of NaCl concentrations (lanes 2-6). With increasing NaCl concentrations, overall BLM unwinding on this structure was reduced; however, this seemed to be a consequence of decreased production of the single stranded product (Figure 4.6B). To determine origin of the single-stranded product, a helicase assay was performed by incubating BLM with *3-way(5'-31nt) in the absence of NaCl at 37°C for 0-15 min (Figure 4.6C). After 1 min, BLM unwound the non-invading strand of *3-way(5'-31nt) producing the larger fork product; however, very little single-stranded product was generated (lane 2). A significant fraction of single strands are not generated until 10 min (lane 5), after production of the

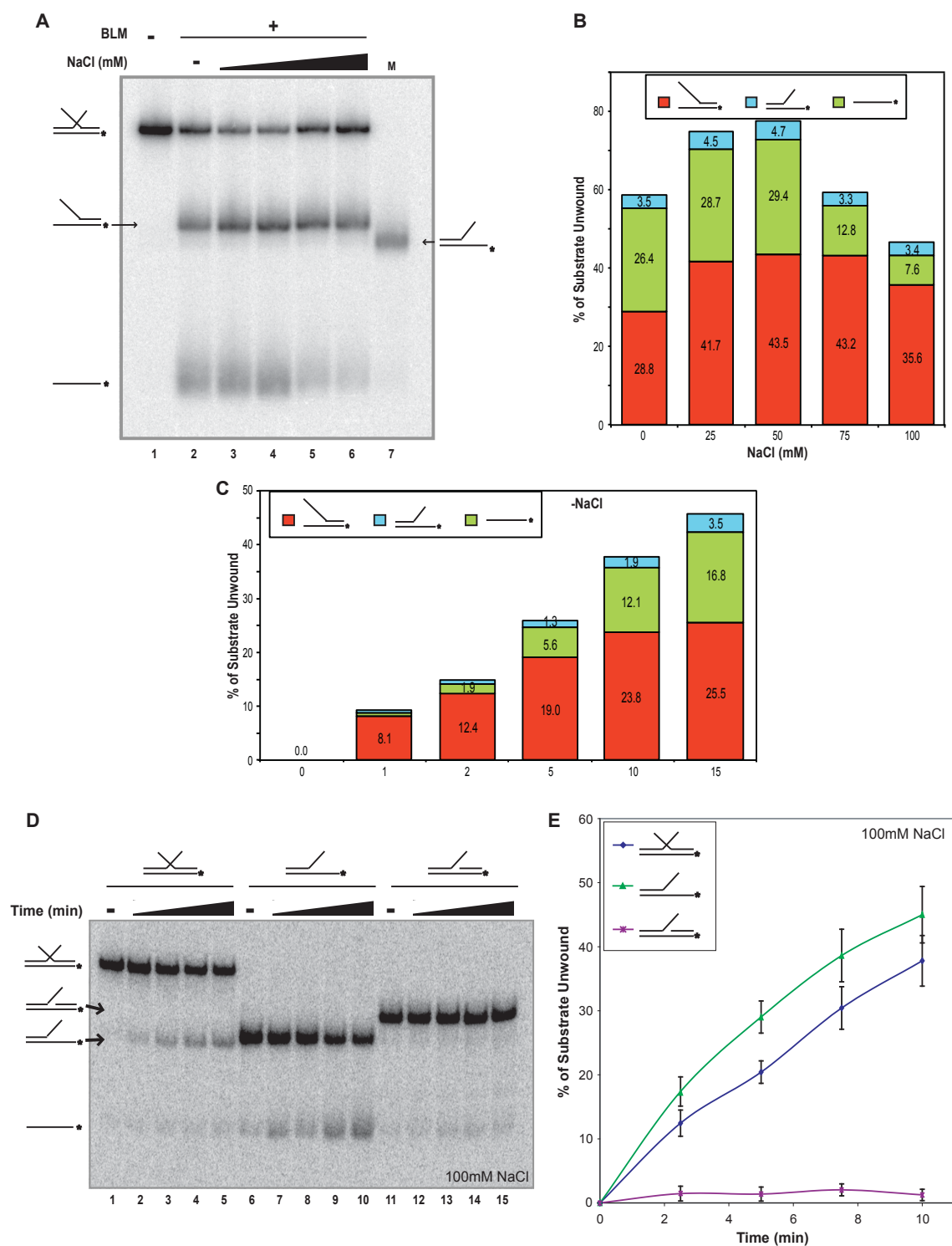


Figure 4.6 BLM directionality and structural preferences are similar to WRN. **A)** Helicase assay to determine unwinding directionality of BLM. BLM (0.31 nM) was incubated with *3-way(5'-31nt) (0.2 nM) in 0-100 mM NaCl at 37°C for 15 min. Unwinding products were analyzed by native PAGE (8%). A marker (M) of the faster migrating fork product is shown. **B)** Bar graph indicating

production of each individual product. **C)** Time course of BLM-mediated unwinding. A helicase assay was performed as described above in the absence of NaCl. Unwinding products were analyzed by native PAGE (8%) (not shown). Bar graph indicating production of each individual product. **D)** Helicase assay to determine structural preference of BLM. BLM (0.31) was incubated with *3-way(5'-21nt) (lanes 1-5), *Fork(3'-21nt) (lanes 6-10), or *3-way(5'-0nt) (lanes 11-15) (0.2 nM) in 100 mM NaCl at 37°C for 0-10 min. Unwinding products were analyzed by native PAGE (6%). **E)** Total unwinding (mean \pm SE) was calculated using three independent experiments. Single-stranded products were not included in quantitation *3-way(5'-21nt) or *3-way(5'-0nt).

fork. Therefore, BLM likely unwinds the larger fork product secondarily following the initial unwinding step, producing a single-stranded product. These results indicate BLM also preferentially unwinds the non-invading strand of a model strand invasion intermediate at physiological salt concentrations.

Although BLM efficiently unwound a model strand invasion intermediate in a salt-resistant manner, BLM may possess different structural preferences than WRN. Therefore, unwinding of a dual-flap structure, a single-flap structure, and a two-stranded fork was compared. To examine the structural requirements for efficient BLM-mediated helicase activity, helicase assays were performed by incubating BLM with *3-way(5'-21nt), *Fork(3'-21nt), and *3-way(5'-0nt) in 100 mM NaCl for 0-10 min at 37°C (Figure 4.6D-E). BLM unwound *3-way(5'-21nt) by primarily displacing a single flap strand, thus producing a fork product (Figure 4.6D, lane 1) in a time-dependent manner (Figure 4.6E). Like WRN, the single-flap structure, *3-way(5'-0nt), was a poor substrate for BLM (Figure 4.6E). However, BLM unwound the two-stranded fork, *Fork(3'-21nt), slightly better than the model strand invasion intermediate (Figure 4.6E), a significantly different result than obtained using WRN (Figure 4.2). These results were consistent at all time points examined. Therefore, these results suggest a substrate and thus functional difference between the RecQ helicases, WRN and BLM. Although BLM does efficiently act at a strand invasion intermediate substrate under physiological conditions and in a direction similar to WRN, BLM likely targets two-stranded forks in addition to strand-invasion intermediates.

E. coli UvrD (Helicase II) is a non-RecQ helicase with a 3' to 5' directionality [Matson 1986] involved in various aspects of repair, including recombination, nucleotide-excision repair (NER), and mismatch repair (MMR) [Husain, Van Houten et al. 1985; Lahue, Au et al. 1989; Mendonca, Kaiser-Rogers et al. 1993]. Like WRN and BLM, the structural preference of UvrD was examined using a model strand invasion intermediate, single-flap structures, and two-stranded forks. Structural preference was examined by performing a helicase assay on *3-way(5'-21nt), *3-way(5'-0nt), *3-way(3'-0nt), *Fork(3'-21nt), or *Fork(5'-21nt) using UvrD in 0-100 mM NaCl at 37°C for 10 min (Figure 4.7). UvrD unwound the model strand invasion intermediate, *3-way(5'-21nt), by primarily displacing the invading strand (Figure 4.7A, lane 2), a directionality opposite of WRN and BLM. Although, in the absence of NaCl UvrD exhibited a slight preference for the model strand invasion intermediate, UvrD helicase activity was significantly reduced at 50 mM NaCl (Figure 4.7B). Due to inefficient helicase activity in NaCl as well as altered directionality, UvrD, and likely other non-RecQ helicases, do not possess the same physiological structural preference as WRN.

DISCUSSION

Cells with defective HR often exhibit increased recombination [van Gent, Hoeijmakers et al. 2001], potentially through illegitimate recombination and/or error-prone NHEJ. Similarly, hyperrecombination is a distinguishing characteristic of WS [Salk, Au et al. 1981], suggesting WRN may play a role in

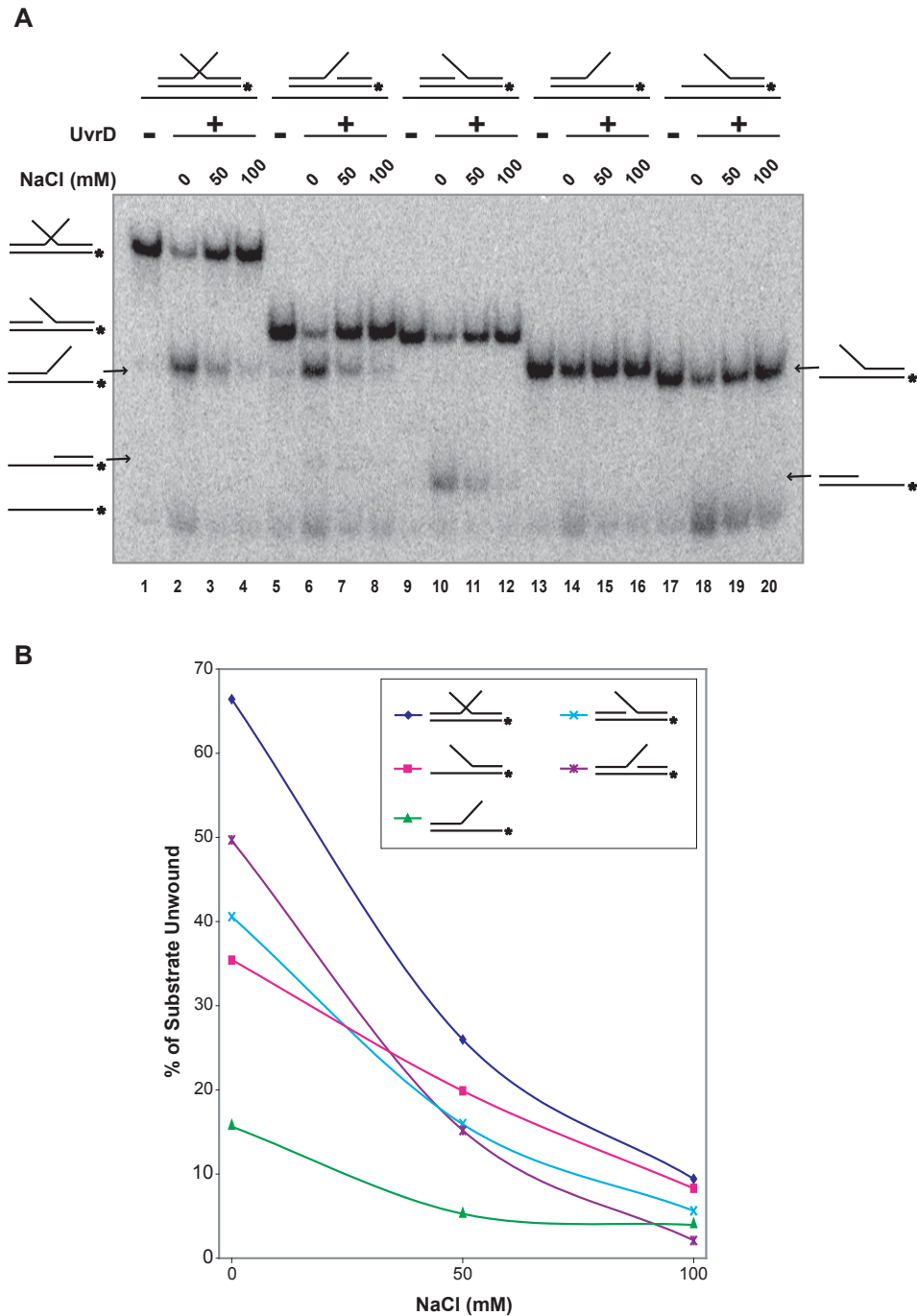


Figure 4.7 Structural preference of UvrD differs from WRN. A) Helicase assay to determine structural preference of UvrD. In 0-100 mM NaCl, UvrD (0.8 nM) was incubated with *3-way(5'-21nt) (lanes 1-4), *3-way(5'-0nt) (lanes 5-8), *3-way(3'-0nt) (lanes 9-12), *Fork(3'-21nt) (lanes 13-16), or *Fork(5'-21nt) (lanes 17-20) at 37°C for 10 min. Unwinding products were analyzed by native PAGE (6%). **B)** Total unwinding was calculated for each substrate at various salt concentrations. Single-stranded products were only included in total unwinding of *Fork substrates.

HR. Hyper-recombination associated with WRN deficiency is also elevated at telomeres [Laud, Multani et al. 2005] and is a consequence of telomere dysfunction [Crabbe, Jauch et al. 2007], suggesting WRN may play a role in telomeric HR. To determine WRN's role in telomeric recombination, I initially examined the structural requirements for efficient WRN-mediated unwinding. Although various recombination intermediates exist, such as D-loops and Holliday junctions, here I focused on WRN's helicase activity on three- stranded invasion intermediates. Importantly, a three-stranded model strand invasion intermediate may act as a favored WRN substrate since this structure is generated during WRN-mediated strand exchange [Machwe, Xiao et al. 2005]. Furthermore, the three-way junction is specifically linked to telomeres since the strand invasion intermediate is a structural component of T-loops, the telomere-protective DNA structure found at the ends of mammalian chromosomes [Griffith, Comeau et al. 1999]. Therefore, activity at this specific HR intermediate may suggest a role of WRN in telomere-specific HR.

To examine WRN's role in telomeric HR, I initially determined the structural requirements needed for efficient WRN-mediated unwinding. I performed comparative helicase assays on a model strand invasion intermediate, single-flap (5' or 3') substrates, and two-stranded fork substrates. WRN more efficiently unwound the model strand invasion intermediate compared to other substrates, especially at physiological salt conditions. This structural discrimination was not a result of differential WRN-mediated annealing, since the bias was observed at earlier time points. Binding assays

confirmed more efficient unwinding of the model strand invasion intermediate was due to more stable WRN-DNA interactions. WRN binding centered around the junction of the model strand invasion intermediate, consistent with previous reports of WRN binding near intersections of single- and double-stranded [Brosh, Waheed et al. 2002; Machwe, Xiao et al. 2002]. From the junction, WRN preferentially unwound the 3' flap strand (non-invading strand), especially at intracellular salt conditions. Importantly, efficient and salt-resistant WRN-mediated displacement of the non-invading strand required presence of a 5' flap, indicating the importance of the invading strand to WRN function. Additionally, invading strand complementarity promoted almost exclusive displacement of the non-invading strand, while bidirectional unwinding was observed with 3' flap complementarity. These results suggest WRN plays a physiological role in promoting branch migration and recombination of homologous sequences during HR. As a protein involved in telomere metabolism, these results support a role for WRN in the promotion of telomeric HR and the development of larger, more stable T-loop structures.

I also examined WRN's specificity for model strand invasion intermediates by determining the structural requirements of RecQ (BLM) and non-RecQ (UvrD) helicases in a range of NaCl concentrations. BLM, a 3' to 5' helicase deficient in the cancer-related syndrome BS [Ellis, Groden et al. 1995; German 1997], unwound the model strand invasion intermediate in a similar salt-resistant manner as WRN with a similar preference for directionality. Compared to WRN, a greater percentage of single strands were generated, but as a

consequence of secondary unwinding of the two-stranded fork product. As previously reported, BLM exhibited a greater preference for a two-stranded fork than WRN [Mohaghegh, Karow et al. 2001], indicating slight structural differences between these two enzymes that may indicate differing biochemical roles. UvrD unwound the model strand invasion intermediate at a similar extent as other related structures tested. In contrast to WRN and BLM, UvrD a 3' to 5' helicase involved in MMR and NER found in *E. coli* [Husain, Van Houten et al. 1985; Lahue, Au et al. 1989] did possess a structural preference for the model strand invasion intermediate and did not exhibit a salt-resistant helicase activity. Furthermore, UvrD primarily displaced the invading strand from all structures, a contrasting directionality from WRN and BLM. Together, these results suggest the RecQ helicase WRN may play a specific and unique role in the resolution of strand-invasion intermediates generated during HR.

The salt resistance of WRN-mediated unwinding of a model strand-invasion intermediate was quite surprising, since previous studies from our lab indicated WRN-mediated unwinding of simpler substrates, such as partial duplexes, was significantly reduced at even low NaCl concentrations, such as 50 mM NaCl (data not shown). Importantly, WRN's preference for the model strand invasion intermediate was even more pronounced at 100-150 mM NaCl, salt concentrations that correspond to the monovalent cation concentration in the intracellular environment [Thier 1986; Rottman, Gilboa et al. 1992]. Therefore, it is likely that the structural preferences of WRN in 100-150 mM NaCl presented here indicate WRN prefers acting at recombination intermediates *in vivo*. Two-

stranded forks were previously reported to act as good substrates for the WRN helicase [Mohaghegh, Karow et al. 2001; Brosh, Waheed et al. 2002]. However, these results suggest the three-way junction, or model strand invasion intermediate, is a more physiological substrate for WRN. Importantly, NaCl concentration also influenced the unwinding directionality. I found WRN unwound a model strand invasion intermediate in both directions, i.e., displaced either the invading or non-invading strand, in the absence of NaCl, a result largely consistent with previous reports [Orren, Theodore et al. 2002; Opresko, Sowd et al. 2009]. However, using a more physiologically relevant salt concentration (100 mM NaCl), WRN almost exclusively displaced the non-invading strand, especially on a substrate with invading strand sequence homology, a directionality that suggests WRN promotes HR and/or T-loop development. Therefore, these results support that strand-invasion intermediates are a physiologically relevant target for WRN, suggesting the helicase may play a role in the promotion of HR or T-loop development.

WS cells undergo elevated telomere recombination [Laud, Multani et al. 2005], suggesting WRN may play a role in telomeric HR. Proper telomeric HR may be particularly critical since the G-rich repetitive sequences composing telomeres pose difficulties for replication. As a result of replication stress, telomeres resemble fragile sites, areas of chromosome breakage and double-strand breaks that are often repaired by the error-free HR pathway [Schwartz, Zlotorynski et al. 2005; Sfeir, Kosiyatrakul et al. 2009]. In addition, the telomere instability associated with WS is a consequence of telomere dysfunction

[Crabbe, Jauch et al. 2007]. T-loops are formed by a similar strand-invasion action as occurs during HR requiring the telomere binding protein TRF2 [Griffith, Comeau et al. 1999; Stansel, de Lange et al. 2001], an interacting partner of WRN [Opresko, von Kobbe et al. 2002; Machwe, Xiao et al. 2004]. WS cells undergo a DNA damage response indicative of T-loop loss [Takai, Smogorzewska et al. 2003; Chang, Multani et al. 2004; Szekely, Bleichert et al. 2005], supporting a role for WRN at this protective structure. These results suggest WRN promotes proper telomeric HR and/or T-loop stabilization by specifically unwinding the non-invading strand, particularly under physiological salt conditions. In the absence of WRN, loss of HR or proper telomere end protection may lead to employment of other more error-prone repair pathways, including NHEJ, resulting in increased illegitimate recombination. As a result, stochastic telomere loss and telomere dysfunction may develop, cellular characteristics of WRN deficiency [Bai and Murnane 2003; Crabbe, Jauch et al. 2007] that are proposed to lead to cellular senescence or apoptosis and premature aging. In conclusion, these results suggest WRN maintains telomere stability by acting as an anti-hyperrecombinational protein, through promotion of error-free HR, suppression of error-prone recombination pathways, and/or enhancement of T-loop development and stability. To further examine WRN's possible role in T-loop formation and HR specifically at telomeres, I consider the effect of telomeric sequence on WRN-mediated unwinding of model strand invasion intermediates in the next chapter.

CHAPTER 5

TELOMERIC SEQUENCE SPECIFICITY OF RECOMBINATIONAL INTERMEDIATES OF WRN AT PHYSIOLOGICAL SALT CONCENTRATIONS

INTRODUCTION

In addition to a general maintenance role throughout the genome, WRN has been suggested to also function at telomeres, as supported by telomere localization during S phase [Crabbe, Verdun et al. 2004; Opresko, Otterlei et al. 2004]. WRN-deficient cells undergo premature senescence, but these cells are able to continue dividing following telomerase expression [Wyllie, Jones et al. 2000], strongly suggesting a telomere defect in WS. However, the greatest breakthrough in linking WS to telomeres came during development of the WS mouse model. Simply knocking out WRN in mice resulted in no obvious aging phenotype [Lombard, Beard et al. 2000]. Mice possess significantly longer telomeres (40 kb) compared to human telomeres (5-15 kb), due to greater expression of telomerase in murine cells [Kipling and Cooke 1990; Rudolph, Chang et al. 1999]. Therefore, in addition to WRN deficiency, telomere shortening was required for several generations (G4-G6) before an aging phenotype was observed [Chang, Multani et al. 2004; Du, Shen et al. 2004]. Importantly, the aging characteristics noted in these G4-G6 $Tert^{-/-}WRN^{-/-}$ mice were similar to WS, including graying and loss of hair, smaller size, cataracts, and osteoporosis [Chang, Multani et al. 2004; Du, Shen et al. 2004]. Cells

derived from these WS mice also exhibited several telomere anomalies, including a reduced telomere length compared to G4-G6 telomerase-deficient mice [Chang, Multani et al. 2004]. However, the telomere loss is potentially a consequence of a single shortened dysfunctional telomere [Wyllie, Jones et al. 2000; Hemann, Strong et al. 2001] since WS cells senesce with longer telomeres than normal cells [Schulz, Zakian et al. 1996].

In Chapter 4, I presented evidence supporting a role of WRN at strand invasion intermediates generated during HR, especially at physiological salt concentrations. WRN-deficient cells undergo elevated telomeric sister chromatid exchange (T-SCE), a defect that is rescued by a helicase-proficient WRN protein [Laud, Multani et al. 2005], suggesting WRN's helicase activity may suppress illegitimate recombination. Therefore, these HR intermediates may be particularly relevant at telomeres, not only in telomeric HR, but also in telomere end protection at T-loops. T-loops, which have been observed in mammalian cells, are formed by invasion of the G-rich 3' telomeric overhang into duplex telomeric regions [Griffith, Comeau et al. 1999]. These specialized structures may protect the ends of linear chromosomes from being recognized as a double-strand break [Chin, Artandi et al. 1999; Denchi and de Lange 2007]. The shelterin protein, TRF2, is believed to play a role in T-loop development and protection [Stansel, de Lange et al. 2001], as loss of TRF2 produces a DNA damage response indicative of telomere dysfunction [van Steensel, Smogorzewska et al. 1998; Takai, Smogorzewska et al. 2003]. Loss of WRN generates a similar damage response [Chang, Multani et al. 2004; Szekely,

Bleichert et al. 2005] that is rescued by TRF2 overexpression [Szekely, Bleichert et al. 2005], strongly supporting a role of WRN in telomere end protection. Therefore, this evidence supports a function of WRN in telomeric recombination and T-loop development as a mechanism to maintain telomere stability. Based on the results obtained in Chapter 4, I examined WRN's helicase activity at model strand invasion intermediates possessing telomere-related sequences on either the invading or non-invading strands. Since these experiments were carried out in conditions favorable for G-rich secondary structure formation, I also considered the effect G-quadruplexes and guanine hairpins have on WRN-mediated unwinding in the context of strand invasion intermediates.

METHODS

Enzymes. WRN-E84A has a point mutation that eliminates the exonuclease activity [Huang, Li et al. 1998] but retains the 3' to 5' helicase activity. WRN-K577M possesses a point mutation that eliminates the helicase activity [Gray, Shen et al. 1997; Machwe, Xiao et al. 2002]. These WRN mutants were purified as described in Chapter 3. T4 polynucleotide kinase, DNase I, and T7 Endonuclease I were purchased from New England Biolabs (Ipswich, MA). BLM and BLM-Y0795A were overexpressed as described in [Karow, Chakraverty et al. 1997] and provided as a gift by Joanna Groden (Ohio State University).

DNA substrates. All oligonucleotides were PAGE-purified and purchased from Integrated DNA Technologies, Inc. (Coralville, IA) (Table 5.1). The oligos G(1)-

Table 5.1 Oligonucleotides used to construct model strand invasion intermediates.

Mobile Junction Oligos

C(1)-83nt
5'-CACTGGTGACCTGTGCAGAGGCGGAAGGCCCTAACCCTAACCCCTAACCCCTAAGCTAGCCTGAGTCGGACTTGAGGTCCAAGTG-3'

C(2)-83nt
5'-CACTGACTCCAGGAAGTGGAGGATGCCTAGGTAAACCCTAACCCCTAACCCCTAATGGCCAGCTGCCGTCCAGACTCAGAGGAGTG-3'

G(1)-83nt
5'-CACTCCTCTGAGTCTGGACGGCAGCTGGCCATTAGGGTTAGGGTTAGGGTTAAGGCCTTCCGCTCTGCACAGGTCACCAAGTG-3'

G(2)-83nt
5'-CACTTGGACCTCAAGTCCGACTCAGGCTAGCTTAGGGTTAGGGTTAGGGTTACCTAGGCATCCTCCAGTTCCTGGAGTCAGTG-3'

Base Oligos

Base
5'-CACTGACTCCAGGAAGTGGAGGATGCCTAGGTGGCCAGCTGCCGTCCAGACTCAGAGGAGTG-3'

5' Flap Oligos

5'flap(31nt)
5'-CACTTGGACCTCAAGTCCGACTCAGGCTAGTCCTAGGCATCCTCCAGTTCCTGGAGTCAGTG-3'

5'flap(21nt)
5'-TCACTTGACAAGTGACTGTGACCTAGGCATCCTCCAGTTCCTGGAGTCAGTG-3'

5'Flap-3.5xG
5'-TTAGGGTTAGGGTTAGGGTTACCTAGGCATCCTCCAGTTCCTGGAGTCAGTG-3'

5'Flap-Gscr
5'-AGTGTGAGTGTGAGTGTGAGTCTAGGCATCCTCCAGTTCCTGGAGTCAGTG-3'

5'Flap-C
5'-TAACCCTAACCCCTAACCCCTAACCTAGGCATCCTCCAGTTCCTGGAGTCAGTG-3'

5'Flap-1xG
5'-TCACTTGACAAGTGAGGGTTACCTAGGCATCCTCCAGTTCCTGGAGTCAGTG-3'

5'Flap-1.5xG
5'-TCACTTGACAAGTTAGGGTTACCTAGGCATCCTCCAGTTCCTGGAGTCAGTG-3'

5'Flap-2xG
5'-TCACTTCTTGGGTTAGGGTTACCTAGGCATCCTCCAGTTCCTGGAGTCAGTG-3'

5'Flap-2.5xG
5'-TCACTTTTAGGGTTAGGGTTACCTAGGCATCCTCCAGTTCCTGGAGTCAGTG-3'

5'Flap-3xG
5'-TCAGGGTTAGGGTTAGGGTTACCTAGGCATCCTCCAGTTCCTGGAGTCAGTG-3'

5'Flap-4xG
5'-AGGGTTAGGGTTAGGGTTAGGGTTACCTAGGCATCCTCCAGTTCCTGGAGTCAGTG-3'

5'Flap-2.5xG-end
5'-TTAGGGTTAGGGTTACTGTGACCTAGGCATCCTCCAGTTCCTGGAGTCAGTG-3'

5'Flap-3.5xT
5'-TTGGGGTTGGGGTTGGGGTTACCTAGGCATCCTCCAGTTCCTGGAGTCAGTG-3'

5'Flap-2.5xT
5'-TCACTTTTGGGGTTGGGGTTACCTAGGCATCCTCCAGTTCCTGGAGTCAGTG-3'

5'Flap-2.5xT-end
5'-TTGGGGTTGGGGTTACTGTGACCTAGGCATCCTCCAGTTCCTGGAGTCAGTG-3'

5'Flap-2.5xT-split
5'-TTGGGGTTT TTTTGGGGTTACCTAGGCATCCTCCAGTTCCTGGAGTCAGTG-3'

5'Flap-3.5xl
5'-TTAGGTTAGGTTAGGGTTACCTAGGCATCCTCCAGTTCCTGGAGTCAGTG-3'

5'flap-WCH
5'-GTTGTCGTAGCGTTTTTCGTACGTTACCTAGGCATCCTCCAGTTCCTGGAGTCAGTG-3'

3' Flap Oligos

3'Flap-G
5'-CACTCCTCTGAGTCTGGACGGCAGCTGGCCATTAGGGTTAGGGTTAGGGTTA-3'

3'Flap-Gscr
5'-CACTCCTCTGAGTCTGGACGGCAGCTGGCCAAGTGTGAGTGTGAGTGTAGT-3'

3'Flap-C
5'-CACTCCTCTGAGTCTGGACGGCAGCTGGCCATAACCCTAACCCCTAACCCCTAA-3'

3'flap(0nt)
5'-CACTCCTCTGAGTCTGGACGGCAGCTGGCCA-3'

Other Oligos

4xGGG²²
5'-AGGGTTAGGGTTAGGGTTAGGG-3'

3xGGG²¹
5'-TTAGGGTTAGGGTTAGGGTTA-3'

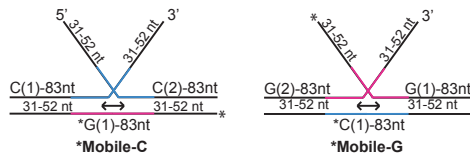
3xCCC²¹
5'-TAACCCTAACCCCTAACCCCTAA-3'

83nt, C(1)-83nt, or base were 5' radiolabeled using ^{32}P - γ -ATP and T4 polynucleotide kinase as described in Chapter 2. To generate three-way junctions (and single-flap substrates) (Figure 5.1), an excess of the appropriate unlabeled oligonucleotides (5' flap and/or 3' flap) were annealed to *base (or *G(1)-83nt or *C(1)-83nt) in 50 mM Tris (pH 8.0) and 10 mM MgCl_2 by heating to 90°C and slow cooling in a step-wise manner as described in Chapter 2. The resulting substrates were purified by native PAGE (6%, 19:1 unless otherwise stated), and the bands corresponding to each substrate were excised. Substrates were eluted in 10 mM Tris (pH 8.0) and 10 mM NaCl.

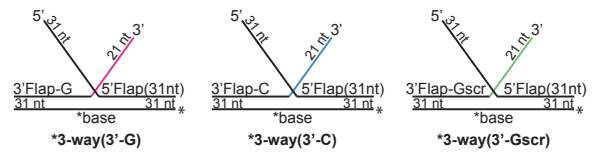
Helicase assay. Unwinding assays were performed as described in Chapter 4. Specific NaCl concentrations (0-300 mM NaCl) used for each experiment are specified in Results. Reactions were performed at 4-37°C with WRN-E84A (0.11-3.4 nM), WRN-K577M (0.2-0.9 nM), BLM (0.16-0.5 nM), or BLM-Y0795A (0.4-36 nM) for 0-15 min. Enzymatic reactions were stopped by addition of 0-0.16% SDS and 4 mM EDTA. Enzymes were digested using 0.4 mg/mL proteinase K at 37°C for 10 min and 1/6 volume of dyes (30% glycerol, 50 mM EDTA, 0.25% bromophenol blue, and 0.25% xylene cyanol) was added. DNA products were separated based on size and shape by native PAGE (6%). Labeled products were visualized and quantitated using the Storm 860 Phosphoimager and ImageQuant software (GE Healthcare).

Electrophoretic mobility shift assay (EMSA). Protein-DNA binding was analyzed by EMSA in WRN helicase buffer, with ATP substituted by 250 μM

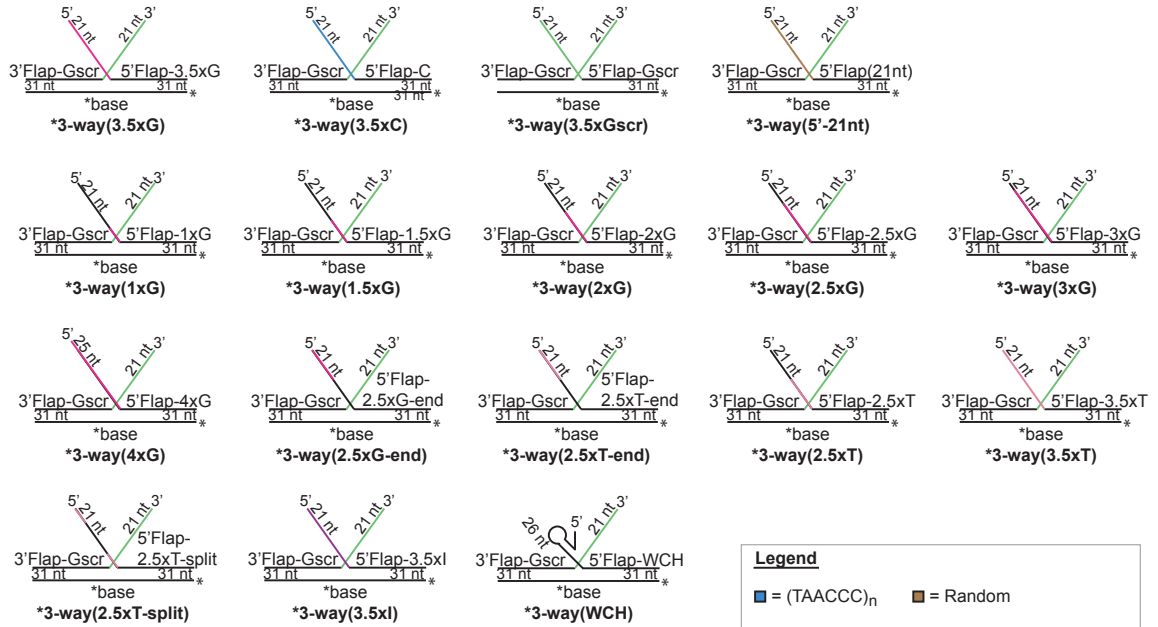
Mobile Junctions



3' Flap Variations



5' Flap Variations



Legend			
■ = (TAACCC) _n	■ = Random	■ = (TTAGGG) _n	■ = (TTAGGG) _n
■ = (TTAGGG) _n	■ = (TTAGGG) _n	■ = (AGTGTG) _n	■ = (TTAGGI) ₂ TTAGGGTTA

Binding Substrates

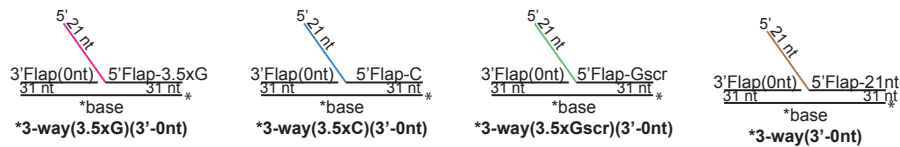


Figure 5.1 Model strand invasion intermediate substrates. Three-way junction substrates were generated by annealing the indicated oligonucleotides. Location of telomeric sequences are indicated (see Legend).

ATPγS, along with 100 mM NaCl in the reaction buffer only. Labeled single-flap substrate (0.2 nM), as specified in Results, and WRN-E84A (1.1-3.4 nM) were incubated at 37°C for 10 min. A 1/6 volume of dyes (see above) was added to the reaction. Protein-DNA complexes were separated from unbound substrate by electrophoresis at 25°C on 3.5% (37.5:1) native polyacrylamide gels without NaCl. Labeled DNA products were analyzed as previously described.

Circular dichroism (CD). The unlabeled short oligonucleotides 3xGGG²¹, 4xGGG²², or 3xCCC²¹ (0.9 O.D.; 4.3-4.7 μM) were prepared in 40 mM Tris (pH 8.0), 5 mM DTT, 1 mM MgCl₂, 1 mM EDTA, and 100 mM KCl (200 μL). The samples were incubated at 90°C for 5 min, slow cooled to 37°C, and incubated at 37°C overnight to allow DNA secondary structure formation. Immediately prior to the experiment, one sample of 3xGGG²¹ was heat denatured at 90°C for 5 min and immediately placed at 4°C. The secondary structures of these DNA oligonucleotides were analyzed by Jasco-J810 spectropolarimeter with a Peltier heating block. Using a 0.1 cm cell length, 200 μL of heated sample was analyzed within the range of 200-350 nm wavelengths at 37°C. Using a scan speed of 50 nm/min, each sample was scanned four times and an average was calculated at each point. Data was plotted as ellipticity (mdeg) at various wavelengths (nm).

Dimethyl sulfate (DMS) protection assay. The short oligonucleotide *3xGGG²¹ or the three way junction with radiolabeled 5' flap, *3-way(3.5xG) (0.2 nM) was treated with 0.5% dimethyl sulfate (DMS) (Sigma-Aldrich; St. Louis,

MO) in helicase buffer (40 mM Tris-HCl (pH 8.0), 1 mM MgCl₂, 5 mM dithiothreitol (DTT), 100 µg/mL bovine serum albumin (BSA), 0.1% NP40, and 250 µM ATP) in 0-200 mM NaCl at room temperature for 10 min, and the reaction was stopped by addition of 250 mM β-mercaptoethanol (BME) and 375 mM sodium acetate (pH 7.0). As a control, 4xGGG²², which was confirmed to form an intramolecular G-quadruplex in Chapter 2, was treated as above but in 0-75 mM KCl. DNA from each sample was collected by standard ethanol precipitation using yeast tRNA (10 µg) as a carrier. The resulting pellet was resuspended in 10% piperidine (Sigma), incubated at 90°C for 30 min, and the liquid was removed using vacuum evaporation. The samples were resuspended in 10 mM Tris (pH 8.0) and an equal volume of formamide loading buffer (95% formamide, 20 mM EDTA, 0.05% bromophenol blue (BPB), and 0.05% xylene cyanol (XC)) was added. To facilitate comparison between samples, equal amounts of radioactivity in individual samples were electrophoresed on a denaturing polyacrylamide (14%) gel. DNA fragments were visualized using Storm 860 Phosphorimager and ImageQuant software (GE Healthcare).

T7 endonuclease I hairpin analysis. In experiments with *3-way(WCH), Watson-Crick hairpin formation was confirmed by treating single-stranded *5'Flap-WCH or the 5' flap-radiolabeled *3-way(WCH) (0.2 nM) with T7 Endo I (20-200 U/mL) in WRN helicase buffer (see above) with 50 mM NaCl at 37°C for 1 hr. For markers, *3-way(WCH) (0.2 nM) was treated with DNase I (0.2-20 U/mL) in WRN helicase buffer with 50 mM NaCl at 37°C for 10 min. Reactions were stopped by addition of 1/6 volume of dyes (30% glycerol, 50 mM EDTA,

0.25% BPB, and 0.25% XC) or equal volume of formamide loading buffer (95% formamide, 20 mM EDTA, 0.05% BPB, and 0.05% XC). Labeled products were electrophoresed on a native (6%) or denaturing (14%) gel and visualized as described above.

RESULTS

G-telomeric sequence on the invading strand enhances WRN-mediated unwinding of a model strand invasion intermediate. In the previous chapter, I demonstrated a model strand invasion intermediate is a preferred substrate for WRN, especially at physiologically relevant salt concentrations (100-150 mM) (Figure 4.2). Although the structure itself is applicable to recombination throughout the genome, further analysis was required to determine how this WRN-mediated activity on a model strand invasion intermediate might be related to telomeric HR. Furthermore, these structures appear to be related to telomere-end protection, as they are generated following invasion of the G-rich 3' telomeric overhang into duplex telomeric sequence during T-loop formation, generating an intermediate with G-telomeric sequence proximal to the junction. Therefore, I explored a possible telomeric sequence preference of WRN by adding G- or C-telomeric sequences in various orientations on a model strand invasion intermediate.

Since the preferred directionality during unwinding involved displacement of the non-invading strand, WRN may preferentially bind to and translocate

along this 3' flap strand in a 3' to 5' orientation. Therefore, model strand invasion intermediates with various telomeric-related sequences located on the 3' flap strand were designed. The sequences used included a G-telomeric (5'-(TTAGGG)₃TTA-3'), C-telomeric (5'-(TAACCC)₃TAA-3'), and a scrambled version of the G-telomeric sequence (5'-(AGTGTG)₃AGT-3'), each encompassing the entire 21 nt 3' flap of their respective substrates. On this set of substrates, the 5' flap consisted of a unique, random sequence, also 21 nt in length. In addition to the two single-stranded flaps, each three-way junction contained 31 bp duplex regions on either side of the junction composed of similar nucleotide compositions to prevent unwinding bias (a preferred unwinding direction due to weaker Watson-Crick interactions), similar to the structures used in Chapter 4 (Figure 5.1). To determine if WRN possessed telomeric sequence specificity, I examined WRN-mediated unwinding of model strand invasion intermediate substrates with G-telomeric (Gtelo), C-telomeric (Ctelo), or a scrambled G-telomeric (Gscr) sequence on the 3' flap in 0-200 mM NaCl at 37°C for 15 min (Figure 5.2). Unless otherwise noted, the exonuclease-deficient mutant WRN-E84A was used throughout this chapter to study the helicase activity of WRN in isolation. The products generated in this helicase assay represent displacement of one or more strands, as indicated by faster product migration on a native polyacrylamide gel. Here, the fork products result from displacement of a single flap strand, either the non-invading 3' flap strand (slower-migrating fork) or the invading 5' flap strand (slightly faster-migrating fork) (Figure 5.2A). In the absence of NaCl, WRN generated multiple labeled products, including two forks and single-stranded base (Figure 5.2A). However,

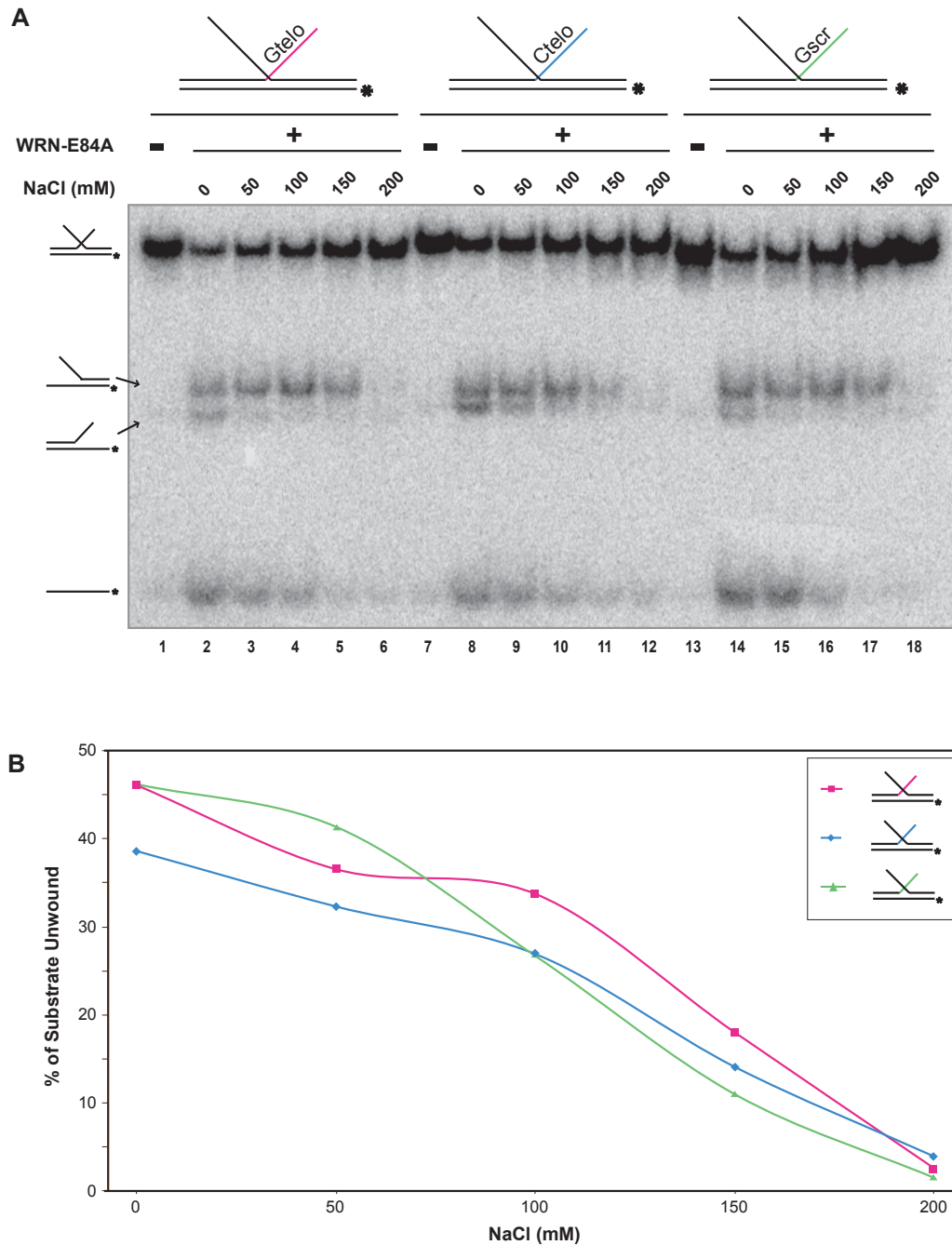


Figure 5.2 Telomeric sequence on 3' flap does not affect WRN-mediated unwinding. **A)** A helicase assay was performed on *3-way(3'-G), *3-way(3'-C), or *3-way(3'-Gscr) (0.2 nM) using WRN-E84A (0.7 nM) in 0-200 mM NaCl at 37°C for 15 min. Unwinding products were analyzed by native PAGE (6%). Structures of resulting DNA products are indicated. **B)** The percentage of original substrate converted to faster migrating products (forks + single strands) was calculated and plotted as a function of NaCl concentration.

at greater NaCl concentrations, WRN primarily displaced the non-invading strand on all substrates (Figure 5.2A), the same directionality observed with non-telomeric sequences (Figure 4.4). WRN exhibited a lesser preference for this directionality on the C-telomeric substrate (Figure 5.2A, lanes 8-12). More importantly, each substrate was unwound at similar levels across the range of NaCl concentrations (Figure 5.2B), indicating that non-invading strand telomeric sequence had little or no effect on WRN-mediated unwinding.

Since the sequence of the 3' flap did not alter WRN-mediated unwinding of a model strand invasion intermediate, I next examined the effect of telomeric sequences on the 5' flap by simply designing new substrates with the same sequences used in the previous experiments in addition to a non-telomeric random sequence on the 5' flap (Figure 5.1). However, scrambled G-telomeric sequence (5'-(AGTGTG)₃AGT-3') now composed the entirety of the 3' flap. To examine the effect of 5' flap sequence, WRN was incubated in 50-200 mM NaCl at 37°C for 15 min with model strand invasion intermediate substrates with G-telomeric (Gtelo), scrambled G-telomeric (Gscr), C-telomeric (Ctelo), or random sequence on the 5' flap (Figure 5.3A-B). Here, and in subsequent experiments, unwinding was not measured in 0 mM NaCl since multiple directionalities were observed under these conditions (Figure 5.2, data not shown). Across the NaCl concentration range, WRN preferentially unwound the non-invading strand (Figure 5.3A), a similar directionality observed in previous experiments (Figure 5.2). However, in marked contrast to substrates possessing 3' flap telomeric sequences, WRN more efficiently unwound the model strand invasion

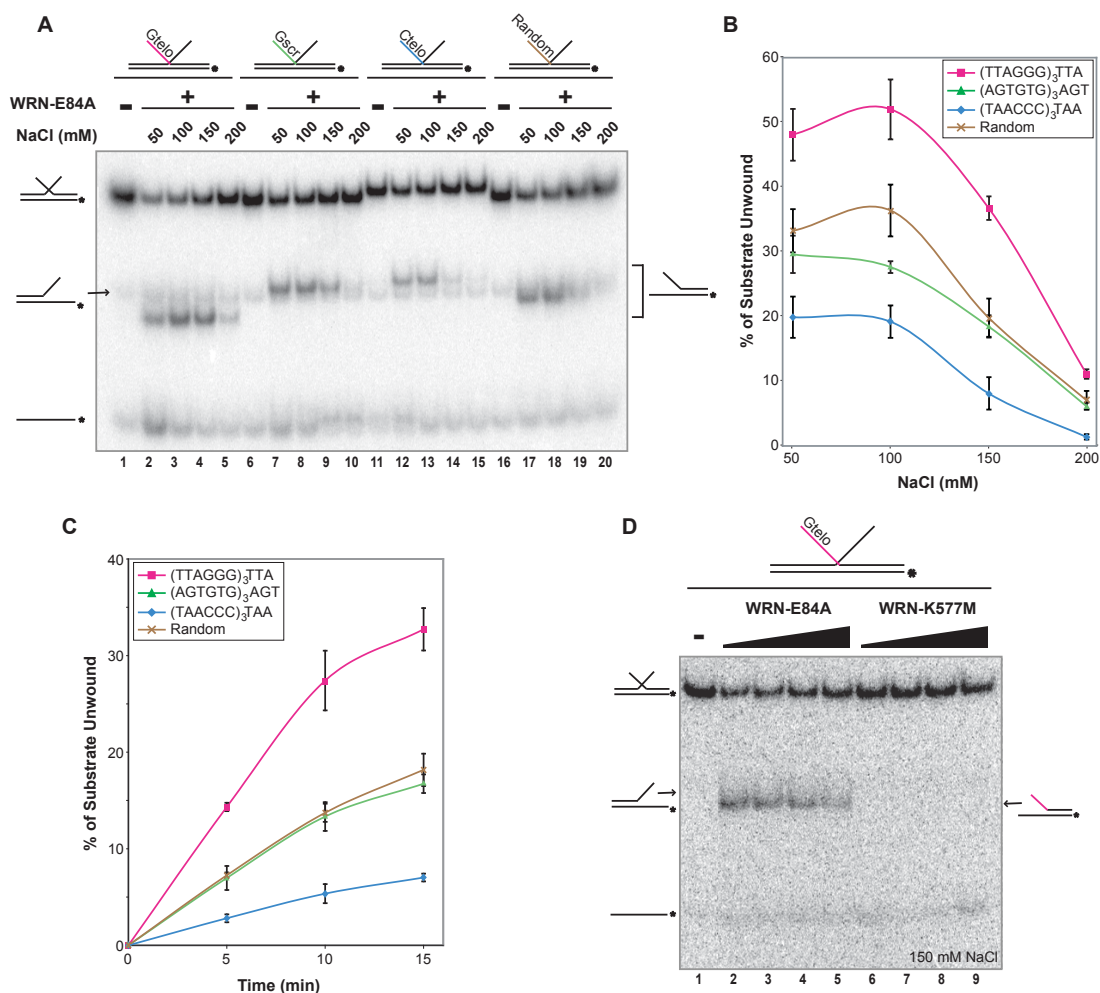


Figure 5.3 WRN preferentially unwinds model strand invasion intermediates with G-telomeric sequence on the 5' flap. **A)** To examine the effect of telomeric sequence on the 5' flap, helicase assays were performed on *3-way(3.5xG), *3-way(3.5xGscr), *3-way(3.5xC), or *3-way(5'-21nt) (0.2 nM) using WRN-E84A (0.24 nM) in 50-200 mM NaCl at 37°C for 15 min. Unwinding products were analyzed by native PAGE (6%). Structures of the unwinding products are indicated. **B)** The percentage of original substrate converted to faster migrating products was calculated (mean \pm SE) using four independent experiments and plotted as a function of NaCl concentration. **C)** WRN-mediated unwinding was further examined by performing a helicase assay of *3-way(3.5xG), *3-way(3.5xGscr), *3-way(3.5xC), or *3-way(5'-21nt) (0.2 nM) using WRN-E84A (0.2 nM) in 150 mM NaCl at 37°C for 0-15 min. Unwinding products were analyzed by native PAGE (6%) (not shown). The percentage of original substrate converted to fork products was calculated (mean \pm SE) using three independent experiments and plotted as a function of time. **D)** A helicase assay was performed on *3-way(3.5xG) (0.2 nM) using WRN-E84A (0.2-0.9 nM) or the helicase-dead mutant WRN-K577M (0.2-0.9 nM) in 150 mM NaCl at 37°C for 15 min. Labeled products were analyzed by native PAGE (6%). Structures of the resulting products are shown.

intermediate with G-telomeric sequence on the 5' flap over other sequences examined here, with the greatest sequence preference occurring at 100-150 mM NaCl (Figure 5.3B). The presence of C-telomeric sequence on the 5' flap resulted in reduced unwinding when compared to scrambled G-telomeric and even non-telomeric sequences (Figure 5.3B). I also examined the rate of unwinding of these substrates in 100 mM NaCl (Figure 5.3C). A similar preference for unwinding model strand invasion intermediates containing G-telomeric sequence on the 5' flap was observed across the examined time range, even after 5 min (Figure 5.3C). Compared to non-telomeric sequences, the presence of C-telomeric sequence also reduced WRN-mediated unwinding after 5 min (Figure 5.3C), consistent with previous results (Figure 5.3A-B). This unwinding activity of WRN is specific to the helicase domain, as WRN-K577M, which has a point mutation that eliminates helicase activity, does not unwind *3-way(3.5xG) (Figure 5.3D). Collectively, these results indicate WRN preferentially unwinds model strand invasion intermediates with G-telomeric sequence on the 5' flap, suggesting WRN may play a role in telomeric HR and/or T-loop development.

Since WRN exhibited a stronger helicase activity associated with G-telomeric sequence, I examined the possibility that WRN more efficiently bound G-telomeric sequences. Initially, I performed binding assays on these same telomeric three-way junctions used in helicase assays; however, no differences in binding were observed (data not shown). Even without telomeric sequences, these model strand invasion intermediates are very stably bound by WRN under

EMSA conditions (Figure 4.3), possibly limiting the ability to observe sequence-specific binding differences. However, a similar structure lacking the 3' flap, *3-way(3'-0nt), was a much poorer binding substrate for WRN (Figure 4.3). Therefore, I examined WRN binding to these structures with varying telomeric sequences on the 5' flap using EMSAs. Using increasing protein concentrations, WRN was incubated with 5' single-flap substrates with G-telomeric (Gtelo), scrambled G-telomeric (Gscr), C-telomeric (Ctelo), or random sequence in 100 mM NaCl at 37°C for 10 min (Figure 5.4). Each substrate was bound by WRN in a protein dependent manner, as evident by the production of a slower migrating WRN-*DNA species (Figure 5.4A). However, the G-telomeric single-flap substrate was more efficiently bound at all WRN concentrations than the other substrates examined (Figure 5.4B). A similar pattern of G-telomeric sequence-specific WRN binding was also observed in EMSAs using single-stranded DNA (data not shown). Therefore, these binding results suggest enhanced WRN-mediated unwinding of G-telomeric strand invasion intermediates is a direct result of more efficient protein binding to DNA structures containing single-stranded G-rich telomeric sequence.

To this point, the most favorable strand invasion intermediate (*3-way(3.5xG)) for WRN-mediated (and NaCl resistant) unwinding had 3.5 G-telomeric repeats ((TTAGGG)₃TTA) on the 5' flap. However, unwinding was significantly reduced when the G-telomeric sequence on the 5' flap was replaced with a random, non-telomeric sequence (*3-way(5'-21nt)) (Figure 5.3). To more closely analyze the G-telomeric sequence requirements for efficient WRN-

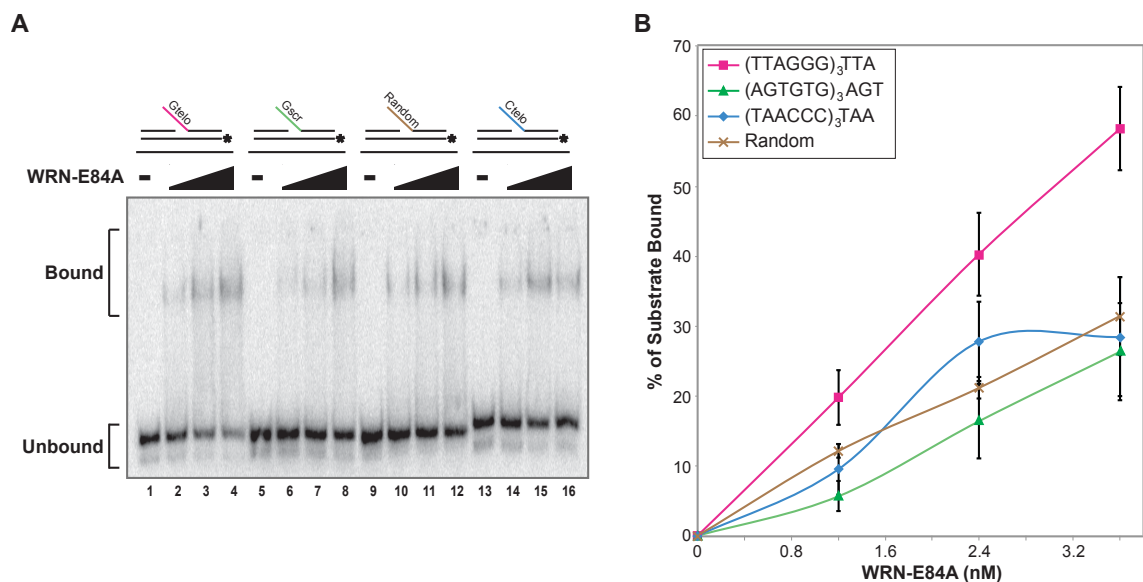


Figure 5.4 WRN preferentially binds G-telomeric sequence. **A)** EMSA's were performed by incubating *3-way(3.5xG)(3'-0nt), *3-way(3.5xGscr)(3'-0nt), *3-way(3'-0nt), or *3-way(3.5xC)(3'-0nt) (0.2 nM) with WRN-E84A (0-3.4 nM) at 37°C for 10 min. NaCl (100 mM) was included only in the reaction volume. Labeled DNA products were analyzed by native PAGE (3.5%, 37.5:1) at 25°C. **B)** The percentage of original substrate lost (mean \pm SE) was calculated using five independent experiments.

mediated unwinding, I created three-way junction substrates with 1-4 G-telomeric repeats extending from the junction on the 5' flap. Each substrate (Figure 5.1) consisted of a 5' flap that was 21 nt long, with repeats proximal to the junction; where applicable, the remainder of the sequence towards the 5' end was comprised of random sequence used previously. As a single exception, *3-way(4xG), with four complete G-telomeric repeats, possessed a 5' flap that was 25 nt long. From this point on, all three-way junctions were constructed with scrambled G-telomeric sequence on the 3' flap (Figure 5.1). A helicase assay was performed by incubating WRN with *3-way(1xG), *3-way(1.5xG), *3-way(2xG), *3-way(2.5xG), *3-way(3xG), *3-way(3.5xG), or *3-way(4xG) in 50-100 mM NaCl at 37°C for 15 min (Figure 5.5). *3-way(3xG) and *3-way(3.5xG), which both contain three GGG repeats, were most efficiently unwound by WRN (Figure 5.5A-B). However, fewer repeats significantly reduced WRN-mediated unwinding, suggesting a threshold of G-telomeric sequence may exist for optimal unwinding of these structures by WRN (Figure 5.5B). These results were consistent across the range of NaCl concentrations tested, except at 150-200 mM NaCl where overall unwinding was very low (Figure 5.5B). Surprisingly, inclusion of an additional GGG tract (*3-way(4xG)) also reduced unwinding (Figure 5.5B). These sequences, which consist of four GGG tracts, may form intramolecular G-quadruplexes, suggesting these secondary structures may alter WRN-mediated unwinding.

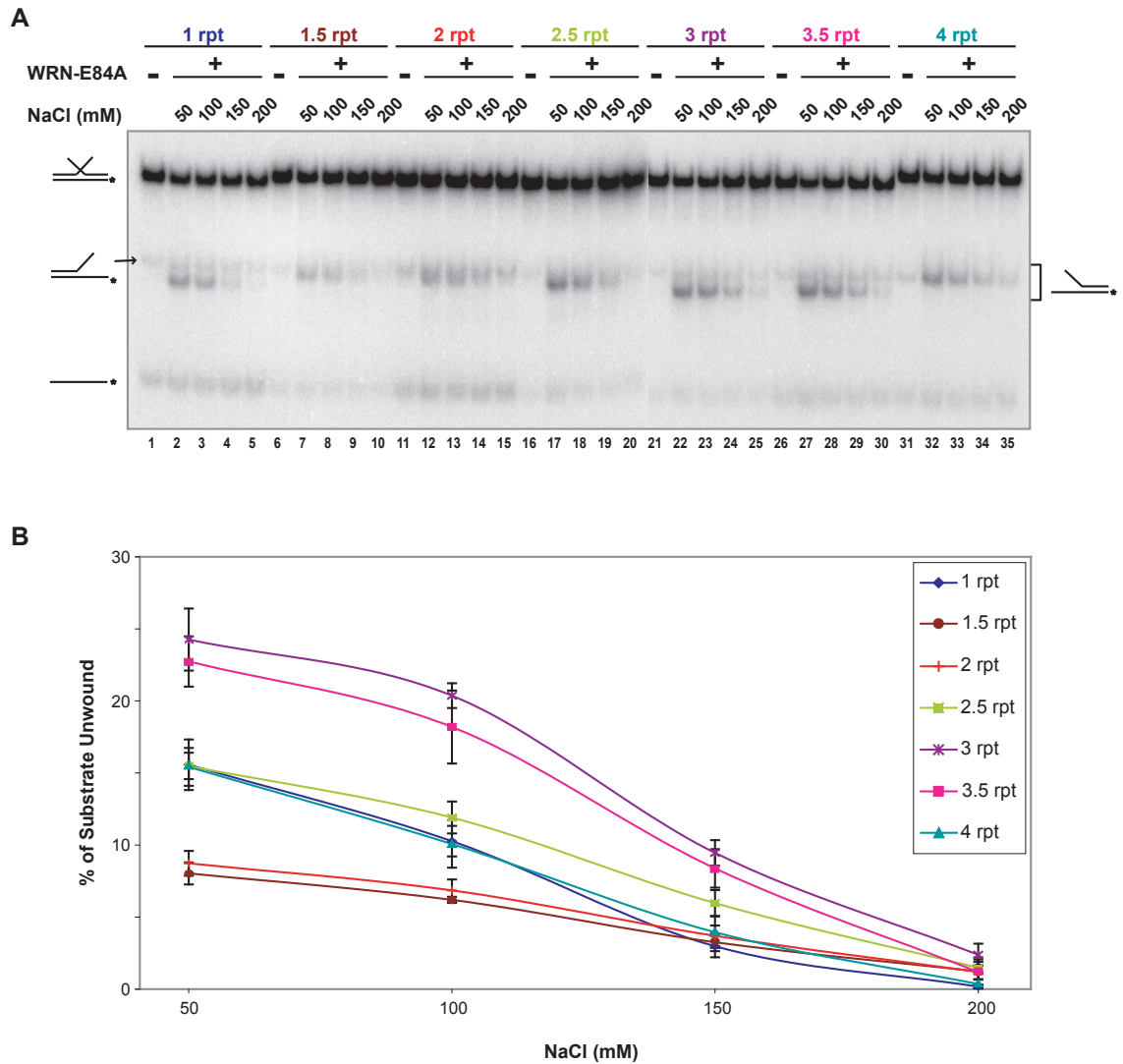


Figure 5.5 At least three G-telomeric repeats are required for efficient WRN-mediated unwinding. **A)** To examine the sequence requirements for efficient unwinding, WRN-E84A (0.23 nM) was incubated with *3-way(1xG), *3-way(1.5xG), *3-way(2xG), *3-way(2.5xG), *3-way(3xG), *3-way(3.5xG), or *3-way(4xG) (0.2 nM) in 50-200 mM NaCl at 37°C for 15 min. Labeled products were analyzed by native PAGE (6%). The resulting structures are indicated. **B)** The percentage of original substrate converted to fork products (mean \pm SE) was calculated from three independent experiments.

Enhanced WRN-mediated unwinding of G-telomeric strand invasion intermediate not due to presence of a G-quadruplex. Telomeric sequences are capable of forming various secondary structures, including G-quadruplexes. As previously discussed (Chapter 2), G-quadruplexes can be formed by the interaction of a single DNA molecule (intramolecular) or two or more strands (intermolecular). These structures are stabilized by monovalent cations, such as Na^+ or K^+ , but Li^+ disfavors G-quadruplex formation [Williamson, Raghuraman et al. 1989]. Notably, the greatest preference for *3-way(3.5xG) occurred in 100-150 mM NaCl (Figure 5.3), raising the possibility that secondary structures on the 5' flap may lead to greater WRN-mediated unwinding. While the 5' flap sequence of *3-way(3.5xG), which consists of only three GGG tracts, does not form an intramolecular G-quadruplex, this sequence may fold into an intermolecular G-quadruplex. Notably, I previously determined the 5' flap sequence of *3-way(4xG), which consists of four GGG tracts, folds into an intramolecular G-quadruplex in 75 mM KCl (Figure 2.3).

To directly examine whether secondary structure or sequence mediated greater WRN-mediated unwinding of model strand invasion intermediates, I compared WRN-mediated unwinding of *3-way(4xG) and *3-way(3.5xG) in 50-200 mM NaCl or LiCl at 37°C for 15 min (Figure 5.6A-B). G-quadruplexes readily form in the presence of Na^+ (or K^+), while the presence of Li^+ disfavors formation of these structures [Sen and Gilbert 1992]. Similar to previous experiments (Figure 5.3A), the primary products observed in reactions performed in NaCl or LiCl were two-stranded forks generated by WRN-mediated

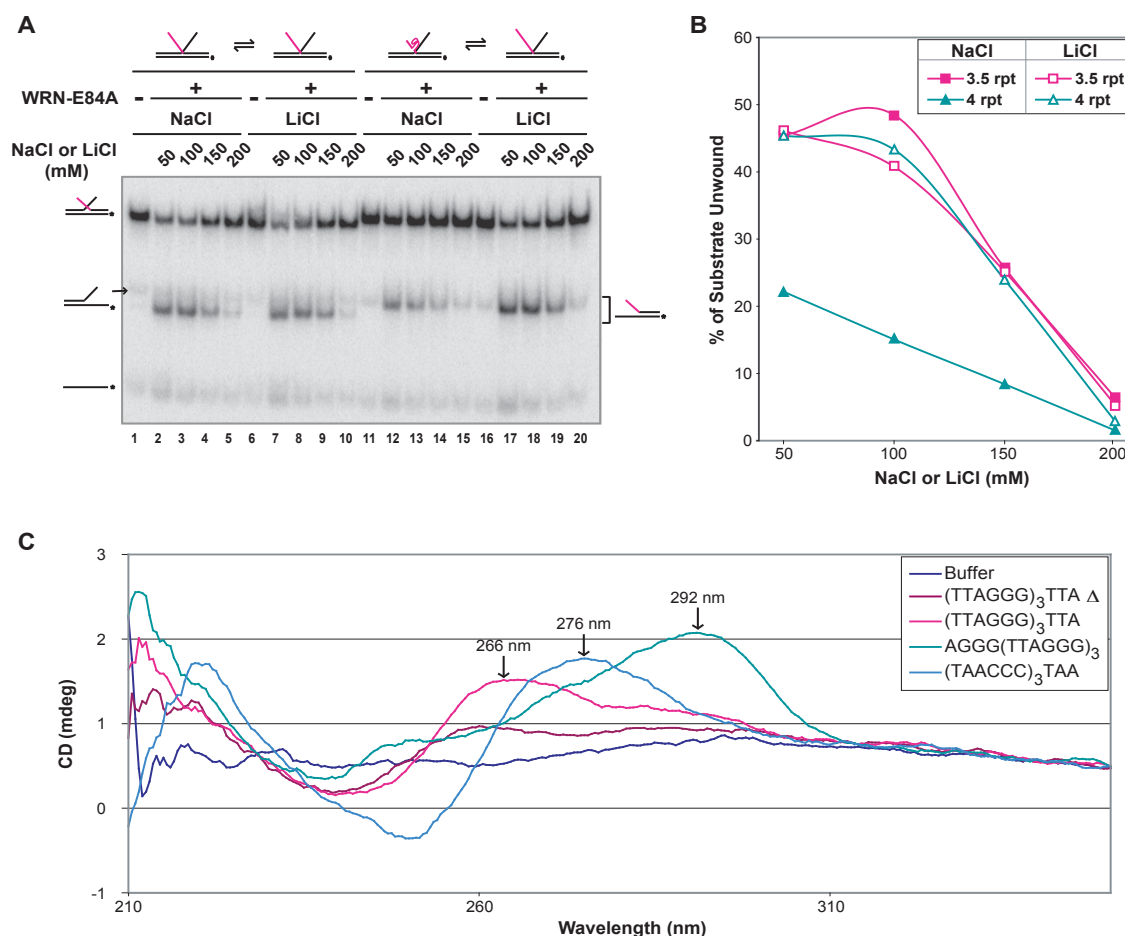


Figure 5.6 Enhanced unwinding of G-telomeric sequence not due to G-quadruplex secondary structure. **A)** A G-quadruplex on the 5' flap reduces WRN-mediated unwinding. In 50-200 mM NaCl or LiCl, WRN-E84A (0.27 nM) was incubated with *3-way(3.5xG) or *3-way(4xG) (0.2 nM) at 37°C for 15 min. Labeled products were analyzed by native PAGE (6%). The structures of the resulting products are indicated. **B)** The percentage of original substrate converted to fork products was calculated. **C)** 4xGGG²² forms an intramolecular G-quadruplex. To examine the secondary structure of the telomeric sequences used on the 5' flaps, CD was performed on 3.5xGGG²¹ (4.5 μM), 4xGGG²² (4.3 μM), or 3.5xCCC²¹ (4.7 μM) in 100 mM KCl at 37°C. The CD was calculated as millidegrees (mdeg) and plotted as a function of wavelength (nm). The maximum peaks are indicated for each sequence.

unwinding of the 3' flap strand (Figure 5.6A). WRN efficiently unwound *3-way(3.5xG) at similar levels in NaCl and LiCl (Figure 5.6B). In LiCl, *3-way(4xG) was unwound at similar levels as *3-way(3.5xG). However, WRN-mediated unwinding of *3-way(4xG) was markedly reduced in NaCl under G-quadruplex forming conditions (Figure 5.6B). These results indicate an intramolecular G-quadruplex on the 5' flap strand reduces WRN-dependent unwinding of a model strand invasion intermediate.

Although *3-way(3.5xG) does not form an intramolecular G-quadruplex, the enhanced unwinding activity may result from intermolecular G-quadruplex formation. I further analyzed the conformation of sequences found on the 5' flap of model strand invasion intermediates using circular dichroism (CD) spectroscopy, a method extensively used to detect DNA secondary structures. In solution, optically active DNA molecules absorb left and right circularly polarized light differently, depending on the structural conformation. CD measures light transmitted through DNA as ellipticity [Woody 1995], which is expressed as millidegrees (mdeg). CD measures ellipticity measured across a range of wavelengths, generating a unique spectrum for each DNA conformation. Using short oligonucleotides of the 5' flap sequences of *3-way(4xG), *3-way(3.5xC), and *3-way(3.5xG), I compared the CD spectra of unlabeled 4xGGG²², 3.5xCCC²¹, and 3.5xGGG²¹ in 100 mM KCl at 37°C (Figure 5.6C). Consistent with formation of an intramolecular G-quadruplex in KCl which exhibits a peak at 295 nm [Xu, Noguchi et al. 2006], I found 4xGGG²² generated a maximum peak at 292 nm, (Figure 5.6C). An oligonucleotide with C-telomeric

sequence, 3.5xCCC, formed a maximum at 276 nm, consistent with unstructured DNA (Figure 5.6C) [Bishop and Chaires 2003; Kaushik, Prasad et al. 2010]. 3xGGG²¹ produced a spectrum with a small peak at 266 nm, and heat denaturation of 3xGGG³¹ eliminated the 266 nm peak (Figure 5.6C). Although the spectrum of 3xGGG²¹ was consistent with a parallel intermolecular G-quadruplex structure [Bishop and Chaires 2003], these experiments were performed in higher DNA concentrations (4.27-4.74 μ M) that tend to promote intermolecular guanine Hoogsteen interactions [Sen and Gilbert 1992]. In contrast, helicase assays are performed using low DNA concentrations (0.2 nM), conditions that are less favorable for intermolecular G-quadruplex formation. However, these results do confirm the 5' flap sequence of *3-way(3.5xG) does not form an intramolecular G-quadruplex in 100 mM KCl.

To determine if the 5' flap of *3-way(3.5xG) formed an intermolecular G-quadruplex under conditions that mimic those of a helicase assay, the dimethyl sulfate (DMS) protection assay was performed. DMS specifically methylates the N⁷ position of guanines not involved in the G-quadruplex structure [Sen and Gilbert 1988; Balagurumoorthy and Brahmachari 1994]. Piperidine randomly cleaves the DNA backbone at methylated guanines, generating a pattern of radiolabeled DNA fragments when analyzed on a denaturing gel. Initially, in 0-200 mM NaCl, single stranded *5'Flap(3.5xG) or *3-way(3.5xG) (with the 5' flap strand radiolabeled) was incubated at 90°C and slow cooled to 25°C to promote any G-quadruplex formation (Figure 5.7). As a positive control for G-quadruplex formation, *4xGGG²² was incubated in 0 or 75 mM KCl (Figure 5.7, lanes 15-

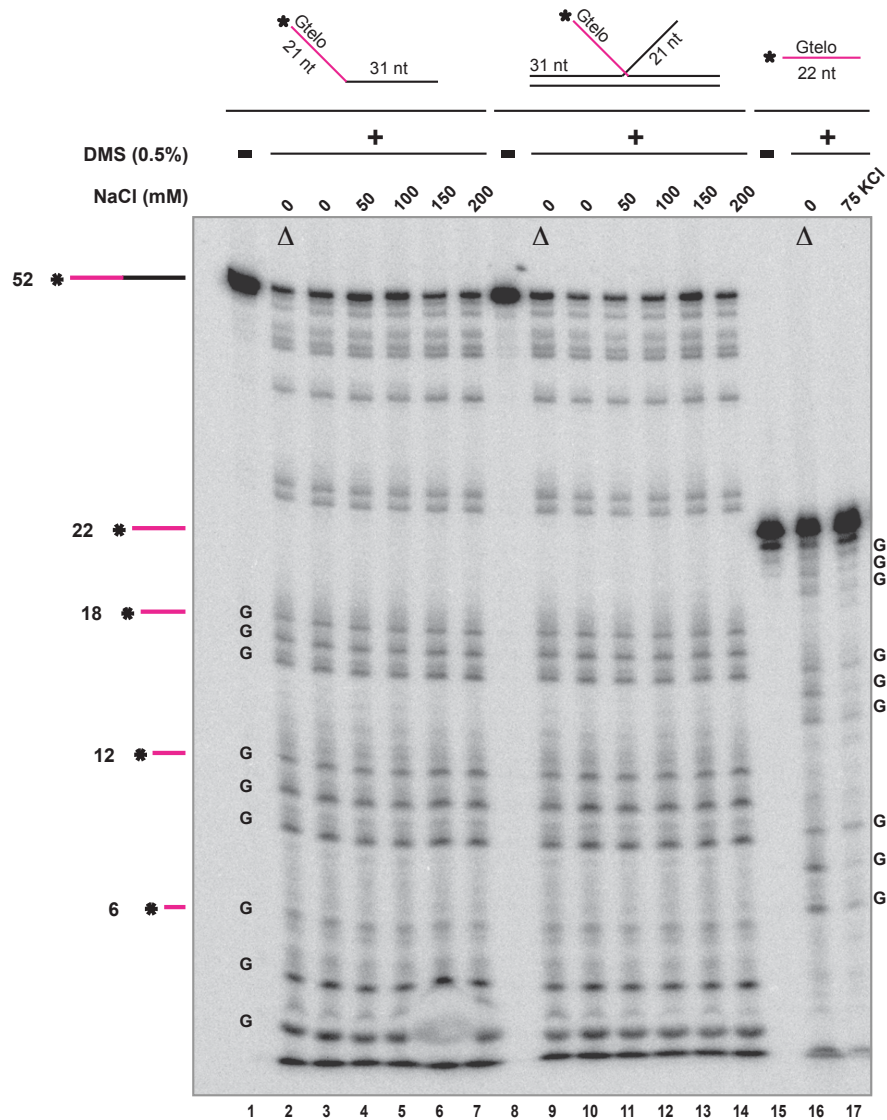


Figure 5.7 A sequence with three G-telomeric repeats does not form a G-quadruplex. To detect G-quadruplex formation, a DMS protection assay was performed on *5'flap-3.5xG or *3-way(3.5xG) (0.2 nM) in WRN buffer conditions containing 0-200 mM NaCl. As a control, *4xGGG²² (0.2 nM) was examined in 0 or 75 mM KCl. Products resulting from cleavage at unmethylated guanine bases are analyzed by denaturing PAGE (14%). Length of resulting DNA fragments are indicated on the left.

17). In the absence of KCl, a pattern of unstructured *4xGGG²² was generated (lane 16), but the intensity of these bands were reduced in 75 mM KCl (lane 17) indicating these guanines were involved in a G-quadruplex structure. However, the unstructured pattern of heat denatured single-stranded *5'Flap(3.5xG) (lane 2) and *3-way(3.5xG) (lane 9) was also observed in 200 mM NaCl (lane 7 and 14 respectively). These results indicate that, under the conditions and DNA concentrations in which these helicase assays were performed, substrates containing 3.5x G-telomeric repeats do not form intermolecular G-quadruplexes and suggest that the enhanced unwinding observed with the *3-way(3.5xG) substrate is not due to an intermolecular G-quadruplex on the 5' flap.

Guanine hairpins may not enhance WRN's preference for G-telomeric model strand invasion intermediates. Although the previous results ruled out formation of an intermolecular G-quadruplex on the 5' flap of *3-way(3.5xG), this sequence might still be capable of forming a hairpin through Hoogsteen interactions. The formation of guanine hairpins, although less stable than G-quadruplexes [Sen and Gilbert 1992], simply requires two tracts with a minimum of 3 consecutive guanines (in this case, two G-telomeric repeats) [Henderson, Hardin et al. 1987]. To examine how these structures may influence WRN-mediated unwinding of model strand invasion intermediates, a series of experiments using conditions that alter potential guanine hairpin stability were designed. Specifically, I examined how sequence location, guanine character, temperature, and flap structure affect WRN-mediated unwinding of model strand invasion intermediates.

The minimal sequence requirement for guanine hairpin formation is two GGG tracts, or two full G-telomeric repeats. With three guanine tracts, *3-way(3.5xG) is capable of forming a guanine hairpin in different frames, including locations proximal or distal to the junction. Therefore, model strand invasion intermediates were generated with two G-telomeric repeats either proximal to the junction (*3-way(2.5xG)) or distal to the junction (*3-way(2.5xG-end)). To examine the effect of G-telomeric repeat location, I performed a helicase assay on *3-way(2.5xG) *3-way(2.5xG-end), and *3-way(3.5xG) using WRN in 50-200 mM NaCl at 37°C for 15 min (Figure 5.8A-B). WRN efficiently unwound *3-way(3.5xG), generating a single fork product (Figure 5.8A, lanes 12-14) with reduced helicase activity at greater NaCl concentrations. Unwinding of both strand invasion intermediate substrates with 2.5 repeats was significantly reduced across the range of NaCl concentrations, except 200 mM NaCl due to reduced overall WRN activity (Figure 5.8B). Importantly, unwinding of both 2.5 repeat substrates was similar at all NaCl concentrations examined (Figure 5.8B).

I performed a similar experiment using strand invasion substrate containing the *Tetrahymena* telomeric sequence, TTGGGG, on the 5' flap. Compared to the human telomeric sequence (TTAGGG), *Tetrahymena* telomeric sequence possesses an extra guanine base and likely forms a more stable guanine hairpin [Henderson, Hardin et al. 1987]. In a similar manner as Figure 5.8A-B, a helicase assay was performed on control, *3-way(3.5xT) and *3-way(3.5xGscr), and test, *3-way(2.5xT) and *3-way(2.5xT-end), substrates using

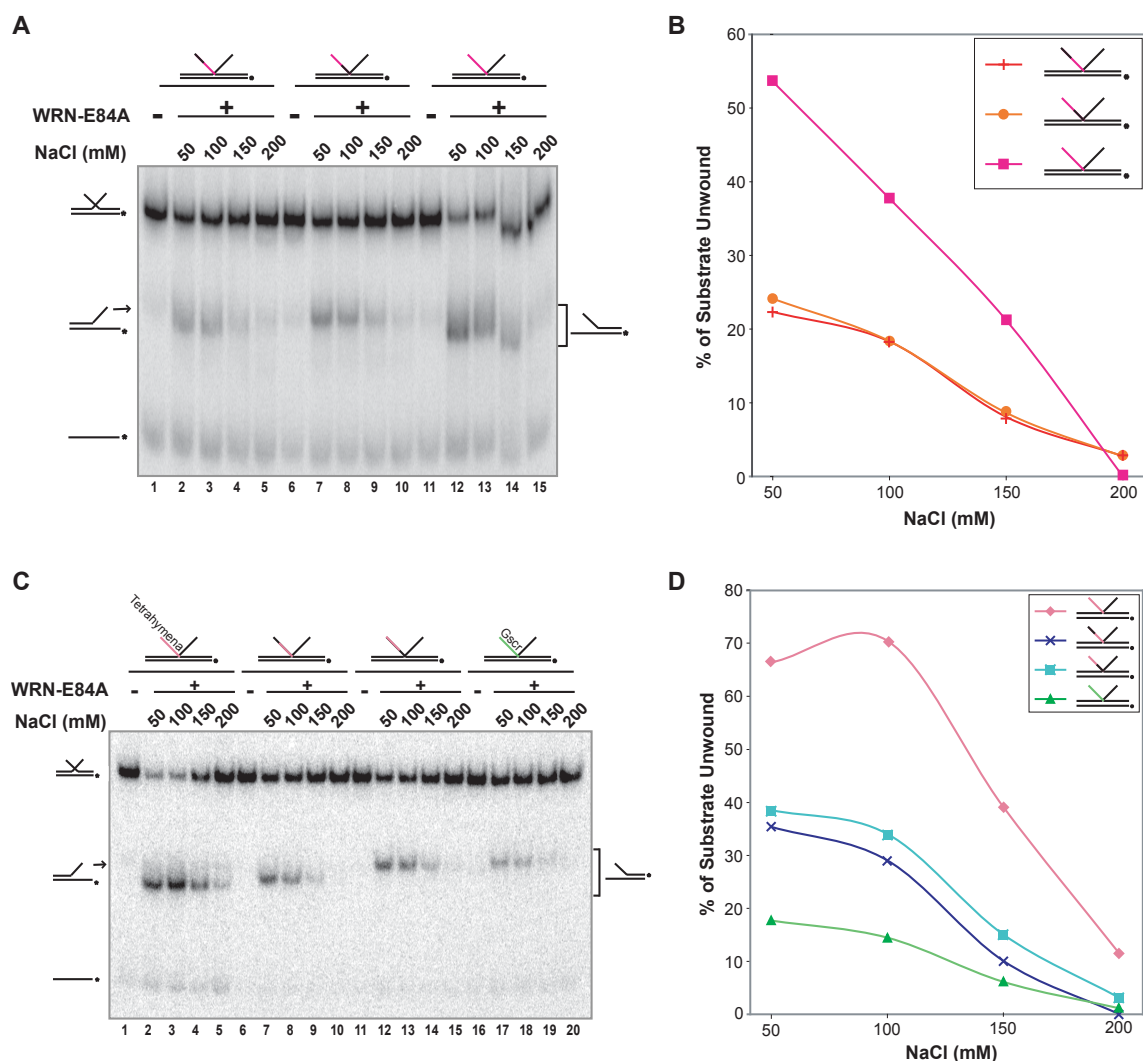


Figure 5.8 Location of G-telomeric repeats does not affect unwinding. A) To examine the effect of location of two human G-telomeric repeats, a helicase assay was performed on *3-way(2.5xG), *3-way(2.5xG-end), or *3-way(3.5xG) (0.2 nM) using WRN-E84A (0.3 nM) in 50-200 mM NaCl at 37°C for 15 min. Labeled unwinding products were analyzed by native PAGE (6%). The structures of the resulting products are indicated. **B)** The percentage of original substrate converted to fork products was quantitated. **C)** To examine the effect of location of two *Tetrahymena* G-telomeric repeats, a helicase assay was performed on *3-way(3.5xT), *3-way(2.5xT), *3-way(2.5xT-end), or *3-way(3.5xGscr) (0.2 nM) using WRN-E84A (0.11 nM) in 50-100 mM NaCl at 37°C for 10 min. *DNA products were analyzed by native PAGE (6%), and structures are indicated. **D)** The percentage of original substrate converted to fork products was calculated.

WRN in 50-200 mM NaCl at 37°C for 10 min (Figure 5.8C-D). The model strand invasion intermediate with 3.5 *Tetrahymena* repeats was efficiently unwound efficiently at all NaCl concentrations examined (Figure 5.8C, lanes 2-5). Unwinding of *3-way(2.5xT) and *3-way(2.5xT-end) were significantly reduced, but levels remained somewhat higher than the control, *3-way(3.5xGscr). However, similarly to substrates with human telomeric repeats, unwinding levels of *3-way(2.5xT) and *3-way(2.5xT-end) were very similar across the range of NaCl concentrations tested (Figure 5.8D).

Since the location of potential guanine hairpins did not appear to alter WRN-mediated unwinding, I next attempted to disrupt the stability of a possible guanine hairpin structure. Here, the sequence on the 5' flap of *3-way(3.5xG) was modified by replacing two guanines with inosine to construct *3-way(3.5xl) substrate. Inosine is identical to guanosine except it lacks the N² amino group that is involved in Hoogsteen interactions (Figure 5.9A). By replacing one guanine in two different G-runs, any potential of *3-way(3.5xl) to form a guanine hairpin has been essentially eliminated. To analyze unwinding of these structures, WRN was incubated with *3-way(3.5xG), *3-way(3.5xl), or *3-way(3.5xGscr) at various NaCl concentrations (50-200 mM) at 37°C for 10 min (Figure 5.9B-C). Inosine substitutions resulted in lesser unwinding compared to the *3-way(3.5xG) (Figure 5.9B). In fact, *3-way(3.5xl) was unwound at similar levels as *3-way(3.5xGscr), and these patterns were consistent across the range of NaCl concentrations tested (Figure 5.9C). In the same experiment, I also compared the *Tetrahymena* telomeric sequence (TTGGGG) of *3-way(3.5xT)

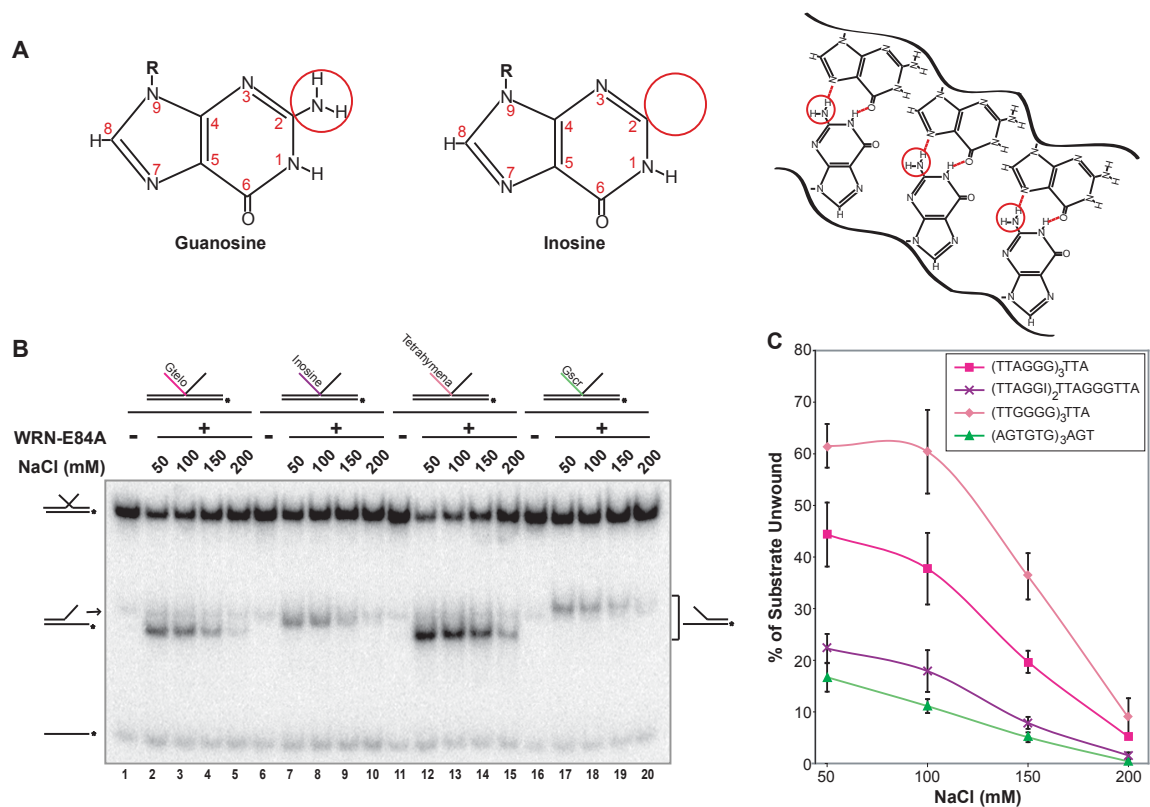


Figure 5.9 More efficient unwinding with presence of longer G-runs. A) Structures of guanosine (left), inosine (middle), and guanine hairpin (right). **B)** To examine how the length of guanine runs affects unwinding efficiency, helicase assays were performed on *3-way(3.5xG), *3-way(3.5xI), *3-way(3.5xT), or *3-way(3.5xGscr) (0.2 nM) using WRN-E84A (0.11 nM) in 50-200 mM NaCl at 37°C for 10 min. Products were analyzed by native PAGE (6%), and the resulting structures are indicated. **C)** The percentage of substrate converted to fork products (mean \pm SE) was calculated using five independent experiments.

directly to the human telomeric sequence (TTAGGG). WRN more efficiently unwound *3-way(3.5xT) (Figure 5.9B-C), suggesting WRN may prefer sequences with longer guanine tracts.

Guanine hairpins are also stabilized by cooler temperatures [Henderson, Hardin et al. 1987]. Therefore, to investigate whether *3-way(3.5xG) forms a guanine hairpin, I examined unwinding of *3-way(3.5xG) at a range of temperatures. The strand invasion intermediate substrates *3-way(3.5xG), *3-way(3.5xT), or *3-way(3.5xGscr) were incubated with WRN in 100 mM NaCl for 10 min at temperatures ranging from 4-37°C (Figure 5.10A-B). WRN more efficiently unwound the *Tetrahymena* substrate, *3-way(3.5xT), compared to the human telomeric substrate, *3-way(3.5xG), across the range of temperatures (Figure 5.10A-B). Interestingly, temperature had a marked effect on WRN-mediated unwinding of these structures; unwinding was significantly enhanced at 18-30°C (Figure 5.10B). These results were particularly interesting since WRN helicase activity is traditionally reduced at temperatures below 37°C (data not shown). However, temperature did not have a marked effect on unwinding of *3-way(3.5xGscr), although under the conditions used here overall unwinding of this substrate was minimal (Figure 5.10B).

To further enhance probability for guanine hairpin formation, I also examined substrates with the *Tetrahymena* sequence at reduced temperatures. In addition to those substrates with two *Tetrahymena* repeats proximal (*3-way(2.5xT)) or distal (*3-way(2.5xT-end)) to the junction, I also included a new

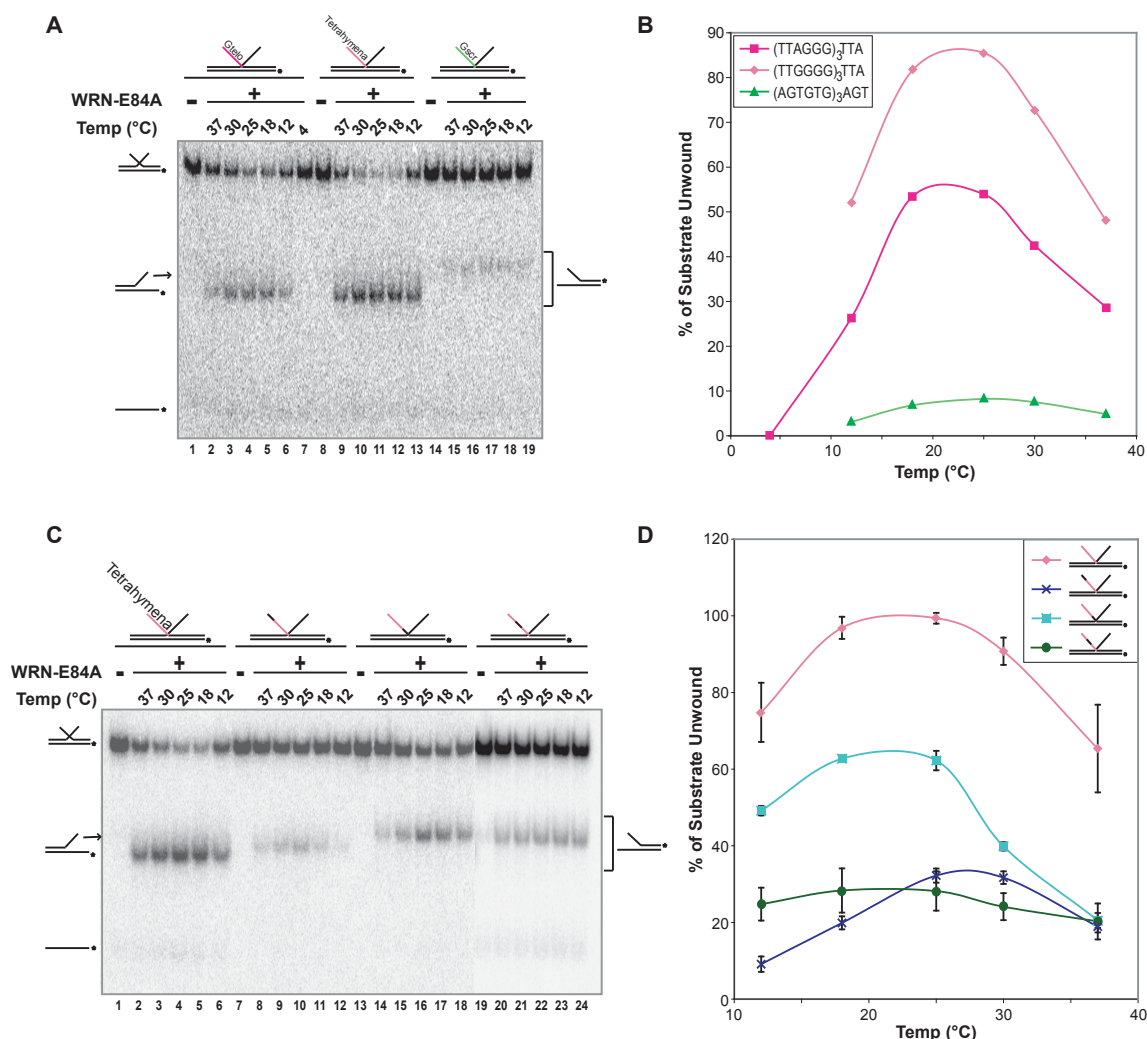


Figure 5.10 WRN-mediated unwinding is altered at lower temperatures. A) To examine the effect of temperature on WRN-mediated unwinding, a helicase assay was performed on *3-way(3.5xG), *3-way(3.5xT), or *3-way(3.5xGscr) (0.2 nM) using WRN-E84A (0.11 nM) in 100 mM NaCl at 4-37°C for 10 min. Labeled products were analyzed by native PAGE (6%). **B)** The percentage of substrate converted to fork products were calculated. **C)** Unwinding of three-way junctions with varying locations of *Tetrahymena* repeats at lower temperatures was analyzed by helicase assays. *3-way(3.5xT), *3-way(2.5xT), *3-way(2.5xT-end), or *3-way(2.5xT-split) (0.2-0.4 nM) was incubated with WRN-E84A (0.11 nM) in 100 mM NaCl at 12-37°C for 10 min. Labeled products were analyzed by native PAGE (6%). The structures of the resulting products are indicated. **D)** The percentage of original substrate converted to fork products (mean \pm SE) was calculated using three independent experiments.

substrate with one *Tetrahymena* repeat near the junction and one repeat near the 5' end (Figure 5.1), which may form a hairpin with a larger loop (*3-way(2.5xT-split)). To examine the effect of potential guanine hairpin position at lower temperatures, WRN was incubated with *3-way(3.5xT), *3-way(2.5xT), *3-way(2.5xT-end), and *3-way(2.5xT-split) using in 100 mM NaCl at 12-37°C for 10 min (Figure 5.10C-D). Consistent with previous results (Figure 5.8C-D), at 37°C, WRN more efficiently unwound *3-way(3.5xT) over other substrates possessing only 2.5 G-telomeric repeats, including *3-way(2.5xT), *3-way(2.5xT-end), and *3-way(2.5xT-split) (Figure 5.10C). However, three-way junctions with distal repeats, such as *3-way(3.5xT) and *3-way(2.5xT-end), were unwound significantly better at lower temperatures (Figure 5.10D). In contrast to substrates with distal repeats, unwinding of *3-way(2.5xT) and *3-way(2.5xT-split) was largely unaffected by temperature (Figure 5.10D).

Although experiments above were designed to investigate the possibility that hairpins formed from Hoogsteen bonding influenced unwinding by WRN, I was not able to conclusively confirm or refute hairpin formation. To examine how a definitive hairpin structure on the 5' flap may affect WRN-mediated unwinding, I generated a substrate that is capable of forming a Watson-Crick (WC) hairpin on the 5' flap, *3-way(WCH) (Figure 5.1). Initially, to determine if *3-way(WCH) formed a WC hairpin, T7 endonuclease I, which cleaves at the first three phosphodiester bonds 5' to the mismatch in the looped region of a hairpin [Babon, McKenzie et al. 2003], was used. On these substrates, formation of a WC hairpin would result in cleavage by T7 endonuclease I,

generating bands in the range of 13-15 nt. Indeed, faster migrating products were generated corresponding to the expected fragment sizes on both native (Figure 5.11A) and denaturing (Figure 5.11B), confirming formation of a WC hairpin on the 5' flap. To examine the effect of a WC hairpin on WRN-mediated unwinding, I performed a helicase assay on *3-way(3.5xG) and *3-way(WCH) using WRN in 50-200 mM NaCl at 37°C for 10 min (Figure 5.11C-D). The presence of a WC hairpin significantly reduced unwinding compared to the control *3-way(3.5xG) across the range of NaCl concentrations tested (Figure 5.11D). Although these results do not directly reflect those of a Hoogsteen-bonding hairpin, they do indicate secondary structure on the invading strand reduces WRN-mediated unwinding of a strand invasion intermediate, consistent with previous results examining the presence of an intramolecular G-quadruplex (Figure 5.6A-B).

In summary, WRN-mediated unwinding of model strand invasion intermediates was not altered by location of 2.5 repeats, the minimal requirement for guanine hairpin formation. Since these substrates were less efficiently unwound compared to those possessing 3.5 repeats, these results suggest the 5' flap of *3-way(3.5xG) is not likely to form a guanine hairpin. In contrast, the reduction in unwinding activity with the substitution of inosine, which disrupts Hoogsteen interactions, suggests the G-telomeric sequence may form a guanine hairpin. However, even the slight structural difference between guanosine and inosine may weaken WRN-DNA interactions resulting in reduced unwinding. Additionally, these results follow a pattern with sequences exhibiting

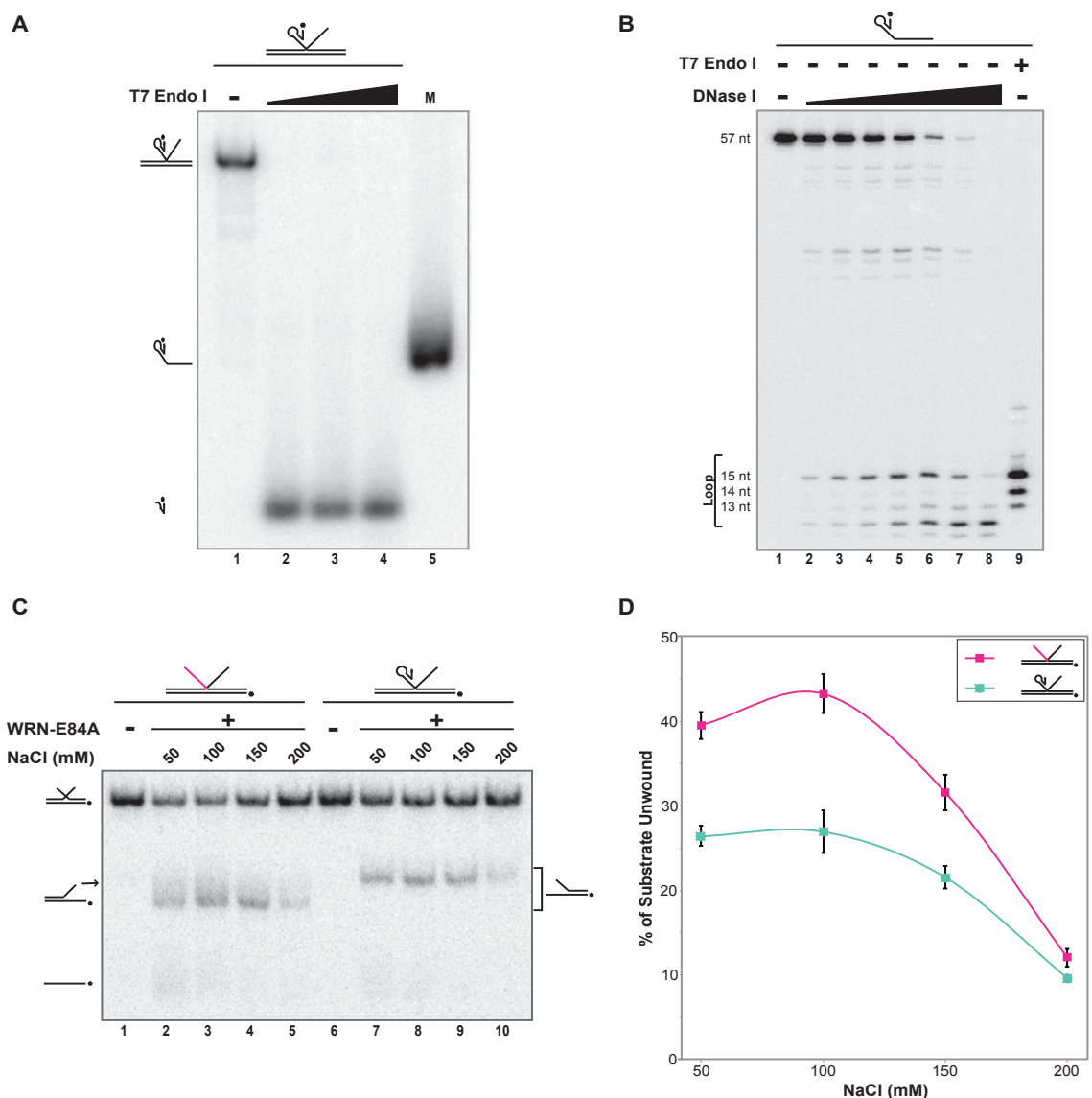


Figure 5.11 WRN-mediated unwinding reduced by Watson-Crick hairpin of 5' flap. **A)** To confirm the 5' flap of *3-way(WCH) forms a hairpin, the substrate (0.2 nM) was incubated with T7 Endo I (20-100 U/mL) at 37°C for 60 min. Labeled products were analyzed by native PAGE (6%). A marker of the 5' flap strand is shown (M). **B)** Further confirmation was obtained by incubating single-stranded *5'flap-WCH (0.2 nM) was incubated with T7 Endo I (200 U/mL) at 37°C for 60 min. For size markers, *5-flap-WCH (0.2 nM) was incubated with DNase I (0.2-20 U/mL) at 37°C for 10 min. Labeled products were analyzed by denaturing PAGE (14%), and approximate fragment sizes are indicated. **C)** To test the effect of a Watson-Crick hairpin on WRN-mediated unwinding, unwinding of *3-way(3.5xG) was compared to *3-way(WCH) (0.2 nM) at 50-200 mM NaCl at 37°C for 10 min using WRN-E84A (1.25 nM). Unwinding products were analyzed by native PAGE (6%). Structures of products are indicated. **D)** The percentage of original substrate converted to faster migrating products (mean \pm SE) was calculated using three independent experiments.

longer guanine tracts enhancing WRN-mediated unwinding, suggesting WRN may prefer sequences with longer G-runs. Also consistent with guanine hairpins enhancing WRN's activity, unwinding of substrates with potential guanine-hairpin forming sequences was enhanced under conditions that would tend to stabilize hairpin structures. However, lower temperatures reduce the molecular motion of DNA, suggesting lesser flap movement at lower temperatures may enhance WRN access to the preferred G-telomeric sequence on the 5' flap and thus, greater unwinding. Likewise, the effect of *Tetrahymena* repeat location on temperature-dependent WRN activity may also be explained by decreased molecular movement which may allow more efficient recognition of the favored sequence at the terminal end of the 5' flap at lower temperatures, and thus, greater unwinding. Taken together, these results likely support an effect of sequence, rather than secondary structure, on WRN-mediated unwinding of model strand invasion intermediates, although the evidence presented here is not conclusive.

The G-telomeric sequence specificity of WRN is further enhanced with mobile three-way junctions. Using helicase and binding assays, these results have demonstrated WRN exhibits a preference for G-telomeric sequence on the 5' flap of strand invasion intermediates. However, HR intermediates and T-loop invasion intermediates would possess homologous sequences on both single-stranded flaps allowing for bidirectional branch migration. Therefore, to examine WRN's G-telomeric sequence specificity on a more physiologically relevant substrate, I generated mobile junction substrates with G-telomeric or C-telomeric

sequence on the single-stranded flaps. The substrate *Mobile-G may include G-telomeric sequence (TTAGGG) on one or both flaps and specifically mimics the three-way junction of T-loops. Due to the mobile nature of these substrates, the length of each flap can vary between 31-52 nt at any point in time, depending on the location of the junction (Figure 5.12A). Likewise, the amount of duplex sequence on either side of the junction can vary in a similar manner. C-telomeric sequence may be found on both flaps of *Mobile-C (Figure 5.1). To compare WRN-mediated unwinding of these substrates, WRN was incubated with *Mobile-G or *Mobile-C in 0-300 mM NaCl at 37°C for 15 min (Figure 5.12). Since *Mobile-C possesses a radiolabeled *base strand, unwinding was detected in a similar manner as in previous experiments. The faster-migrating fork was generated by displacement of the 5' flap strand, while displacement of the 3' flap strand produces the slower-migrating fork. As with non-mobile substrates, two fork products are generated in the absence of NaCl (Figure 5.12A, lane 2), but WRN preferentially displaces the non-invading strand in greater NaCl concentrations. In contrast, *Mobile-G was composed using a radiolabeled 5' flap strand which results in production of a single fork product in addition to low amounts of single-stranded 5' flap strand. Here, the fork product is generated by displacement of the 3' flap strand, while the opposite directionality is observed by production of single strands (Figure 5.12A). In a similar manner as *Mobile-C, both directionalities are observed with *Mobile-G in the absence of NaCl (lane 10), but WRN preferentially unwinds the non-invading strand at greater NaCl concentrations. Both substrates were unwound to a large extent in the absence of NaCl (Figure 5.12B). However, while WRN-mediated

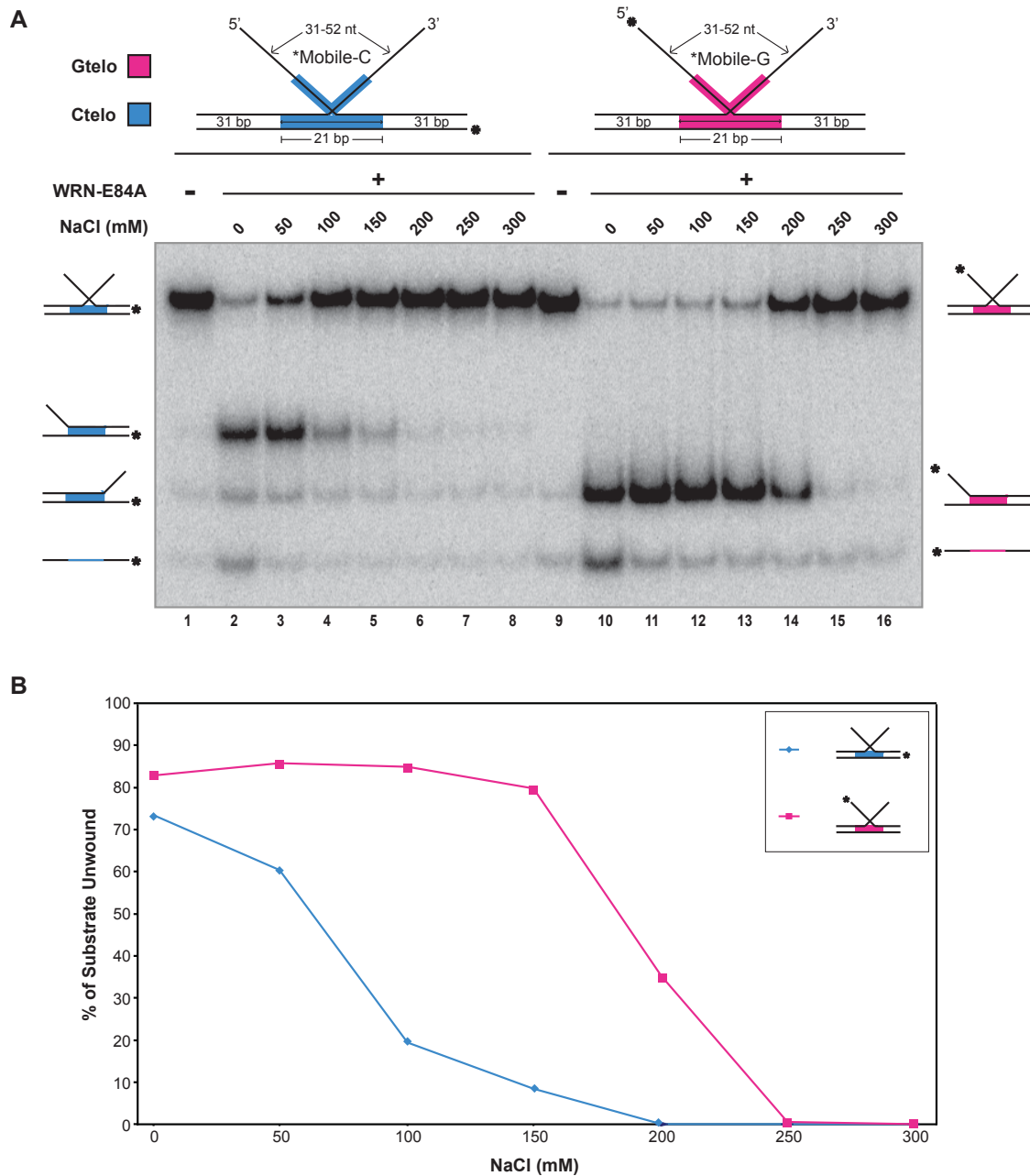


Figure 5.12 G-telomeric mobile junctions are more effectively unwound.
A) Unwinding of G-telomeric (*Mobile-G) and C-telomeric (*Mobile-C) (0.2 nM) were compared in 0-300 mM NaCl at 37°C for 15 min using WRN-E84A (1.2 nM). Here, Mg^{2+} was replaced with Mn^{2+} . Labeled products were analyzed by native PAGE (6%). Product structures are indicated. **B)** The percentage of original substrate converted to fork product was calculated.

unwinding of *Mobile-G was largely unaffected in up to 150 mM NaCl, *Mobile-C unwinding was significantly reduced (Figure 5.12B). In fact, some unwinding of Mobile-G was even observed at 200 mM NaCl (Figure 5.12B); thus WRN action on this substrate was even more “salt resistant” than observed using non-mobile substrates (Figure 5.3). Since T-loops are formed by invasion of the G-rich 3' telomeric overhang, these results are even more supportive of a role for WRN in the promotion of telomeric HR and/or T-loop development.

BLM possesses a similar G-telomeric sequence specificity as WRN.

Previous results presented here suggested BLM possessed a similar structural preference as WRN. Since WRN also exhibited a G-telomeric sequence preference, I examined the sequence specificity of BLM. BLM-mediated unwinding of model strand invasion intermediate substrates with G-telomeric (*3-way(3.5xG)), scrambled G-telomeric (*3-way(3.5xGscr)), C-telomeric (*3-way(3.5xC)), or random (*3-way(5'-21nt)) in 50-200 mM NaCl at 37°C for 15 min was compared (Figure 5.13A-B). Similar to WRN, BLM, by primarily displacing the non-invading strand, more efficiently unwound the G-telomeric strand invasion intermediate (Figure 5.13A, lanes 1-5) compared to the other substrates examined (Figure 5.13B). Similar to WRN, unwinding activity and salt resistance was enhanced on a G-telomeric mobile three-way junction (data not shown). BLM's unwinding activity was also dependent on the number of GGG tracts, since activity was significantly reduced in the presence of 2.5 G-telomeric repeats (Figure 5.13C). In a similar manner to WRN, BLM-mediated unwinding required a functional helicase domain, since no unwinding occurred in

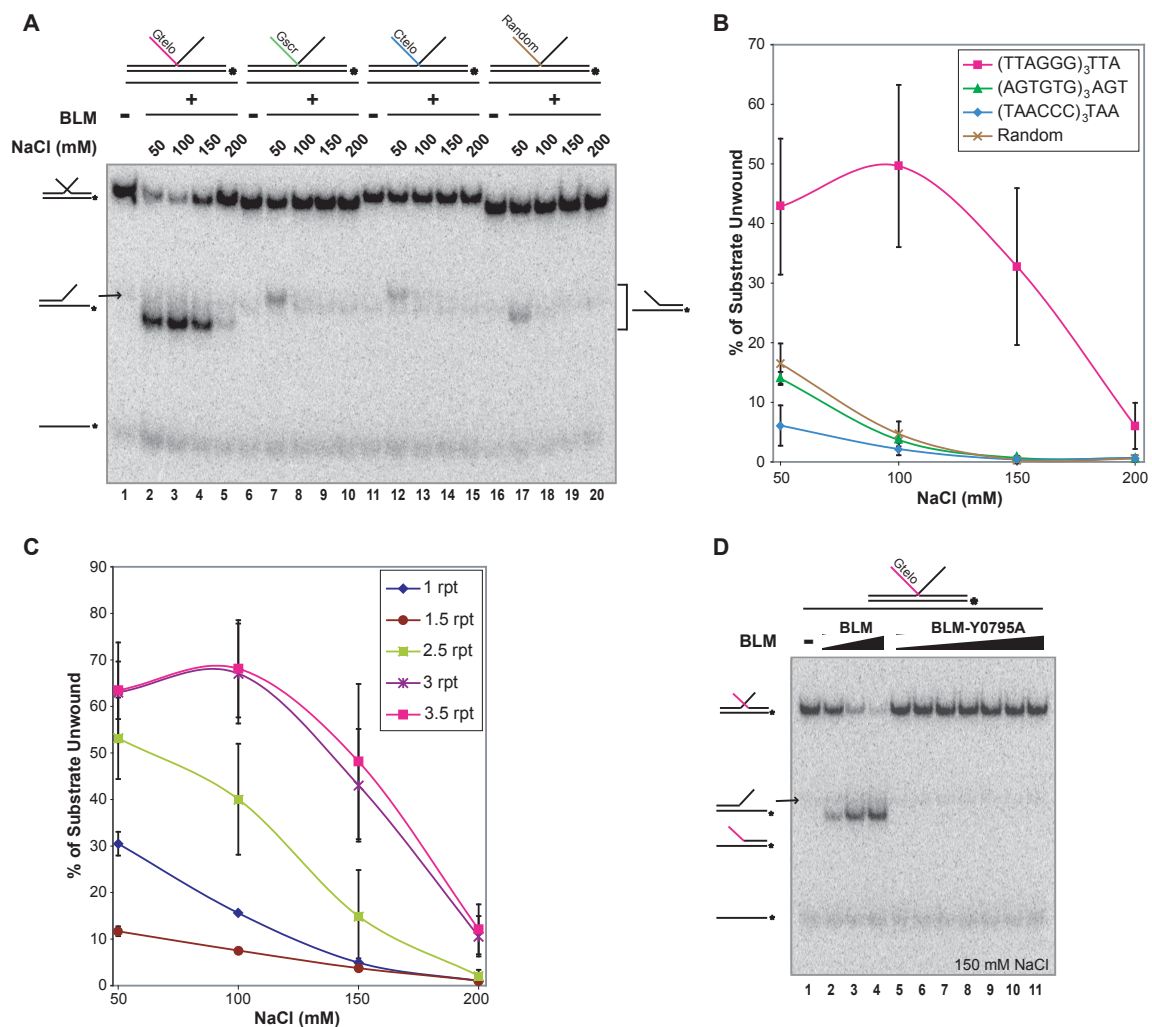


Figure 5.13 BLM preferentially unwinds model strand invasion intermediates with G-telomeric sequence. **A)** To examine the telomeric sequence specificity of BLM, a helicase assay was performed by incubating BLM (0.16 nM) with *3-way(3.5xG), *3-way(3.5xGscr), *3-way(3.5xC), or *3-way(5'-21nt) (0.2 nM) in 50-200 mM NaCl at 37°C for 15 min. Labeled unwinding products were analyzed by native PAGE (6%). Product structures are indicated. **B)** The percentage of original substrate converted to fork products (mean \pm SE) was calculated. **C)** To examine the sequence requirements of BLM, a helicase assay was performed by incubating *3-way(3.5xG), *3-way(3xG), *3-way(2.5xG), *3-way(1.5xG), or *3-way(1xG) (0.2 nM) in 50-200 mM NaCl at 37°C for 15 min. Labeled products were analyzed by native PAGE (6%) (not shown). The percentage of original substrate converted to fork products (mean \pm SE) was calculated. **D)** To determine if unwinding was dependent on BLM helicase domain, a helicase assay was performed by incubating wild-type BLM (0.13-0.5 nM) or helicase-deficient BLM-Y0795A (0.4-36 nM) with *3-way(3.5xG) (0.2 nM) in 150 mM NaCl at 37°C for 15 min. Labeled products were analyzed by native PAGE (6%). Unwinding product structures are indicated.

the presence of a helicase-dead mutant (BLM-Y0795A) (Figure 5.13D). Other RecQ helicases, such as RecQ4 and *E. coli* RecQ, did not possess a telomeric sequence preference on model strand invasion intermediates (data not shown). These results indicate BLM and WRN possess a similar G-telomeric sequence preference in the context of a model strand invasion intermediate. However, it is important to consider BLM exhibited a greater preference for two-stranded forks (Figure 4.6D-E), a somewhat different structural specificity than WRN (Chapter 4).

DISCUSSION

WRN has been suggested to function at telomeres, as initially evidenced by the extended replicative lifespan of WS cells expressing telomerase [Wyllie, Jones et al. 2000]. Additional physiological evidence was obtained during the development of a WS mouse model, which required several generations of telomerase deficiency before a WS phenotype could be observed [Lombard, Beard et al. 2000; Chang, Multani et al. 2004; Du, Shen et al. 2004]. WS cells undergo elevated telomere recombination [Laud, Multani et al. 2005] and exhibit a DNA damage response indicative of telomere dysfunction [van Steensel, Smogorzewska et al. 1998; Takai, Smogorzewska et al. 2003; Chang, Multani et al. 2004; Szekely, Bleichert et al. 2005], suggesting WRN may function in telomere maintenance and telomere-end protection. Telomeres may be protected by T-loops, a structure identified in mammalian cells that forms via a recombinogenic event involving invasion of the G-rich 3' telomeric overhang into

the homologous duplex repeats [Griffith, Comeau et al. 1999]. Previously, I presented evidence that WRN preferentially unwinds model strand invasion intermediates (Chapter 4), a structure that mimics a HR intermediate as well as the T-loop junction. To more closely examine a potential role of WRN in telomeric HR, I investigated the effect telomeric sequences have on WRN's helicase activities at model strand invasion intermediates. Previous studies have not demonstrated a sequence preference for WRN. For the first time, I show that G-rich telomeric sequences in context of HR intermediates allows for greater WRN activity.

In Chapter 4, I demonstrated that WRN preferentially unwound a model strand invasion intermediate by specifically displacing the non-invading strand, particularly in physiological salt conditions. To analyze how sequence influences WRN-mediated unwinding, I placed telomeric sequences consisting of 3.5 repeats on the 3' or 5' flap of model strand invasion intermediates. While no sequence preference associated with the 3' flap was observed, WRN preferentially unwound model strand invasion intermediates with at least three G-telomeric repeats (5'-(GGGTTA)₃-3') proximal to the junction on the 5' flap when compared to similar substrates with C-telomeric or non-telomeric sequences. Consistent with previous results using non-telomeric substrates, unwinding was achieved by primarily displacing the non-invading strand, especially in physiological salt conditions. In the more physiologically relevant KCl [Thier 1986], not only was a similar sequence preference observed, but WRN also possessed greater overall unwinding activity (data not shown). Under

these high salt conditions, G-quadruplexes may form [Wang and Patel 1993; Xu, Noguchi et al. 2006; Phan, Kuryavyi et al. 2007]. Therefore, the possibility G-quadruplexes might be mediating WRN's preference for the G-telomeric model strand invasion intermediate was considered. However, these results indicated the 5' flap sequence consisting of 3.5 G-telomeric repeats did not form a G-quadruplex. Furthermore, in conditions favorable for G-quadruplex formation, the model structure with four G-telomeric repeats, *3-way(4xG), was a poorer substrate, suggesting G-quadruplexes reduce WRN-mediated unwinding of model strand invasion intermediates. Although G-quadruplexes are *in vitro* substrates for WRN [Fry and Loeb 1999; Mohaghegh, Karow et al. 2001], it is believed the reduced unwinding of *3-way(4xG) is not due to these structures sequestering WRN from the single-stranded/double-stranded junction. Further supporting a G-telomeric sequence specificity, WRN more effectively bound single-flap structures as well as single-stranded DNA possessing G-telomeric sequence. However, these studies only indicated a telomeric sequence specificity of WRN's helicase activity, as WRN's exonuclease activity, as observed on the radiolabeled base strand, was unaffected by sequence (not shown). Most importantly, WRN's preference for G-telomeric model strand invasion intermediates was greatest in salt conditions that mimic the intracellular environment, suggesting these structures may be physiological targets of WRN.

These results indicated a G-quadruplex did not form on the 5' flap of *3-way(3.5xG) and thus did not enhance WRN's preference for G-telomeric model strand invasion intermediates. Therefore, this study considered WRN's G-

telomeric sequence specificity may be driven by the less stable guanine hairpin or may simply result as an effect of sequence. Supporting a sequence-based mechanism, model strand invasion intermediates with two human or *Tetrahymena* telomeric repeats, the minimal requirement for guanine hairpin formation, were less efficiently unwound than those with their three repeat counterparts. However, sequences that support more stable hairpin formation (*Tetrahymena*) enhance WRN-mediated unwinding, while sequences that destabilize or disrupt guanine hairpins (inosine) suppress it. While these results are suggestive of a favorable effect of guanine hairpins on WRN-mediated unwinding, these results may also reflect a preference of WRN for sequences with longer guanine tracts. Furthermore, conditions such as lower temperatures, that support guanine hairpin stabilization promoted more efficient unwinding, but it is important to consider the effect lower temperatures also have on molecular motion. At lower temperatures, the reduced movement of particularly single strands may provide better opportunities for WRN to recognize a preferred sequence, particularly near the free end of the 5' flap, thus leading to greater unwinding activity. Moreover, altering the non-guanine sequence immediately proximal to the junction, a change that should have no effect on guanine hairpin formation, also reduced WRN-mediated activity (data not shown). Therefore, based on the entirety of the results, it is our belief that primary, unstructured G-telomeric sequence consisting of a minimal three repeats located proximal to the junction most likely drives preferential WRN-mediated unwinding of strand invasion intermediates. However, additional experiments will be required to confirm this hypothesis.

I also examined the specificity of WRN's role at telomeric strand invasion intermediates by studying other RecQ helicases, including BLM, which performs similar biochemical activities [Mohaghegh, Karow et al. 2001; Machwe, Xiao et al. 2005; Machwe, Xiao et al. 2006]. While WRN preferentially unwound a model strand invasion intermediate, BLM preferentially unwound a two-stranded fork although the protein also efficiently acted at model strand invasion intermediates (Chapter 4). Like WRN, BLM more efficiently unwound a model strand invasion intermediate with a minimal three G-telomeric repeats on the invading strand, by specifically displacing the non-invading strand. Since these studies were performed at physiological salt conditions and BLM disrupts G-quadruplexes *in vitro* [Sun, Karow et al. 1998; Mohaghegh, Karow et al. 2001], the possibility remains that G-quadruplexes or other secondary structures may enhance BLM's G-telomeric sequence preference. However, due to the fact both WRN and BLM exhibited similar activities, it is likely these two proteins will possess a similar sequence-based mechanism of unwinding. The vast similarities of these two RecQ helicases also suggest WRN and BLM may perform similar functions in the cell. Consistent with this notion, *Tert*^{-/-}WRN^{-/-}BLM^{-/-} triple knockout mice exhibited a more severe phenotype [Du, Shen et al. 2004] suggesting some redundancy does exist between WRN and BLM. However, other RecQ helicases examined in this study, RecQ4 and *E. coli* RecQ, did not exhibit a G-telomeric sequence preference related to model strand invasion intermediates (not shown), suggesting telomeric recombination intermediates may not be targeted by all RecQ proteins.

In this study, I presented evidence that WRN preferentially unwinds strand invasion intermediates with invading strand G-telomeric sequence. Although these structures may also represent telomeric HR intermediates, they directly mimic the invasion site of the 3' overhang into the duplex repeats. The directionality observed in this study supports a role of WRN in T-loop formation and/or stabilization through generation of longer duplex regions at the T-loop junction. Consistent with WRN maintaining these protective telomere structures, WRN-deficient cells undergo elevated telomere recombination [Laud, Multani et al. 2005] as a consequence of telomere dysfunction [Crabbe, Jauch et al. 2007]. In addition, these cells exhibit a DNA damage response indicative of telomere dysfunction [van Steensel, Smogorzewska et al. 1998; Takai, Smogorzewska et al. 2003; Chang, Multani et al. 2004; Szekely, Bleichert et al. 2005]. Therefore, WRN may protect against telomere dysfunction and a DNA-damage response by aiding in the formation and/or stabilization of T-loops. However, it is important to consider that similar structures may be found in other locations, possibly at the other end of the T-loop, and these sites may indicate other roles for WRN. Furthermore, WRN functionally interacts with TRF2 [Opresko, von Kobbe et al. 2002; Machwe, Xiao et al. 2004], the only identified protein involved in T-loop formation [Stansel, de Lange et al. 2001]. Loss of TRF2 leads to telomere fusions and instability as well as a DNA damage response at telomeres [van Steensel, Smogorzewska et al. 1998; Takai, Smogorzewska et al. 2003], similar to characteristics of WRN deficiency [Chang, Multani et al. 2004; Szekely, Bleichert et al. 2005]. I have demonstrated TRF2 enhances WRN-

mediated strand exchange of telomeric sequences (not shown), suggesting these proteins may cooperate at T-loops to promote loop formation in addition to stabilization. Together, these results suggest, in the absence of WRN, fewer T-loops may be generated, thus leading to telomere dysfunction. In response to telomere deprotection, activation of cell cycle checkpoints leads to senescence and consequently aging. Telomere end fusions and additional instability also result from dysfunctional telomeres [van Steensel, Smogorzewska et al. 1998], supporting tumor development. Therefore, to protect against telomere instability, premature aging, and cancer, WRN may maintain telomere functionality by promoting formation of stable T-loops.

CHAPTER 6

CONCLUSIONS AND FUTURE DIRECTIONS

Found at the terminal ends of all linear chromosomes, telomeres possess several elements that make these specialized structures unique. This abundant sequence consist of six-nucleotide repeats and acts as a buffer to protect the important internal genetic information [McClintock 1941; Szostak and Blackburn 1982; Moyzis, Buckingham et al. 1988; de Lange, Shiue et al. 1990]. These repeats generate a specific binding sequence for the shelterin DNA-binding proteins TRF1, TRF2, and POT1 [Zhong, Shiue et al. 1992; Billaud, Brun et al. 1997; Broccoli, Smogorzewska et al. 1997; Baumann and Cech 2001; de Lange 2005]. Additionally, the repeating nature of telomeres allows strand invasion of the G-rich 3' overhang, a process that generates a specialized protective T-loop structure that is unique to telomeres [Griffith, Comeau et al. 1999]. As a G-rich sequence, the telomeric lagging strand possesses the potential to form a G-quadruplex within single-stranded regions generated during DNA metabolism [Huppert and Balasubramanian 2005; Lipps and Rhodes 2009]. These telomere-specific DNA binding proteins, specialized protective structures, and secondary structures have to potential to impede telomeric replication. As a result of the unidirectional nature of telomeric replication [Gilson and Geli 2007], these blocks may generate more severe consequences at telomeres. Therefore, additional mechanisms are likely required to support proper telomeric maintenance and metabolism.

The goal of this study was to examine WRN's role in telomere maintenance, particularly during replication, repair of stalled replication forks, and maintenance of telomere protective structures. Supporting a functional telomeric role of WRN, WS cells undergo premature senescence, but telomerase expression extends their replicative lifespan [Wyllie, Jones et al. 2000]. A physiological link between WRN and telomeres has been identified during development of a WS mouse model. WRN-deficient mice have no discernable phenotype [Lombard, Beard et al. 2000], due to extremely long murine telomeres [Kipling and Cooke 1990; Rudolph, Chang et al. 1999]. However, following several generations of telomerase deficiency, WRN loss leads to an external phenotype reminiscent of WS [Chang, Multani et al. 2004; Du, Shen et al. 2004], directly linking telomere dysfunction to premature aging associated with WS. Cells deficient of WRN suffer several metabolic anomalies [Salk, Au et al. 1981; Goto, Miller et al. 1996; Lebel and Leder 1998; Pichierri, Franchitto et al. 2001; Poot, Yom et al. 2001] suggesting WRN may function in telomere maintenance and/or metabolism. The results presented in this study suggest G-quadruplexes pose a barrier to telomeric replication and support a role for WRN in targeting G-rich telomeric sequences to promote proper telomeric maintenance and metabolism as methods to maintain proper telomere structure and function.

REPLICATION OF G-QUADRUPLEX FORMING SEQUENCES

The initial focus of this study was to examine the impact G-quadruplex-forming sequences, including telomeres, may have on replication. These results revealed that although telomeric intramolecular G-quadruplexes appear to exist in a dynamic equilibrium under physiological conditions, these secondary structures still blocked several replicative polymerases, thus suggesting intramolecular G-quadruplexes may impede replication. While these telomeric G-quadruplexes were dynamic in nature, it is important to consider that other G-rich sequences found throughout the genome may form more stable G-quadruplexes that could more effectively block these polymerases. This study also indicated intramolecular G-quadruplexes even blocked translesion polymerases that typically bypass bulky, fork-blocking DNA lesions, which suggests an high probability for replication fork blockage and subsequent fork collapse within G-rich sequences. Indeed, G-quadruplex-forming sequences have been shown to induce genomic instability [Betous, Rey et al. 2009; Damerla, Knickelbein et al. 2010], and our results are consistent with this notion. Importantly, the main polymerase in synthesis of the G-rich telomeric lagging strand, pol δ [Nick McElhinny, Gordenin et al. 2008] was blocked, indicating these secondary structures are also likely to impede telomere lagging strand replication. Due to the unidirectional nature of telomere synthesis, incomplete telomere replication can result in telomere loss. Directly or over time, loss of telomeric sequences can lead to critically shortened dysfunctional telomeres that trigger a DNA damage response. To more directly investigate how G-

quadruplexes may impact telomeric stability within a cellular environment, telomerase-deficient primary fibroblasts may be treated with telomestatin, a highly specific human telomeric G-quadruplex binding ligand that serves to stabilize these secondary structures [Kim, Vankayalapati et al. 2002]. Stabilization by telomestatin would be expected to exacerbate the effects of G-quadruplexes on telomere replication, such as telomere loss. Therefore, telomere length could be examined in response to telomestatin treatments to study the effect G-quadruplexes have on replication. Additionally, telomere-dysfunction induced foci (TIF) may be detected as markers of telomere dysfunction in response to G-quadruplex formation [Takai, Smogorzewska et al. 2003]. Since telomere dysfunction may also contribute to senescence, these telomestatin-treated cells may be tested for β -galactosidase, a marker of senescence. Increased senescence in these cells may suggest a connection between telomeric G-quadruplexes and aging.

More than 300,000 sequences across the genome have the potential to form a G-quadruplex [Huppert and Balasubramanian 2005; Huppert and Balasubramanian 2007]. However, unperturbed cells do not exhibit the widespread genomic instability that may result from frequent replication fork stalling at G-quadruplexes. Therefore, other protein(s) may be involved in the resolution of G-quadruplexes. While several helicases, including WRN, BLM, and FANCD1, have been shown to unwind G-quadruplexes *in vitro* [Sun, Karow et al. 1998; Fry and Loeb 1999; Mohaghegh, Karow et al. 2001; London, Barber et al. 2008; Wu, Shin-ya et al. 2008], molecular evidence is available supporting a

role for WRN in the resolution of G-quadruplexes at telomeres. Importantly, the loss-of-function diseases associated with these proteins generate genome instability, suggesting these proteins may also promote efficient replication. However, due to the substantial evidence supporting a functional interaction between WRN and the lagging strand polymerase pol δ , additional experiments should be focused on WRN's role in telomeric lagging strand replication at G-quadruplexes. Using the primer extension protocol used in this study, it would be informative to examine the effect of WRN, as well as other helicases such as BLM and/or FANCDJ, on particularly pol δ extension opposite an intramolecular G-quadruplex-forming template. These experiments should provide valuable information regarding identification of potential replication-assisting helicase(s) at G-quadruplexes. The effect of G-quadruplexes on genome stability has been previously studied through transfection of plasmids containing G-quadruplex-forming sequences [Betous, Rey et al. 2009; Damerla, Knickelbein et al. 2010]. Using a similar method, the impact of WRN loss on genome stability related to G-quadruplexes could be examined. Following transfection of normal and WRN-deficient cells with a non-integrated plasmid containing a control sequence that does not form G-quadruplexes or a G-quadruplex-forming sequence, isolated plasmids could be detected for mutations particularly within the G-rich region using sequencing methods. Compared to control cells, loss of WRN may result in loss of sequence or more frequent mutations within the G-rich region.

ROLES FOR WRN DURING TELOMERIC REPLICATION AND RECOMBINATION

WRN-mediated regression of replication forks stalled in telomeric regions.

The unidirectional nature of telomere synthesis indicates that blockage of replication forks by proteins, damage, or secondary structures may result in more severe consequences at telomeres, such as telomere loss and/or dysfunction. While replication fork regression is proposed to be an initial response to blocked replication forks, repeating sequences may become misaligned during this process, resulting in sequence loss or expansion. By continuing studies performed in our lab that identified fork regression as a complex activity of WRN [Machwe, Xiao et al. 2006; Machwe, Xiao et al. 2007], I presented *in vitro* evidence that WRN properly aligns telomeric and shorter dinucleotide repeats during the coordinated action of replication fork regression. Through proper alignment, these results support the idea that WRN-mediated fork regression is a highly coordinated process [Machwe, Xiao et al. 2007], rather than separate unwinding and annealing events which would likely result in misaligned sequences. Furthermore, the results presented here indicate WRN regression may also be utilized in difficult to replicate regions, including telomeres [Sfeir, Kosiyatrakul et al. 2009] that consist of repeating sequences. These results are consistent with previous reports that WRN responds to blocked replication forks [Lebel and Leder 1998; Pichierri, Franchitto et al. 2001; Poot, Yom et al. 2001; Pirzio, Pichierri et al. 2008]. Replication restart through the proper alignment of telomeric repeats would prevent excessive telomere loss

during synthesis, theoretically protecting against the telomere instability and dysfunction observed in WS [Laud, Multani et al. 2005; Crabbe, Jauch et al. 2007]. Therefore, in the absence of WRN, blocked replication forks may lead to fork collapse and subsequent telomere loss, consistent with the stochastic telomere loss observed in WS [Bai and Murnane 2003].

At telomeres, the replication fork can encounter a number of potential blocks, including G-quadruplexes, telomere binding proteins, and T-loops. However, the consequences of replication fork blockage may be more severe at telomeres, as the repeating nature of the sequence allows for more opportunities for errors through recombination repair pathways that may result in telomere dysfunction. While regression activity of WRN might apply throughout the genome, WRN's ability to properly align repeats during fork regression suggests WRN's role at telomeres may be especially crucial. Therefore, it would be informative to examine the effect WRN has on telomeric replication efficiency, particularly in response to fork-blocking DNA damage. This could be accomplished by treating normal and WRN-deficient cells with a DNA damaging agent, such as cisplatin which would generate greater damage at G-rich sequences such as telomeres [Blommaert, van Dijk-Knijnenburg et al. 1995]. Replication efficiency could then be detected by measuring the rate of nucleotide incorporation at telomeres. Reduced telomeric synthesis in WRN-deficient cells in response to DNA damage will support a role of WRN in promotion of efficient telomeric replication. However, WS cells would likely exhibit reduced replication efficiency even in the absence of exogenous agents due to other forms of fork

blocks, including endogenous DNA damage, DNA-binding proteins, or secondary structures. Furthermore, replication fork blocks at telomeres may lead to fork collapse and telomere loss due to a lack of a converging replication fork. Since WRN deficient cells are likely to possess a greater number of blocked replication forks in response to DNA damage, they retain a greater probability of fork collapse and telomere loss. Therefore, following treatment with DNA damage agents, telomere lengths may be measured within normal and WRN knockdown cells. These studies may provide valuable evidence linking inefficient replication in the absence of WRN to telomere instability.

WRN-mediated action on recombinational and telomeric structures. Since WS cells also develop genomic instability associated with elevated telomeric recombination [Laud, Multani et al. 2005], this study examined a potential role of WRN in not only HR, but at a similar homology-based strand invasion intermediate found at the protective T-loop structure [Griffith, Comeau et al. 1999]. WRN's function in telomeric recombination and end protection was examined by investigating the protein's helicase activity at model strand invasion intermediates that mimic telomeric HR and the junction at T-loops. I demonstrated WRN preferentially unwinds model strand invasion intermediates, a structure that mimics HR intermediates, supporting the notion WRN functions in HR. Strongly supporting a telomeric function of WRN, a minimum of three G-telomeric repeats (TTAGGG) located proximal to the single-stranded/double-stranded junction enhanced WRN's activity on these structures. Importantly, these G-telomeric structures directly mimic a recombination intermediate

generated by invasion of the G-telomeric strand during telomeric HR, especially at the T-loop, consistent with a potential role of WRN in telomere end-protection [Chang, Multani et al. 2004; Szekely, Bleichert et al. 2005]. These studies addressed a possible physiological role of WRN at telomeric recombination intermediates and/or at the T-loop. Importantly, the directionality observed is consistent with WRN promoting telomeric HR in addition to T-loop formation and stabilization, through generation of a longer duplex region at the T-loop junction. Therefore, in the absence of WRN, unstable or even non-existent T-loops may result leaving the telomere ends unprotected and dysfunctional. However, it is also important to consider these structures may be found at other locations, such as the other end of the T-loop invasion site, where the observed directionality would support a counteractive T-loop resolution activity; therefore, additional studies may be performed to identify WRN's precise role at T-loops. Unresolved T-loops in the absence of WRN may block the replication fork, also resulting in stochastic telomere loss and subsequent telomere dysfunction. Regardless of WRN's directionality of action, WRN deficiency would potentially allow more error-prone repair pathways such as NHEJ to become implemented, leading to greater instability at telomeres. Therefore, loss of proper WRN-mediated recombination potentially allows greater utilization of aberrant, error-prone recombination, which may be responsible for generating dysfunctional telomeres and cellular senescence or death.

Although these studies only examined the helicase activity of WRN, it is unclear how the exonuclease activity may function in these processes. Under

normal conditions used for *in vitro* WRN studies, others have demonstrated that WRN's exonuclease activity disrupts D-loops [Orren, Theodore et al. 2002; Opresko, Sowd et al. 2009]. Limited studies from our lab have indicated WRN's exonuclease activity is reduced in physiological salt conditions (data not shown), although we have not fully investigated a potential telomeric sequence effect on the exonuclease function.

While the results presented in this study only indicate a stabilization function of WRN at T-loops, WRN may also promote the initial strand invasion and formation of these structures. T-loop formation involves TRF2, a member of the shelterin complex [Stansel, de Lange et al. 2001]. TRF2, which functionally interacts with WRN [Opresko, von Kobbe et al. 2002], enhances WRN-mediated strand exchange of telomeric sequences *in vitro* (data not shown), supporting the notion that these proteins may cooperate to promote strand invasion of the 3' overhang, generating T-loops. In addition to TRF2, WRN functionally interacts with POT1, and each of these proteins stimulate one or more WRN activity [Opresko, von Kobbe et al. 2002; Machwe, Xiao et al. 2004; Opresko, Mason et al. 2005]. Limited studies to date have indicated POT1 neither enhances nor inhibits WRN's helicase activity on G-telomeric model strand invasion intermediates (data not shown). However, it is important to consider that TRF2 or POT1 alone, or in combination with one or more of the six shelterin proteins may still alter WRN's activity at model strand invasion intermediates. Although these results indicate WRN may promote T-loop formation, additional experiments should be performed using an established protocol to generate

large T-loops [Stansel, de Lange et al. 2001] to determine if WRN alone, or in combination with TRF2, is capable of forming T-loops *in vitro*. These results, which are supportive of a role of WRN in T-loop development, would suggest that loss of WRN reduces the number of these structures. Therefore, T-loops could be counted in WRN-deficient and wild-type cells using electron microscopy.

Since the experiments performed here showed that WRN exhibited greatest preference for G-telomeric strand invasion intermediates in physiological salt conditions that are supportive of a secondary structure, the potential that G-quadruplexes and/or guanine hairpin structures enhanced WRN-mediated unwinding was considered. However, at least in the context of a model strand invasion intermediate, intramolecular G-quadruplexes did not mediate WRN's preference for G-telomeric sequences. Yet, sufficient evidence does not exist to conclusively determine how G-quadruplexes may influence certain biochemical activities. Experiments using various methods to alter stability of any potential guanine hairpin, including temperature and sequence alterations, provided results largely supporting a sequence effect. The difficulty in confirming hairpin formation of telomeric sequences prevented development of more certain conclusions; therefore, additional experimentation will be necessary. For example, using lower temperatures to generate more stable hairpins, temperature-dependent electrophoresis has previously been demonstrated to detect guanine hairpins [Henderson, Hardin et al. 1987]. This method could be utilized to determine if the 3.5-repeat G-telomeric sequence

that conferred maximal WRN-mediated unwinding forms a guanine hairpin. Likewise, as temperature disrupts these DNA conformations, they absorb UV light differently. Therefore, the 3.5-repeat human G-telomeric sequence can be analyzed for guanine hairpin formation by examining absorbance at differing temperatures, similar to a protocol performed previously [Henderson, Hardin et al. 1987]. These methods may also be used on other non-telomeric sequences that consist of greater G-rich character and thus, are likely to form more stable guanine hairpins.

RELEVANCE OF RESULTS IN THE CONTEXT OF WERNER SYNDROME

These studies have provided additional evidence supporting a role of WRN in telomere maintenance and stability. Specifically, these results indicate telomere replication may be inherently difficult as a result of secondary structure formation and the repeating nature of these sequences. My results also support a potential role of WRN in promoting telomere replication by regressing blocked replication forks. Furthermore, WRN possesses a three-repeat G-telomeric sequence specificity associated with the invading strand, particularly under physiological salt conditions, thus suggesting WRN may promote proper telomeric HR and/or T-loop development. Biochemically, these functions support a potential function of WRN in not only in telomere replication and recombination but also telomere-end protection. These roles are consistent with WRN protecting against the telomere instability associated with WS [Laud, Multani et al. 2005], which occurs as a result of telomere dysfunction [Crabbe,

Jauch et al. 2007] and replication defects [Lebel and Leder 1998; Pichierri, Franchitto et al. 2001; Poot, Yom et al. 2001]. Also utilizing previous evidence, a model was developed based on the results presented here describing how WRN loss may lead to the premature aging and cancer phenotypes observed in WS (Figure 6.1). In the absence of WRN, frequent replication fork blockage within telomeric sequences, potentially as a result of G-quadruplexes, may lead to fork collapse and accelerated telomere loss, thus prematurely producing shortened, unprotected telomeres. In a similar manner, loss of WRN may lead directly to premature telomere deprotection due to an inability to properly develop T-loops, producing free telomere ends and an enhanced potential for telomere and genomic instability. Illegitimate recombination may also occur independently in the absence of WRN potentially generating additional instability, which along with loss/gain of tumorigenic regulators may lead to cancer. Alternatively, a DNA damage response to unprotected telomere ends may induce cell cycle checkpoints, resulting in senescence or apoptosis, a proposed mechanism for the development of some aging characteristics. Even though additional experiments need to be performed to fully conclude WRN's role in telomere metabolism, these results provided additional clues to WRN's potential function in telomere replication, recombination, and end protection.

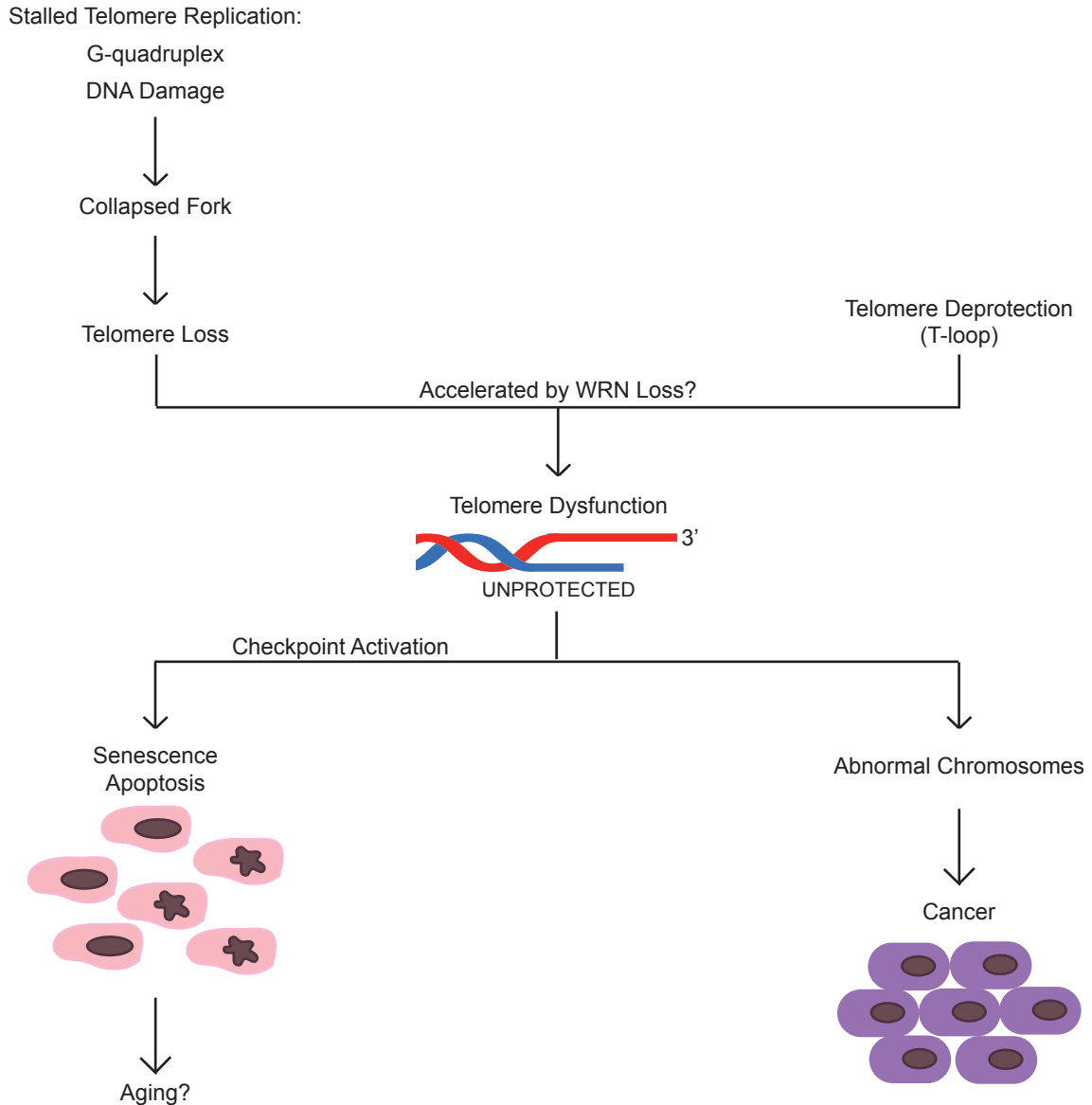


Figure 6.1 Graphic demonstrating downstream consequences of nonfunctional WRN. Loss of WRN may lead to greater replication fork stalling, particularly at telomeres, due to G-rich secondary structures (G-quadruplexes), DNA damage, etc. Without a functional WRN protein, more error-prone methods of telomeric recombination may occur at stalled or collapsed replication forks, leading to stochastic telomere loss. WRN deficiency may destabilize T-loop structures, exposing the telomere ends. As a result of telomere loss and/or telomere deprotection, telomeres become dysfunctional and activation of cell-cycle checkpoints render the cells non-functional through senescence or apoptosis, a pathway that results in premature development of aging characteristics. Abnormal chromosomes can develop from short, unprotected telomeres, potentially leading to cancer.

RELEVANCE OF RESULTS IN CONTEXT OF NORMAL AGING PHENOTYPES (INCLUDING CANCER) AND IMPLICATIONS FOR DELAYING AGE-RELATED HEALTH PROBLEMS AND FOR CANCER THERAPY

While the proposed activities of WRN in telomere metabolism and protection are consistent with phenotype of WS, these results are also applicable to normal aging and cancer. Although WRN acts to help maintain telomere structure and functionality, telomere loss still occurs throughout the lifespan of a normal cell due to the end replication problem [Watson 1972; Harley, Futcher et al. 1990] or as a result of replicative and recombinational inaccuracies. Individuals with lesser WRN activity, potentially as a result of particular polymorphisms in the WRN gene or WRN silencing, may possess inefficient WRN-mediated metabolic functions and may age more rapidly than normal individuals. WRN expression has also been reported to decline in blood cells with aging [Polosak, Kurylowicz et al. 2011], suggesting the potential metabolic functions for WRN discussed here may become less effective in older individuals and even greater telomere loss can result, particularly in combination with DNA damage. Additionally, environmental DNA-damaging agents, such as UV radiation, generate bulky lesions on the DNA that can block replication, and my results suggest WRN may aid in the repair of these damaged sites. However, greater exposure to these agents increases the probability for errors during replication or even recombination and may contribute to greater telomere loss and earlier development of certain aging characteristics. Regardless of how telomere loss occurs, critically short, unprotected telomeres may become

recombinogenic as a result of fusing with another telomere end, thus contributing to a tumorigenic phenotype.

These results may also be applied to develop potential therapies to delay aging and treat cancer. Long telomeres are likely to remain protected; therefore, expression of telomerase would potentially extend the replicative lifespan of cells and thus delay aging. As a protein involved in preventing premature aging, increasing WRN protein levels may further delay the development of an aging phenotype. My results suggest increased WRN protein levels may provide better telomere capping and enhance telomeric replication and recombination to maintain telomere structure and function. A similar effect may be generated by enhancing WRN activity through post-translational modifications, such as acetylation, which serves to stabilize WRN in response to some types of DNA damage [Li, Wang et al. 2010]. However, based on these results, increased WRN activity would also be favorable for survival of some types of tumors. In fact, some forms of cancers exhibit reduced expression of WRN but are more responsive to chemotherapy [Agrelo, Cheng et al. 2006; Kawasaki, Ohnishi et al. 2008]. Traditional forms of chemotherapy damage DNA to block the replication machinery and induce apoptosis, but my studies implied WRN may counteract the effectiveness of these drugs. Therefore, inhibiting WRN function in combination with chemotherapy may lead to more blocked replication forks, greater telomere loss, and greater apoptosis. In the process of tumorigenesis, cancer cells activate a telomere lengthening mechanism, typically through telomerase activation [Wright and Shay 1992; Shay, Van Der Haegen et al.

1993]. Therefore, eliminating telomerase and WRN together may lead to short unprotected telomeres, forcing these immortal cells to “age” and undergo apoptosis. WRN also possesses a G-telomeric sequence specificity, as demonstrated in Chapter 5. Thus, introduction of G-telomeric oligonucleotides into tumor cells will potentially compete with telomeres for WRN binding. In addition, these oligonucleotides are capable of recruiting other shelterin proteins including TRF1 and TRF2 (if double-stranded telomeric DNA) or POT1. Eliminating WRN and other proteins potentially involved in telomere-end protection may induce apoptosis in tumor cells. With these opportunities to develop new treatment regimens for aging and/or cancer, further research of WRN and telomeres may generate new possibilities for the enhancement of human health.

APPENDIX

LIST OF ABBREVIATIONS

53BP1: p53-Binding Protein 1

ATM: Ataxia Telangiectasia Mutated

ATP: Adenine Triphosphate

ATR: Ataxia Telangiectasia and Rad3 Related

BLM: Bloom's Syndrome Protein

bp: base pair(s)

BS: Bloom's Syndrome

BME: β -mercaptoethanol

BPB: Bromophenol Blue

BSA: Bovine Serum Albumin

CD: Circular Dichroism

cm: centimeter(s)

DMS: Dimethyl Sulfate

DTT: Dithiothreitol

dATP: Deoxyadenosine Triphosphate

dCTP: Deoxycytidine Triphosphate

dGTP: Deoxyguanosine Triphosphate

dNTP: Deoxyribonucleotide Triphosphate

dTTP: Deoxythymidine Triphosphate

EDTA: Ethylenediaminetetraacetic Acid

EMSA: Electrophoretic Mobility Shift Assay

FANCI: Fanconi Anemia, Complementation Group J

G4: G-quadruplex

HR: Homologous Recombination

kb: kilobase(s)

Kexo⁺: Klenow Fragment (3' to 5' exo⁺)

mdeg: millidegree(s)

μg: microgram(s)

μL: microliter(s)

MEF: Mouse Embryonic Fibroblast

mM: millimolar

MMR: Mismatch Repair

NER: Nucleotide Excision Repair

NHEJ: Non-Homologous End Joining

nM: nanomolar

nt: nucleotide(s)

OD: Optical Density

PAGE: Polyacrylamide Gel Electrophoresis

PCNA: Proliferating Cell Nuclear Antigen

pM: picomolar

POT1: Protection of Telomeres 1

RAP1: Ras-related Protein 1

Rb: Retinoblastoma protein

RPA: Replication Protein A

RTS: Rothmund-Thomson Syndrome

Sgs1: Slow Growth Suppressor 1

Tert: Telomerase

TIF: Telomere-dysfunction Induced Foci

TIN2: TRF1-Interacting Protein 2

TPP1: Tripeptidyl Peptidase 1

TRF1: Telomere Repeat-binding Factor 1

TRF2: Telomere Repeat-binding Factor 2

T-SCE: Telomeric Sister Chromatid Exchange

WC: Watson-Crick base pairing

WRN: Werner's Syndrome Protein

WS: Werner's Syndrome

XC: Xylene Cyanol

REFERENCES

- Agrelo, R., W. H. Cheng, F. Setien, S. Ropero, J. Espada, M. F. Fraga, M. Herranz, M. F. Paz, M. Sanchez-Cespedes, M. J. Artiga, D. Guerrero, A. Castells, C. von Kobbe, V. A. Bohr, M. Esteller (2006). "Epigenetic inactivation of the premature aging Werner syndrome gene in human cancer." Proc Natl Acad Sci U S A **103**(23): 8822-8827.
- Allsopp, R. C., H. Vaziri, C. Patterson, S. Goldstein, E. V. Younglai, A. B. Futcher, C. W. Greider, C. B. Harley (1992). "Telomere length predicts replicative capacity of human fibroblasts." Proc Natl Acad Sci U S A **89**(21): 10114-10118.
- Arnaudeau, C., C. Lundin, T. Helleday (2001). "DNA double-strand breaks associated with replication forks are predominantly repaired by homologous recombination involving an exchange mechanism in mammalian cells." J Mol Biol **307**(5): 1235-1245.
- Arnoult, N., C. Saintome, I. Ourliac-Garnier, J. F. Riou, A. Londono-Vallejo (2009). "Human POT1 is required for efficient telomere C-rich strand replication in the absence of WRN." Genes Dev **23**(24): 2915-2924.
- Babon, J. J., M. McKenzie, R. G. H. Cotton. (2003). "The use of resolvases T4 endonuclease VII and T7 endonuclease I in mutation detection." Mol Biotechnol **23**(1): 73-81.
- Bachrati, C. Z., R. H. Borts, I. D. Hickson (2006). "Mobile D-loops are a preferred substrate for the Bloom's syndrome helicase." Nucleic Acids Res **34**(8): 2269-2279.

- Bai, Y. and J. P. Murnane (2003). "Telomere instability in a human tumor cell line expressing a dominant-negative WRN protein." Hum Genet **113**(4): 337-347.
- Balagurumoorthy, P. and S. K. Brahmachari (1994). "Structure and stability of human telomeric sequence." J Biol Chem **269**(34): 21858-21869.
- Baumann, P. and T. R. Cech (2001). "Pot1, the putative telomere end-binding protein in fission yeast and humans." Science **292**(5519): 1171-1175.
- Betous, R., L. Rey, G. Wang, M. J. Pillaire, N. Puget, J. Selves, D. S. Biard, K. Shin-ya, K. M. Vasquez, C. Cazaux, J. S. Hoffmann. (2009). "Role of TLS DNA polymerases eta and kappa in processing naturally occurring structured DNA in human cells." Mol Carcinog **48**(4): 369-378.
- Bilaud, T., C. Brun, K. Ancelin, C. E. Koering, T. Laroche, E. Gilson (1997). "Telomeric localization of TRF2, a novel human telobox protein." Nat Genet **17**(2): 236-239.
- Bishop, G. R. and J. B. Chaires (2003). "Characterization of DNA structures by circular dichroism." Curr Protoc Nucleic Acid Chem **Chapter 7**: Unit 7 11.
- Blommaert, F. A., H. C. van Dijk-Knijnenburg, F. J. Dijt, L. den Engelse, R. A. Baan, F. Berends, A. M. Fichtinger-Schepman (1995). "Formation of DNA adducts by the anticancer drug carboplatin: different nucleotide sequence preferences in vitro and in cells." Biochemistry **34**(26): 8474-8480.
- Bohr, V. A. (2008). "Rising from the RecQ-age: the role of human RecQ helicases in genome maintenance." Trends Biochem Sci **33**(12): 609-620.

- Broccoli, D., A. Smogorzewska, L. Chong, T. de Lange (1997). "Human telomeres contain two distinct Myb-related proteins, TRF1 and TRF2." Nat Genet **17**(2): 231-235.
- Brosh, R. M., Jr., D. K. Orren, J. O. Nehlin, P. H. Ravn, M. K. Kenny, A. Machwe, V. A. Bohr (1999). "Functional and physical interaction between WRN helicase and human replication protein A." J Biol Chem **274**(26): 18341-18350.
- Brosh, R. M., Jr., J. Waheed, J. A. Sommers (2002). "Biochemical characterization of the DNA substrate specificity of Werner syndrome helicase." J Biol Chem **277**(26): 23236-23245.
- Burgers, P. M. (2009). "Polymerase dynamics at the eukaryotic DNA replication fork." J Biol Chem **284**(7): 4041-4045.
- Campisi, J. (2005). "Senescent cells, tumor suppression, and organismal aging: good citizens, bad neighbors." Cell **120**(4): 513-522.
- Chang, S., A. S. Multani, N. G. Cabrera, M. L. Naylor, P. Laud, D. Lombard, S. Pathak, L. Guarente, R. A. DePinho (2004). "Essential role of limiting telomeres in the pathogenesis of Werner syndrome." Nat Genet **36**(8): 877-882.
- Chavez, A., A. M. Tsou, F. B. Johnson (2009). "Telomeres do the (un)twist: helicase actions at chromosome termini." Biochim Biophys Acta **1792**(4): 329-340.
- Chin, L., S. E. Artandi, Q. Shen, A. Tam, S. L. Lee, G. J. Gottlieb, C. W. Greider, R. A. DePinho (1999). "p53 deficiency rescues the adverse effects of

- telomere loss and cooperates with telomere dysfunction to accelerate carcinogenesis." Cell **97**(4): 527-538.
- Clark, J. M., C. M. Joyce, G. P. Beardsley (1987). "Novel blunt-end addition reactions catalyzed by DNA polymerase I of Escherichia coli." J Mol Biol **198**(1): 123-127.
- Constantinou, A., M. Tarsounas, J. K. Karow, R. M. Brosh, V. A. Bohr, I. D. Hickson, S. C. West (2000). "Werner's syndrome protein (WRN) migrates Holliday junctions and co-localizes with RPA upon replication arrest." EMBO Rep **1**(1): 80-84.
- Crabbe, L., A. Jauch, C. M. Naeger, H. Holtgreve-Grez, J. Karlseder (2007). "Telomere dysfunction as a cause of genomic instability in Werner syndrome." Proc Natl Acad Sci U S A **104**(7): 2205-2210.
- Crabbe, L., R. E. Verdun, C. I. Hagglblom, J. Karlseder (2004). "Defective telomere lagging strand synthesis in cells lacking WRN helicase activity." Science **306**(5703): 1951-1953.
- Damerla, R. R., K. E. Knickelbein, D. Kepchia, A. Jackson, B. A. Armitage, K. A. Eckert, P. L. Opresko (2010). "Telomeric repeat mutagenicity in human somatic cells is modulated by repeat orientation and G-quadruplex stability." DNA Repair (Amst) **9**(11): 1119-1129.
- de Lange, T. (2005). "Shelterin: the protein complex that shapes and safeguards human telomeres." Genes Dev **19**(18): 2100-2110.
- de Lange, T., L. Shiue, R. M. Myers, D. R. Cox, S. L. Naylor, A. M. Killery, H. E. Varmus (1990). "Structure and variability of human chromosome ends." Mol Cell Biol **10**(2): 518-527.

- Denchi, E. L. and T. de Lange (2007). "Protection of telomeres through independent control of ATM and ATR by TRF2 and POT1." Nature **448**(7157): 1068-1071.
- Dimri, G. P., X. Lee, G. Basile, M. Acosta, G. Scott, C. Roskelley, E. E. Medrano, M. Linskens, I. Rubelj, O. Pereira-Smith, M. Peacocke, J. Campisi (1995). "A biomarker that identifies senescent human cells in culture and in aging skin in vivo." Proc Natl Acad Sci U S A **92**(20): 9363-9367.
- Doetsch, P. W., G. L. Chan, W. A. Haseltine. (1985). "T4 DNA polymerase (3'-5') exonuclease, an enzyme for the detection and quantitation of stable DNA lesions: the ultraviolet light example." Nucleic Acids Res **13**(9): 3285-3304.
- Du, X., J. Shen, N. Kugan, E. E. Furth, D. B. Lombard, C. Cheung, S. Pak, G. Luo, R. J. Pignolo, R. A. DePinho, L. Guarente, F. B. Johnson (2004). "Telomere shortening exposes functions for the mouse Werner and Bloom syndrome genes." Mol Cell Biol **24**(19): 8437-8446.
- Ellis, N. A., J. Groden, T. Z. Ye, J. Straughen, D. J. Lennon, S. Ciocchi, M. Proytcheva, J. German (1995). "The Bloom's syndrome gene product is homologous to RecQ helicases." Cell **83**(4): 655-666.
- Epstein, C. J., G. M. Martin, A. L. Schultz, A. G. Motulsky (1966). "Werner's syndrome a review of its symptomatology, natural history, pathologic features, genetics and relationship to the natural aging process." Medicine (Baltimore) **45**(3): 177-221.

- Fry, M. and L. A. Loeb (1994). "The fragile X syndrome d(CGG)_n nucleotide repeats form a stable tetrahelical structure." Proc Natl Acad Sci U S A **91**(11): 4950-4954.
- Fry, M. and L. A. Loeb (1999). "Human werner syndrome DNA helicase unwinds tetrahelical structures of the fragile X syndrome repeat sequence d(CGG)_n." J Biol Chem **274**(18): 12797-12802.
- Fujiwara, Y., T. Higashikawa, M. Tatsumi (1977). "A retarded rate of DNA replication and normal level of DNA repair in Werner's syndrome fibroblasts in culture." J Cell Physiol **92**(3): 365-374.
- German, J. (1997). "Bloom's syndrome. XX. The first 100 cancers." Cancer Genet Cytogenet **93**(1): 100-106.
- Gilson, E. and V. Geli (2007). "How telomeres are replicated." Nat Rev Mol Cell Biol **8**(10): 825-838.
- Goto, M. (1997). "Hierarchical deterioration of body systems in Werner's syndrome: implications for normal ageing." Mech Ageing Dev **98**(3): 239-254.
- Goto, M., R. W. Miller, Y. Ishikawa, H. Sugano. (1996). "Excess of rare cancers in Werner syndrome (adult progeria)." Cancer Epidemiol Biomarkers Prev **5**(4): 239-246.
- Goto, M., Y. Yamabe, M. Shiratori, M. Okada, T. Kawabe, T. Matsumoto, M. Sugimoto, Y. Furuichi (1999). "Immunological diagnosis of Werner syndrome by down-regulated and truncated gene products." Hum Genet **105**(4): 301-307.

- Gray, M. D., J. C. Shen, A. S. Kamath-Loeb, A. Blank, B. L. Sopher, G. M. Martin, J. Oshima, L. A. Loeb (1997). "The Werner syndrome protein is a DNA helicase." Nat Genet **17**(1): 100-103.
- Greider, C. W. and E. H. Blackburn (1985). "Identification of a specific telomere terminal transferase activity in Tetrahymena extracts." Cell **43**(2 Pt 1): 405-413.
- Greider, C. W. and E. H. Blackburn (1987). "The telomere terminal transferase of Tetrahymena is a ribonucleoprotein enzyme with two kinds of primer specificity." Cell **51**(6): 887-898.
- Griffith, J. D., L. Comeau, S. Rosenfield, R. M. Stansel, A. Bianchi, H. Moss, T. de Lange (1999). "Mammalian telomeres end in a large duplex loop." Cell **97**(4): 503-514.
- Harley, C. B., A. B. Futcher, C. W. Greider (1990). "Telomeres shorten during ageing of human fibroblasts." Nature **345**(6274): 458-460.
- Harmon, F. G. and S. C. Kowalczykowski (1998). "RecQ helicase, in concert with RecA and SSB proteins, initiates and disrupts DNA recombination." Genes Dev **12**(8): 1134-1144.
- Hayflick, L. (1965). "The Limited in Vitro Lifetime of Human Diploid Cell Strains." Exp Cell Res **37**: 614-636.
- Hayflick, L. (1976). "The cell biology of human aging." N Engl J Med **295**(23): 1302-1308.
- Hemann, M. T., M. A. Strong, L. Y. Hao, C. W. Greider (2001). "The shortest telomere, not average telomere length, is critical for cell viability and chromosome stability." Cell **107**(1): 67-77.

- Henderson, E., C. C. Hardin, S. K. Walk, I. Tinoco, Jr., E. H. Blackburn. (1987). "Telomeric DNA oligonucleotides form novel intramolecular structures containing guanine-guanine base pairs." Cell **51**(6): 899-908.
- Henderson, E. R. and E. H. Blackburn (1989). "An overhanging 3' terminus is a conserved feature of telomeres." Mol Cell Biol **9**(1): 345-348.
- Hiom, K. (2001). "Recombination: homologous recombination branches out." Curr Biol **11**(7): R278-280.
- Huang, S., B. Li, M. D. Gray, J. Oshima, I. S. Mian, J. Campisi (1998). "The premature ageing syndrome protein, WRN, is a 3'-->5' exonuclease." Nat Genet **20**(2): 114-116.
- Hubscher, U., G. Maga, S. Spadari. (2002). "Eukaryotic DNA polymerases." Annu Rev Biochem **71**: 133-163.
- Huppert, J. L. and S. Balasubramanian (2005). "Prevalence of quadruplexes in the human genome." Nucleic Acids Res **33**(9): 2908-2916.
- Huppert, J. L. and S. Balasubramanian (2007). "G-quadruplexes in promoters throughout the human genome." Nucleic Acids Res **35**(2): 406-413.
- Husain, I., B. Van Houten, D. C. Thomas, M. Abdel-Monem, A. Sancar (1985). "Effect of DNA polymerase I and DNA helicase II on the turnover rate of UvrABC excision nuclease." Proc Natl Acad Sci U S A **82**(20): 6774-6778.
- Johnson, R. E., S. Prakash, L. Prakash. (1999). "Efficient bypass of a thymine-thymine dimer by yeast DNA polymerase, Poleta." Science **283**(5404): 1001-1004.

- Johnson, R. E., M. T. Washington, S. Prakash, L. Prakash. (2000). "Fidelity of human DNA polymerase ϵ ." J Biol Chem **275**(11): 7447-7450.
- Kamath-Loeb, A. S., E. Johansson, P. M. Burgers, L. A. Loeb (2000). "Functional interaction between the Werner Syndrome protein and DNA polymerase δ ." Proc Natl Acad Sci U S A **97**(9): 4603-4608.
- Kamath-Loeb, A. S., L. A. Loeb, E. Johansson, P. M. Burgers, M. Fry. (2001). "Interactions between the Werner syndrome helicase and DNA polymerase δ specifically facilitate copying of tetraplex and hairpin structures of the d(CGG)_n trinucleotide repeat sequence." J Biol Chem **276**(19): 16439-16446.
- Karow, J. K., R. K. Chakraverty, I. D. Hickson (1997). "The Bloom's syndrome gene product is a 3'-5' DNA helicase." J Biol Chem **272**(49): 30611-30614.
- Karow, J. K., L. Wu, I. D. Hickson (2000). "RecQ family helicases: roles in cancer and aging." Curr Opin Genet Dev **10**(1): 32-38.
- Kaushik, M., M. Prasad, S. Kaushik, A. Singh, S. Kukreti (2010). "Structural transition from dimeric to tetrameric i-motif, caused by the presence of TAA at the 3'-end of human telomeric C-rich sequence." Biopolymers **93**(2): 150-160.
- Kawasaki, T., M. Ohnishi, Y. Suemoto, G. J. Kirkner, Z. Liu, H. Yamamoto, M. Loda, C. S. Fuchs, S. Ogino (2008). "WRN promoter methylation possibly connects mucinous differentiation, microsatellite instability and CpG island methylator phenotype in colorectal cancer. Mod Pathol **21**(2): 150-158.

- Kettani, A., R. A. Kumar, D. J. Patel (1995). "Solution structure of a DNA quadruplex containing the fragile X syndrome triplet repeat." J Mol Biol **254**(4): 638-656.
- Kim, M. Y., H. Vankayalapati, K. Shin-Ya, K. Wierzb, L. H. Hurley (2002). "Telomestatin, a potent telomerase inhibitor that interacts quite specifically with the human telomeric intramolecular g-quadruplex." J Am Chem Soc **124**(10): 2098-2099.
- Kipling, D. and H. J. Cooke (1990). "Hypervariable ultra-long telomeres in mice." Nature **347**(6291): 400-402.
- Kitao, S., A. Shimamoto, M. Goto, R. W. Miller, W. A. Smithson, N. M. Lindor, Y. Furuichi (1999). "Mutations in RECQL4 cause a subset of cases of Rothmund-Thomson syndrome." Nat Genet **22**(1): 82-84.
- Kruk, P. A., N. J. Rampino, V. A. Bohr (1995). "DNA damage and repair in telomeres: relation to aging." Proc Natl Acad Sci U S A **92**(1): 258-262.
- Kunkel, T. A. (1986). "Frameshift mutagenesis by eucaryotic DNA polymerases in vitro." J Biol Chem **261**(29): 13581-13587.
- Lahue, R. S., K. G. Au, P. Modrich (1989). "DNA mismatch correction in a defined system." Science **245**(4914): 160-164.
- Laud, P. R., A. S. Multani, S. M. Bailey, L. Wu, J. Ma, C. Kingsley, M. Lebel, S. Pathak, R. A. DePinho, S. Chang (2005). "Elevated telomere-telomere recombination in WRN-deficient, telomere dysfunctional cells promotes escape from senescence and engagement of the ALT pathway." Genes Dev **19**(21): 2560-2570.

- Lebel, M. and P. Leder (1998). "A deletion within the murine Werner syndrome helicase induces sensitivity to inhibitors of topoisomerase and loss of cellular proliferative capacity." Proc Natl Acad Sci U S A **95**(22): 13097-13102.
- Lebel, M., E. A. Spillare, C. C. Harris, P. Leder (1999). "The Werner syndrome gene product co-purifies with the DNA replication complex and interacts with PCNA and topoisomerase I." J Biol Chem **274**(53): 37795-37799.
- Lee, J. Y., B. Okumus, D. S. Kim, T. Ha. (2005). "Extreme conformational diversity in human telomeric DNA." Proc Natl Acad Sci U S A **102**(52): 18938-18943.
- Li, K., R. Wang, E. Lozada, W. Fan, D. K. Orren, J. Luo (2010). "Acetylation of WRN protein regulates its stability by inhibiting ubiquitination." PLoS One **5**(4): e10341.
- Lipps, H. J. and D. Rhodes (2009). "G-quadruplex structures: in vivo evidence and function." Trends Cell Biol **19**(8): 414-422.
- Lombard, D. B., C. Beard, B. Johnson, R. A. Marciniak, J. Dausman, R. Bronson, J. E. Buhlmann, R. Lipman, R. Curry, A. Sharpe, R. Jaenisch, L. Guarente (2000). "Mutations in the WRN gene in mice accelerate mortality in a p53-null background." Mol Cell Biol **20**(9): 3286-3291.
- London, T. B., L. J. Barber, G. Mosedale, G. P. Kelly, S. Balasubramanian, I. D. Hickson, S. J. Boulton, K. Hiom. (2008). "FANCD1 is a structure-specific DNA helicase associated with the maintenance of genomic G/C tracts." J Biol Chem **283**(52): 36132-36139.

- Machwe, A., E. M. Lozada, L. Xiao, D. K. Orren (2006). "Competition between the DNA unwinding and strand pairing activities of the Werner and Bloom syndrome proteins." BMC Mol Biol **7**: 1.
- Machwe, A., L. Xiao, J. Groden, S. W. Matson, D. K. Orren (2005). "RecQ family members combine strand pairing and unwinding activities to catalyze strand exchange." J Biol Chem **280**(24): 23397-23407.
- Machwe, A., L. Xiao, J. Groden, D. K. Orren (2006). "The Werner and Bloom syndrome proteins catalyze regression of a model replication fork." Biochemistry **45**(47): 13939-13946.
- Machwe, A., L. Xiao, R. G. Lloyd, E. Bolt, D. K. Orren (2007). "Replication fork regression in vitro by the Werner syndrome protein (WRN): holliday junction formation, the effect of leading arm structure and a potential role for WRN exonuclease activity." Nucleic Acids Res **35**(17): 5729-5747.
- Machwe, A., L. Xiao, D. K. Orren (2004). "TRF2 recruits the Werner syndrome (WRN) exonuclease for processing of telomeric DNA." Oncogene **23**(1): 149-156.
- Machwe, A., L. Xiao, S. Theodore, D. K. Orren (2002). "DNase I footprinting and enhanced exonuclease function of the bipartite Werner syndrome protein (WRN) bound to partially melted duplex DNA." J Biol Chem **277**(6): 4492-4504.
- Mahdi, A. A., G. S. Briggs, G. J. Sharples, Q. Wen, R. G. Lloyd (2003). "A model for dsDNA translocation revealed by a structural motif common to RecG and Mfd proteins." EMBO J **22**(3): 724-734.

- Matson, S. W. (1986). "Escherichia coli helicase II (uvrD gene product) translocates unidirectionally in a 3' to 5' direction." J Biol Chem **261**(22): 10169-10175.
- Matsumoto, T., A. Shimamoto, M. Goto, Y. Furuichi (1997). "Impaired nuclear localization of defective DNA helicases in Werner's syndrome." Nat Genet **16**(4): 335-336.
- Maxam, A. M. and W. Gilbert (1980). "Sequencing end-labeled DNA with base-specific chemical cleavages." Methods Enzymol **65**(1): 499-560.
- McClintock, B. (1941). "The Stability of Broken Ends of Chromosomes in Zea Mays." Genetics **26**(2): 234-282.
- McElligott, R. and R. J. Wellinger (1997). "The terminal DNA structure of mammalian chromosomes." EMBO J **16**(12): 3705-3714.
- Mendonca, V. M., K. Kaiser-Rogers, S. W. Matson (1993). "Double helicase II (uvrD)-helicase IV (helD) deletion mutants are defective in the recombination pathways of Escherichia coli." J Bacteriol **175**(15): 4641-4651.
- Mohaghegh, P., J. K. Karow, R. M. Brosh, Jr., V. A. Bohr, I. D. Hickson. (2001). "The Bloom's and Werner's syndrome proteins are DNA structure-specific helicases." Nucleic Acids Res **29**(13): 2843-2849.
- Moser, M. J., A. S. Kamath-Loeb, J. E. Jacob, S. E. Bennett, J. Oshima, R. J. Monnat, Jr. (2000). "WRN helicase expression in Werner syndrome cell lines." Nucleic Acids Res **28**(2): 648-654.
- Moyzis, R. K., J. M. Buckingham, L. S. Cram, M. Dani, L. L. Deaven, M. D. Jones, J. Meyne, R. L. Ratliff, J. R. Wu (1988). "A highly conserved

- repetitive DNA sequence, (TTAGGG)_n, present at the telomeres of human chromosomes." Proc Natl Acad Sci U S A **85**(18): 6622-6626.
- Myung, K., A. Datta, C. Chen, R. D. Kolodner (2001). "SGS1, the *Saccharomyces cerevisiae* homologue of BLM and WRN, suppresses genome instability and homeologous recombination." Nat Genet **27**(1): 113-116.
- Nick McElhinny, S. A., D. A. Gordenin, C. M. Stith, P. M. Burgers, T. A. Kunkel. (2008). "Division of labor at the eukaryotic replication fork." Mol Cell **30**(2): 137-144.
- Opresko, P. L., W. H. Cheng, V. A. Bohr (2004). "Junction of RecQ helicase biochemistry and human disease." J Biol Chem **279**(18): 18099-18102.
- Opresko, P. L., P. A. Mason, E. R. Podell, M. Lei, I. D. Hickson, T. R. Cech, V. A. Bohr (2005). "POT1 stimulates RecQ helicases WRN and BLM to unwind telomeric DNA substrates." J Biol Chem **280**(37): 32069-32080.
- Opresko, P. L., M. Otterlei, J. Graakjaer, P. Bruheim, L. Dawut, S. Kolvraa, A. May, M. M. Seidman, V. A. Bohr (2004). "The Werner syndrome helicase and exonuclease cooperate to resolve telomeric D loops in a manner regulated by TRF1 and TRF2." Mol Cell **14**(6): 763-774.
- Opresko, P. L., G. Sowd, H. Wang (2009). "The Werner syndrome helicase/exonuclease processes mobile D-loops through branch migration and degradation." PLoS One **4**(3): e4825.
- Opresko, P. L., C. von Kobbe, J. P. Laine, J. Harrigan, I. D. Hickson, V. A. Bohr (2002). "Telomere-binding protein TRF2 binds to and stimulates the

- Werner and Bloom syndrome helicases." J Biol Chem **277**(43): 41110-41119.
- Orren, D. K., R. M. Brosh, Jr., J. O. Nehlin, A. Machwe, M. D. Gray, V. A. Bohr (1999). "Enzymatic and DNA binding properties of purified WRN protein: high affinity binding to single-stranded DNA but not to DNA damage induced by 4NQO." Nucleic Acids Res **27**(17): 3557-3566.
- Orren, D. K., S. Theodore, A. Machwe (2002). "The Werner syndrome helicase/exonuclease (WRN) disrupts and degrades D-loops in vitro." Biochemistry **41**(46): 13483-13488.
- Phan, A. T., V. Kuryavyi, K. N. Luu, D. J. Patel. (2007). "Structure of two intramolecular G-quadruplexes formed by natural human telomere sequences in K⁺ solution." Nucleic Acids Res **35**(19): 6517-6525.
- Pichierri, P., A. Franchitto, P. Mosesso, F. Palitti (2001). "Werner's syndrome protein is required for correct recovery after replication arrest and DNA damage induced in S-phase of cell cycle." Mol Biol Cell **12**(8): 2412-2421.
- Pichierri, P., F. Rosselli, A. Franchitto (2003). "Werner's syndrome protein is phosphorylated in an ATR/ATM-dependent manner following replication arrest and DNA damage induced during the S phase of the cell cycle." Oncogene **22**(10): 1491-1500.
- Pirzio, L. M., P. Pichierri, M. Bignami, A. Franchitto. (2008). "Werner syndrome helicase activity is essential in maintaining fragile site stability." J Cell Biol **180**(2): 305-314.
- Polosak, J., A. Kurylowicz, M. Roszkowska-Gancarz, M. Owczarz, M. Puzianowska-Kuznicka (2011). "Aging is accompanied by a progressive

- decrease of expression of the WRN gene in human blood mononuclear cells." J. Gerontol A Biol Sci Med Sci **66**(1): 19-25.
- Poot, M., H. Hoehn, T. M. Runger, G. M. Martin (1992). "Impaired S-phase transit of Werner syndrome cells expressed in lymphoblastoid cell lines." Exp Cell Res **202**(2): 267-273.
- Poot, M., J. S. Yom, S. H. Whang, J. T. Kato, K. A. Gollahon, P. S. Rabinovitch (2001). "Werner syndrome cells are sensitive to DNA cross-linking drugs." FASEB J **15**(7): 1224-1226.
- Ribeyre, C., J. Lopes, J. B. Boule, A. Piazza, A. Guedin, V. A. Zakian, J. L. Mergny, A. Nicolas. (2009). "The yeast Pif1 helicase prevents genomic instability caused by G-quadruplex-forming CEB1 sequences in vivo." PLoS Genet **5**(5): e1000475.
- Rodriguez-Lopez, A. M., D. A. Jackson, F. Iborra, L. S. Cox (2002). "Asymmetry of DNA replication fork progression in Werner's syndrome." Aging Cell **1**(1): 30-39.
- Rodriguez-Lopez, A. M., D. A. Jackson, J. O. Nehlin, F. Iborra, A. V. Warren, L. S. Cox (2003). "Characterisation of the interaction between WRN, the helicase/exonuclease defective in progeroid Werner's syndrome, and an essential replication factor, PCNA." Mech Ageing Dev **124**(2): 167-174.
- Rottman, A., H. Gilboa, Y. Schechter, B. L. Silver (1992). "The determination of intracellular sodium concentration in human red blood cells: nuclear magnetic resonance measurements." Anal Biochem **201**(1): 48-51.

- Rudolph, K. L., S. Chang, H. W. Lee, M. Blasco, G. J. Gottlieb, C. Greider, R. A. DePinho (1999). "Longevity, stress response, and cancer in aging telomerase-deficient mice." Cell **96**(5): 701-712.
- Salas, T. R., I. Petruseva, O. Lavrik, A. Bourdoncle, J. L. Mergny, A. Favre, C. Saintome (2006). "Human replication protein A unfolds telomeric G-quadruplexes." Nucleic Acids Res **34**(17): 4857-4865.
- Salk, D., K. Au, H. Hoehn, G. M. Martin (1981). "Cytogenetics of Werner's syndrome cultured skin fibroblasts: variegated translocation mosaicism." Cytogenet Cell Genet **30**(2): 92-107.
- Schaffitzel, C., I. Berger, J. Postberg, J. Hanes, H. J. Lipps, A. Pluckthun. (2001). "In vitro generated antibodies specific for telomeric guanine-quadruplex DNA react with *Stylonychia lemnae* macronuclei." Proc Natl Acad Sci U S A **98**(15): 8572-8577.
- Schulz, V. P., V. A. Zakian, C. E. Ogburn, J. McKay, A. A. Jarzebowicz, S. D. Edland, G. M. Martin (1996). "Accelerated loss of telomeric repeats may not explain accelerated replicative decline of Werner syndrome cells." Hum Genet **97**(6): 750-754.
- Schwartz, M., E. Zlotorynski, M. Goldberg, E. Ozeri, A. Rahat, C. le Sage, B. P. Chen, D. J. Chen, R. Agami, B. Kerem (2005). "Homologous recombination and nonhomologous end-joining repair pathways regulate fragile site stability." Genes Dev **19**(22): 2715-2726.
- Searle, M. S., H. E. Williams, C. T. Gallagher, R. J. Grant, M. F. Stevens. (2004). "Structure and K⁺ ion-dependent stability of a parallel-stranded

- DNA quadruplex containing a core A-tetrad." Org Biomol Chem **2**(6): 810-812.
- Sen, D. and W. Gilbert (1988). "Formation of parallel four-stranded complexes by guanine-rich motifs in DNA and its implications for meiosis." Nature **334**(6180): 364-366.
- Sen, D. and W. Gilbert (1992). "Guanine quartet structures." Methods Enzymol **211**: 191-199.
- Sfeir, A., S. T. Kosiyatrakul, D. Hockemeyer, S. L. MacRae, J. Karlseder, C. L. Schildkraut, T. de Lange. (2009). "Mammalian telomeres resemble fragile sites and require TRF1 for efficient replication." Cell **138**(1): 90-103.
- Shay, J. W. and S. Bacchetti (1997). "A survey of telomerase activity in human cancer." Eur J Cancer **33**(5): 787-791.
- Shay, J. W., B. A. Van Der Haegen, Y. Ying, W. E. Wright (1993). "The frequency of immortalization of human fibroblasts and mammary epithelial cells transfected with SV40 large T-antigen." Exp Cell Res **209**(1): 45-52.
- Shay, J. W. and W. E. Wright (2005). "Senescence and immortalization: role of telomeres and telomerase." Carcinogenesis **26**(5): 867-874.
- Shay, J. W., W. E. Wright, H. Werbin (1991). "Defining the molecular mechanisms of human cell immortalization." Biochim Biophys Acta **1072**(1): 1-7.
- Shen, J. C., M. D. Gray, J. Oshima, A. S. Kamath-Loeb, M. Fry, L. A. Loeb (1998). "Werner syndrome protein. I. DNA helicase and dna exonuclease reside on the same polypeptide." J Biol Chem **273**(51): 34139-34144.

- Stansel, R. M., T. de Lange, J. D. Griffith (2001). "T-loop assembly in vitro involves binding of TRF2 near the 3' telomeric overhang." EMBO J **20**(19): 5532-5540.
- Stewart, E., C. R. Chapman, F. Al-Khodairy, A. M. Carr, T. Enoch (1997). "rqh1+, a fission yeast gene related to the Bloom's and Werner's syndrome genes, is required for reversible S phase arrest." EMBO J **16**(10): 2682-2692.
- Streisinger, G., Y. Okada, J. Emrich, J. Newton, A. Tsugita, E. Terzaghi, M. Inouye (1966). "Frameshift mutations and the genetic code. This paper is dedicated to Professor Theodosius Dobzhansky on the occasion of his 66th birthday." Cold Spring Harb Symp Quant Biol **31**: 77-84.
- Sun, H., R. J. Bennett, N. Maizels. (1999). "The *Saccharomyces cerevisiae* Sgs1 helicase efficiently unwinds G-G paired DNAs." Nucleic Acids Res **27**(9): 1978-1984.
- Sun, H., J. K. Karow, I. D. Hickson, N. Maizels (1998). "The Bloom's syndrome helicase unwinds G4 DNA." J Biol Chem **273**(42): 27587-27592.
- Sundquist, W. I. and A. Klug (1989). "Telomeric DNA dimerizes by formation of guanine tetrads between hairpin loops." Nature **342**(6251): 825-829.
- Szekely, A. M., F. Bleichert, A. Numann, S. Van Komen, E. Manasanch, A. Ben Nasr, A. Canaan, S. M. Weissman (2005). "Werner protein protects nonproliferating cells from oxidative DNA damage." Mol Cell Biol **25**(23): 10492-10506.
- Szostak, J. W. and E. H. Blackburn (1982). "Cloning yeast telomeres on linear plasmid vectors." Cell **29**(1): 245-255.

- Takai, H., A. Smogorzewska, T. de Lange (2003). "DNA damage foci at dysfunctional telomeres." Curr Biol **13**(17): 1549-1556.
- Takeuchi, F., F. Hanaoka, M. Goto, M. Yamada, T. Miyamoto (1982). "Prolongation of S phase and whole cell cycle in Werner's syndrome fibroblasts." Exp Gerontol **17**(6): 473-480.
- Tang, J., Z. Y. Kan, Y. Yao, Q. Wang, Y. H. Hao, Z. Tan. (2008). "G-quadruplex preferentially forms at the very 3' end of vertebrate telomeric DNA." Nucleic Acids Res **36**(4): 1200-1208.
- Thier, S. O. (1986). "Potassium physiology." Am J Med **80**(4A): 3-7.
- van Gent, D. C., J. H. Hoeijmakers, R. Kanaar (2001). "Chromosomal stability and the DNA double-stranded break connection." Nat Rev Genet **2**(3): 196-206.
- van Steensel, B., A. Smogorzewska, T. de Lange (1998). "TRF2 protects human telomeres from end-to-end fusions." Cell **92**(3): 401-413.
- Veldman, T., K. T. Etheridge, C. M. Counter (2004). "Loss of hPot1 function leads to telomere instability and a cut-like phenotype." Curr Biol **14**(24): 2264-2270.
- von Kobbe, C. and V. A. Bohr (2002). "A nucleolar targeting sequence in the Werner syndrome protein resides within residues 949-1092." J Cell Sci **115**(Pt 20): 3901-3907.
- Wang, Y. and D. J. Patel (1993). "Solution structure of the human telomeric repeat d[AG3(T2AG3)3] G-tetraplex." Structure **1**(4): 263-282.

- Washington, M. T., R. E. Johnson, S. Prakash, L. Prakash. (2001). "Mismatch extension ability of yeast and human DNA polymerase ϵ ." J Biol Chem **276**(3): 2263-2266.
- Watson, J. D. (1972). "Origin of concatemeric T7 DNA." Nat New Biol **239**(94): 197-201.
- Watt, P. M., E. J. Louis, R. H. Borts, I. D. Hickson (1995). "Sgs1: a eukaryotic homolog of E. coli RecQ that interacts with topoisomerase II in vivo and is required for faithful chromosome segregation." Cell **81**(2): 253-260.
- Werner, O. (1904). On cataract in conjunction with scleroderma. Kiel, Kiel University. **Doctoral dissertation.**
- Williamson, J. R., M. K. Raghuraman, T. R. Cech. (1989). "Monovalent cation-induced structure of telomeric DNA: the G-quartet model." Cell **59**(5): 871-880.
- Whitby, M. C. and R. G. Lloyd (1998). "Targeting Holliday junctions by the RecG branch migration protein of Escherichia coli." J Biol Chem **273**(31): 19729-19739.
- Woody, R. W. (1995). "Circular dichroism." Methods Enzymol **246**: 34-71.
- Wright, W. E. and J. W. Shay (1992). "The two-stage mechanism controlling cellular senescence and immortalization." Exp Gerontol **27**(4): 383-389.
- Wu, L. and I. D. Hickson (2006). "DNA helicases required for homologous recombination and repair of damaged replication forks." Annu Rev Genet **40**: 279-306.
- Wu, Y. and R. M. Brosh, Jr. (2010). "G-quadruplex nucleic acids and human disease." FEBS J **277**(17): 3470-3488.

- Wu, Y., K. Shin-ya, R. M. Brosh, Jr. (2008). "FANCD1 helicase defective in Fanconi anemia and breast cancer unwinds G-quadruplex DNA to defend genomic stability." Mol Cell Biol **28**(12): 4116-4128.
- Wyllie, F. S., C. J. Jones, J. W. Skinner, M. F. Haughton, C. Wallis, D. Wynford-Thomas, R. G. Faragher, D. Kipling (2000). "Telomerase prevents the accelerated cell ageing of Werner syndrome fibroblasts." Nat Genet **24**(1): 16-17.
- Xu, Y., T. Ishizuka, K. Kurabayashi, M. Komiyama. (2009). "Consecutive formation of G-quadruplexes in human telomeric-overhang DNA: a protective capping structure for telomere ends." Angew Chem Int Ed Engl **48**(42): 7833-7836.
- Xu, Y., Y. Noguchi, H. Sugiyama (2006). "The new models of the human telomere d[AGGG(TTAGGG)₃] in K⁺ solution." Bioorg Med Chem **14**(16): 5584-5591.
- Yamagata, K., J. Kato, A. Shimamoto, M. Goto, Y. Furuichi, H. Ikeda (1998). "Bloom's and Werner's syndrome genes suppress hyperrecombination in yeast sgs1 mutant: implication for genomic instability in human diseases." Proc Natl Acad Sci U S A **95**(15): 8733-8738.
- Yan, H., J. McCane, T. Toczylowski, C. Chen (2005). "Analysis of the Xenopus Werner syndrome protein in DNA double-strand break repair." J Cell Biol **171**(2): 217-227.
- Yang, L., T. Suwa, W. E. Wright, J. W. Shay, P. J. Hornsby (2001). "Telomere shortening and decline in replicative potential as a function of donor age in human adrenocortical cells." Mech Ageing Dev **122**(15): 1685-1694.

- Yu, C. E., J. Oshima, Y. H. Fu, E. M. Wijsman, F. Hisama, R. Alisch, S. Matthews, J. Nakura, T. Miki, S. Ouais, G. M. Martin, J. Mulligan, G. D. Schellenberg (1996). "Positional cloning of the Werner's syndrome gene." Science **272**(5259): 258-262.
- Zaug, A. J., E. R. Podell, T. R. Cech. (2005). "Human POT1 disrupts telomeric G-quadruplexes allowing telomerase extension in vitro." Proc Natl Acad Sci U S A **102**(31): 10864-10869.
- Zhang, M. L., X. J. Tong, X. H. Fu, B. O. Zhou, J. Wang, X. H. Liao, Q. J. Li, N. Shen, J. Ding, J. Q. Zhou. (2010). "Yeast telomerase subunit Est1p has guanine quadruplex-promoting activity that is required for telomere elongation." Nat Struct Mol Biol **17**(2): 202-209.
- Zhong, Z., L. Shiue, S. Kaplan, T. de Lange (1992). "A mammalian factor that binds telomeric TTAGGG repeats in vitro." Mol Cell Biol **12**(11): 4834-4843.

VITA

DEANNA NICOLE EDWARDS

Date of Birth: October 27, 1982
Place of Birth: Paducah, Kentucky

EDUCATION

- 2005-Present** **Doctoral Student**, Graduate Center for Toxicology, University of Kentucky, Lexington, KY
- 2001-2005** **Bachelor of Science, Biochemistry**, Lipscomb University, Nashville, TN

PROFESSIONAL EXPERIENCE

- 2006-present** **Research assistant**, Graduate Center for Toxicology, University of Kentucky
- 2004-2005** **General Chemistry Tutor**, Athletic Department, Lipscomb University

HONORS/AFFILIATIONS

- 2010** **First Place, Poster Presentation**, Midwest DNA Repair Symposium, Louisville, KY

- 2009 Exemplary Scholar, Environmental Health Sciences Fellows Showcase, Cincinnati, OH**
- 2008-2010 Treasurer, Toxicology Student Forum, University of Kentucky**
- 2008-2011 American Association of the Advancement of Science**
- 2006-2009 Predoctoral Fellow, NIEHS Training Grant in Molecular Mechanisms of Toxicity, University of Kentucky**
- 2005-2006 Graduate School Academic Year Fellowship, University of Kentucky**
- 2004-2005 Atlantic Sun All-Academic Team, Track, Lipscomb University**
- 2003-2004 Atlantic Sun All-Academic Team, Cross Country, Lipscomb University**
- 2002-present Alpha Chi Honor Society, Lipscomb University**

POSTER PRESENTATIONS

Edwards, D. N., Machwe, A., and D. K. Orren. The Werner syndrome protein (WRN) preferentially acts at model strand invasion intermediates with G-rich telomeric sequences. Midwest DNA Repair Symposium. May 19-20, 2012. Cincinnati, OH.

Edwards, D. N., Machwe, A., and D. K. Orren. The Werner syndrome protein (WRN) preferentially acts at model strand invasion intermediates with G-rich

telomeric sequences. Markey Cancer Center Research Day. May 16, 2012. Lexington, KY.

Edwards, D. N., Karale, R., Machwe, A., Wang, Z., and D. K. Orren. Effect of G-quadruplex structures on DNA synthesis by replicative and translesion polymerases. Markey Cancer Center Research Day. March 22, 2011. Lexington, KY.

Edwards, D. N., Machwe, A., and D. K. Orren. The Werner's syndrome (WS) helicase specifically acts at strand invasion intermediates at physiological salt concentrations. Midwest DNA Repair Symposium. May 15-16, 2010. Louisville, KY.

Edwards, D. N., Singh, J., and D. K. Orren. Chronic cisplatin treatment accelerates premature senescence of normal human fibroblasts. Environmental Health Sciences Fellows Showcase. September 18, 2009. Cincinnati, OH.

Edwards, D. N., Machwe, A., and D. K. Orren. The Werner syndrome protein (WRN) mediates proper alignment of repeated sequences during replication fork regression. Molecular Genetics of Aging. September 24-28, 2008. Cold Spring Harbor, NY.

PRESENTATIONS

Edwards, D. N., Singh, J., and D. K. Orren. Chronic cisplatin treatment accelerates premature senescence of normal human fibroblasts. Environmental Health Sciences Fellows Showcase. September 18, 2009. Cincinnati, OH.

SEMINARS

Relationships between telomeric sequences and structures, DNA replication, and the function of the Werner Syndrome Protein. July 13, 2012. Lexington, KY.

The action of Werner syndrome protein (WRN) on telomeric structures. University of Kentucky. April 26, 2010. Lexington, KY.

PUBLICATIONS

Edwards, D. N., Karale, R., Machwe, A., Wang, Z., and D. K. Orren. Effect of G-quadruplex structures on DNA synthesis by replicative and translesion polymerases. (manuscript to be submitted September 2012).

Edwards, D. N., Machwe, A., and D. K. Orren. The Werner syndrome protein (WRN) accurately aligns regions containing telomeric or dinucleotide repeats during replication fork regression. (manuscript in preparation).

Edwards, D. N., Machwe, A., and D. K. Orren. The Werner's syndrome (WS) helicase specifically acts at strand invasion intermediates at physiological salt concentrations. (manuscript in preparation)

Edwards, D. N., Machwe, A., and D. K. Orren. The Werner syndrome protein (WRN) preferentially acts at model strand invasion intermediates with G-rich telomeric sequences. (manuscript in preparation)

Singh, J., **Edwards, D.N.** and D.K. Orren. Chronic DNA damaging treatments accelerates the cellular senescence of normal human fibroblasts. (manuscript in preparation)